Experimental Study of Wing-in-Ground Effects in the AFIT 5-foot Wind Tunnel

Thesis

Laywn C. Edwards
Major, U.S. ARMY

AFIT/GAE/AA/87M-1

DEPARTMENT OF THE AIR FORCE
AIR UNIVERSITY
AIR FORCE INSTITUTE OF TECHNOLOGY

Wright-Patterson Air Force Base, Ohio

DISCLAIMER NOTICE

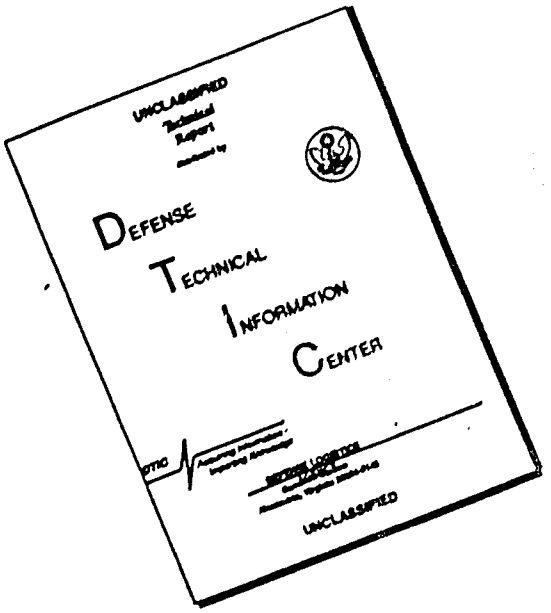

THIS DOCUMENT IS BEST QUALITY AVAILABLE. THE COPY FURNISHED TO DTIC CONTAINED A SIGNIFICANT NUMBER OF PAGES WHICH DO NOT REPRODUCE LEGIBLY.

AFIT/GAE/AA/87M-1

Experimental Study of Wing-in-Ground Effects in the AFIT 5-foot Wind Tunnel

Thesis

Laywn C. Edwards
Major, U.S. ARMY

AFIT/GAE/AA/87M-1

AFIT/GAE/AA/87M-1

EXPERIMENTAL STUDY OF WING-IN-GROUND EFFECTS IN THE AFIT 5-FOOT WIND TUNNEL

THESIS

Presented to the Faculty of the School of Engineering
of the Air Force Institute of Technology
Air University
in Partial Fulfillment of the
Requirements for the Degree of
Master of Science in Aeronautical Engineering

Lawyn C. Edwards
Major, U.S. Army

March 1987

Approved for public release; distribution unlimited

A Dedication

This thesis is dedicated to my loving wife, [redacted], who supplied constant encouragement and displayed great patience and tolerance during the entire course of my graduate study. Without this support, I would not have successfully completed this project. It is also dedicated to my newly born twins, [redacted] who created a lot of additional incentive as well as diversion from the AFIT studies. I now hope to get to know them all again.

Preface

In this study, I have investigated the effects of flying close to the ground on flight characteristics. My interest with this subject stems from my belief, as a combat aviator, that the only way for Army Aircraft to survive in the coming combat is to fly proficiently in the nap-of-the-earth technique; in other words, in and below the trees, hills, and ditches.

First of all, my thanks are due to Dr. Mangal D. Chawla of the Special Projects Group in Flight Dynamics Laboratory at WPAFB, Ohio, who sponsored this project. His own work and continuous technical support, from the model design and test planning stage through data analysis, is sincerely appreciated.

Next, of course, I owe my thanks to my thesis advisor, Dr. Milton E. Franke, for his guidance and encouragement during this study and my entire rocky-road throughout AFIT. Without that support, I probably would not be here to finish my degree. In addition, I thank the other members of my thesis committee, namely MAJ Lanson J. Hudson, who helped with the computer and scheduling, and MAJ Terry D. Hinnerichs. All of the committee members were very helpful and supportive of my work. My thanks are also due to Professor Emeritus Harold C. Larson who offered ideas and constructive criticism for running tests in the wind tunnel.

Technical support came from all directions and was the best I have ever seen. Messieurs Dave Driscoll and Tim Hancock worked long and hard under Mr. Jack Tiffany's direction in getting the

model and the ground boards built and ready. Mr. Andy Riessenschneider manipulated the wind tunnel as if they were born together. Messieurs Nick Yardich, Jay Anderson and Leroy Cannon provided a lot of technical and logistical support. Finally, without Mr. Jim Grove none of the data would have been stored, printed, plotted or thesis completed.

Most importantly, without God's support and guidance I would not have finished this project. Motivation is sometimes hard to come by.

Clay Edwards

Zenith Z-100/Wordstar, Math Text/Enhanced Epson FX100

Table of Contents

List of Figures

List of Tables

List of Symbols

b, b_1	span of wing
b_m	span of wing's image
c, c_{MAC}	mean aerodynamic chord
C	tunnel cross section area
C_D	drag coefficient
C_{D_i}	induced drag coefficient
C_L	lift coefficient
C_M	moment coefficient
C_p	pressure coefficient
c_r	root chord
c_t	tip chord
D_i	induced drag
e	distance from end of flap to bottom of plate
g	gravity constant
h	height of plates
H	height above ground surface
H/c	height to chord ratio
L, L_1	lift of wing
L_m	lift of wing's image
M	momentum
P	pressure
q	dynamic pressure
S	surface planform area of wing
t	boundary layer thickness
u	denotes data uncorrected based on freestream q

V	velocity
V_a	leakage flow velocity
α	angle of attack
α_b	angle between deflected flap and horizontal
α_a	$\alpha + \alpha_b$
δ	boundary correction factor
ε	h/c
θ	flap angle
μ	viscosity coefficient
ρ	density
σ	Prandtl's Interference Factor
∞	freestream condition

Configurations

OO	no center or end plates
OL	large end plates
LL	large center and end plates
OM	medium end plates
MM	medium center and end plates
OS	small end plates
SS	small center and end plates

List of Abbreviations

ACWIG	air cushion wing-in-ground
AFIT	Air Force Institute of Technology
AR	Aspect Ratio
DC	Direct Current
IGE	in-ground effects
L/D	lift to drag ratio
LE	leading edge of wing
MDL	Mobility Development Laboratory
NACA	National Advisory Committee for Aeronautics
OGE	out-of-ground effects
PAR-WIG	power augmented ram-wing in-ground
TE	trailing edge of wing
WIG	wing-in-ground
WPAFB	Wright-Patterson Air Force Base, Ohio

ABSTRACT

The effect of flying close to the earth's surface on the lift to drag ratio (L/D) was investigated. This was accomplished with the model of a NACA 4415 wing in the AFIT 5-foot Wind Tunnel.

The model was equipped with a full-span adjustable flap and three sets of end and center plates. Ground boards were placed in the tunnel to simulate the earth's surface. Five different heights of the model above the ground boards were selected to represent in and out of ground effects regimes.

Data were collected for forces and pressures on the model and on the board. The graphical representation of results displayed the effects of changing model parameters versus force, moment and pressure coefficients.

These conclusions were compared to theory and other literature for correlation. Results were conclusive. The effects of center plates and the variation of plate size were negligible. The presence of the set of end plates was beneficial near the surface but was negligible out of ground effects. The height of the model above the board produced noticeable differences in results. Angle of attack was shown to have a marked influence along with flap angle. Pressure plots also appeared to provide a method of predicting the amount of lift produced.

I. Introduction

Purpose

This investigation determined the ground effects on a wing when it was flying in close proximity to the ground. These wing-in-ground (WIG) effects, as they are commonly called, are generally experienced in the form of increased lift and reduced induced drag. Ground effects slowly diminish as the object is flying away from the ground surface and eventually disappear. Thus the entire regime of WIG effects can be further subdivided into three zones, namely a) In-Ground Effects (IGE) zone where these effects are very predominant, b) Out-of-Ground Effects (OGE) zone, where these effects are disappearing, and c) Free Stream zone, where these effects are absent.

The transition from one zone to the other is gradual. This study has defined and established boundaries for these zones in addition to determining quantitatively the ground effects and how they can best be used. For this study, a NACA 4415 wing with Aspect Ratio (AR) equal to 2.33 was selected. The selection of the airfoil shape and AR was deliberate. The Mobility Development Laboratory (MDL) of the Flight Dynamics Lab at WPAFB used this wing in power augmented ram wing-in-ground (PAR-WIG) effect studies. The present effort was aimed at supplementing the MDL work. Effort was made to study the effect of different variables on the aerodynamic characteristics of the wing, singly and in combination with the other parameters, in order to find the configuration which exhibited

the highest L/D. Various parameters considered were the angle of attack, α, flap angle, θ, height, H/c, and the size of the end plates.

The present study will help explain the gliding mode of a body when it is flying close to the ground. This situation is encountered during take-off and landing stages. In the present study, no engines were used. Thus, while flying near the ground, the ground effects experienced are the result of the air cushion developed in the cavity between the underside of the body and the ground. So, in reality, it becomes a case of air cushion wing-in-ground (ACWIG) effects.

The research contained in this study is part of a program directed at the development of a horizontal launch system for transatmospheric-type vehicles. To date, all such vehicles sent into space have been launched vertically. Even the sup-posedly resuable space shuttle requires many throw away sections that must be heaved into orbit through massive expenditures of power, money, time, and loss of flexibility. With more common use of the shuttle system coming along, a concept which can reduce life-cycle costs and provide greater flexibility is required. A possibility exists in the PAR-WIG launcher. The PAR-WIG launch system is a piggy-back transporter which will allow horisontal take-off of shuttle-type vehicles from conventional airfields with very short response times. Besides providing nearly unlimited flexibility, this transporter system will provide huge savings in man-hours, launch platforms, power requirements and,

thus, affect cost savings. The ACWIG studies will help determine the additional effects encountered in PAR-WIG effect flying mode.

Background

When an aircraft takes off in normal operation, it does not climb immediately to its flight altitude. For the first few moments, it stays close to the surface in nearly horizontal flight to gather the speed, and thus generate lift, required to be able to support itself and climb. While close to the surface, the wing is able to generate additional lift for the aircraft with less power than is possible during flight at high altitudes.

It is generally accepted from previous studies that IGE are experienced within one wing chord height above the surface. As the wing gets closer to the surface, lift increases very rapidly. Larger lift produces an increased lift to drag ratio (L/D) near the surface. As the vehicle approaches the ground, a reduction in the induced drag also occurs. As drag is reduced, the L/D is further increased.

The primary result of the phenomenon is that the vehicle can carry a heavier load than an aircraft flying at higher altitudes, "out-of-ground effect". This may provide the basis for a potential launch platform.

This WIG effect phenomenon was first observed when, during the landing phase, pilots noticed that their aircraft tended to

"float" as if on a cushion of air. It is also noticed in helicopters that less power is required to hover IGE than OGE. The associated reduction in induced drag was first capitalized upon in the Dornier DO X-12 Flying Boat to increase its range for scheduled crossings of the Atlantic during the 1930's. A by-product of the IGE phenomenon was the safe return of many pilots and damaged aircraft when pilots capitalized upon it during combat in World War II.

The evaluation of IGE started in the 1920's and is probably the result of observations made during the flight intensive years of World War I. The first work in the 1920's and 1930's was done by Warner (20). He studied low Aspect Ratio and ram-wing configurations. T. Kaario (20), a Finnish engineer, developed the first true WIG concept. During 1932 he built a craft called a flying wing which worked well near the ground. However, when he tried to fly it higher, it developed severe instability problems. In 1935 he built and flew another craft which generated a L/D of almost 15. He kept up his studies until the early 1960's. During World War II, N. Troong (20), in Switzerland, built and tested a craft weighing up to 30 tons but these studies were never completed.

Most of the studies of WIG vehicles since World War II have been carried out in the United States and the Soviet Union. However, since the fuel shortage, research has been reawakened in the Federal Republic of Germany and Japan as well as in the U.S. and U.S.S.R. The Soviets have seriously outpaced all

others in their efforts even though they claim "the U.S. has conducted detailed and exhaustive work on surface effect craft since World War II" (20).

In the U.S., experiments have been conducted by Alexander Lippish (20) from West Germany and H. Weiland (20) from Sweden. These experiments resulted in the design and development of the 1000-ton "Weilandcraft", which was dropped from building and further testing in 1964 after the model failed. The U.S. Maritime Administration let a contract for research and development that resulted in the "Columbia" which had such enormous cost overruns that it was discontinued after only a few tests.

Prior to the 1970's, technological advancements alone were the driving force behind the experiments. It was not until the fuel shortages and the dynamic leaps made in air defense systems demonstrated in the 1973 Arab-Israeli War that new interest was started in the WIG capability. Since then, the WIG effort in the U.S. has been primarily a naval effort. The use of hovercraft has become prominent. The only true high speed, low flying WIG vehicle currently in use is the Soviet "Caspian Sea Monster" capable of long-range transport of heavy cargo or large numbers of troops. Possible WIG missions include anti-submarine warfare, anti-shipping warfare, minelaying, reconnaissance, search and rescue, troop and logistic support, and amphibious operations. WIG vehicles offer advantages of low fuel consumption rates, the speed of an aircraft, low altitudes,

better payload capability, lower detection threshold, and at least four modes of operation. They will fly 1) in ground effect, 2) maneuver on the surface, 3) stationkeep (hover), and 4) fly out of ground effect. They provide a perfect platform for weapons or sub-vehicle launch and, in some cases, sub-vehicle retrieval.

To provide power, engines are mounted on the vehicle as they would be in a conventional aircraft, or even further forward of the wing than normal. These engines, however, would have adjustable pitch to provide for thrust vectoring. By varying this engine angle, the exhaust gases and thrust help provide additional flow under the wings to allow more lift, greater L/D, and lower speeds. This is called power augmentation. This configuration would eventually fly and be used in the final development at which this study is aimed.

Objectives and Scope

The stipulated purpose of the present study has been to show that greater amounts of lift and higher L/D are generated close to the surface of the earth. The objectives were:

1. Design wind tunnel experiments which would simulate flight of a wing close to the ground and generate the aerodynamic data required for various heights and flight control settings.
2. Establish a data reduction methodology for the experiments of objective 1.
3. Reduce and plot the results with varying parameters to deduce the effectiveness of each variable.

4. Determine recommendations for further study to accomplish the final stages of launch vehicle development.

The scope was limited to a non-powered system. The power augmented ram-wing would have entailed a more sophisticated model. That may follow the present effort. By using the wing without power, the characteristics were determined for a glide mode. Differences in values were not as dramatic as in a PAR-WIG experiment but the characteristics exhibited by each step could be determined.

The model was limited in size by the use of the Air Force Institute of Technology's (AFIT) 5-foot Wind Tunnel. Atmospheric air was the medium of study at low sub-sonic speeds. The dynamic pressure was kept low, at 10 psf, to stay within the limitations of the instrumentation.

II. Theory

The aerodynamic characteristics of a wing operating at or near the surface of the earth have interested many researchers since the end of World War I. Those interested in a more efficient mode of flight have considered flying in ground effect to be efficient not only in production of increased lift but also in reduction of induced drag, thus resulting in fuel savings.

Drag

Wieselberger (43) studied 'Wing Resistance Near the Ground' in 1921 and was the first experimenter to document "that the wing resistance diminishes on approaching the ground, while the lift increases somewhat, thereby making the lift to drag ratio more favorable". In order to solve for the change in induced drag (ΔD_i), Wieselberger used the theory of images or principle of reflection. He thus replaced the ground surface by a mirror creating an image below of the wing above. Then, to calculate the drag, he used a method similar to the one used for computing the drag of a multiplane from that of a monoplane. As the wing flies above the surface at a height, h, creating lift, L_1, the mirror image wing flies below the surface of the earth at the same distance and yielding lift, $-L_2$. The change in induced drag due to one wing's influence upon another is given by:

$$\Delta D_i = \frac{\sigma L_1(-L_2)}{\pi q b_1 b_2} \qquad (1)$$

For a mirror image case,

$b_1 = b_2 = b$, therefore $L_1 = L_2 = L$

so equation (1) becomes:

$$\triangle D_i = \frac{-\sigma L^2}{\pi q b^2} \qquad (2)$$

Induced drag on a wing is given by:

$$D_i = \frac{L^2}{\pi q b^2} \qquad (3)$$

So, when flying close to the ground where the mirror image wing has an effect, the drag is then changed to:

$$D_i = \frac{L^2}{\pi q b^2} - \frac{\sigma L^2}{\pi q b^2} = \frac{L^2}{\pi q b^2} \ (1-\sigma) \qquad (4)$$

Change in drag coefficient $\triangle C_{Di}$ when flying close to the ground is therefore given by:

$$\triangle C_{Di} = \frac{\triangle D_i}{q\ S} \qquad (5)$$

Combining (2) and (5) gives:

$$\triangle C_{Di} = \frac{-\sigma\ L^2}{\pi q^2 S \cdot b^2} = -\ \sigma\ \frac{C_L^{\ 2}}{\pi} \cdot \frac{S}{b^2} \qquad (6)$$

Equation (6) shows that the changes in induced drag ($\triangle C_{Di}$) vary as the square of the lift coefficient (C_L)

(ΔC_{Di}) vary as the square of the lift coefficient (C_L) while in ground effect.

The limitations in the Wieselberger theory were that it considered a one-dimensional case and that the wing considered was without end plates.

Lift

The lift coefficient (C_L) near the ground is greater than the C_L in freestream primarily due to the effects of shedding bound and trailing vortices. The ground proximity provides this new C_L which is a combination of freestream, $C_{L\infty}$, plus a change due to a ground cushion, $\Delta C_{L_{WIG}}$.

$$C_L = C_{L\infty} + \Delta C_{L_{WIG}} \qquad (7)$$

Since the value for $\Delta C_{L_{WIG}}$ is positive , the final value for C_L is greater than when out of ground effect.

Gallington, Miller, and Smith (18) developed a one-dimensional theory using "The Ram-Wing Surface Effect Vehicle". Their vehicle had end plates. They compared their theoretical results with their wind tunnel and freestream results. In the study, leakage underneath the end plates was considered and assumed to be due to the elevated pressure in the channel underneath the wing, i.e., an increase in pressure. (See Fig. 1).

$$\Delta p = 1/2\ \rho V_o^2 \qquad (8)$$

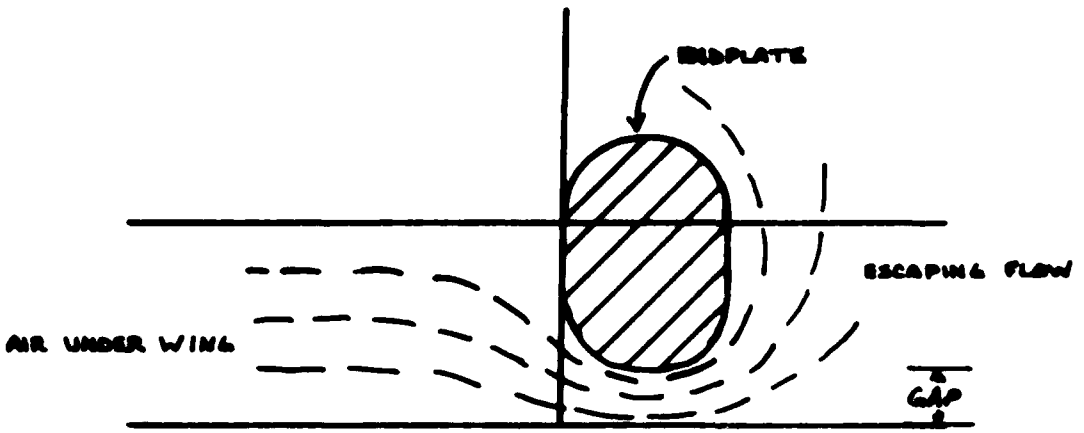

Fig. 1 End Plate Leakage

surfaces on the top and bottom whereas Model II was a flat bottomed airfoil. The latter model showed better correlation with theory.

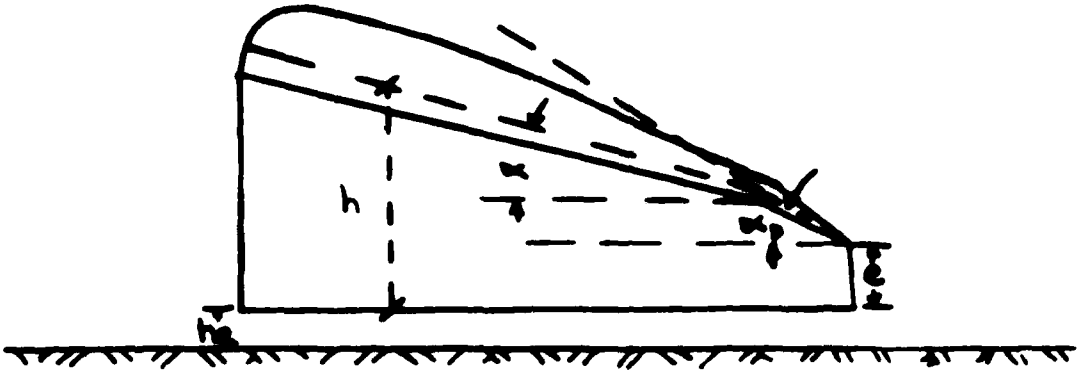

Fig. 2 End Plate Dimensions

Gallington et al., developed the following set of equations:

$$C_D = C_{D_M} + C_{D_p} \tag{9}$$

where C_{D_M} = momentum drag coefficient

$$= 2Y * \tan \alpha_D * C_{L_{WIG}} \left[1 - \sqrt{1 - C_{L_{WIG}}} \right] \tag{10}$$

$$\text{where } Y = \frac{2\, h_m}{b \tan \alpha_D} \tag{11}$$

$$C_{L_{WIG}} = \frac{V_n^2}{V_\alpha^2} \tag{12}$$

C_{D_p} = profile drag, independent of ground surface

= 0.145 (assumption for Model II)

Widnall and Barrows (42), working at M.I.T. in 1969, developed an analytic solution for two- and three-dimensional cases of wings in ground effect. They used lifting surface theory for a ram-wing operating in close proximity to a solid boundary. This study determined that flying in close proximity to the ground had definite performance advantages. Very high C_L and L/D can be achieved with such vehicles. Widnall and Barrows found that for a ram-wing IGE, the lowest order solution for the C_L was given by:

$$C_L = \frac{\alpha}{\tau} \tag{13}$$

Next order solution is:

$$C_L = \frac{\alpha}{\tau} + \frac{2}{\pi}\alpha \left[2 \ln \frac{\pi}{\tau} + 1 \right] \tag{14}$$

and so on.

Using the value of C_L from above, the induced drag coefficient is given by:

$$C_{Di} = \frac{C_L^2}{\pi K AR} \tag{15}$$

where K AR is called the Effective Aspect Ratio. Also,

$$K = \frac{2}{3\pi\tau} \tag{16}$$

Combining the above equations yields

$$C_{Di} = \frac{1.5\ C_L^2 \epsilon}{AR} \qquad (17)$$

In the three-dimensional case there will be an additional contribution to C_L.

Goetz (22), at AFIT, tried to predict the lift and drag characteristics of an AR 2 wing, with and without end plates, operating in ground effect by using the PANAIR higher order panel method. Goetz obtained excellent agreement between a numerical solution and the experimental data for the wing without end plates up to low values of H/c ratios. However, for the wing with end plates, the numerical results showed large variation from the experimental data up to an H/c of twenty percent. The gap between numerical and experimental data narrows down for higher altitudes. The modeling technique needs further refinement to account for other variables like end plate size, angle of attack, and flap deflection.

Boundary Layer Effect.

In this particular study, ground boards were used to simulate the surface of the earth. In much of the literature and theory, the thought process utilized the imaging system discussed earlier and shown in Fig. 3. A few experiments have actually been run with this system also. It is, theoretically, a better method than the ground board.

The ground board will create a boundary layer that does

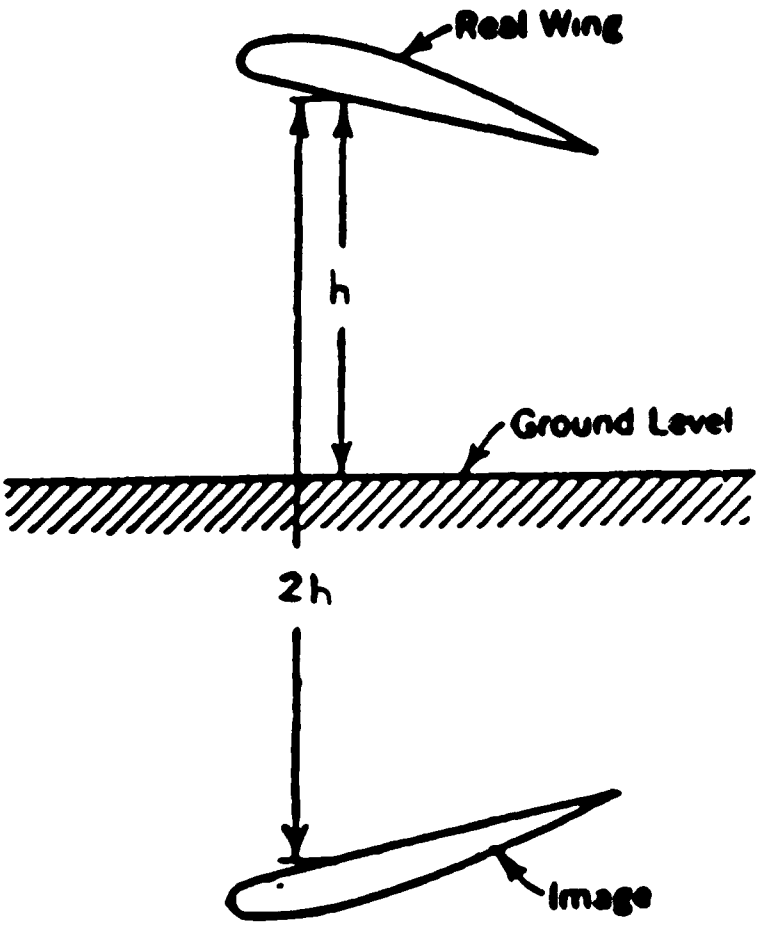

Fig. 3 Wing Model Imaging

The ground board will create a boundary layer that does not exist in nature. This boundary layer's thickness depends upon the freestream velocity, the length of the board in front of the model, and the roughness of the board. The boundary layer can theoretically affect the results if the model is inside the layer as it could be when flying near the surface of the board. Inside the boundary layer, viscosity must be taken into consideration. Potential flow solutions cannot be used. However, at H/c greater than one half, potential flow solutions would be acceptable. The main shortcoming in Goetz' solution was that he did not take the boundary layer into account.

The main purpose of this study is to maximize the L/D by flying close to the ground surface as this results in the maximum power available for propulsion and acceleration. To assure realistic simulation for as close to the surface as possible, the boundary layer effects need to be negated. To negate boundary layer effects, the imaging technique should be used. Comparing imaging results with the results of this study would show if the boundary layer affected the present study.

III. Experimental Apparatus

The experimental apparatus for this study was made up of the model, the ground boards, the AFIT 5-foot Wind Tunnel, the instrumentation and calibration, and the computer hardware and software. Each will be addressed separately.

Model

In order to study IGE and OGE, an ACWIG model was designed and built in the AFIT model shops. The model was built to match a model used on the static table at the Air Force Wright Aeronautical Laboratories Mobility Branch by Dr. M.D. Chawla in a similar PAR-WIG experiment. The model represents a 1/102 scale of a prototype of 180 ft span (see Figs 4 to 6). The salient features of the wing include:

Wing Profile	NACA 4415 airfoil
Aspect Ratio, AR	2.33
span, b	20.97 in
root chord, c_r	10.66 in
tip chord, c_t	7.34 in
mean aero chord, c_{MAC}	9.00 in
Flap (0.2 c_{MAC})	1.80 in
wing planform area, S	1.31 ft^2
wing sweep angle	17.54 deg
End and Center Plates	0.125c_{MAC}, 0.15c_{MAC}, 0.2c_{MAC}

The model size was designed so that, along with the ground board

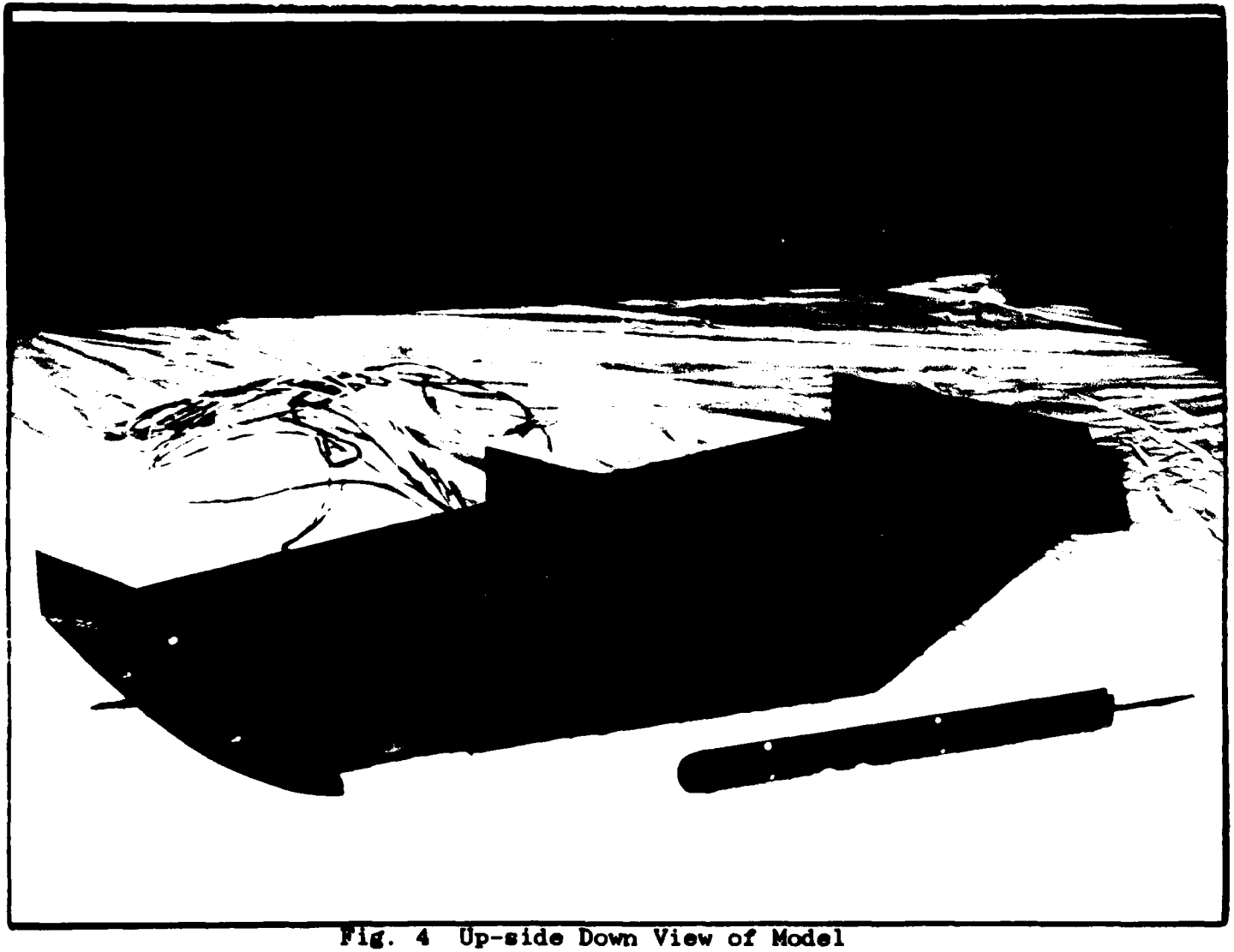

Fig. 4 Up-side Down View of Model

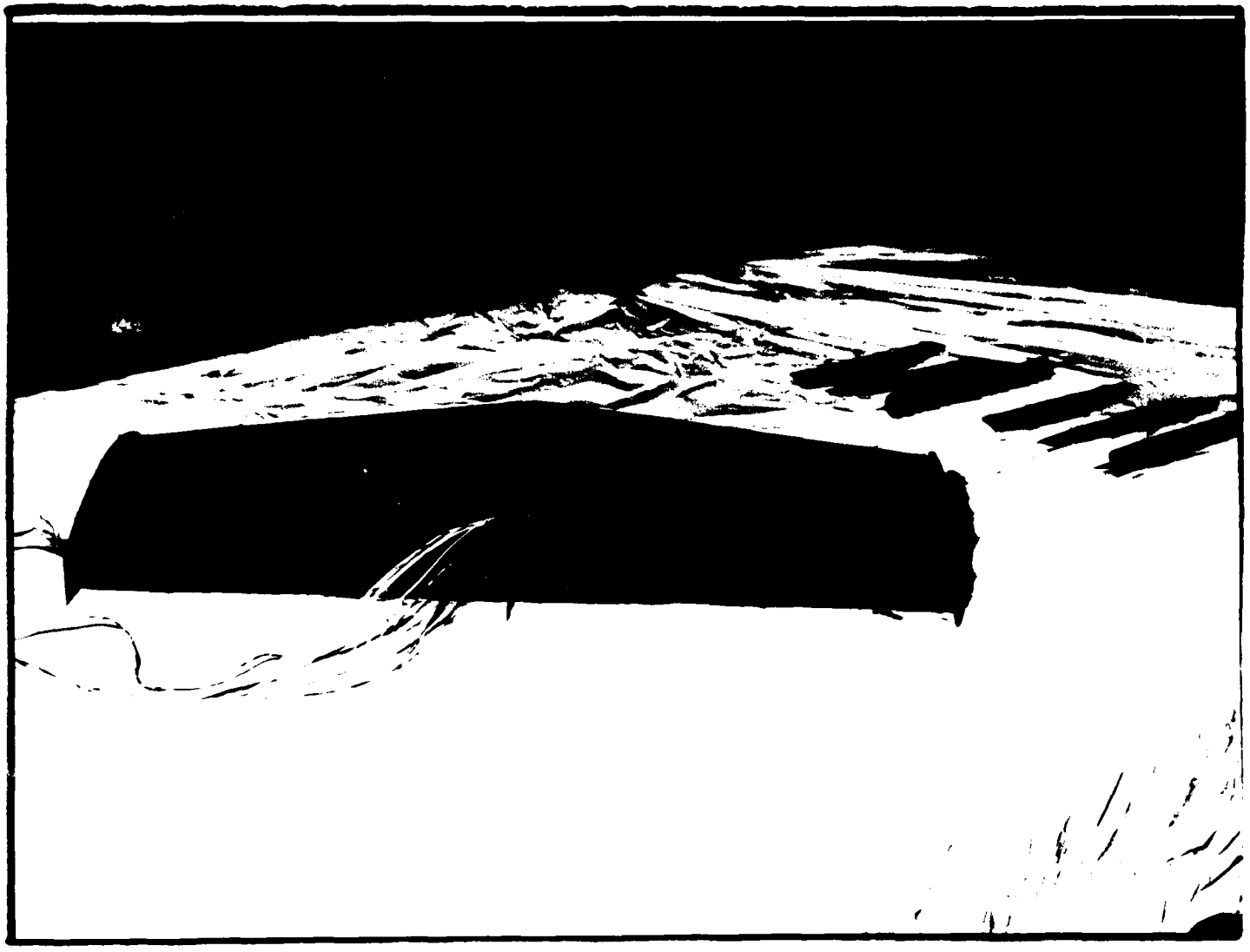

Fig. 5 Model Showing Flap, Plates, Instrumentation, and Tools

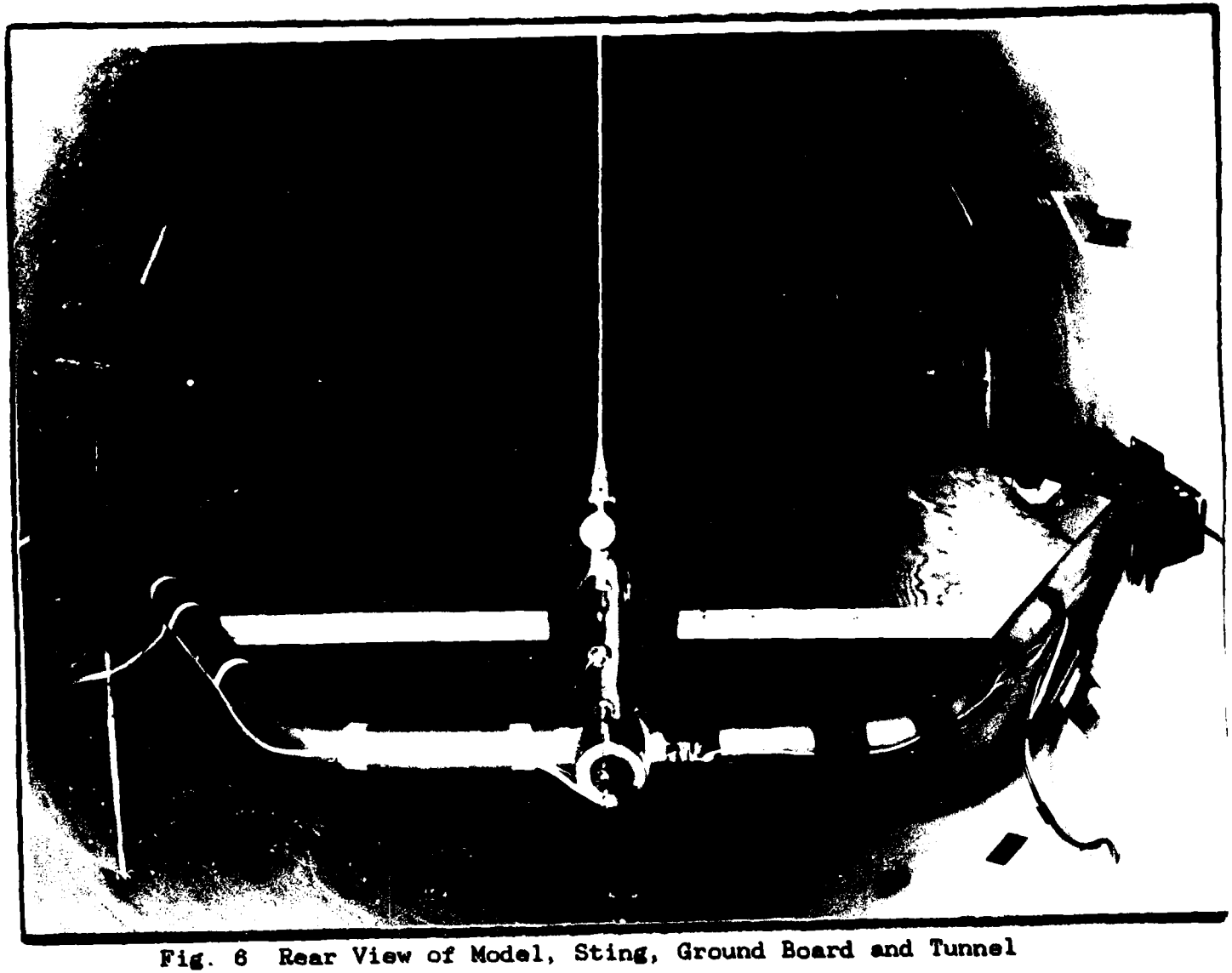

Fig. 6 Rear View of Model, Sting, Ground Board and Tunnel

and the model pitched through the maximum angle of attack, the percentage blockage area did not exceed 7 percent.

The model was constructed of 1/16 in high strength, high temperature casting resin with wooden internal supports. Before the top was attached to the bottom of the wing, provisions were made for wiring, tubing and Scanivalve placement.

The model was built with a machined circular metal balance receiver in the trailing edge to accommodate the sting which held the model in place in the tunnel and acted as a mount for the load balance. The model angle of attack was changed by changing the angle of the sting. When mounted on the sting, angle of attack and yaw angle could be adjusted. In the present case, yaw angle was kept constant at zero.

The flap on the trailing edge was a constant $0.2c_{MAC}$ all along the span. It was hinged so that it could be set manually at angles ranging from 0 to 90 deg plus. For this study, the flap angle was varied from 0 to 30 deg in 5 deg increments. The flap was split at mid-span to accommodate the center plate when it was attached. The flap was held in place by four set screws in the top of the main wing (see Fig. 7).

Three complete sets of plates were constructed for this study. A set of plates consisted of two end plates and one center plate. The plates were made in different sizes to study the effect of the plate size. The model was tested without plates, with only end plates, and with all plates to determine the effectiveness of only end plates, end plates with center

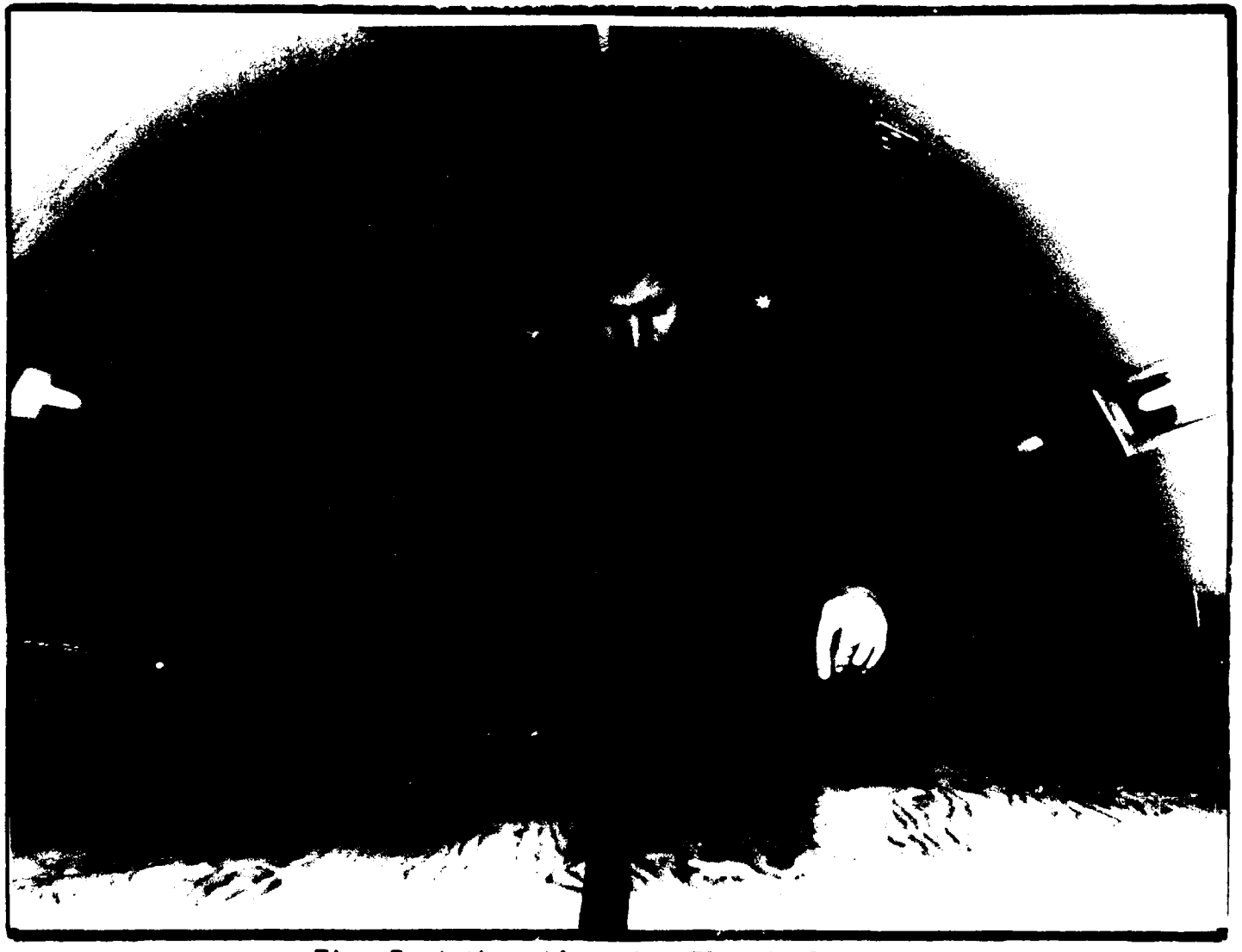

Fig. 7 Author Adjusting Flap Angle

plate and plate size. The height of the plates was measured at the 1/4 mean aero chord point from the chord to the bottom of the end plate. The upper edge of the plate followed the wing profile. The center plate was attached in the middle of the model. The center plate bottom was flat like that of the end plates. The model was canted upwards at a 5 deg angle to the horizontal and the bottom edges of the plates were horizontal in this position. The back edges of the plates were vertical. The plates were attached to the sides and bottom of the model by screws.

Pressure taps were drilled on the left side of the wing around the mean aero chord location as shown in Fig 8. The tubing for these pressure taps was built into the model before it was closed up. These tubes were run to a Scanivalve model T compartment inside the wing (see Fig. 9). The weights of the Scanivalve and tubing were taken into account in balancing the model by adding weights on the side opposite the valve. Wiring was run from the Scanivalve to the center receptacle to exit along with the balance wires to feed pressure data to the computer for reduction.

Ground Boards

The surface of the earth was simulated by various flat ground boards. At first, a board was to be placed inside the tunnel and the model was to be raised and lowered above it to provide in-ground and out-of-ground effect conditions. The engineering problems entailed in this system were immense. To

MEAN AERO CHORD SECTION
PRESSURE TAPS

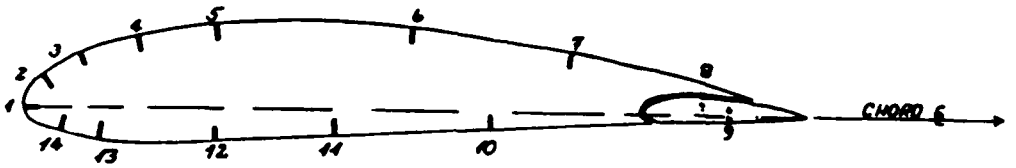

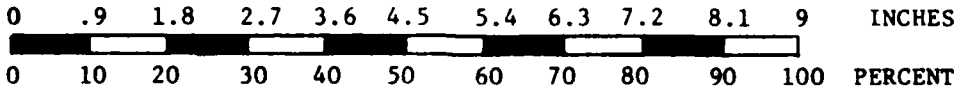

TEST STATION #	PERCENT MEAN AERO CHORD
1	0
2	2.5
3	7.5
4	15
5	25
6	50
7	70
8	86.88
9	90
10	60
11	38.88
12	25
13	10
14	5

Fig. 8 Mean Aero Chord Section Pressure Taps

Fig. 9 Front View of Model Showing Plates, Wiring, and Balance Block

alleviate these problems, three ground boards of different widths were built in the AFIT shops to simulate the earth's surface at five heights. Each 3/4 in plywood board was 8 ft long and reinforced to 1.5 in at the edges. The width of each board was determined by the wind tunnel width at the height the model was to be located. The board at the top-most location accommodated three different model heights by simply using extending brackets. The small gaps in widths at those three heights was less than one inch. These gaps were closed by using duct tape.

The leading edge of the board was first designed to be of aerodynamic shape. It was discovered that this shape resulted in an undue amount of turbulence. Professor Larson of AFIT suggested reducing turbulence by placing an elliptical leading edge on the board at both top and bottom. He recommended a 4 or 5 to 1 ratio of major to minor axes. A 4 to 1 ratio was selected since the reinforced edge of the board was only 1.5 in thick giving a minor axis of 0.75 in. These edges were fabricated from 2x4's and glued to the ends of the ground boards.

The boards were provided with clamps which bolted into brackets screwed to the sides of the tunnel. Also attached to the bottom of the two higher boards was a large retaining bolt (jack-screw) attached to the tunnel floor. These points of attachment were sufficient for conditions during this study. The lower board did not use the jack-screw as the board was so

close to the floor of the tunnel.

The boards also had pressure taps drilled into the right side. The 21 pressure taps were spaced one inch apart for twenty inches on a line directly under the mean aero chord of the model (see Fig. 10). The number eleven (center) pressure tap was set at the 1/4 chord point on the wing. A Scanivalve model S was screwed to the bottom of each ground board to read and transfer the pressure readings along the board to the computer for data collection.

The Tunnel

The AFIT 5-foot Wind Tunnel was constructed in 1919 at McCook Field in Dayton, Ohio. In 1931 it was moved to its current site at Wright-Patterson AFB. It has a closed test section measuring 5 ft inside diameter, 18 ft long, and is constructed entirely of wood. The entrance contraction ratio is 3.7 to 1. The tunnel is open at both ends and is located inside a large building which serves both as an inlet plenum and a discharge chamber (see Fig. 11).

The flow is driven by two 12-ft counter-rotating fans which are each powered by two 400-horsepower DC electric motors. The tunnel is capable of velocities up to 293 ft/sec for a maximum unit Reynolds number of approximately 1.876 x 10^6/ft. Total pressure is atmospheric, and static pressure is measured by a manifold containing eight static ports, 30 in downstream from the tunnel entrance and 6.5 ft upstream of the test section. Dynamic pressure is measured by use of a Validyne

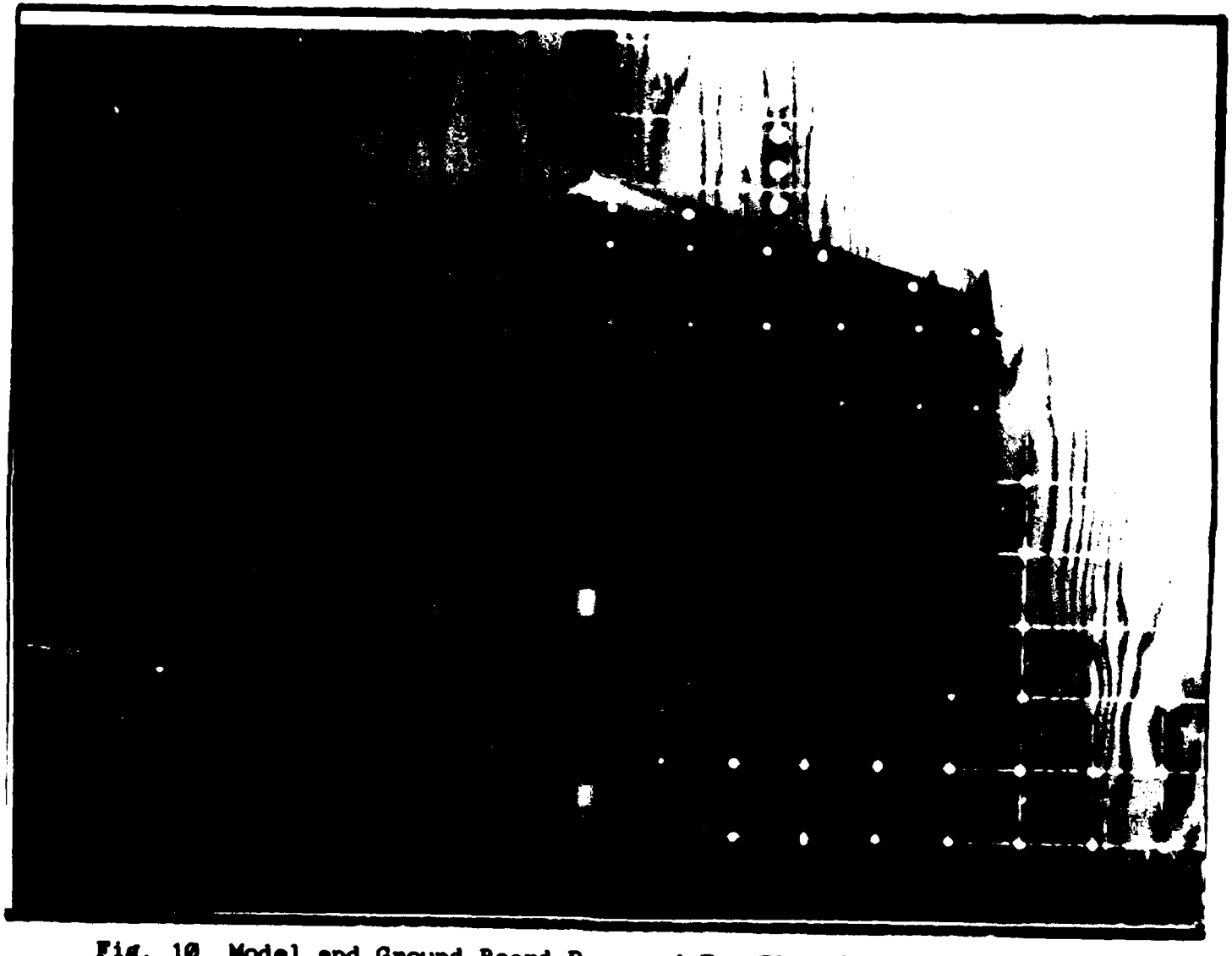

Fig. 10 Model and Ground Board Prepared For Flow Visualisation

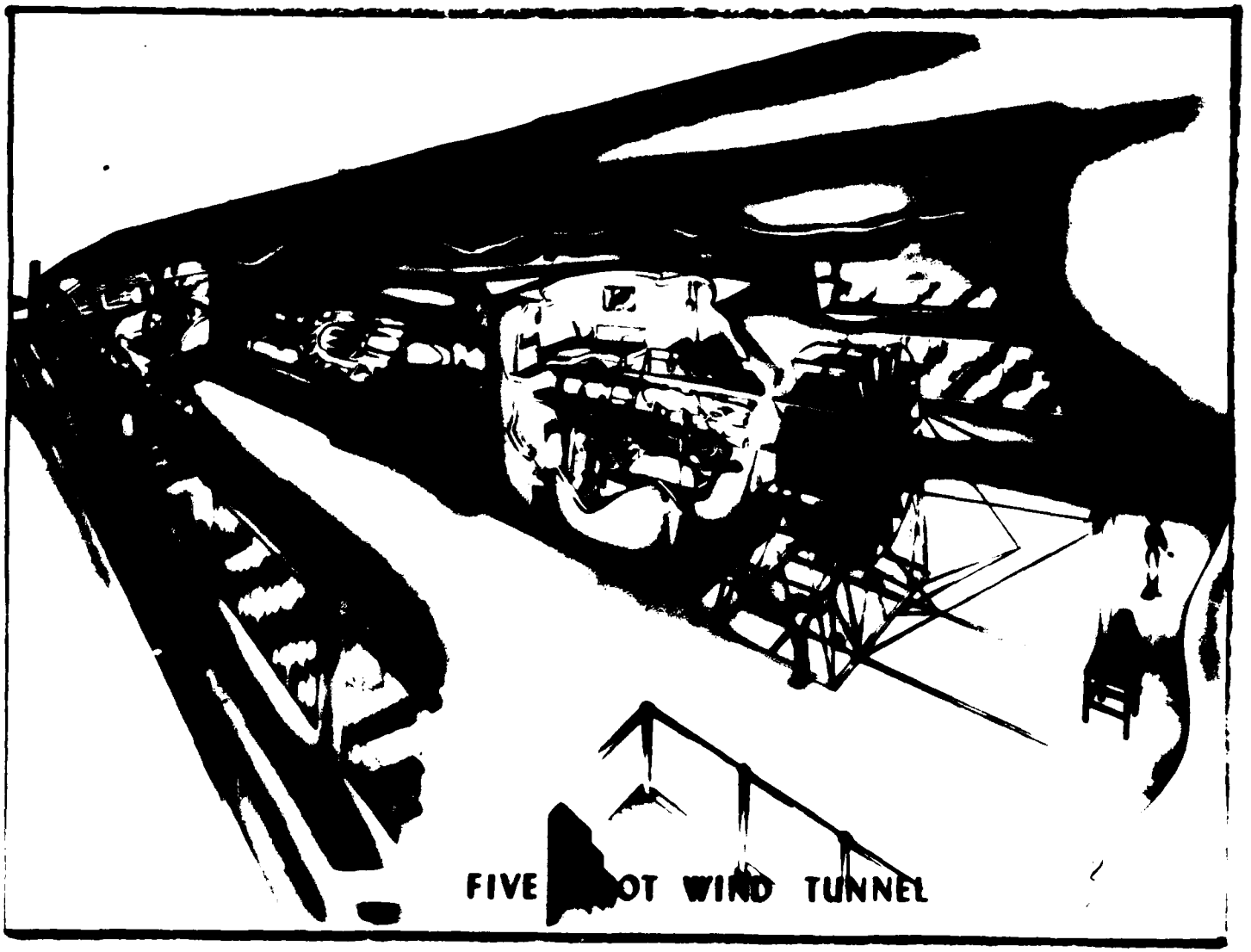

Fig. 11 Caricature of AFIT 5-Foot Wind Tunnel

Model DP15 pressure transducer with a range of 0.1 psi differential and a micromanometer as a backup. The transducer was calibrated against the micromanometer prior to data collection. Dynamic pressure is controlled by varying the speed of DC motors driving the fans.

Instrumentation

Internal Balance. A sting mounting is used with an internal strain gauge balance. The balance was fitted with a Task Corporation, model MK1, six-component strain gauge sensor provided by the Air Force Flight Dynamics Laboratory. The balance had a diameter of 3/4 inches, and was calibrated up to 25 lbf normal force, 20 lbf side and axial forces, and 60 in-lbf of rolling moment. The balance was rated at a maximum of 40 lbf per gauge of normal and axial force, 20 lbf per gauge of side force, and 60 in-lbf of rolling moment. The balance, mounted inside the model at its aerodynamic center, measured axial, normal, and side forces; pitch, yaw, and rolling moments. The balance output was monitored by a Hewlett-Packard (HP) 3497A Data Acquisition/Control Unit. The data were stored on floppy disks, and later converted to model stability axis coefficients, by an HP 9826 computer. A 3-component wire balance was also available for use.

Pressure Scanners. The pressure scanners used in both the model and under the ground board were DC motor-driven pulse scanners with step controller from Scanivalve Corporation. Both

were fitted with 2.5 psi transducers with a sensitivity of 25mV. The board scanner was attached to the underside of the board and was a model S valve. The smaller model scanner was a model T placed in a receptacle built into the model (see Fig. 9). Both Scanivalve outputs ran to an electronics terminal channel input which stored the data for reduction later.

Support Apparatus. For the internal balance test, the model was mounted to a steel sting and yoke apparatus. When the model was mounted horisontally, operation of this equipment permitted angle of attack limits of -6 to +26 deg and $\pm$6 deg sideslip, while keeping the model in the center of the test section. To attain sideslip angles of up to 26 deg, the model can be rolled vertically and a prebend in the sting used for step increases of 10 and 20 deg for the model's angle of attack. The model's sideslip would then correspond to the vertical movement of the yoke, -6 to + 26 deg. A prebend of 20 deg with a +6 deg lateral movement by the yoke would provide the maximum 26 deg angle of attack. However, with the use of the prebend, the model would move outside the center of the test section in increasing amounts, depending on the prebend angle. The prebend and sideslip were not used in the study.

Computer

The Data Acquisition System. The data taken on the sting mounted internal balance was recorded using an HP 9826 computer and an HP 3497 Data Acquisition/Control Unit. Each of the

balance force component voltages was sampled ten times in approximately two seconds and averaged at each data point. These, as well as the dynamic pressure, temperature, barometric pressure, angle of attack, sideslip angle, and other information were stored by the computer. Dynamic pressure was measured by the same transducer which was used to control dynamic pressure. Temperature was measured by a copper-constantan thermocouple. Angle of attack and sideslip were measured by rheostats attached to the electric motors which set the angle of the model. Barometric pressure was measured by a Heath Kit Digital Weather computer which had been checked against a standard barometer. Plotting capability was obtained by using an HP 9872C plotter.

Software. A program written by Mr. Jim Grove of Flight Dynamics Lab, Aerodynamics and Airframes Branch, and Mr. Steve Coates of AFIT was used to reduce the internal balance forces into coefficient form and was also used to drive the plotter.

IV. Experimental Procedure

Calibrations

Flow Angularity. The wing model was used for a series of preliminary tests to determine flow angularity in the tunnel. The air in a wind tunnel does not flow perfectly straight at every location. A correction had to be made to determine the actual angle of attack of the model. The correction is called flow angularity. Angularity was determined by running the model upright and then inverted, and plotting the value of lift coefficient for the two runs on the same plot. The angularity is then half the value of the difference between the point where lift crosses zero on each plot. Angularity as measured was a mean value which depended upon the ratio of the span of the model to the tunnel diameter and the amount the model was off the center line.

Angle of Attack. The angle of attack was determined by the voltage reading from the rheostat attached to the electric motor which sets the angle of the model. Motor movement was stopped when the correct voltage was read for the desired angle of attack. To determine these voltages in question for this study, a level balance such as an M-2 Artillery Gunner's Quadrant was placed on the block of wood fitted to the model (see Fig. 9). The top surface of this block of wood was parallel to the center line of the model. The angle set into the gunner's quadrant was attained when the level bubble centered. The voltage reading was taken for each desired angle of attack. This procedure was

repeated and the values averaged. The curve drawn from voltages versus angle of attack was linear.

Dynamic Pressure. Prior to the model being placed in the tunnel, complete runs were made for each ground board. The presence of the ground board changed the dynamic pressure from the tunnel harness reading mentioned earlier. A reading was taken of dynamic pressure, q, at the model location, above and below the board. This gave local 'q' and forces on the board. The local 'q' values above the board were integrated into the computer program for data reduction at the model. The difference in q's above and below the board furnished the knowledge that a force of 240 lbf was being exerted downward on the board, reinforcing the retaining brackets. Each set of runs with any board was preceeded with a run using yarn tufts on the board surface. No undue turbulence or burbling over the edges was noticed at any spot on any board.

All data runs were conducted at a constant dynamic pressure of 10 psf. The tests originally began at a q of 20 psf. However, this quickly exceeded the limitations of the balance instrumentation to their limits. Three check-runs were conducted to determine the effect of q on the coefficients. Data for these check-runs were then superimposed on a graph. As can be seen in Figs. 12 to 15, no difference is noticeable amongst the coefficient values for the different q's. Tests were restarted with a new q of 10 psf and this was held constant throughout the rest of the study. Due to the open nature of the

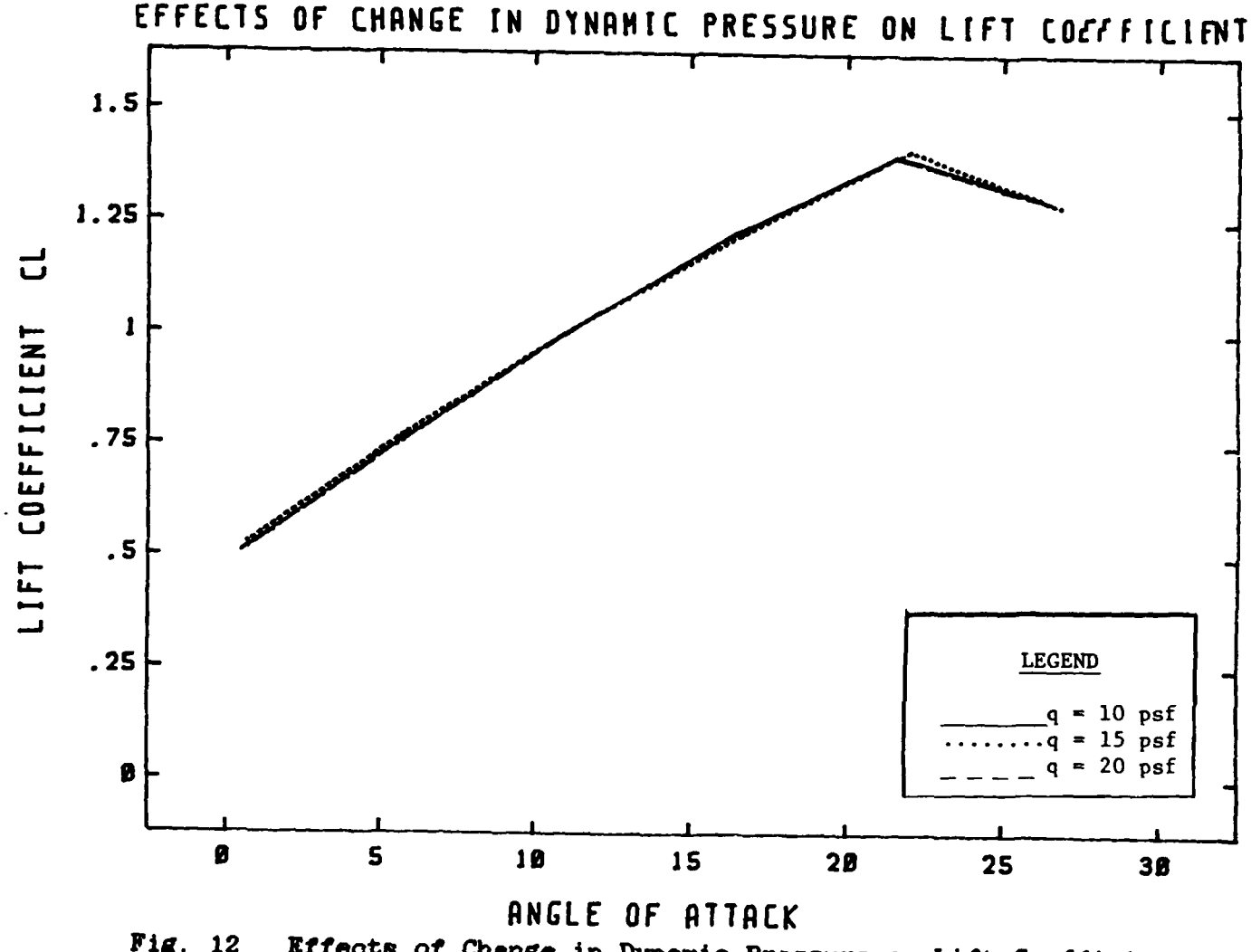

Fig. 12 Effects of Change in Dynamic Pressure on Lift Coefficient

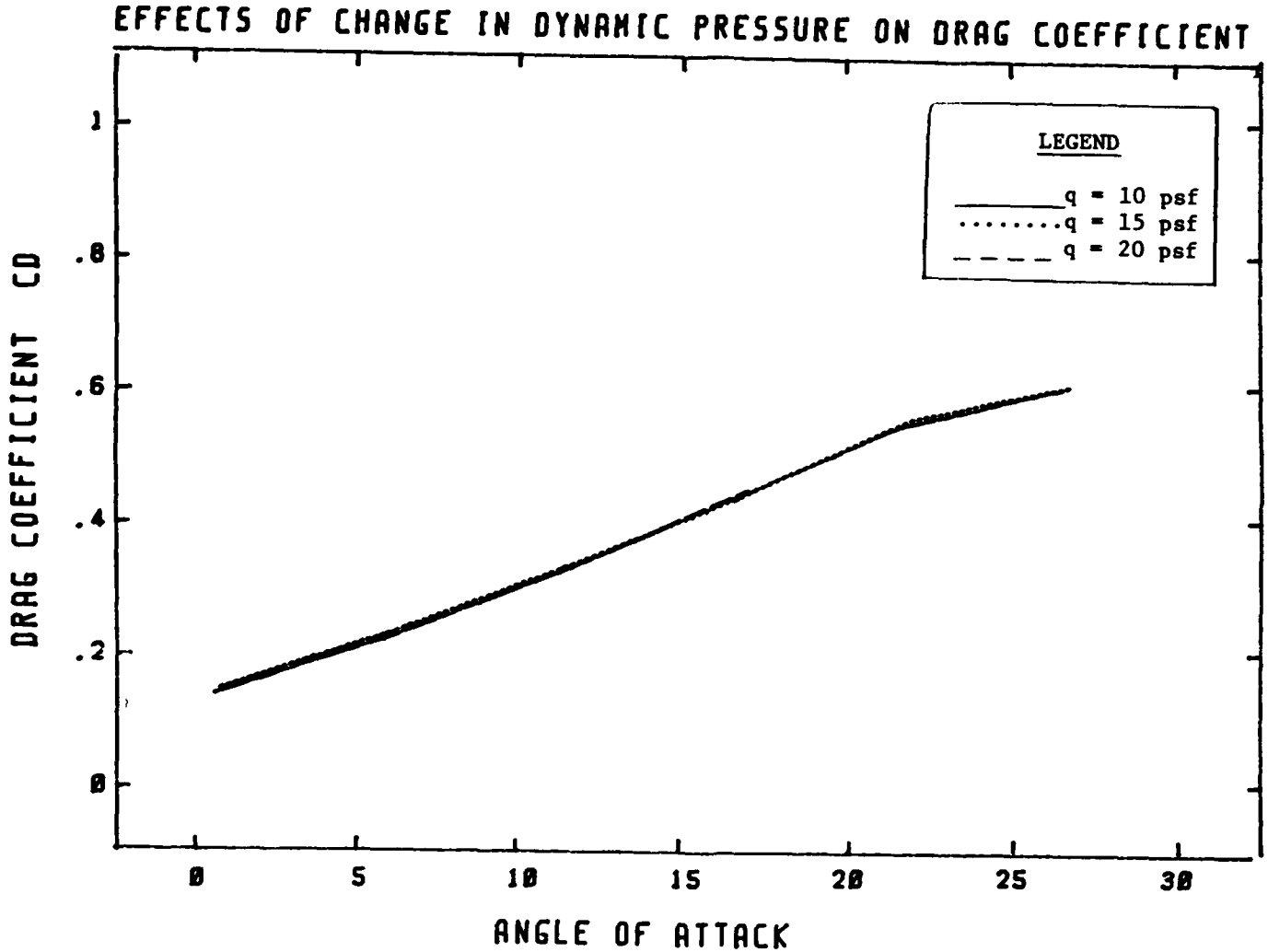

Fig. 13 Effects of Change in Dynamic Pressure on Drag Coefficient

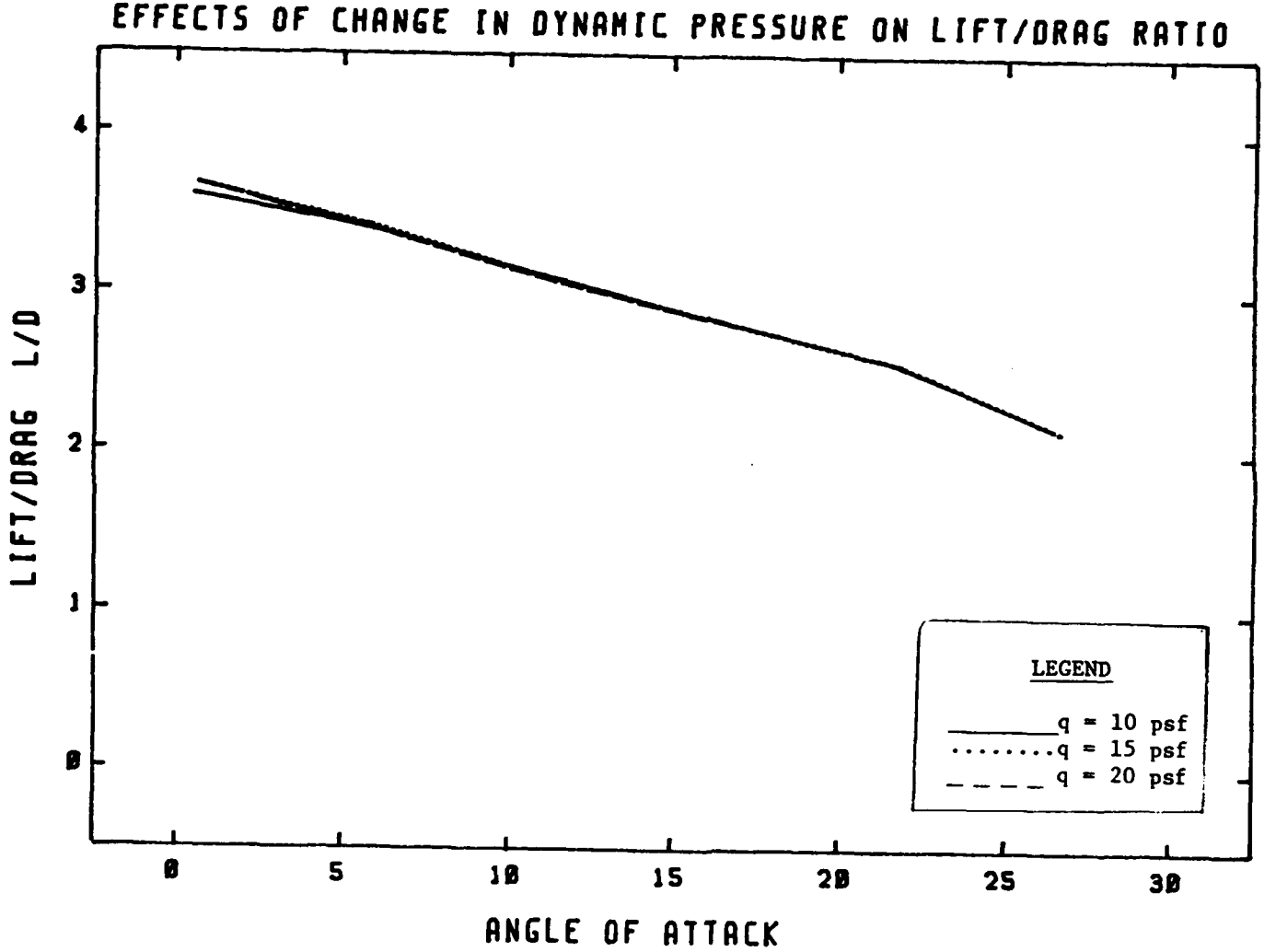

Fig. 14 Effects of Change in Dynamic Pressure on Lift/Drag Ratio

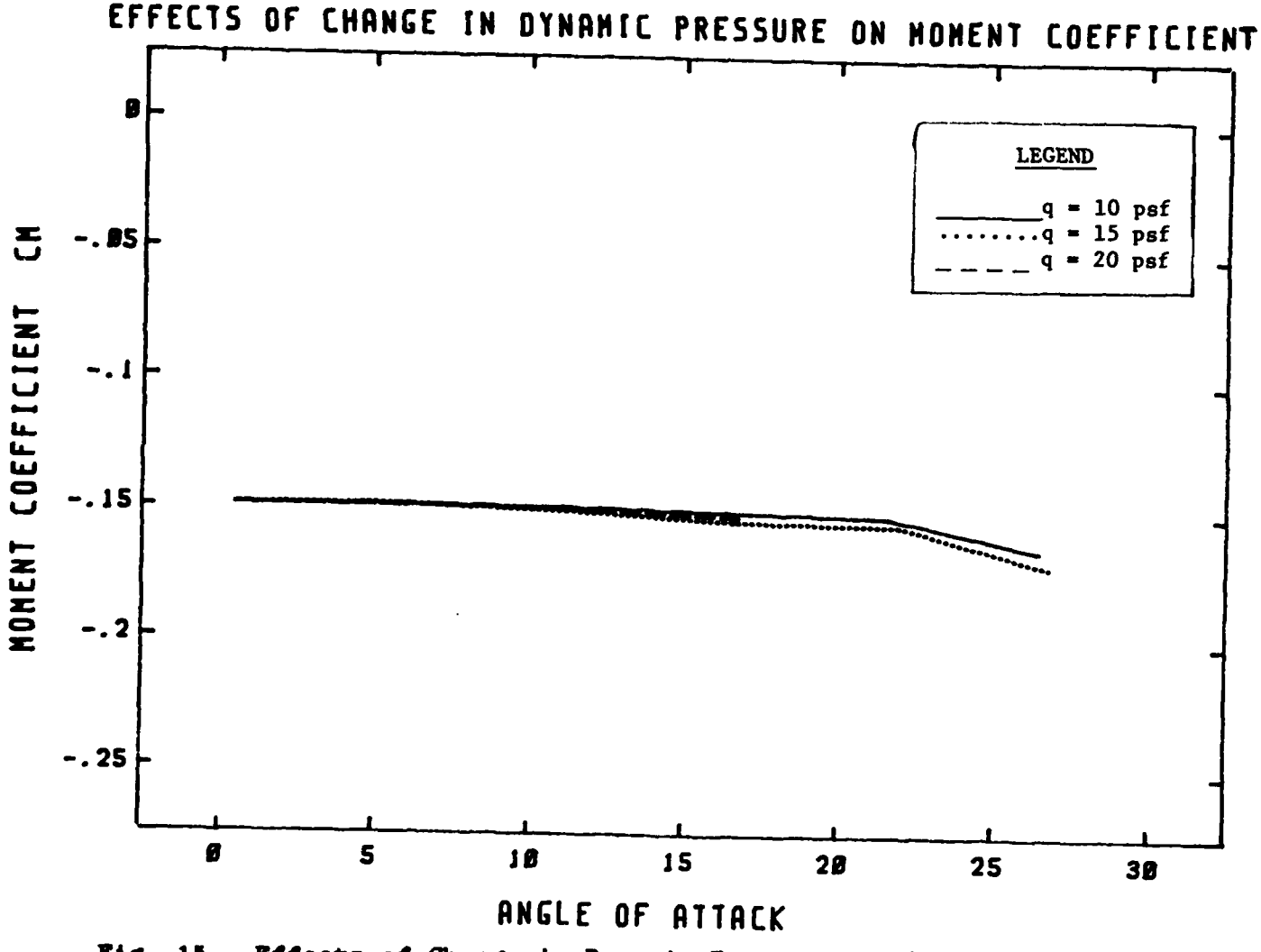

Fig. 15 Effects of Change in Dynamic Pressure on Moment Coefficient

AFIT 5-foot tunnel, it was impossible to hold temperature and atmospheric pressure constant. Temperature varied from 58 to 82F and barometric pressure ranged between 28.79 and 29.82 in Hg. This fact caused variations in the Reynolds number, velocity and Mach number. The unit Reynolds number varied from 6.Ø1 x $1Ø^{6}$/ft to 6.45 x $1Ø^{6}$/ft. Velocity was between 68.3 mph and 71.9 mph and Mach number stayed between Ø.Ø89 and Ø.Ø93.

Transducers. The transducers in the Scanivalves used in the model and under the board were calibrated. This was done by using an Ametek/Mansfield and Greene Division self-regulating, dead weight tester with a range of 4 to 254 in H_2O. Several tests were conducted on each transducer. The pressure was applied to the transducer which provided a voltage readout. The voltage readouts were averaged over numerous runs. The average voltage was integrated into the computer program and used to calculate pressures and coefficients in the data reduction program.

Flow Separation. One last point of interest in calibration and test verification was flow separation. The possibility that the air flow over the wing could separate from the wing and cause false readings was significant. If flow separation occurred, the data collected would not provide a true depiction of forces in flight. To show that the present experimental set-up would render accurate and truthful dta, flow visualization runs were made. These runs were made to show that there was air flow across the entire surface of the wing.

Oil spots were placed on the model and the ground board as in Fig. 11. Some flow visualization runs were also run without the ground board. The model was then placed in the configurations as delineated by the cards displayed in Figs. 16 to 23. The wind tunnel was turned on and brought up to test speeds. As can be seen in the figures related, the oil drops across the entire model and all along the ground board show that there was air flow over the entire experimental area. Flow separation did not occur to the extent that data integrity was compromised. From these runs, it was determined that flow separation and boundary layer effects did not disrupt data and this experiment was candid in these respects.

Procedure Variables

There were several variables involved which were incremented gradually to study their effect. The variables and their ranges are:

1) Angle of attack, α, from Ø to 25 deg
2) Flap angle, θ, from Ø to 3Ø deg
3) Model height, H/c, at Ø.15, Ø.25, Ø.5, 1.Ø and 2.35
4) End plate size and configuration to include:
   a) no plates, OO
   b) large end plates only, OL
   c) large center and end plates, LL } Ø.2Ø c.
   d) medium end plates only, OM
   e) Medium center and end plates, MM } Ø.15 c.

f) small end plates only, OS
g) small center and end plates, SS

} Ø.125 c.

All heights and configurations that were physically possible amongst the combinations listed above were tested. Graphs and plots were then made to view and study the collected data. For this study, some height assumptions were made. The heights, H/c, represented ranges for in-ground effect (Ø.15, Ø.25, and Ø.5), out-of-ground effect (1.Ø), and freestream (2.35).

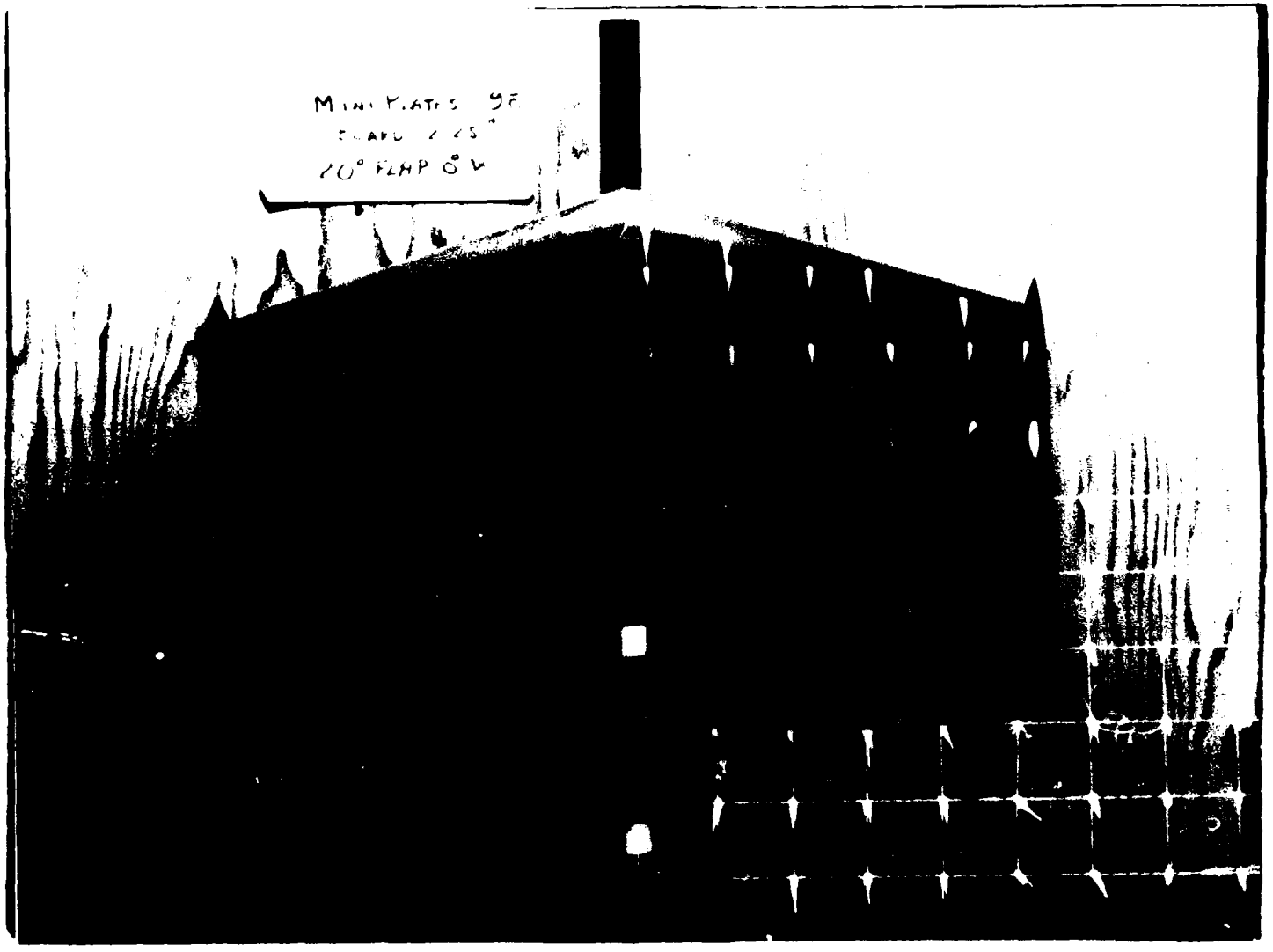

Fig. 16 Flow Visualization With Ground Board

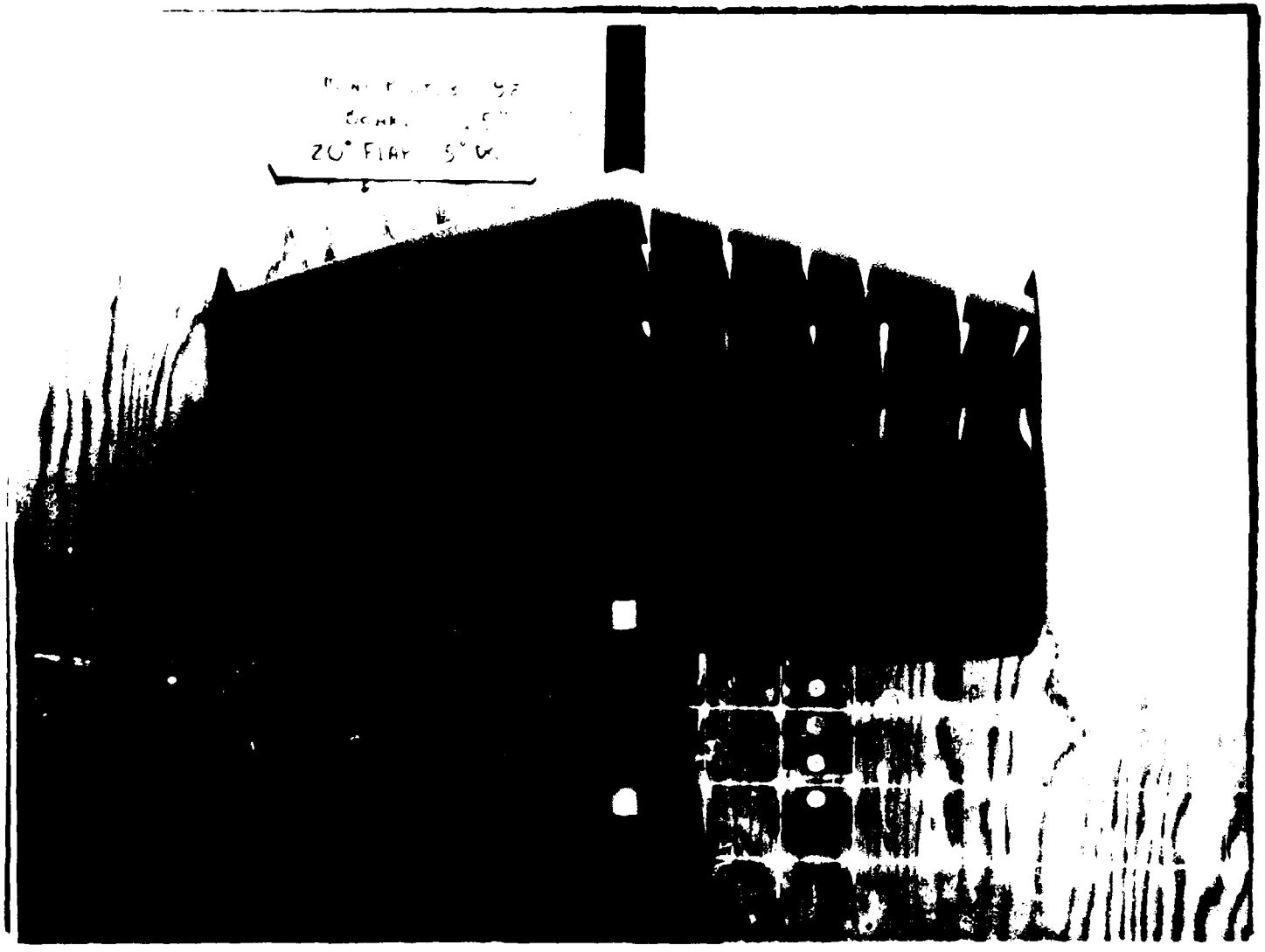

Fig. 17 Flow Visualisation With Ground Board

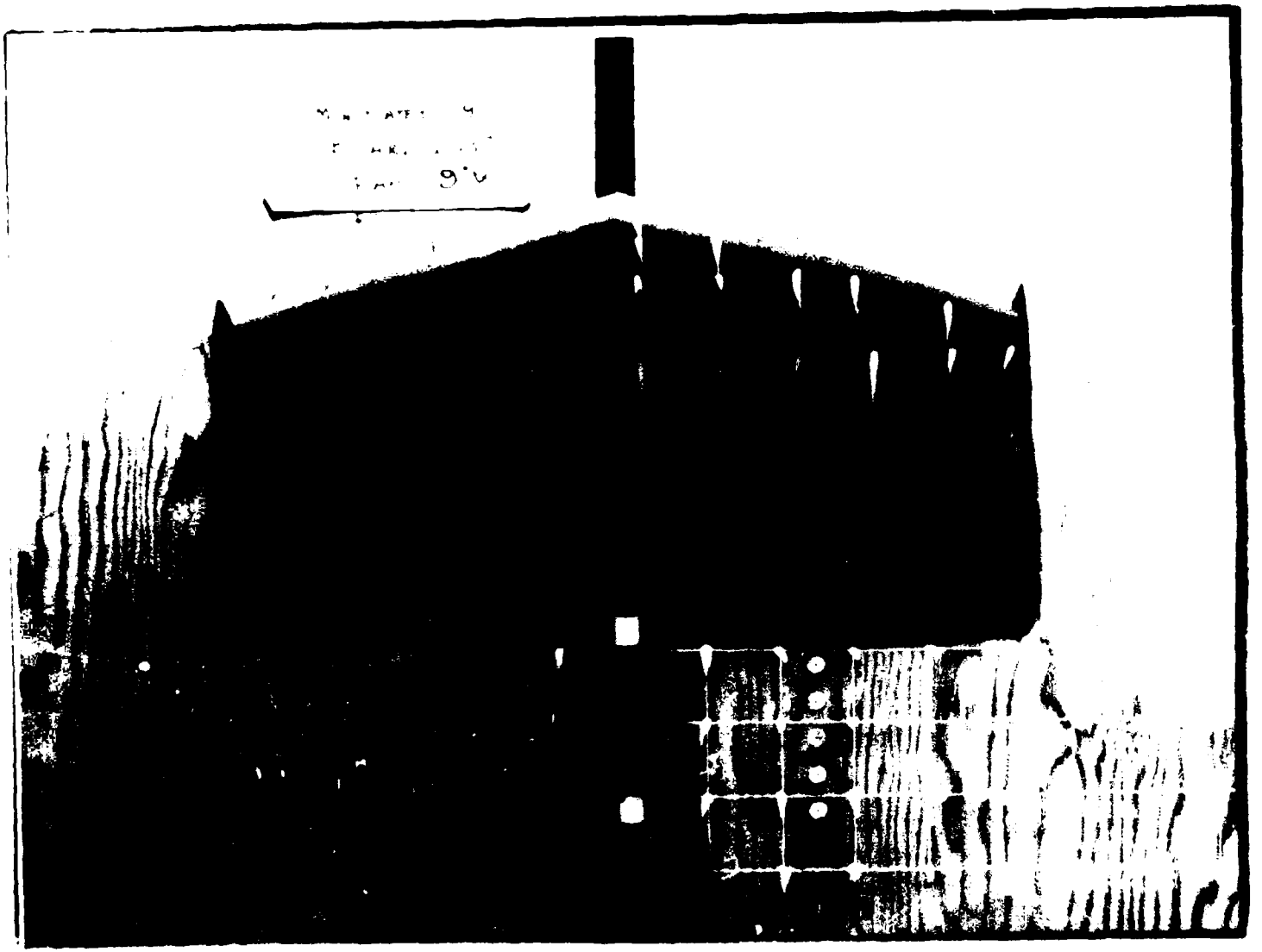

Fig. 18 Flow Visualisation With Ground Board

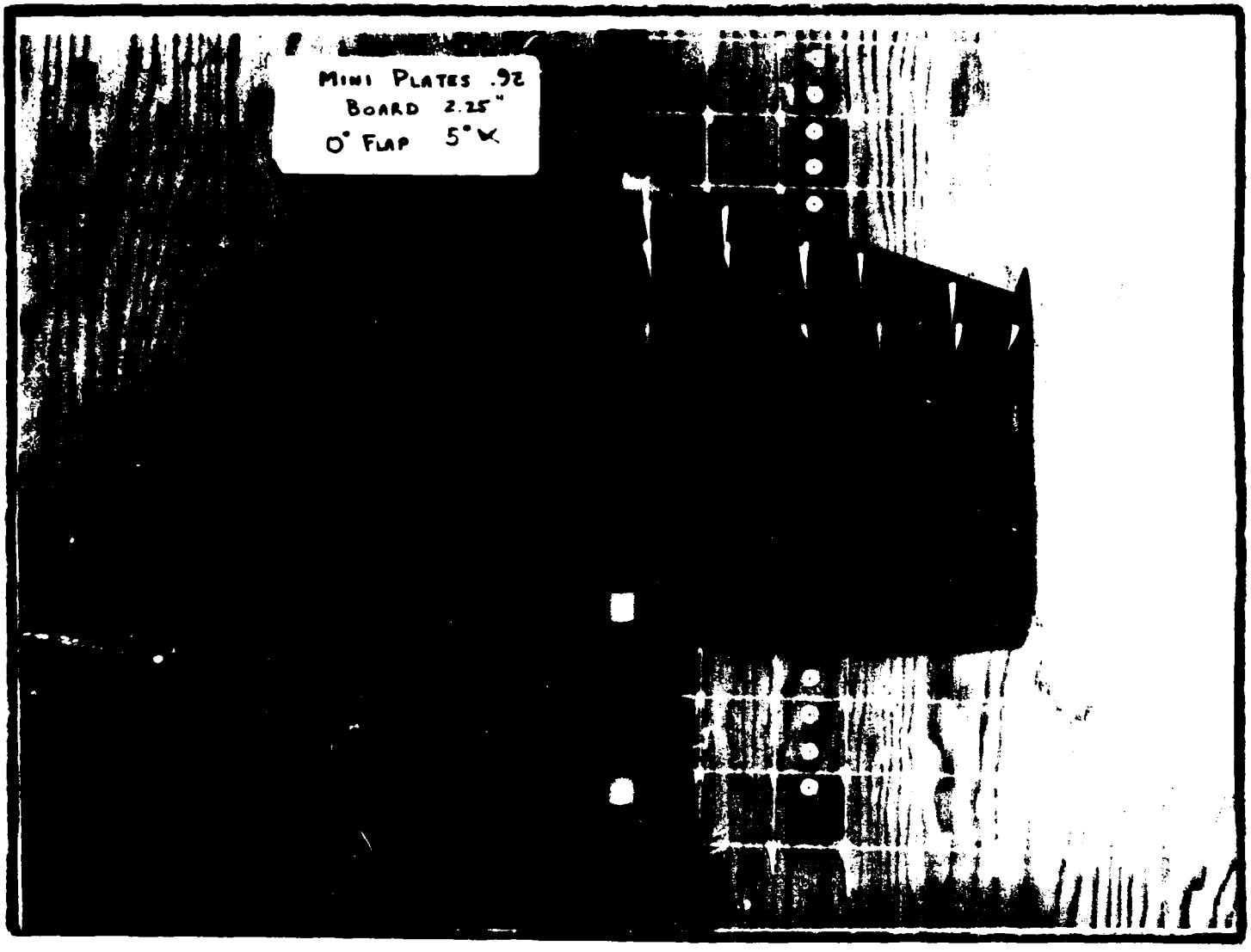

Fig. 19 Flow Visualization With Ground Board

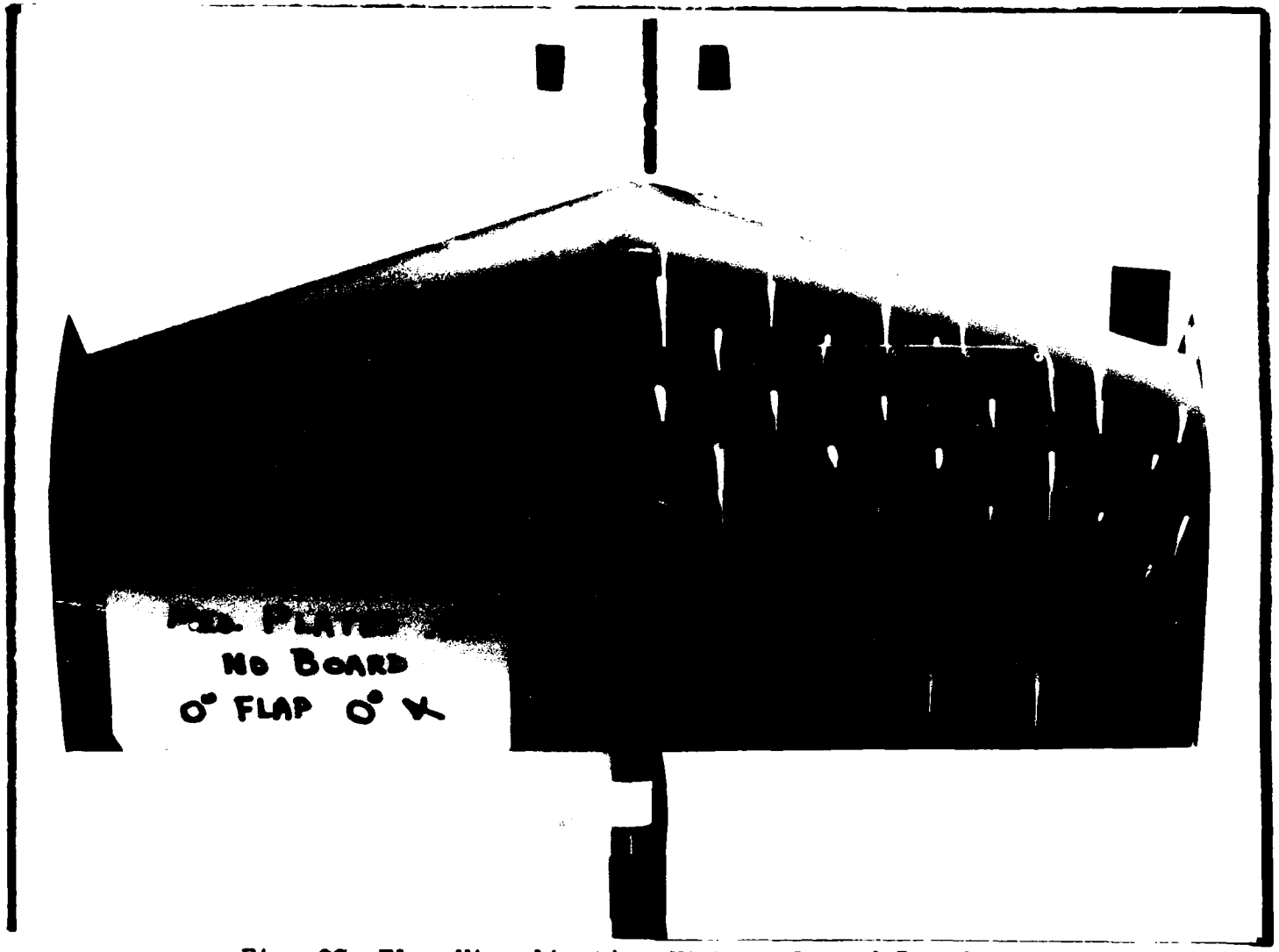

Fig. 20 Flow Visualization Without Ground Board

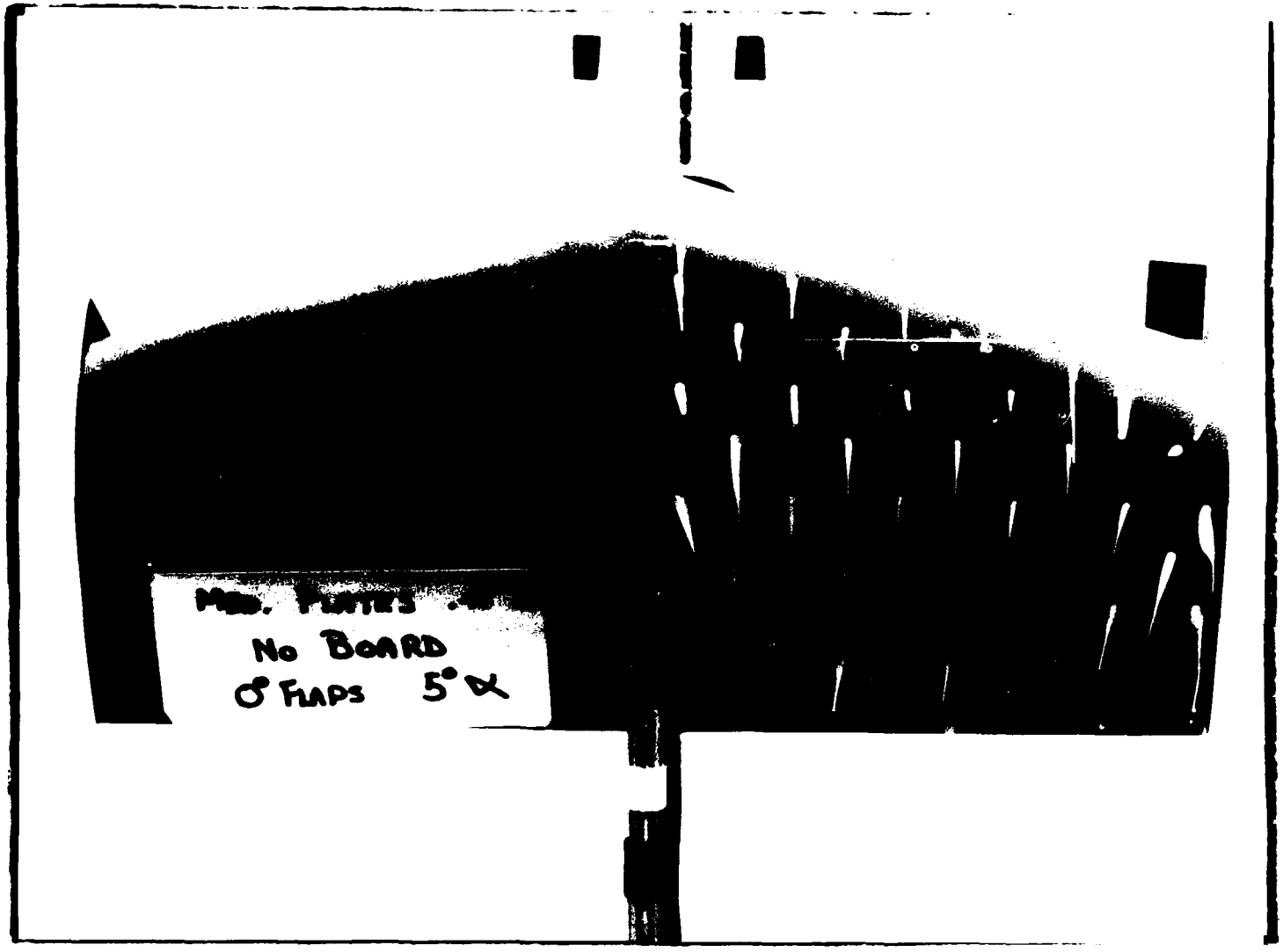

Fig. 21 Flow Visualization Without Ground Board

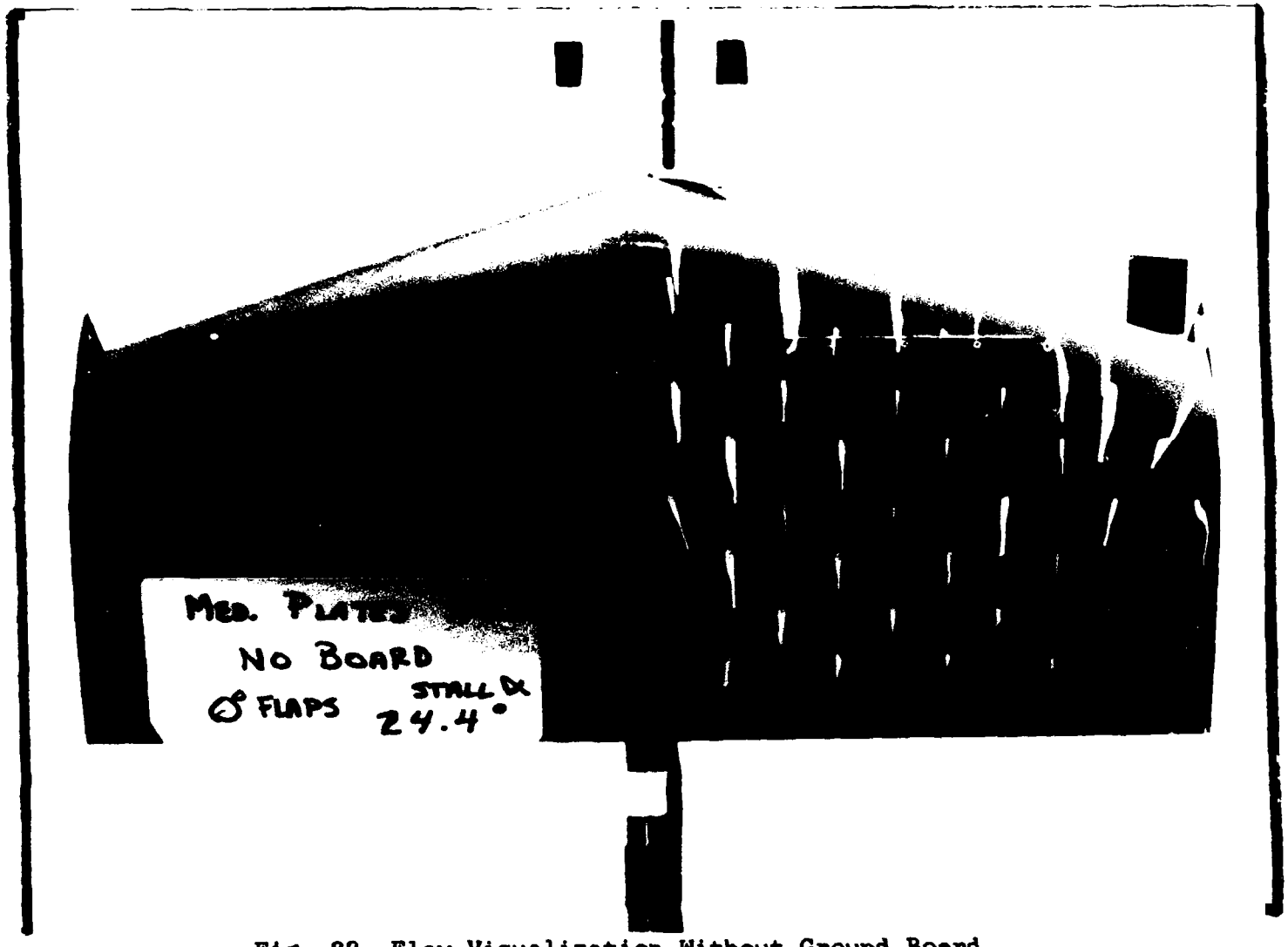

Fig. 22 Flow Visualization Without Ground Board

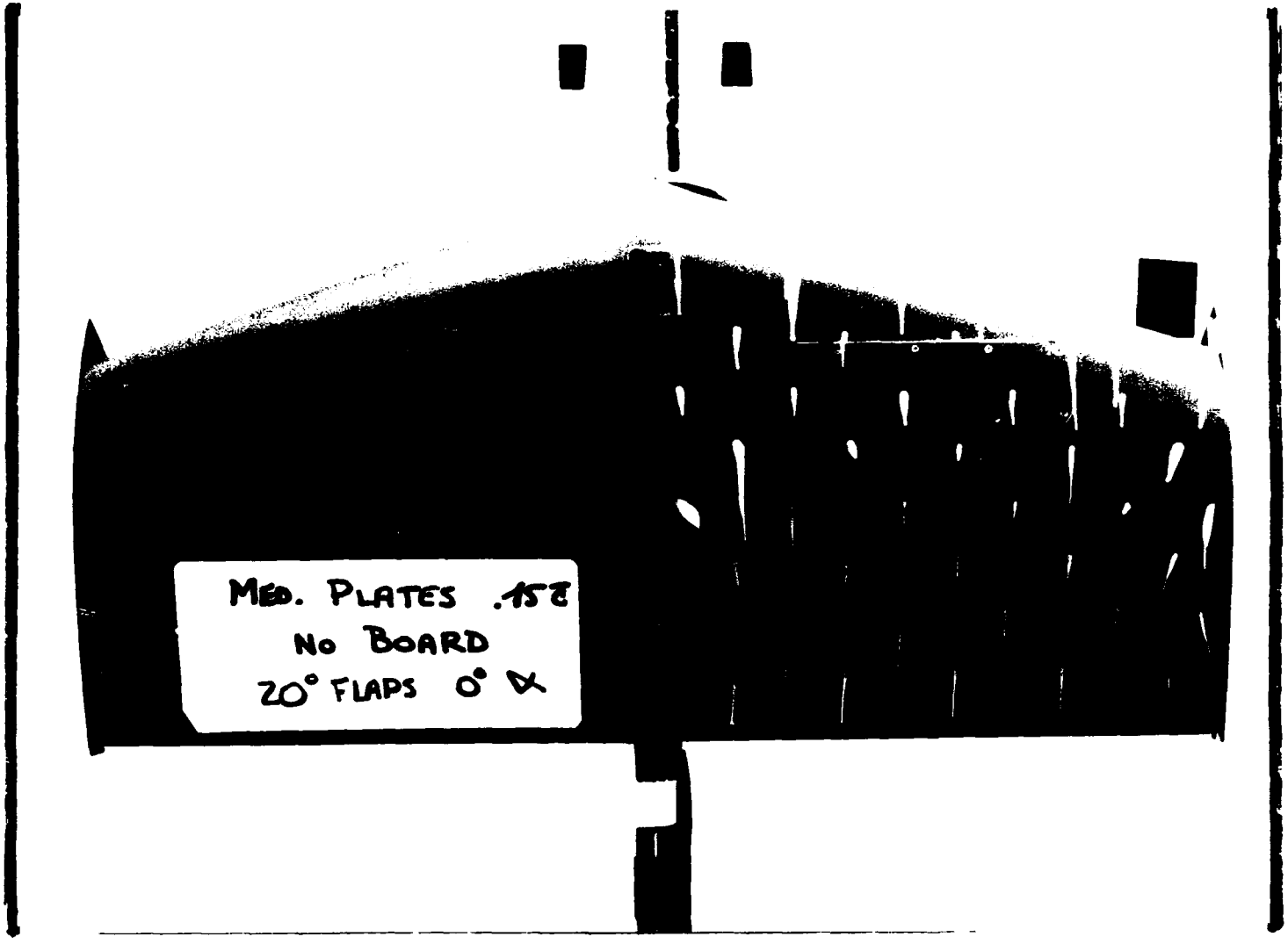

Fig. 23 Flow Visualization Without Ground Board

V. Results and Discussion

Results are presented as a function of several parameters. The mode of presentation chosen was a series of curves that were discussed in groups. These groups related to the various parameters which accentuate the effects of proximity to the ground upon the flight characteristics of an aircraft. These data were compared amongst themselves to determine and reinforce trends. They were also compared against theoretical expectations and the conclusions of previously run experiments.

The plots presented in this chapter were all the results of the same data runs. Each different set of plots merely rearranges the data being compared to highlight the specific effects of each parameter.

The first variable to be checked was the effect of a center plate. For this study, tests were run with all plate sizes, but data are presented for the medium plates only. The other plate sizes gave similar results. The three configurations plotted are OO, OM, and MM at H/c values of Ø.5, 1.Ø, and 2.35, and the angle of attack selected is 15 deg. These plots were then compared taking into account the effects of α, θ, and H/c.

Plots were made of C_L, C_D, L/D, and C_M vs θ. From the plots shown at Figs. B-1 to B-4, it is concluded that the presence or absence of a center plate does not have any noticeable effect upon the coefficients studied. The effect of the center plate alone in increasing L/D was not addressed in any literature studies. The only effect of a center plate noted in literature

was that the center plate might help in breaking up vortices which may develop under the wing causing instabilities (12).

The next effects investigated were the effects of the presence of end plates, as well as their size. Theoretically, end plates will noticeably increase the lift characteristics of a wing flying near the surface (35). These end plates have been found to serve two basic functions. First, they act as containment walls for a high pressure air cushion being forced under the wing by the forward velocity of the wing. Secondly, they tend to serve as a vehicle support system at low speeds which allows greater ground clearance. However, the end plates could eventually replace the landing gear system. Their use as landing gear would then entail design of a ground handling system to move the aircraft around on the surface. The first function is the primary concern of the aerodynamicist studying improved lift.

There is a detraction from this first benefit of end plates, however. When flying close to the surface, the vehicle maintains a clearance between the bottom of the plates and the ground. This clearance is necessary to maintain structural integrity in flight and to reduce frictional drag. This clearance allows the air cushion discussed earlier to leak out the sides under the plates, as well as being forced out the rear. This leakage not only causes a loss of potential lift but also acts as a brake since it is operating normal to the direction of travel. From this theory, it is concluded that end

plates not very near to the surface will detract, not aid, in the increase of L/D.

The configurations used in this study were OO, LL, MM, and SS at H/c values of Ø.25, Ø.5, 1.Ø, and 2.35. Flap angle, θ, was varied from Ø to 3Ø deg and angle of attack, α, from Ø to 25 deg. Tests were conducted, and graphs plotted, of C_L, C_D, L/D, and C_M vs θ. It was found that for each value of H/c, lift increased with the addition of the end plates to varying extents. The drag stayed almost exactly the same. This resulted in a rise in L/D. These graphs are shown in Figs. B-5 to B-2Ø. Thus, it was established that it is of significant advantage to have the end plates.

In ground effect, the values for L/D ranged from 5.7 to 4.5 at H/c = Ø.25 and 5.8 to 4.1 at H/c = Ø.5Ø for large center and end plates. If the plates were removed, this range decreased to 5.4 to 3.9 at H/c = Ø.25 and 5.5 to 3.7 at H/c = Ø.5Ø. For the beginning of the out-of-ground regime, i.e., at H/c = 1.Ø, L/D values with plates ranged from 5.Ø to 3.5 and without plates were 5.Ø to 3.2. For freestream effects, the range with plates was 5.3 to 3.6, and without plates, 5.2 to 3.2. These last two heights have near identical values for all plate configurations. The plots show that there is little effect of plate size and that conditions at H/c = 1.Ø were nearly equivalent to free-stream effects at H/c = 2.35.

The next parameter to be isolated for its effects was H/c, i.e., the effects of ground proximity. Again for this study

the data for medium plates were used to show results. Angle of attack, α, was 5, 15 and 25 deg and flap angle, θ, used was 0, 10, 20, and 30 deg.

In the plots shown from Figs. B-21 to B-36, C_L, C_D, L/D, and C_M were plotted vs height, H/c. Comparing Figs. B-21, B-25, B-29 and B-33, it was very clear that C_L decreased as height was increased. However, C_L increased with α to the point where stall was reached. Thereafter, it did not add any more lift. As observed in this study, the model stalled between 22 and 25 deg depending upon the configuration. Drag coefficient, C_D, was very nearly level for each value across the spectrum of height. However, as α increased, the drag increased quite dramatically. The plot of C_M vs H/c showed a stabilizing effect by being close to the surface. The data shown here definitely agreed with the theory of flying in ground effect. It showed directly the conclusions reached when ground effects were first noticed (43). As the aircraft flew closer to the surface, a noticeable increase in lift, decrease in drag, and the corresponding increase in L/D, was realized. As to be expected also from theory, when flap angle was increased, the drag increased so the L/D decreased. Every experimental study has shown the same results.

The next step was to attempt to delineate the boundaries of the various regions. It was stated in Chapter 4 that H/c = 0.15 to 0.50 were assumed to represent IGE. It was in this zone that most of the effects were prevalent. At H/c = 1.0, out of ground

effects began. The IGE were not seen at this altitude. At approximately H/c = 2.0, the freestream case is encountered. This statement more or less agrees with the observation of other investigators that the ground effects persist until about one chord height.

The data collected and exhibited in the set of plots at Figs. B-37 to B-44 more or less reinforced these divisions of the various regimes. (Recall, straight lines were drawn between points on these plots. The only true data collected were the point values of H/c mentioned previously.) The gaps between heights tested left some voids and made for inaccuracies hidden in the straight lines drawn between test points. It was unknown whether the changes between two test points occurred dramatically at the beginning of the gap, at the end of the gap, in between, or if possibly the changes were gradual. However, from the data plots and the additional lines drawn in on Fig. B-43, regime boundaries were inferred. The data supportted the assumptions made in Chapter 4.

The values are shown in these figures by comparing the ratio of C_L, C_D, L/D, and C_M to their respective values at freestream conditions vs H/c. For example, as H/c = 2.35 values have been taken for freestream values in this study, C_L / C_{L_∞} at H/c = 2.35 is necessarily equal to 1. The increase in lift and L/D is apparent near the surface in these plots.

Pressures were also investigated in this study. There is much less information available in literature upon this facet of

interest with wings-in-ground effect. There were two kinds of pressures which were recorded and studied; ground pressure on the ground boards and the wing pressure profile on the model itself. Pressures were taken for flap angle, θ, from 0 to 30 deg at 10 deg increments (see Figs. 24 and 25).

There were 21 pressure taps in the ground board covering a distance of 20 in located under the right mean aero chord. Pressure tap #11 was placed directly under the quarter chord point. The 14 pressure taps in the model were placed at a slight angle across the left mean aero chord of the wing. Eight taps were on the top of the model and six were on the bottom. Model pressure tap #1 was on the leading edge of the wing. See Fig. 8 for details.

Ground pressures were of primary interest as the information in the literature on this subject was rare. In the plots that are at Figs. C-1 to C-12, the change in pressure along the ground board can be observed. Whether the pressure was positive or negative (suction) is determined for the specific configuration of that test run. Of importance to this study was the absolute value of the pressure and whether it followed theory as expected.

Given Bernoulli's equation and the conservation of mass,

$$p + 1/2\rho V^2 = \text{constant}; \quad \rho_1 A_1 V_1 = \rho_2 A_2 V_2$$

it is understood that when the flow area decreases, the velocity must increase given constant density. It is also understood that as the velocity increases, the pressure must decrease. Of

MODEL CP'S

RUN #= 43 TP #= 2 Q BOARD= 11.53

UPPER SURFACE CP'S

.75	-.13	-.60	-.72	-.76	-.67	-.49	-.38

LOWER SURFACE CP'S

.32	.06	-.03	-.18	-.32	-.32

RUN #= 43 TP #= 3 Q BOARD= 11.55

UPPER SURFACE CP'S

.66	-.85	-1.17	-1.12	-1.04	-.83	-.58	-.46

LOWER SURFACE CP'S

.30	.07	.03	-.03	0.00	.16

RUN #= 43 TP #= 4 Q BOARD= 11.72

UPPER SURFACE CP'S

-.11	-1.76	-1.78	-1.55	-1.35	-.94	-.68	-.53

LOWER SURFACE CP'S

.27	.05	.09	.09	.24	.47

RUN #= 43 TP #= 5 Q BOARD= 11.51

UPPER SURFACE CP'S

-1.56	-2.85	-2.49	-2.10	-1.61	-1.09	-.78	-.60

LOWER SURFACE CP'S

.22	.02	.11	.16	.39	.57

RUN #= 43 TP #= 6 Q BOARD= 11.52

UPPER SURFACE CP'S

-3.51	-3.94	-3.23	-2.34	-1.86	-1.17	-.82	-.63

LOWER SURFACE CP'S

.18	.01	.15	.24	.48	.55

RUN #= 43 TP #= 7 Q BOARD= 11.72

UPPER SURFACE CP'S

-4.47	-4.00	-3.23	-2.11	1.76	-1.09	-1.06	-.90

LOWER SURFACE CP'S

.08	-.08	.14	.24	.47	.44

Fig. 24 Example, Model Pressure Coefficients Printout

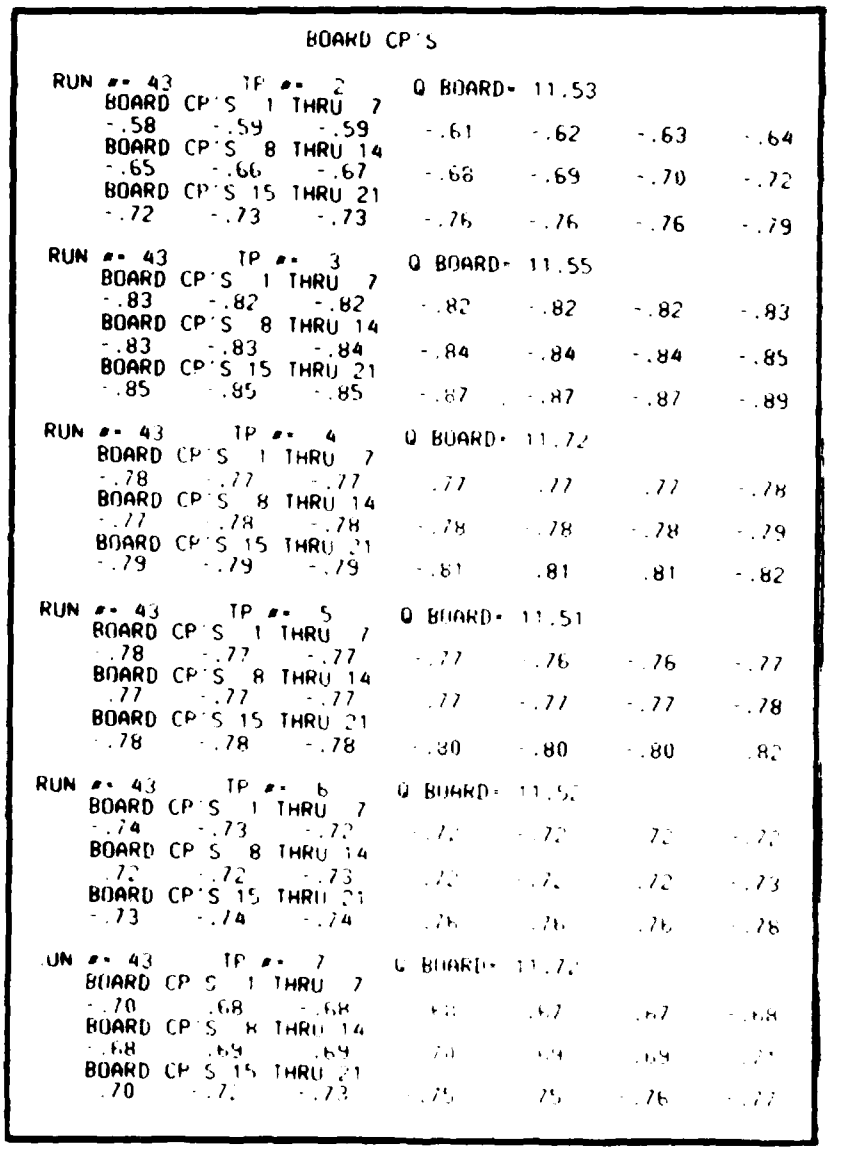

BOARD CP'S

RUN #= 43 TP #= 2 Q BOARD= 11.53

BOARD CP'S 1 THRU 7

-.58 -.59 -.59 -.61 -.62 -.63 -.64

BOARD CP'S 8 THRU 14

-.65 -.66 -.67 -.68 -.69 -.70 -.72

BOARD CP'S 15 THRU 21

-.72 -.73 -.73 -.76 -.76 -.76 -.79

RUN #= 43 TP #= 3 Q BOARD= 11.55

BOARD CP'S 1 THRU 7

-.83 -.82 -.82 -.82 -.82 -.82 -.83

BOARD CP'S 8 THRU 14

-.83 -.83 -.84 -.84 -.84 -.84 -.85

BOARD CP'S 15 THRU 21

-.85 -.85 -.85 -.87 -.87 -.87 -.89

RUN #= 43 TP #= 4 Q BOARD= 11.72

BOARD CP'S 1 THRU 7

-.78 -.77 -.77 .77 .77 .77 -.78

BOARD CP'S 8 THRU 14

-.77 -.78 -.78 -.78 -.78 -.78 -.79

BOARD CP'S 15 THRU 21

-.79 -.79 -.79 -.81 .81 .81 -.82

RUN #= 43 TP #= 5 Q BOARD= 11.51

BOARD CP'S 1 THRU 7

-.78 -.77 -.77 -.77 -.76 -.76 -.77

BOARD CP'S 8 THRU 14

.77 -.77 -.77 .77 -.77 -.77 -.78

BOARD CP'S 15 THRU 21

-.78 -.78 -.78 -.80 -.80 -.80 .82

RUN #= 43 TP #= 6 Q BOARD= 11.52

BOARD CP'S 1 THRU 7

-.74 -.73 -.72 -.72 -.72 .72 -.72

BOARD CP'S 8 THRU 14

.72 -.72 -.73 .72 -.72 .72 -.73

BOARD CP'S 15 THRU 21

-.73 -.74 -.74 .76 .76 .76 -.76

RUN #= 43 TP #= 7 Q BOARD= 11.72

BOARD CP'S 1 THRU 7

-.70 .68 -.68 .68 .67 .67 -.68

BOARD CP'S 8 THRU 14

-.68 .69 .69 .70 .69 .69 -.71

BOARD CP'S 15 THRU 21

.70 -.72 -.73 .75 .75 -.76 -.77

Fig. 25 Example, Ground Board Pressure Coefficients Printout

course, the opposite is also true.

Referring to Fig. C-1 for example, the leading edge of the wing at the mean aero chord is just forward of test station #9. The trailing edge is just short of test station #18. As the air rushed at the wing, the highest pressure encountered was at the nose of the wing or slightly in front of it. This is shown on the plot by the large absolute value of the pressure coefficients (C_p) at this point. As seen on the plot, as the air travelled along the chord of the wing, the pressure was decreased. The area of flow between the wing and the surface was being decreased due to the camber and angle of attack of the wing. Due to continuity, as this area decreased, the flow accelerated to maintain mass flow rate. The C_p's on the plot verified this by decreasing their absolute value. At the trailing edge, the area was the smallest it would get. At or slightly past this point, the flow began to expand thus increasing the area and decreasing the flow velocity and increasing the pressure shown by the C_p's turning away from the zero line in Fig. C-1. These plots show how well the present study correlates with theory and expected results.

The angle of attack changed the C_p curve itself but the movements of the C_p's followed the same pattern around the wing regardless. This can be seen by comparing the lines on each individual plot. Also, as the flap angle changed, varying constriction of the flow between the wing and the ground board was realized. The flap formed a nozzle with the board and moved

the C_p value up and down the Y-axis. This is seen by comparing plots of differing θ such as Figs. C-10, C-11 and C-12.

As the wing was rotated through various angles of attack and flap angle changes, more of the air flow which entered under the leading edge of the wing was forced out under the plates on the sides. Continuity was still preserved, of course, but the nozzle was greatly expanded and inefficient. This caused more variations in the pressures felt under the wing and presented additional bulges in the pressure profile and aberrations in C_p values and graphs. This leakage caused as much difficulty in interpretation of pressure data as it caused losses in lift. Gallington et al, (18) mentioned this same phenomenon and the need to overcome it. By staying close to the surface with the bottom of the end plates, much of this loss was stopped. Further study could show what angle of attack and flap angle provides the greatest lift and pressure data without large losses from the sides.

Wing pressure profiles are shown in Figs. D-1 to D-24. Referring to Fig. D-1 as an example, the area between the curves represents the total lift experienced by the wing section identified by the pressure tap locations shown in Fig. 8. If a large number of these sections were taken and the areas between all of the curves were quantified and summed, the lift would approach that given by the force balance data for that run. The upper surface experienced a vacuum over its surface while the lower surface had a slight positive pressure.

This, of course, is the real cause of lift.

Searching through the figures of wing pressure profile, it was observed that an increase in flap angle increased the lift produced but the curve stays nearly the same shape. As angle of attack was varied, this shape changed. The curves for each angle of attack maintained their shape for all heights above the surface. The area between the curves, however, changed with the height. Comparing Figs. D-1 and D-19 shows the loss of lift coincidental with flying out of the ground effects experienced in Fig. D-1.

Because the several curve shapes are maintained and with the variation of area between the curves as a result of height changes, it is quite possible to use these curves to predict the lift that will be generated at various conditions and configurations. It is feasible to use this pressure data for analytical studies in the future to better understand the behavior of flying in and out of ground effects.

The inferences drawn from the pressure data in Figs. D-1 to D-24 can be compared to the inferences which stem from the force data presented earlier in this chapter. Using Tables 1 and 2, lift and L/D present general trends which change with H/c, α, and θ. Equivalent trends were noted from the pressure plots.

Referring to Table 1, select H/c = 1.0 and 0.5 with α = 5 deg. Total lift increased as H/c decreased. Comparing the area between the curves on Figs. D-9 and D-15 gave this same

TABLE 1

Examples of Lift Variation with Flap Angle, θ, and Angle of Attack, α (MM)

	θ	H/c = 0.25	H/c = 0.5	H/c = 1.0	H/c = 2.35
	0	-	2.16	-	2.30
$\alpha = 0$	10	-	3.92	-	3.63
	30	-	8.66	-	7.61
	0	9.16	6.97	6.19	6.23
$\alpha = 5$	10	11.41	8.98	7.92	7.85
	30	15.79	13.65	12.05	11.89
	0	-	16.01	-	13.76
$\alpha = 15$	10	-	17.83	-	15.74
	30	-	21.75	-	19.62

TABLE 2

Examples of L/D Variation with Flap Angle, ϕ, and Angle of Attack, α (MM)

	ϕ	H/c = Ø.25	H/c = Ø.5	H/c = 1.Ø	H/c = 2.35
	Ø	-	4.25	-	4.42
α = Ø	1Ø	-	4.6Ø	-	4.62
	3Ø	-	3.88	-	3.26
	Ø	5.71	5.58	4.98	5.23
α = 5	1Ø	5.41	5.11	4.54	4.78
	3Ø	4.53	3.94	3.43	3.56
	Ø	-	4.52	-	4.ØØ
α = 15	1Ø	-	4.2Ø	-	3.68
	3Ø	-	3.51	-	2.96

impression. By also comparing Figs. B-9 and B-13, the same results were again obtained with C_L as the variable.

On Table 2, for the same H/c and α, the L/D increased as H/c decreased. Comparing Figs. B-11 and B-15 rendered the corresponding conclusion which lead to a belief that L/D can be predicted by knowledge of pressure curves.

The effects of angle of attack and flap angle upon the L/D were studied more carefully by plotting another set of graphs to combine other data. These plots were made for all heights studied and with all different plate configurations. For each angle of attack the flap angles used were Ø, 1Ø, 2Ø and 3Ø deg. This reduced the congestion of the graphs.

Comparing the plots was quite simple as the scales were the same. These plots verified quite a bit of information already addressed. First, the addition of center plates did not affect the results. An identifiable difference was perceived in the presence or absence of end plates in general, however, what size plates were used was not a factor. All plates sizes used showed similar effects. Thus, the two remaining sets of data for no plates and medium center and end plates at Figs. E-1 to E-8 were chosen. Both sets of plots demonstrate the same general effects of L/D and verify the same conclusions.

The difference between H/c = 1.Ø and 2.35 is negligible. Quite a bit of difference is noted below H/c = 1.Ø. The L/D increased dramatically in ground effect.

The effect of plates on the wing are negated once the wing

is out of ground effect. However, in ground effect, the plates do illustrate an advantageous effect. These plots verify results postulated by studying other parameters earlier in this chapter.

As flap angle increased, the lift increased but the drag increased to a greater extent. This caused the L/D to drop. The L/D decreased each time flap angle was increased. Again, these results verified previous conclusions.

The angle of attack had a major effect upon the L/D. As seen in all of the figures listed for this subject, $\alpha = 0$ deg did not provide the best ratio. In actuality, pilots know not to take-off or land at zero degrees angle of attack. The aircraft is always rotated to gain lift. This study always showed a climb in L/D up to $\alpha = 5$ deg and then a decrease from then on. It was not known for sure where this decrease began but it was between 5 and 10 deg. The normal take-off approach angle for helicopters is taught as 7 to 10 deg thus supporting this data. A steep approach angle (read "higher power required") is 15 deg, to be used only if necessary since it is not very efficient.

At small angles of attack, both the lift and the drag coefficient are small. At large angles of attack, the lift coefficient grows larger but the drag coefficient did the same. It was found in other studies that increasing only 1.5 to 2 deg over the angle which presented the minimum drag coefficient only slightly increased drag while it greatly increased lift (42). This point should give the greatest L/D.

From these discussions, it was obvious that flying in ground effect will raise the L/D. The ratio of C_L to C_D provides the same value as the ratio of the forces, L/D, themselves. If C_L becomes greater and C_D lesser, then the ratio is greater.

The present study confirmed the generally accepted results of theory and previous studies. Even though some curve shapes were unexplainable, (see Figs. B-43 and B-44) the apparent inconsistencies did not appear throughout the study. These odd-shaped curves were believed to have resulted from experimental error rather than from actual phenomenon of flight. In other words, they were from bad data; a glitch in the apparatus. They were rare and the large majority of data and curves were consistent rendering conclusive results.

VI. Conclusions

As stated at the beginning of this study, the primary purpose of this effort was to show that greater amounts of lift and higher L/D are obtained by flying close to the surface of the earth. The conclusions of this study were definitive and correspond quite well with trends expected from theoretical analysis as well as those trends identified in other studies.

Most importantly, the height above the surface had a profound effect upon the L/D. The wing flew more efficiently due to reduced power requirements, a result of increased lift and decreased drag experienced near the surface. The effects of the proximity to the surface were reduced as height was increased until freestream values were approximated in the vicinity of H/c = 1.Ø.

Control surfaces and the attitude of flight affected the production of lift and drag and therefore, necessarily, their ratio. As the angle of attack of the wing increased from Ø to 5 deg, the L/D increased. However, somewhere between 5 and 1Ø deg, the rise in L/D reversed and began to fall. For all further increases in angle of attack, the L/D decreased. As the flap angle was increased from zero, the drag increased at a faster rate than lift. This resulted in a rapid decline in L/D.

Changing the configuration of the wing by adding end and center plates caused some noticeable effects. Addition of end plates resulted in an increase in L/D when the wing was in ground effects. This was caused by trapping air between the

wing, the surface, and the plates. Trapping the air created a cushion of air which resulted in greater lift. The plates added only minutely to the drag on the wing. The size of the plates used did not cause any appreciable benefit or loss as long as they were present and near the surface. Once the wing was out of ground effect, there was no longer a cushion of air trapped under the wing and the additional benefit was lost. The end plates alone created as much a benefit as they did when combined with a center plate.

Pressure profiles from ground and wing pressure readings correspond to theoretical expectations as well as other experimental results. Due to the repetitive pattern the distributions exhibited, it is deduced that the pressure distributions can be used to predict the lift generated by a wing under varying control inputs and configurations.

VII. Recommendations

The results of this study allow for continued work. If further work is done, the model, instrumentation, set-up, and methodology can be refined and improved to provide more accurate and automated model changes and data collection. Some changes in the experiment are needed. Also, from this study, it can be determined that the ranges of variable changes can be narrowed for closer study and more detailed analysis to keep from repeating segments that do little to meet the primary purpose of this study. These include:

1. Angle of attack should be narrowed to values between Ø and 1Ø deg as this range has shown the greatest L/D. More increments in this range should be taken.
2. The flap angles should be narrowed to values between 0 and 15 deg for L/D maximization.
3. The AR should be increased from 2 to perhaps 6 or as high as 1Ø because other studies have shown that higher AR may be more advantageous for yielding higher L/D values.
4. There should be a larger variation in the size of the plates to determine if any more assistance is available with the use of end plates.
5. The imaging of the model to run the test should be attempted to do away with the ground boards which are restrictive, inaccurate, and quite bulky. Imaging the system will be an engineering marvel in itself but would improve the quality of data.

6. Consideration should be given to the possibility of using the wire balance system rather than the sting and yoke. The sting and yoke assembly presented problems to surmount in the construction of boards, etc.
7. The closeness of the lines in many of the plots in the study show that little effect was registered in many aspects. To enhance the study and provide more realism, and to refine the effects of configuration changes, some sort of engines should be added to the model. This would change the study from the glider mode to the PAR-WIG mode. The flow generated by the engines would certainly enhance the performance of the model near the ground and may further show the benefits of end plates over conventional landing gear systems.
8. If additional tests are run, the effect of surface roughness of the board should be varied to simulate different terrains. Flat surfaces do not usually exist in nature, other than at Edwards Air Force Base, and to simulate readiness at various locations, a rough, vegetated, broken surface should be tested.
9. The ground board should extend a greater distance behind the model. This will negate the possibilities of any turbulence bubbling up over the rear lip and travelling upstream, thus interfering with the model performance. This will necessitate changes and redesign in the yoke assembly.

10. From the present study, there does not seem to be much advantage in using the end plates on wings flying substantially higher above the ground than two times the chord height. Plates may be retracted like the landing gear itself. The possibility of retracting the end plates into the wings of the aircraft, much like landing gear, could be studied for flight out of ground effect.
11. A computer program such as PANAIR should be used before the physical tests are run. The program should duplicate the model and the boundary conditions as closely as possible so that computer prediction will directly resemble the real-life output obtained in the test.
12. H/c can be narrowed to values equal to and less than 1.0 since this study shows that there is very little change between H/c = 1.0 and 2.35. Instead, more heights in this smaller range could be tested to obtain full data in the most promising area. (If flight out-of-ground effects is contemplated, stability problems in that regime will need to be tested.)

Appendix A

Computer Program

This section describes the program used by the HP9826 desk top computer to convert the raw data (voltages from the voltmeter) to stability axes force and moment coefficients, and to collect and store pressure data.

The final output array S(30,13) of stability axes coefficients and associated parameters (for up to 30 test points) consists of:

S(I,1): Test point number

S(I,2): Corrected angle of attack

S(I,3): Corrected dynamic pressure

S(I,4): Stability axes yawing moment coefficient

S(I,5): Stability axes rolling moment coefficient

S(I,6): Center of pressure

S(I,7): Stability axes lift coefficient

S(I,8): Stability axes drag coefficient

S(I,9): Stability axes pitching moment coefficient

S(I,10): Stability axes side force coefficient

S(I,11): Yaw angle

S(I,12): Not Used

S(I,13): Not Used

The test point number is a consecutive number, starting with one, assigned to each point in a given run by the computer. As stated above, this program will handle up to 30 data points per run. Most runs consisted of 7 data points.

The process of computing the stability axes forces and moments from the balance loads is rather complex. The computer reads the bridge excitation voltage from the six volt power supply and the temperature of the air entering the tunnel from a thermocouple located just outside the mouth of the tunnel one time each. The computer then reads the base pressure gauge nine times, the forward normal force gauge nine times, the aft normal force gauge nine times, the forward side force gauge nine times, the aft side force gauge nine times, the rolling moment gauge nine times, and the axial force gauge nine times. It repeats the cycle from the forward normal force gauge to the axial force gauge five times, yielding 45 readings of each balance gauge. The program averages the 45 values for each gauge. The computer operator inputs the tare code to be used, the configuration code, the run number, and the type of data point (wind off point, tare point, wind on point, final point). All voltages input to the computer by the voltmeter are in volts. The balance calibration constants are in units per millivolt so the balance calibration constants are multiplied by 1000. The temperature calibration constants are then used to convert the temperature voltage to Fahrenheit, which is then converted to Rankine.

Next, the program subtracts the wind off values at zero angle of attack of the six balance voltages and the base pressure in pounds per square foot from the respective values of these quantities at each test point. The balance gauge interactions are then calculated. The program uses the gauge interactions,

the calibration constants and the balance loads to calculate gauge loads. From these loads, the forces and moments are calculated. The normal force and pitching moment are calculated from the two normal force gauge loads, the rolling moment from the rolling moment gauge loads, and the axial force from the axial force gauge load. These forces are the forces printed out under "Balance Loads (Tares Not Removed)". (See Fig. A-1.)

At this point the program splits into two branches - one for calculating tare slopes and one for calculating force and moment coefficients. The tare slopes are used to correct the data for model weight at angle of attack. If the data type input by the operator is tare data, the program next calculates four tare slopes from loads from the six balance gauges. To check the calculated tare slopes, the tare slopes are applied to the balance loads in the tare data and the appropriate values subtracted from the tare loads. These differences are printed out so the operator can verify they are approximately zero. The four calculated tare slopes are then stored.

The second branch of the program calculates force and moment coefficients from the wind on data. The angle of attack is determined as follows. The computer takes the voltage read from the angle of attack voltmeter at the tunnel operator's station and converts the voltage to degrees angle of attack (α) using the angle of attack calibration. This value is printed out as "Theta" in the section "Balance Loads (Tares Not Removed)" (See Fig. A-1). This is the angle of attack printed out with the body

DATA COLLECTED 08:53:50 4 Nov 1986

RUN NUMBER 46
FOREBEND 0 ROLL ANGLE 0
HEIGHT OF BOARD (IN INCHES): 21.15
FLAP DEFLECTION (IN DEGREES): 15

BALANCE LOADS (TARES NOT REMOVED)

TPN	Bgrav DEGREE	THETA DEGREE	NFB LBS	PMOMB LB-IN	SFB LBS	YMOMB LB-IN	RMOMB LB-IN	AXFB LBS
2.	-.01	.01	4.709	-22.922	.057	-.414	2.008	1.046
3.	-.01	4.95	9.078	-31.212	.056	-.222	2.160	1.390
4.	-.01	10.00	13.514	-39.847	.164	-.186	2.022	1.241
5.	-.01	14.99	17.558	-47.688	.121	-.196	1.709	.638
6.	-.01	19.98	20.828	-53.978	.069	.165	2.374	-.304
7.	-.01	25.04	19.166	-55.776	-.330	3.872	8.750	.164

BODY AXIS COEFFICIENTS

TPN	ALPHA	CN	CA	CM	CS	Cn	Cl
2.	.31	.3106	.0688	-.0954	.0037	-.0009	.0064
3.	5.56	.5837	.0737	-.0888	.0035	-.0004	.0067
4.	10.94	.8558	.0491	-.0858	.0103	.0004	.0063
5.	16.22	1.1107	-.0020	-.0849	.0076	0.0000	.0053
6.	21.43	1.3109	-.0748	-.0845	.0042	.0007	.0073
7.	26.33	1.2045	-.0686	-.1203	-.0214	.0095	.0262

DATA COLLECTED 08:53:50 4 Nov 1986

STABILITY AXIS

TPN	ALPH	L	D	MPIT	S	MYAW	MROLL	L/D
2.	.31	4.70	1.07	-13.02	.06	-.31	2.03	4.40
3.	5.56	8.92	2.02	-12.42	.05	-.33	2.16	4.42
4.	10.94	13.10	3.32	-12.17	.16	-.28	2.06	3.95
5.	16.22	16.82	4.86	-12.04	.12	-.47	1.69	3.46
6.	21.43	19.72	6.48	-12.03	.07	-.65	2.33	3.05
7.	26.33	17.47	7.44	-17.04	-.34	-1.03	9.19	2.35

Fig. A-1 Example, Reduced Data Printout, Sheet 1

WING-IN-GROUND EFFECTS

AFIT 5-FOOT TUNNEL

TEST # 1112

RUN # 46

Q PSF	VELOC. MPH	MACH NO.	TEMP. (F)	REYN.# PER FT	PATM IN.HG	WAREA SQ.FT	TARE CODE	FLAP ANGLE
11.93	69.3	.091	60.5	6.26E+05	29.29	1.310	6.	15.

TPN	ALPHA DEG	PSI DEG	CL	CD	CM	CS	CN	CRL
	Q PSF	CP IN.FR.NS	BLANK	BLANK	PBASE PSF			
2.	.31	-.01	.3102	.0705	-.0954	.0037	-.0010	.0064
	11.57	6.75	0.000	0.000	3.154			
3.	5.56	-.01	.5738	.1299	-.0888	.0035	-.0010	.0066
	11.86	5.32	0.000	0.000	3.095			
4.	10.94	-0.00	.8310	.2106	-.0858	.0103	-.0008	.0062
	12.03	4.83	0.000	0.000	2.994			
5.	16.22	-0.00	1.0671	.3082	-.0849	.0076	-.0014	.0051
	12.03	4.60	0.000	0.000	2.942			
6.	21.43	-0.00	1.2476	.4094	-.0845	.0042	-.0020	.0070
	12.07	4.47	0.000	0.000	3.123			
7.	26.33	-.04	1.1100	.4726	-.1203	-.0214	-.0031	.0277
	12.01	4.79	0.000	0.000	7.196			

Fig. A-2 Example, Reduced Data Printout, Sheet 2

axes coefficients (to be discussed later). The program then uses the sting deflection coefficients (included in the program like the balance constants and tunnel constants) to calculate the horizontal and vertical displacement and rotation of the sting due to aerodynamic loads. From these deflections and "theta", it calculates pitch angle. These pitch angles, model constants, and the tare slopes are used to correct the forces and moments calculated above. The forces and moments are now in the body axis.

The next step is to correct dynamic pressure for blockage corrections. To calculate the dynamic pressure, the program averages the ten readings of each of the eight pressure ports 2.5 ft upstream to get an average uncorrected dynamic pressure for the 10 ft test section. These values are then corrected, by use of 'delta q' which was determined in the board only runs for local 'q' at the model. It then converts this value to pounds per square foot, subtracts the wind off value, and corrects for compressibility using the following equation:

$$q = (3.5)\,(\text{static pressure})\left[\left(\frac{\text{static pressure}}{\text{atmospheric pressure}}\right)^{-0.2857} - 1\right]$$

where q is the dynamic pressure corrected for compressibility and the static pressure is the difference between the dynamic pressure before the compressibility correction is made and the atmospheric pressure. (The atmospheric pressure is the value typed in by the operator, converted from in Hg to psf The corrected dynamic pressure is found by applying the following

combined solid and wake blockage correction:

q_{corr} = (dynamic pressure after compressibility correction) * (1 + total blockage corrections)^2

The total blockage correction is calculated from:

Total blockage = 1/4 (model frontal area)/(test section area)

The dynamic pressure printed with the stability axes force and moment coefficients, both for each data point and the value averaged over all points in the run, and in the final output array is q_{corr}.

Next the axial force is corrected for base pressure.

corrected axial force = axial force (body axis) - (base area)*(base pressure)

The base area is a model constant. For the model used, it was 0.0062 ft^2. Using this corrected axial force and the other forces and moments after the tare slopes correction, the program calculates 1) the body axes force coefficients by dividing by the body axis forces by the product of q_{corr} and the wing area, and 2) the pitching moment coefficient by dividing the product of q_{corr}, the wing area, and the mean aerodynamic chord. It then corrects α for downwash using the following equation:

$$\alpha_{corr} = \alpha + \frac{(\delta)\ (\text{model reference area})}{(\text{tunnel cross-sectional area})}$$

where δ is a boundary correction for downwash and sidewash from Pope and Rae (33:380).

Next the program uses α_{corr} from the above equation to convert the body axis forces and moments to stability axes forces and moments. The stability axes coefficients are calculated from these stability axes forces and moments. The program corrects the drag coefficient and drag as follows: (this is an induced drag correction)

$$C_{D_{corr}} = (\text{stability axes drag coefficient}) + \frac{(\delta)(\text{model ref. area})(\text{stability axes lift coeff.})^2}{(\text{tunnel cross-sectional area})}$$

$$D_{corr} = (C_{D_{corr}})\,(q_{corr})\,(\text{model reference area})$$

The program then uses $C_{D_{corr}}$, D_{corr}, α_{corr}, and the stability axes lift to recalculate the axial and normal forces. Using these axial and normal forces, and pitching moments after the tare slopes correction, the program recomputes the body axes coefficients and stability axes forces and moments. These are the body axes coefficients and the stability axes forces and moments which are printed out. The stability axes forces and moments printed out are then converted to stability axes coefficients in the same manner the previous forces and moments have been converted to coefficients, and printed out.

There are several other miscellaneous pieces of information printed out with the stability axes coefficients. The center of pressure, measured from the nose, is essentially the distance from

the nose to the moment reference center minus the quantity of the pitching moment divided by the normal force. The base pressure is printed out as a delta pressure (p static- p base). The tare code, the configuration code, and atmospheric pressure are as input by the operator. The wing area is a model constant. The temperature is the measured temperature converted to Fahrenheit, averaged over all points in the run. The velocity and unit Reynolds number calculations require the density. The density is obtained from the measured temperature and a corrected static pressure. The corrected static pressure is found by subtracting q_{----} from the atmospheric pressure.

The velocity and unit Reynolds numbers were calculated from:

$$\text{velocity} = (2\ q_{----}/\text{density})^{1/2}$$

$$R_L/ft = \frac{(\text{density})(\text{velocity})}{(2.27)\{[\text{temp in Rankine}]^{1.5}/[\text{temp in Rankine} + 198.6]\}\ (10^{-8})}$$

respectively and averaged over all the test points in the run.

The Mach number is:

$$\text{Mach No.} = \frac{\text{velocity}}{(49.07)\ (\text{measured temperature in } ^\circ R)^{1/2}}$$

averaged over all test points in the run. The two columns labeled "P left" and "P right" were not used.

If desired, this program will collect and store pressure data for up to 30 test points. The computer reads each of the 14 model and 21 ground board pressure ports ten times and averages the values for each port. This program does not print out any

pressure data. The pressure data output file, consists of the average pressure values, the dynamic pressure voltage, the atmospheric pressure in inches of Mercury, the test point number, the data type, and the run number, in that order, for each data point. Another program was used to reduce and print out the pressure data.

Run Schedule

The run schedule was set up to acquire all data needed at a given height of the model before moving to the next height. When the model height became very low, several of the plates would not fit on the model. In some cases, the plates fit but left no room for variation of angle of attack. The runs at each height consisted of seven plate configurations: 1) no plates, 2) large end plates only, 3) large center and end plates, 4) medium end plates only, 5) medium center and end plates, 6) small end plates only, and 7) small center and end plates.

Integrated into each of these different configurations was variation of flap angle, ϕ, from 0 to 30 deg at 5 deg increments; and angle of attack, α, from 0 to 25 deg at 5 deg increments. Yaw was fixed at 0 deg. Before data were collected for reduction, a tare value was taken with each weight change (plate configuration) to subtract the weight components of the model from the forces collected in the software.

The ground boards were set at heights of $0.15c_{MAC}$, $0.25c_{MAC}$, $0.5c_{MAC}$, $1.0c_{MAC}$ and $2.35c_{MAC}$, ie., 1.35 in to 21.15 in. The lower three heights represented in-ground effect conditions.

1.0c_{MAC} represents the borderline between in- and out-of-ground effects. 2.35c_{MAC} represents freestream conditions.

APPENDIX B: FORCE PLOTS

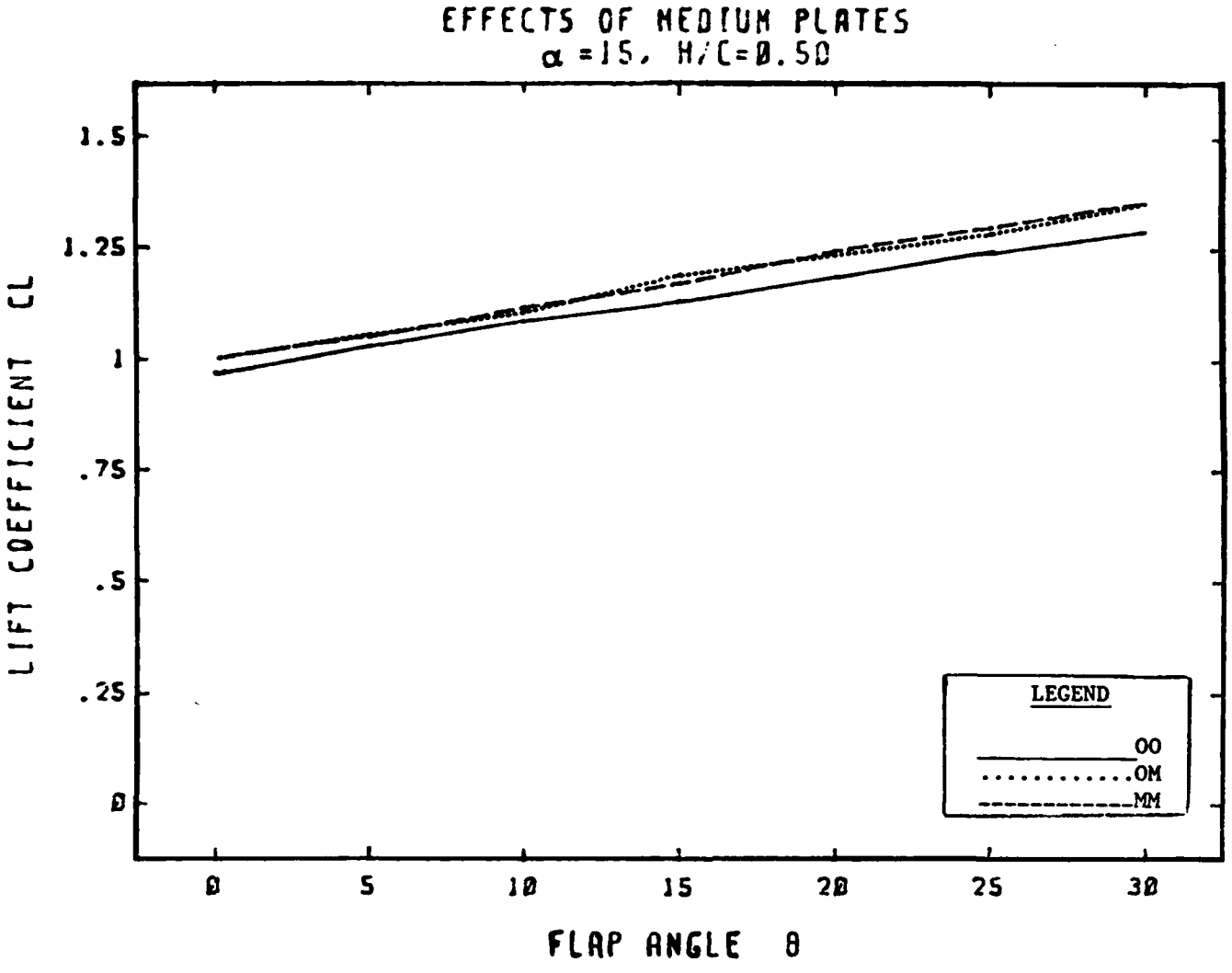

Fig. B-1 Effects of Medium Plates, CL

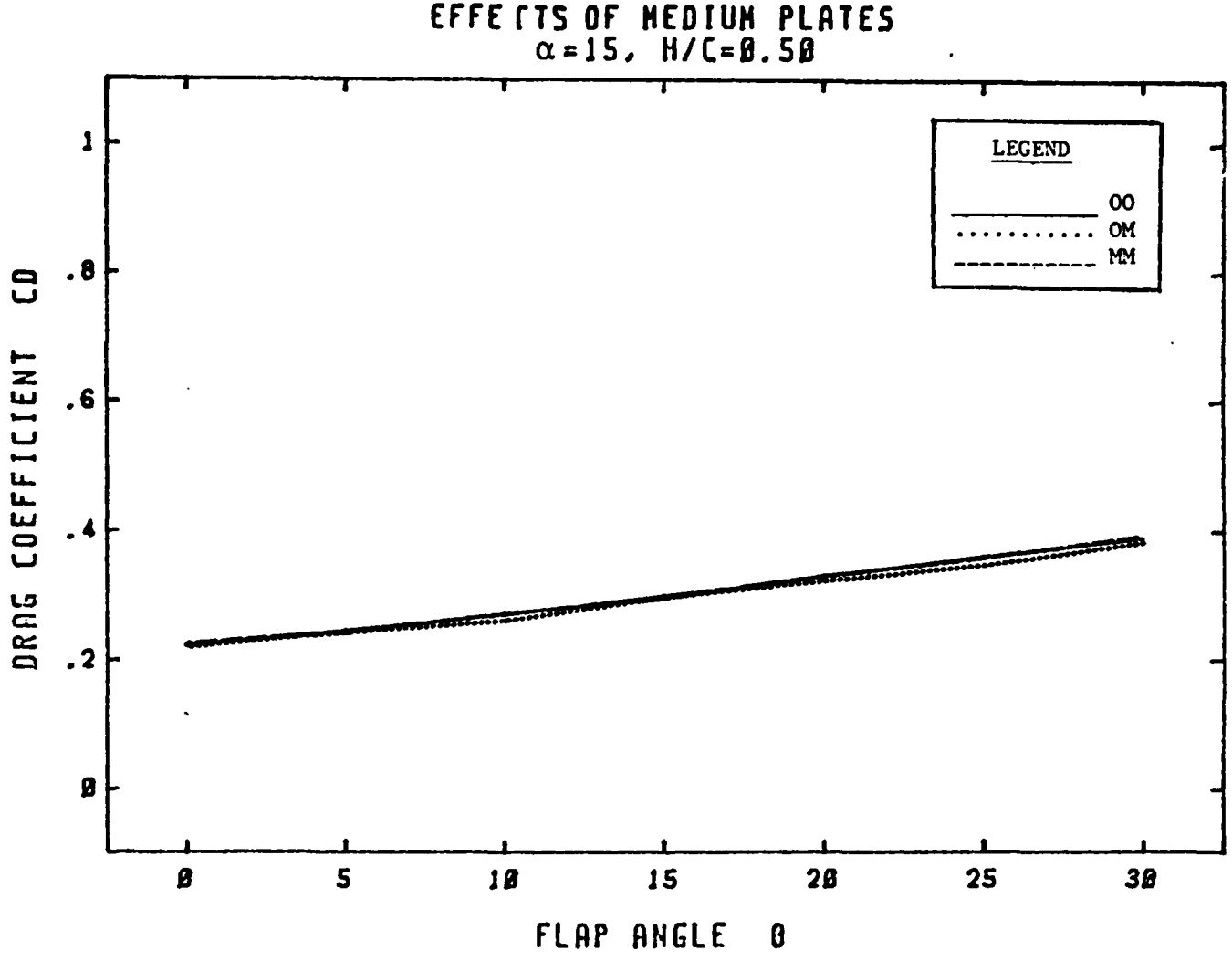

Fig. B-2 Effects of Medium Plates, CD

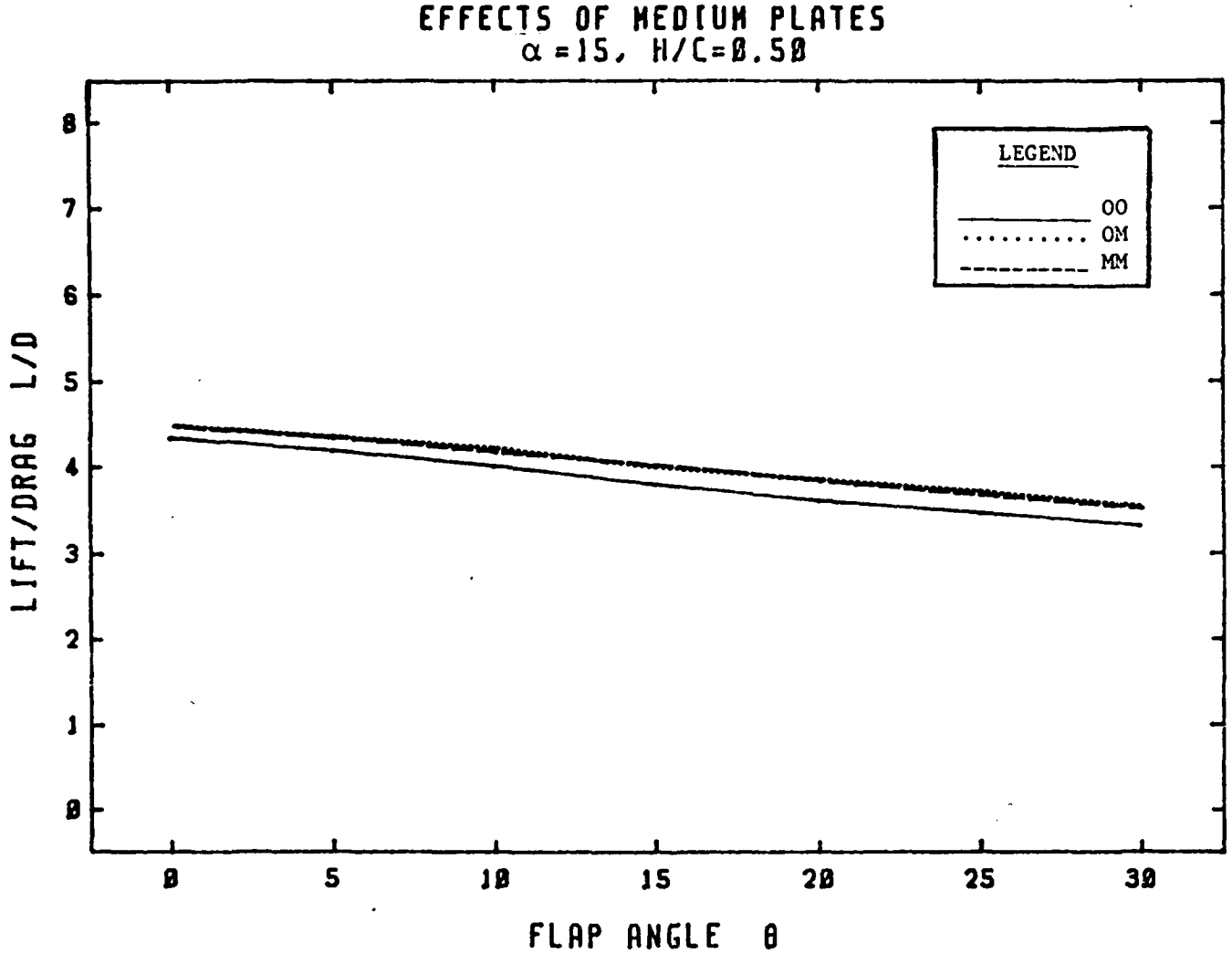

Fig. B-3 Effects of Medium Plates, L/D

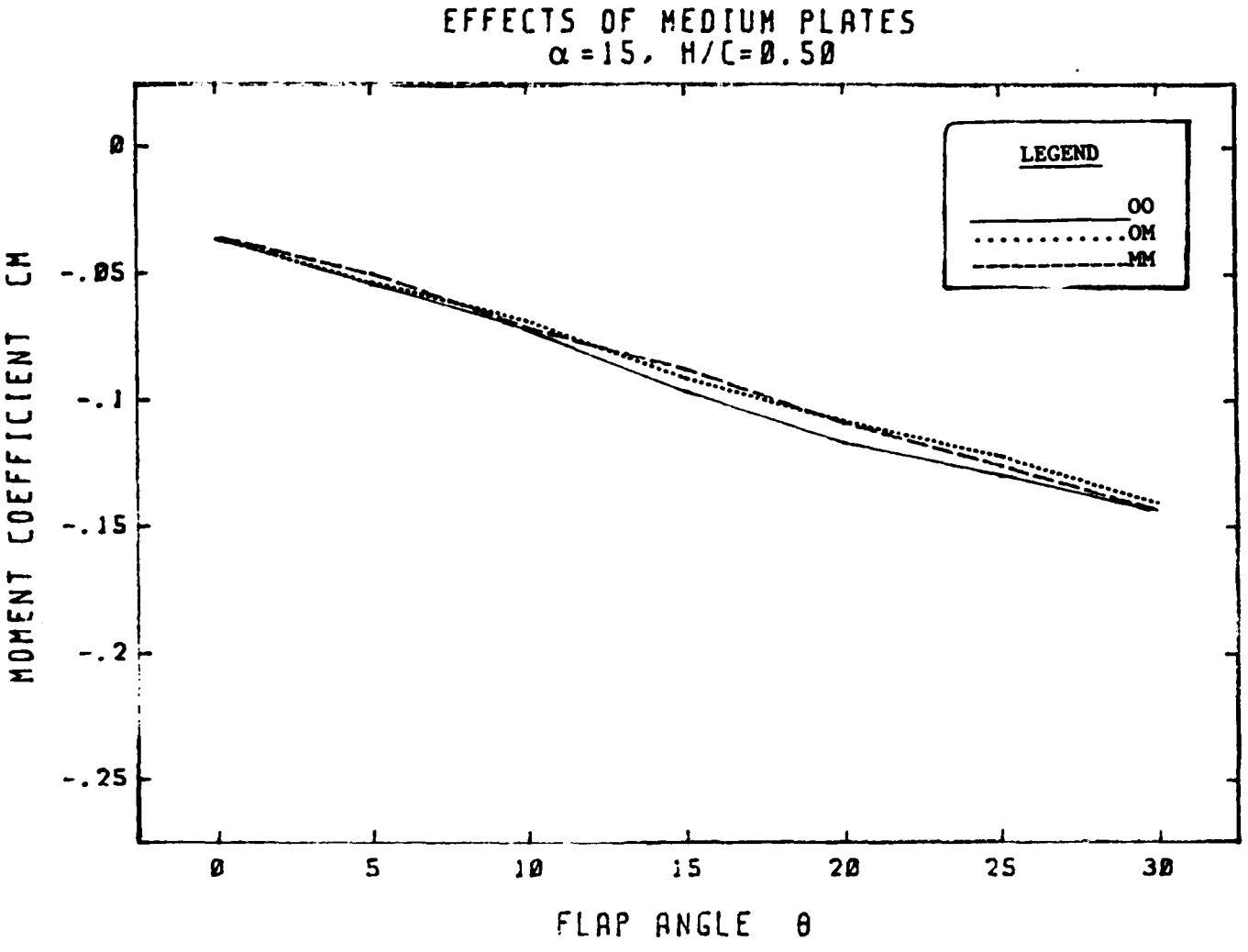

Fig. B-4 Effects of Medium Plates, CM

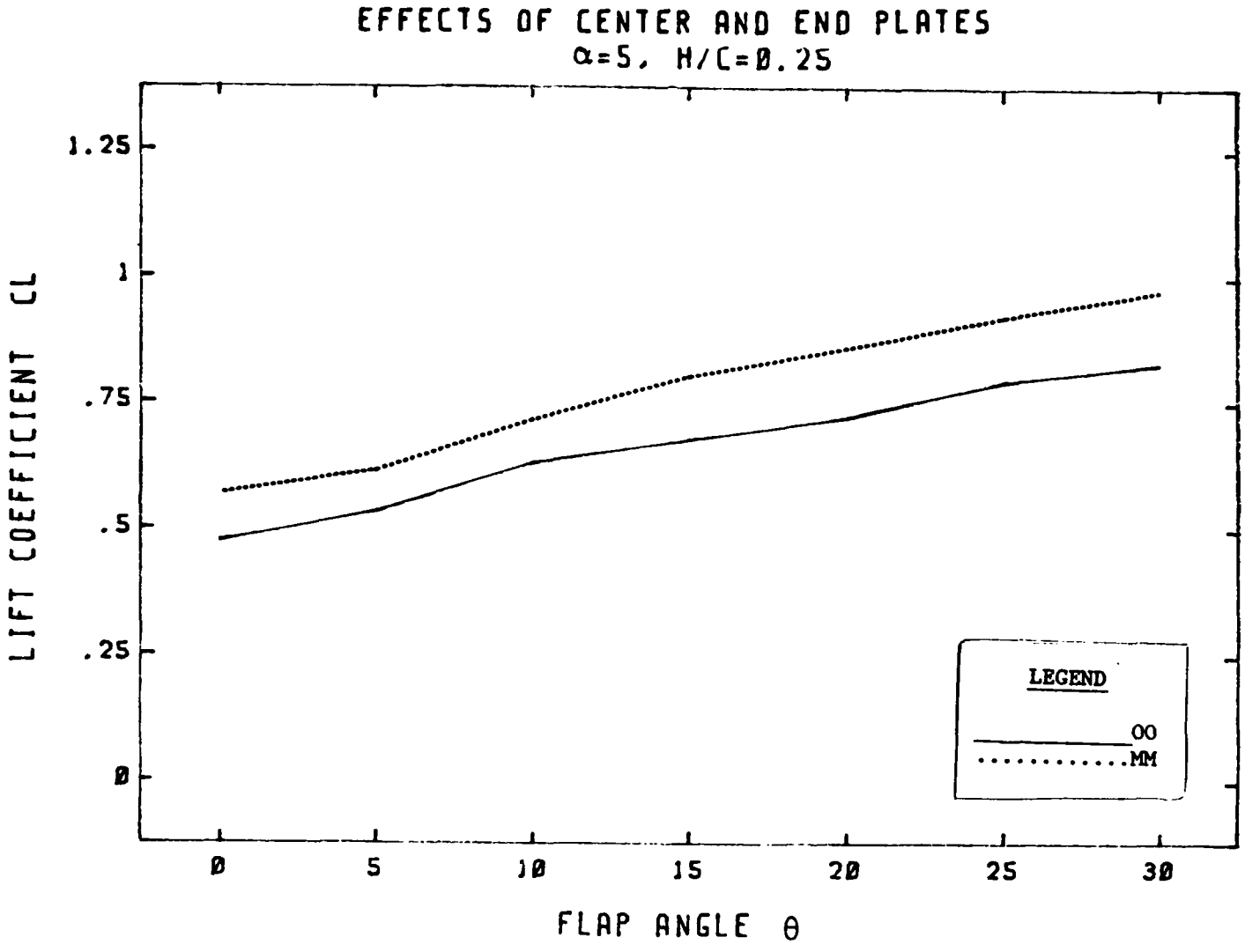

Fig. B-5 Effects of Center and End Plates, CL

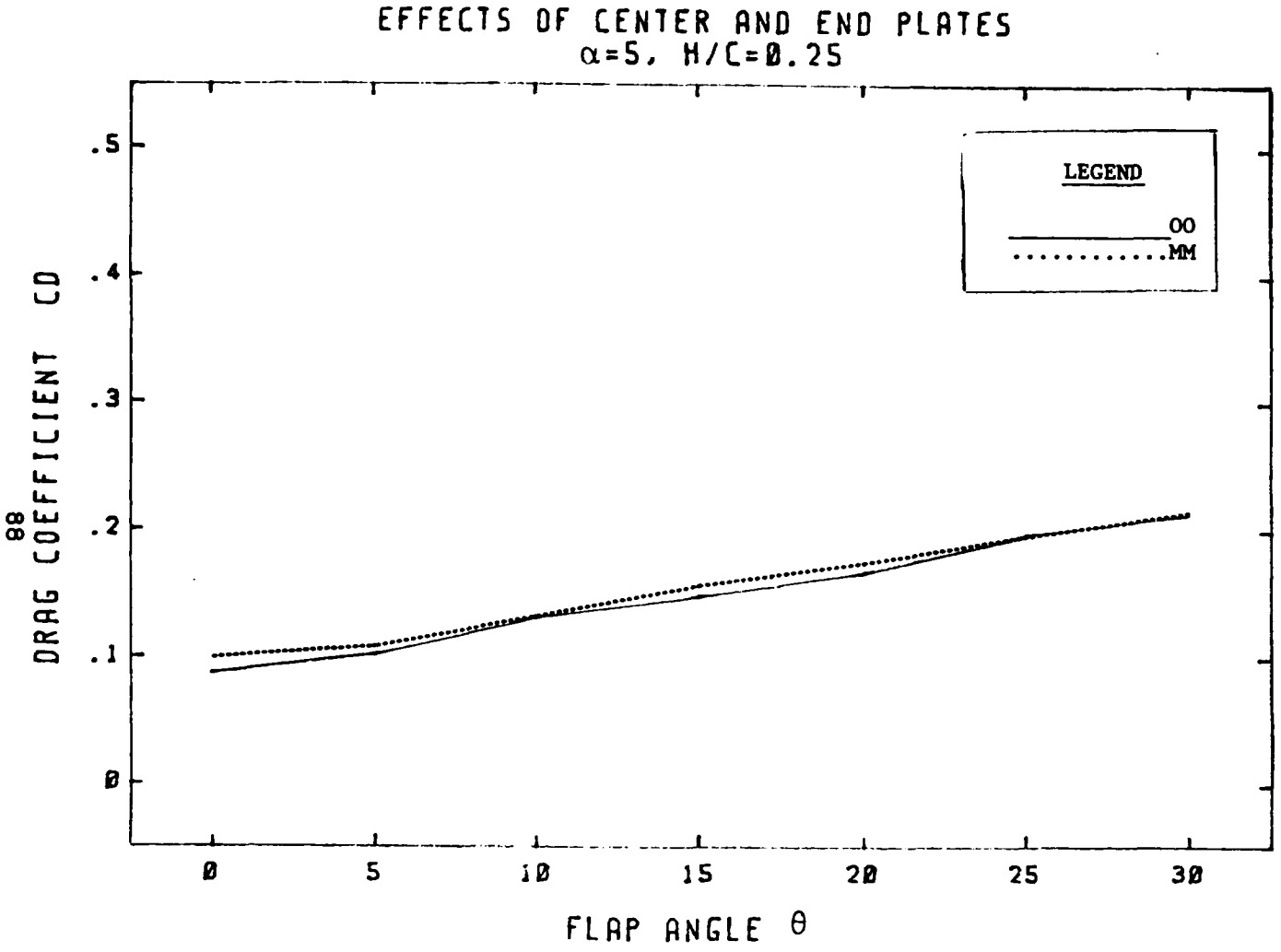

Fig. B-6 Effects of Center and End Plates, CD

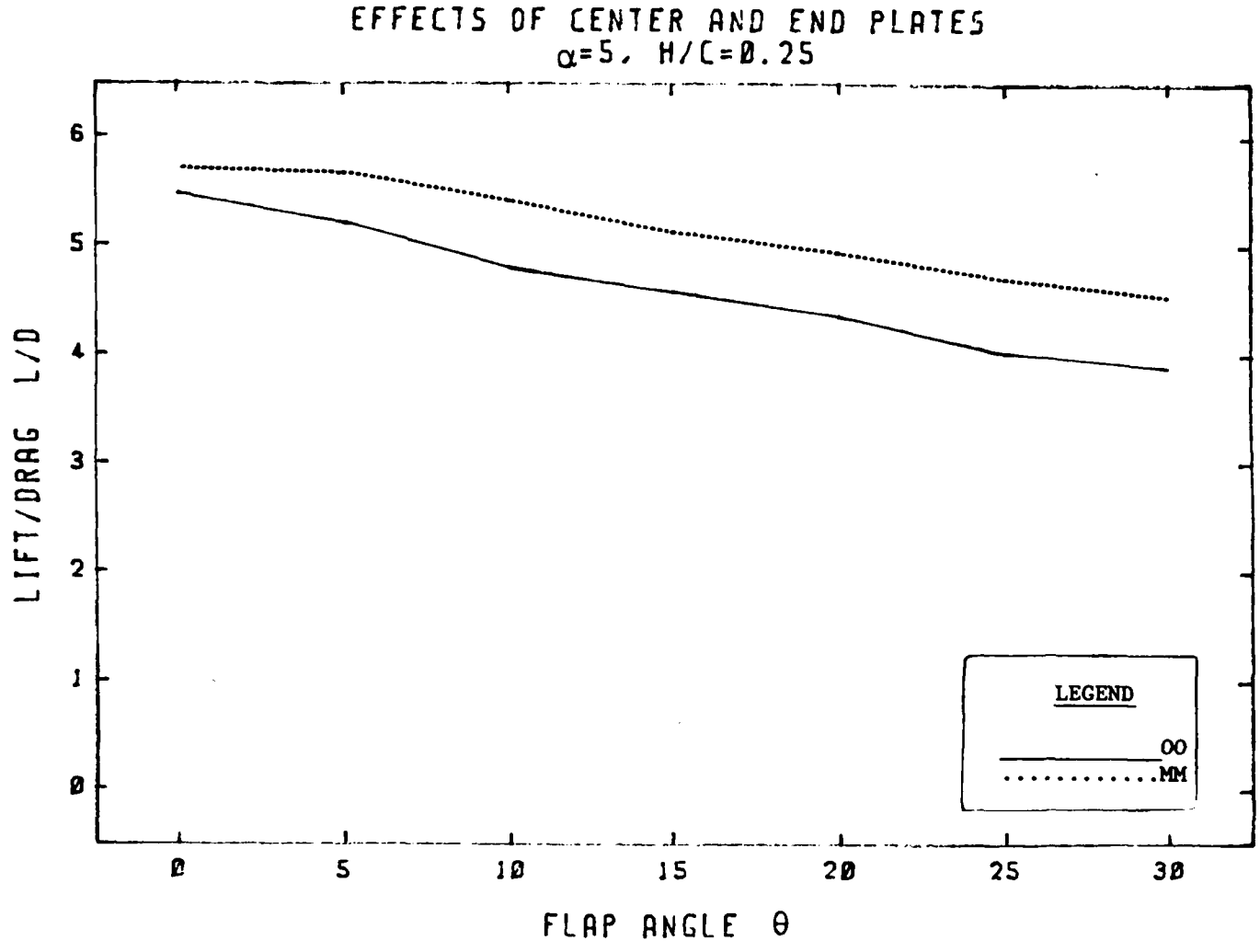

Fig. B-7 Effects of Center and End Plates, L/D

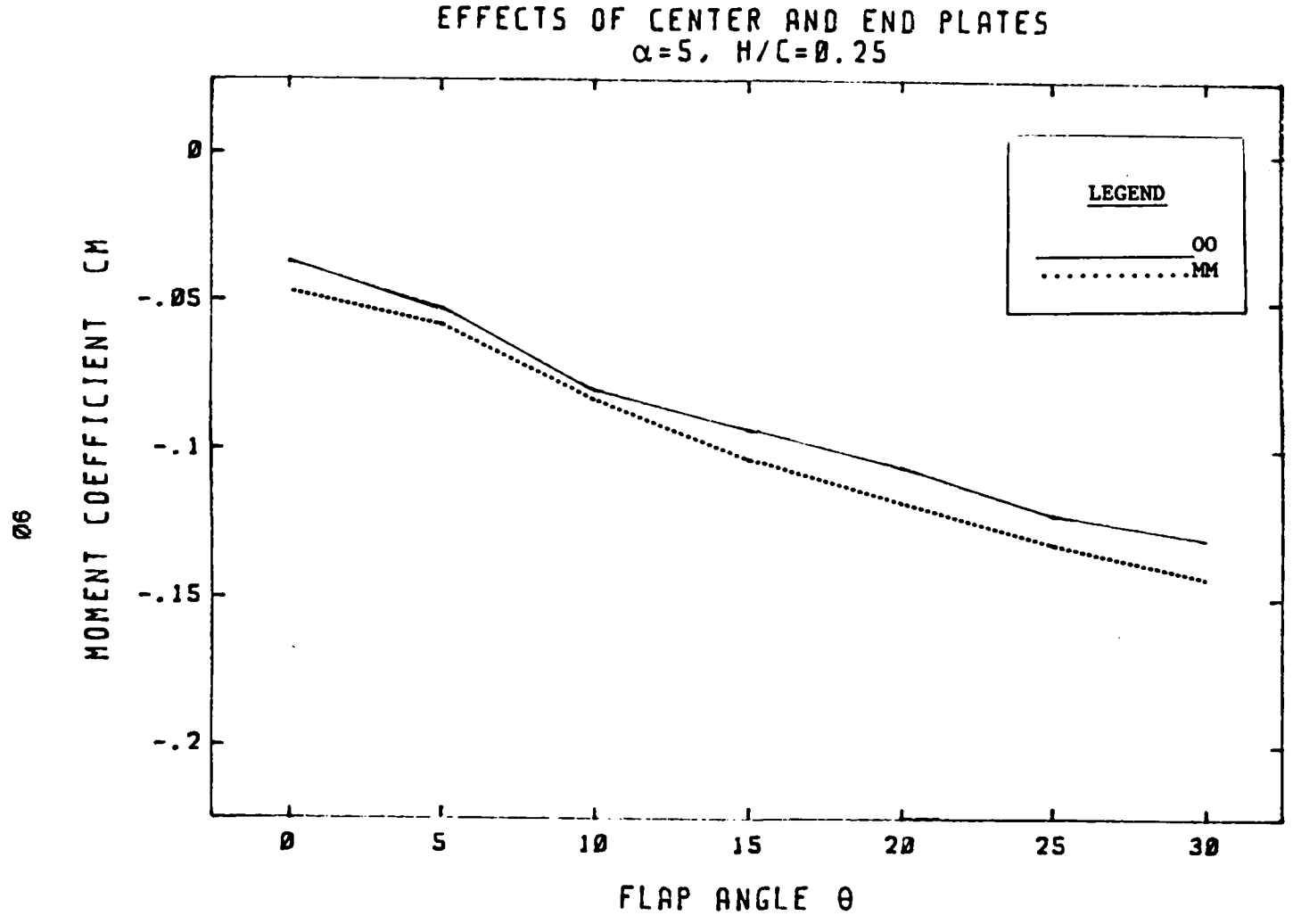

Fig. B-8 Effects of Center and End Plates, CM

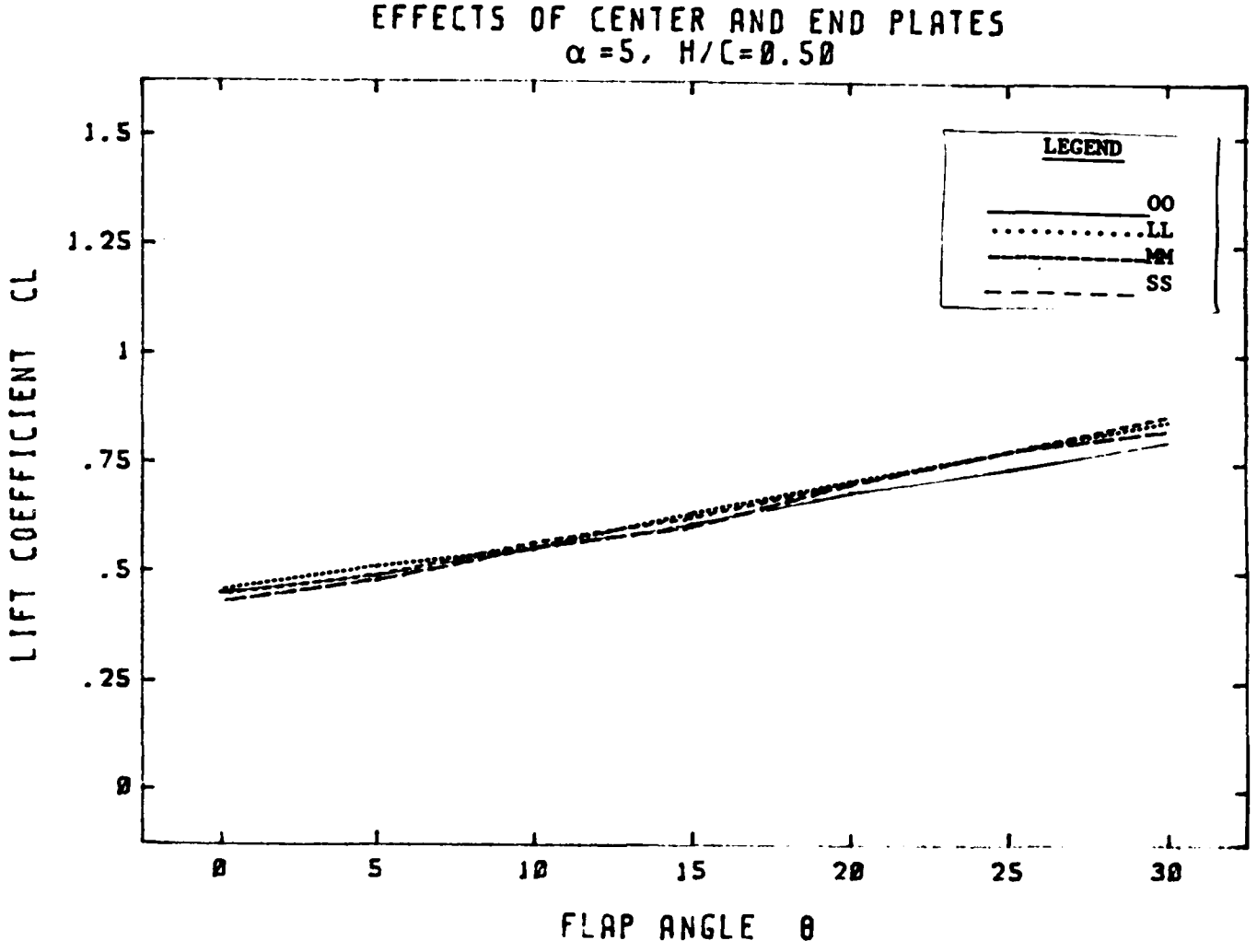

Fig. B-9 Effects of Center and End Plates, CL

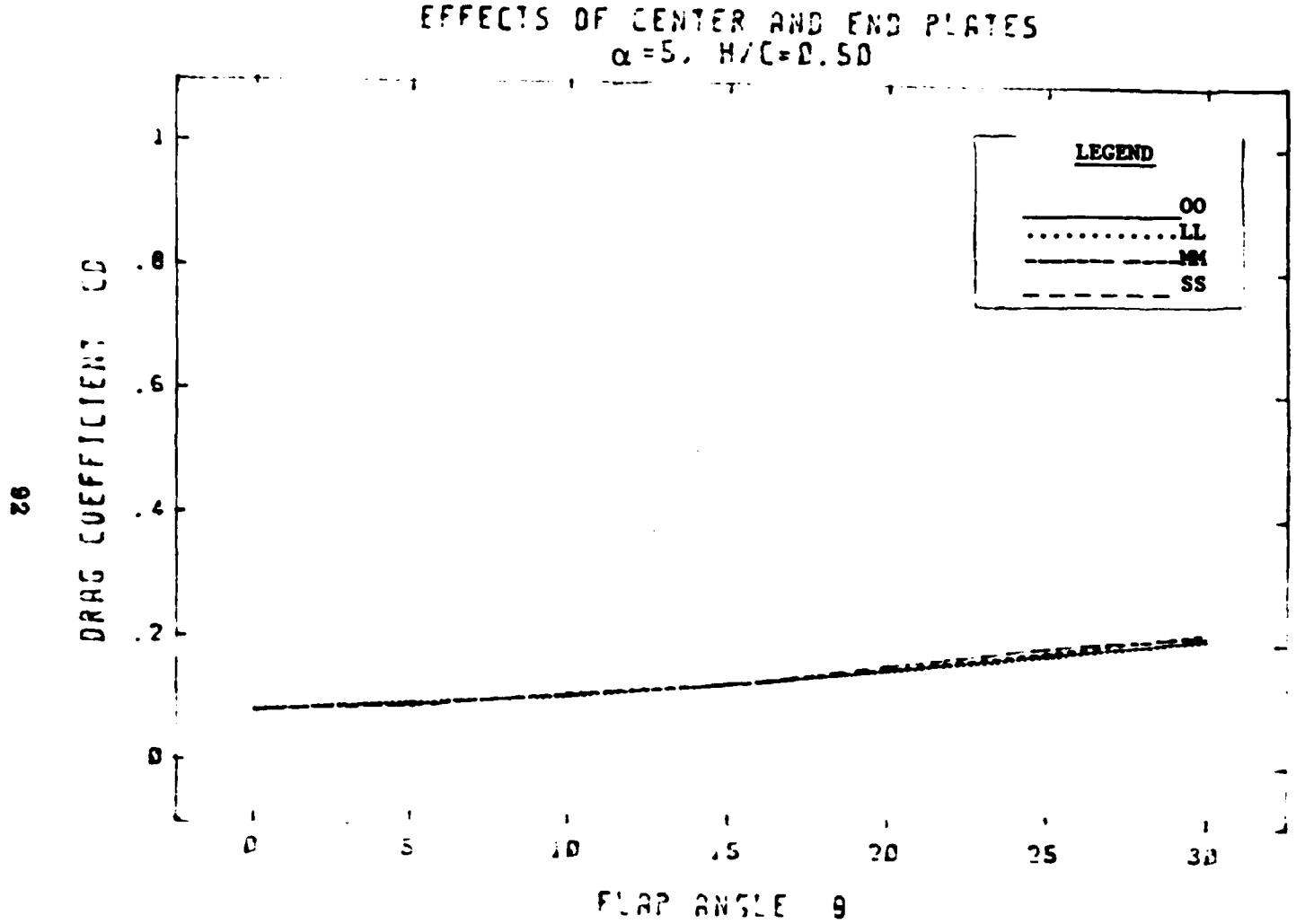

Fig. B-10 Effects of Center and End Plates, CD

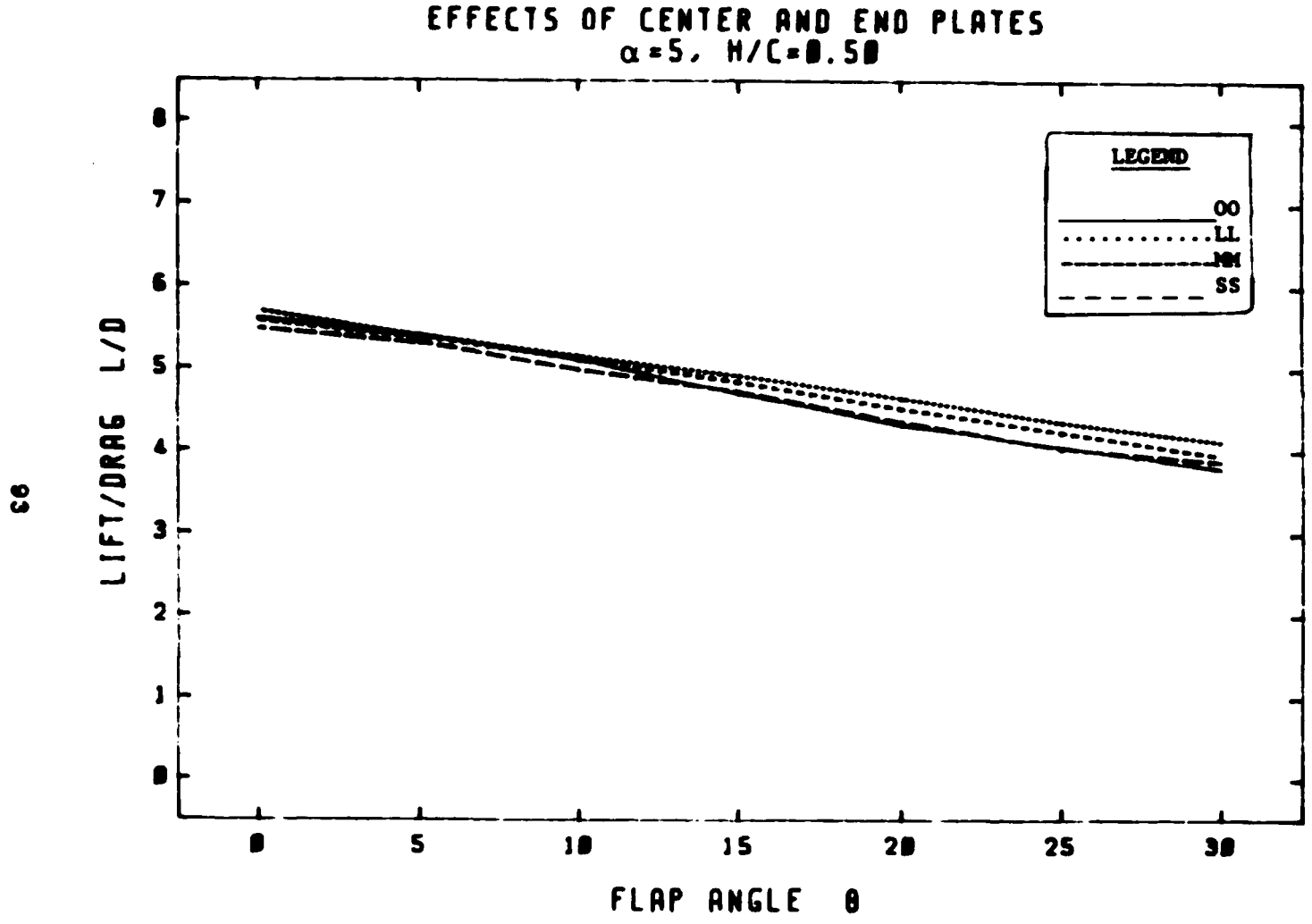

Fig. B-11 Effects of Center and End Plates, L/D

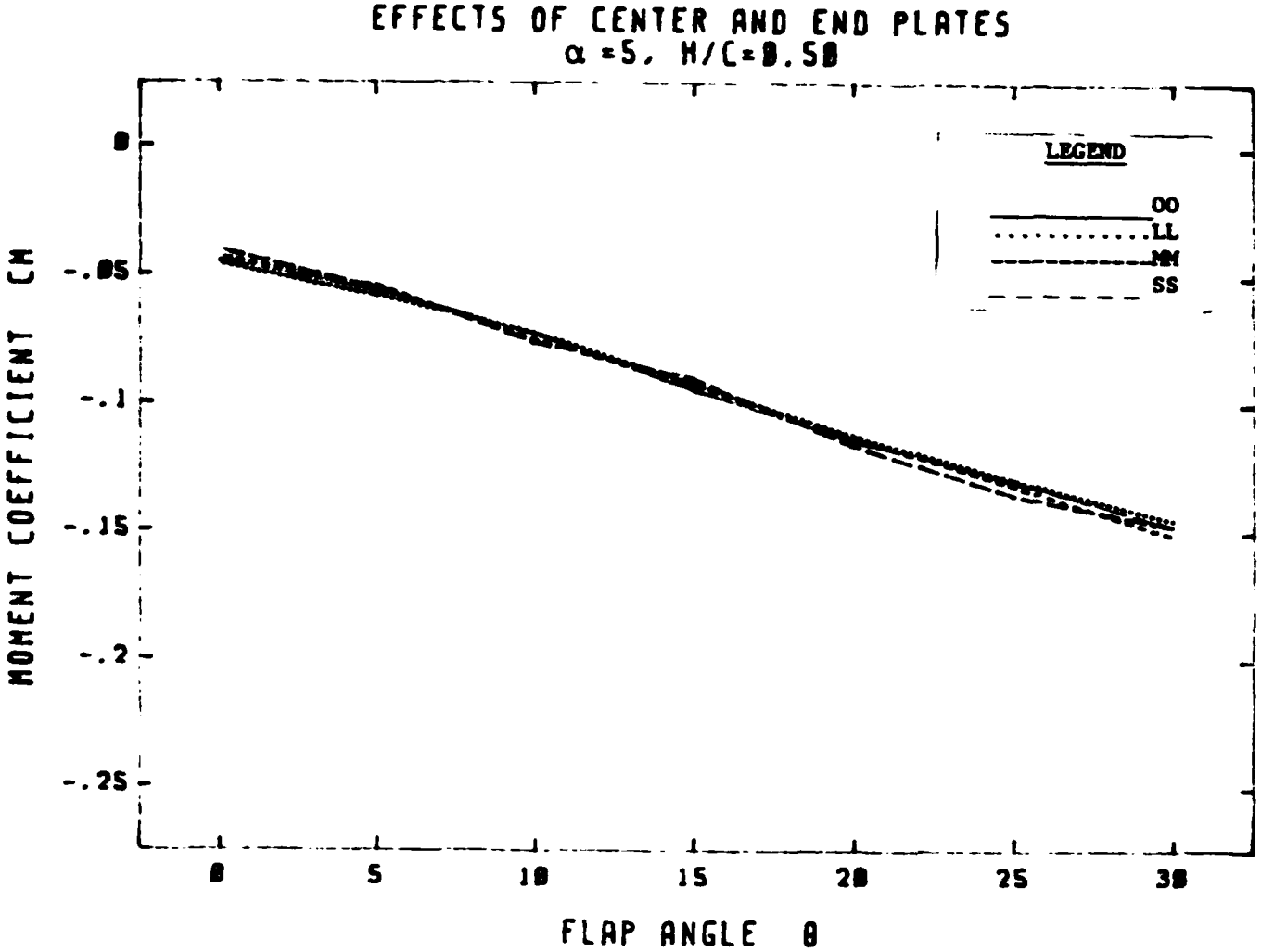

Fig. B-12 Effects of Center and End Plates, CM

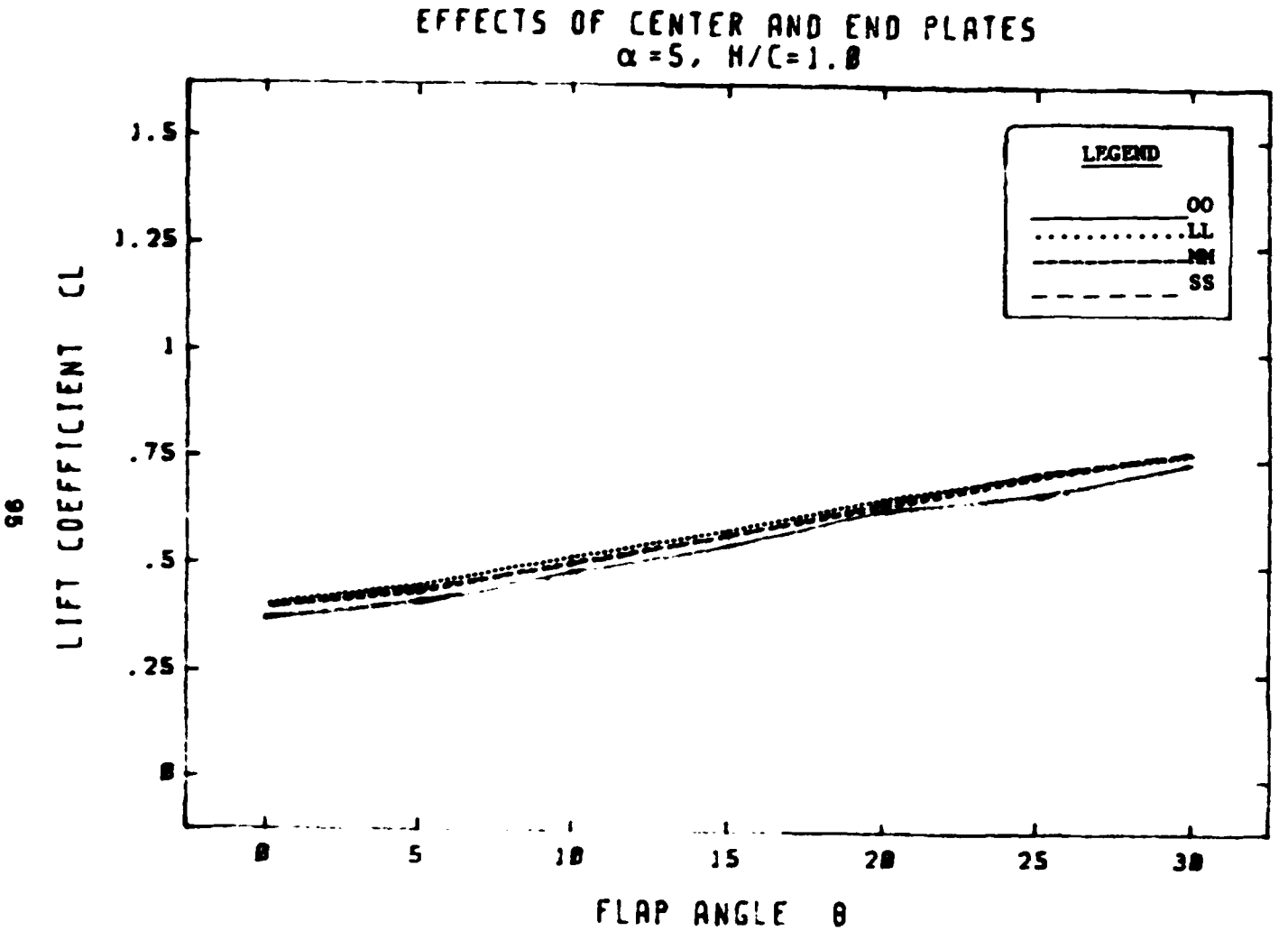

Fig. B-13 Effects of Center and End Plates, CL

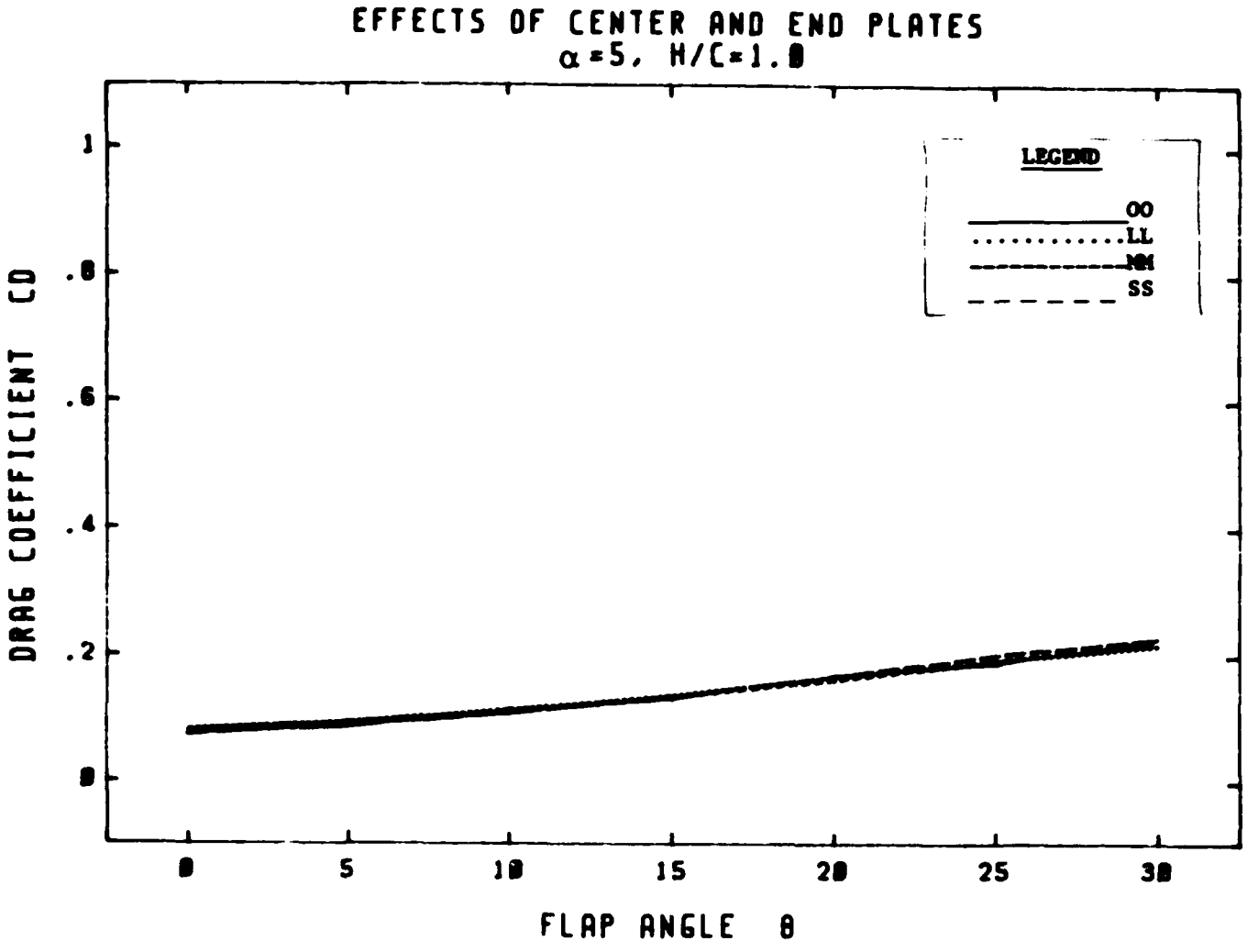

Fig. B-14 Effects of Center and End Plates, CD

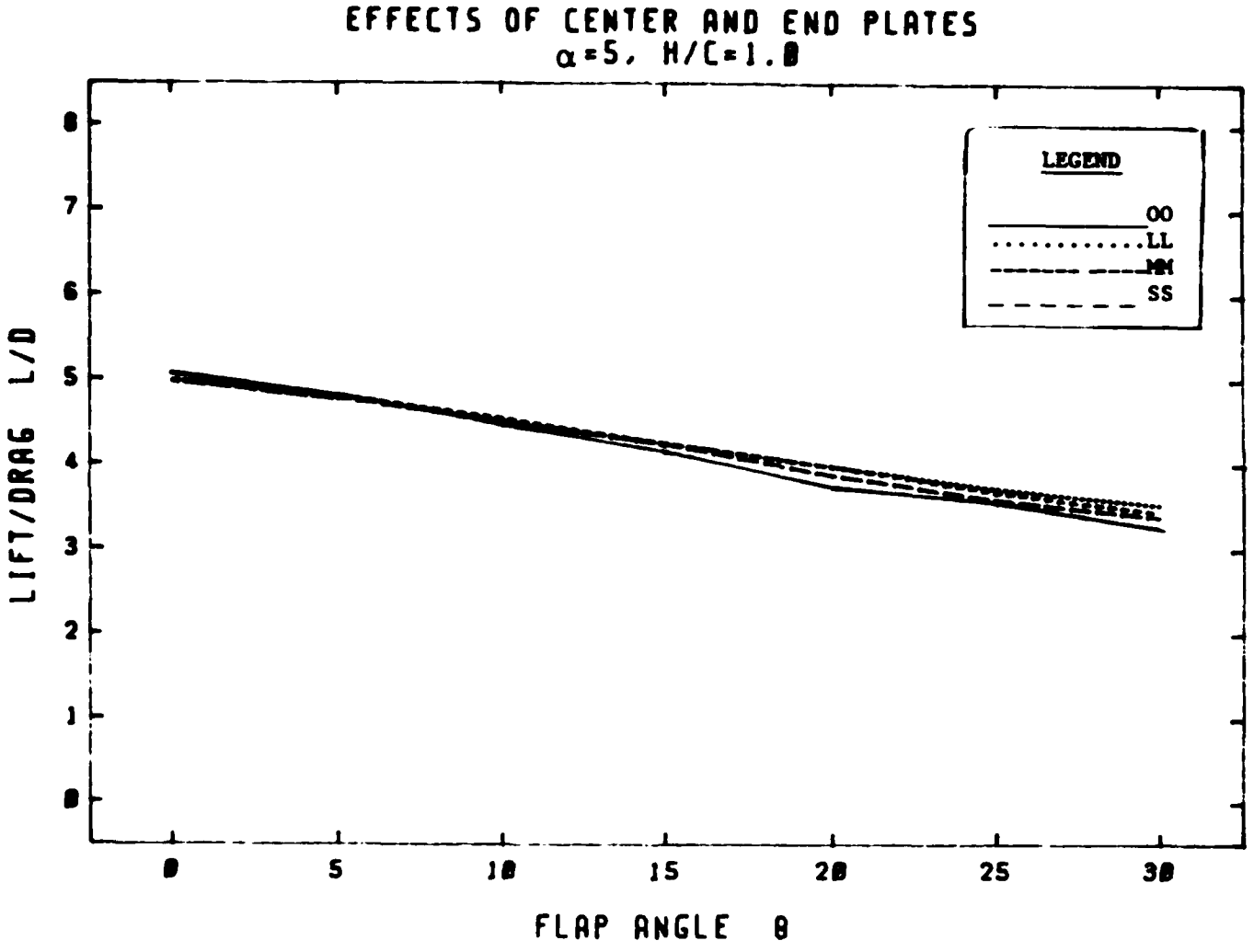

Fig. B-15 Effects of Center and End Plates, L/D

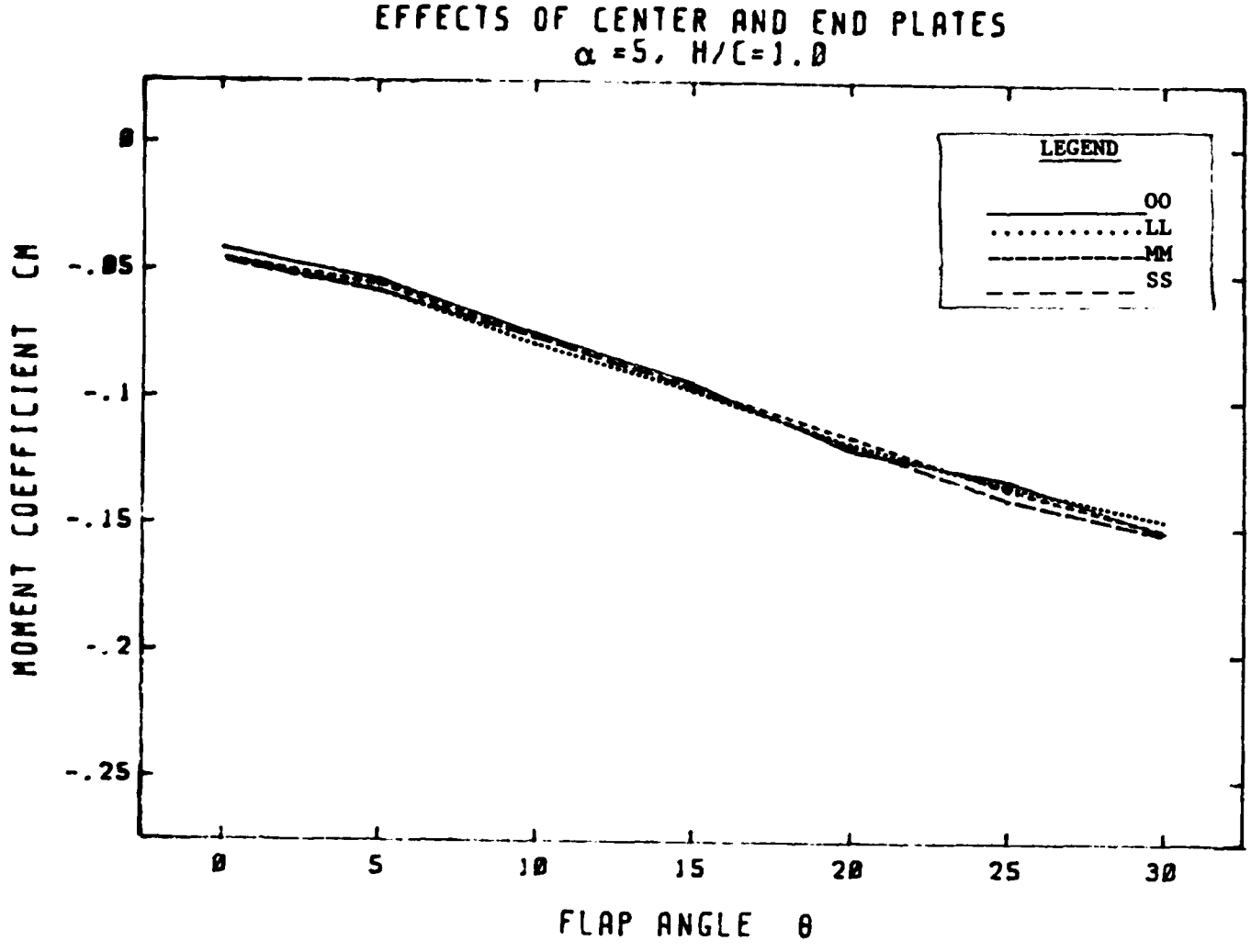

Fig. B-16 Effects of Center and End Plates, CM

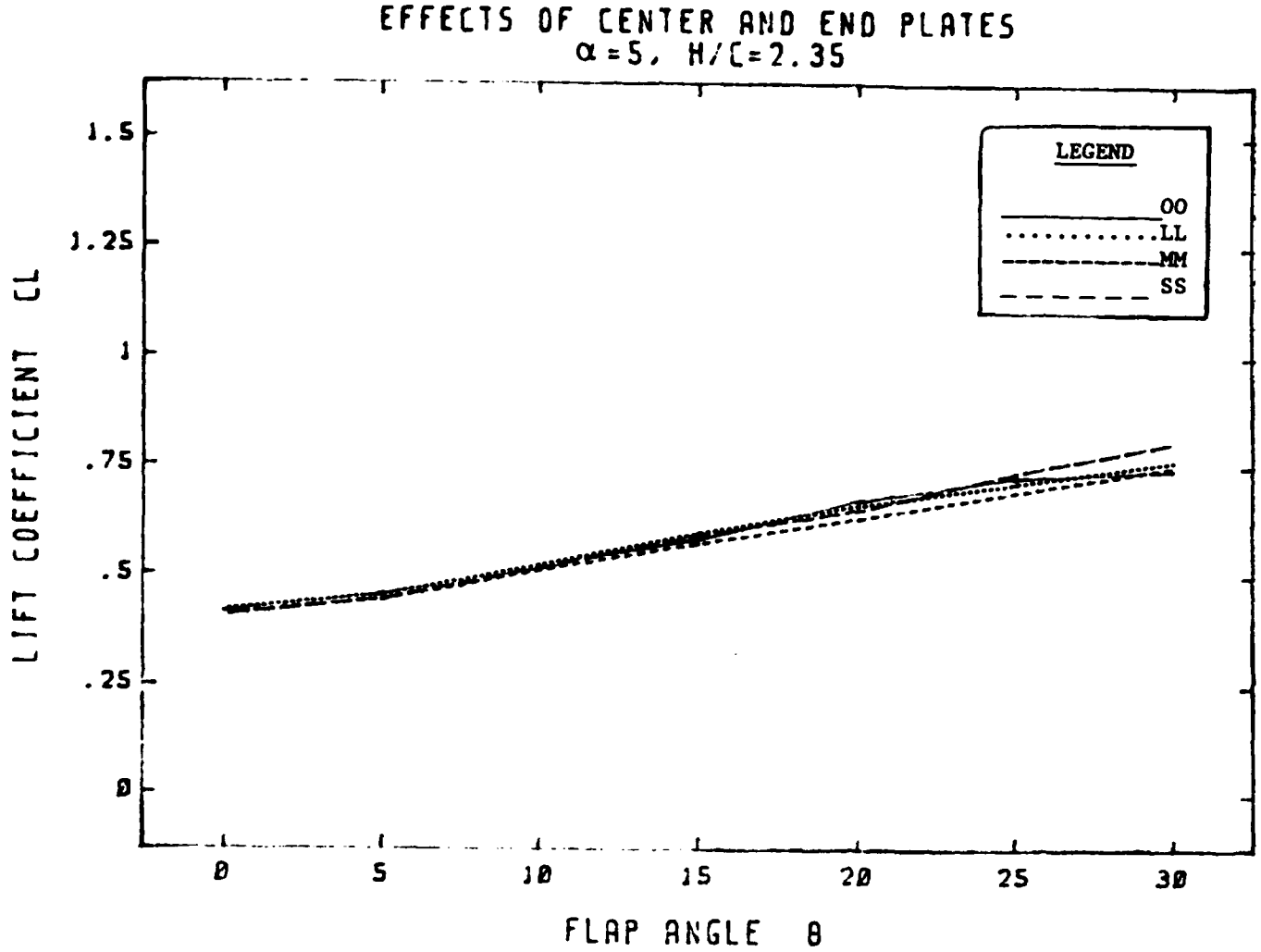

Fig. B-17 Effects of Center and End Plates, CL

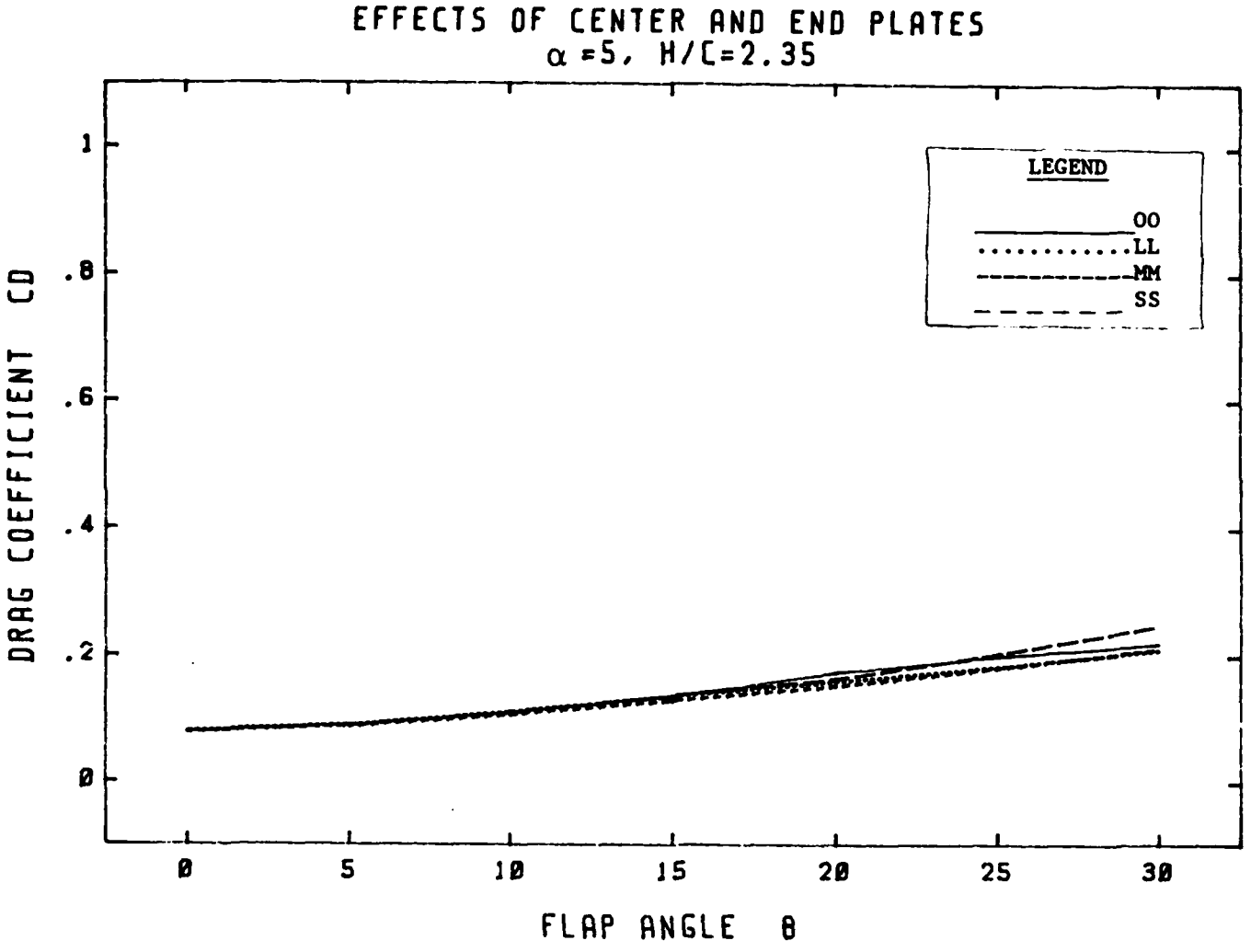

Fig. B-18 Effects of Center and End Plates, CD

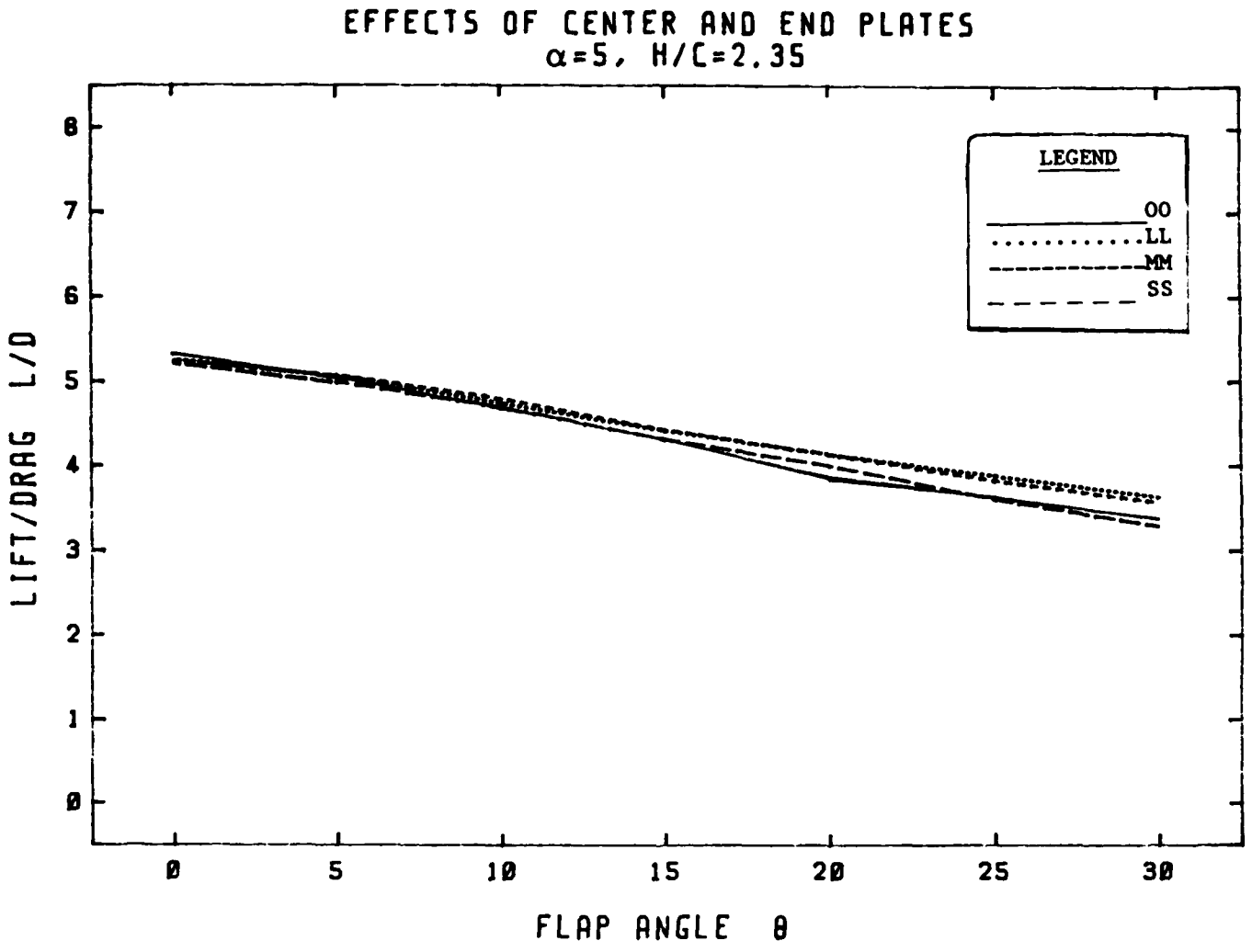

Fig. B-19 Effects of Center and End Plates, L/D

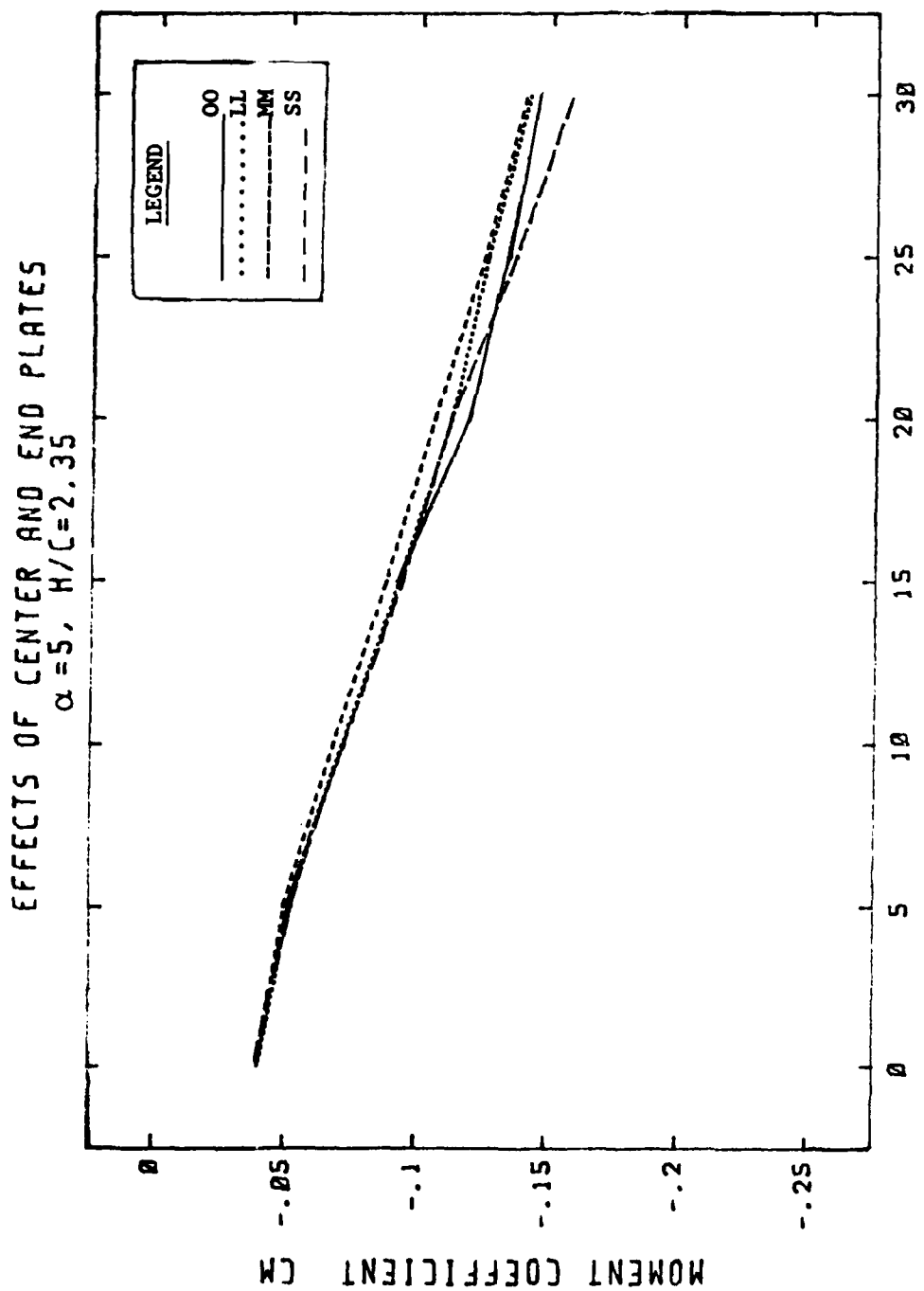

Fig. B-20 Effects of Center and End Plates, CM

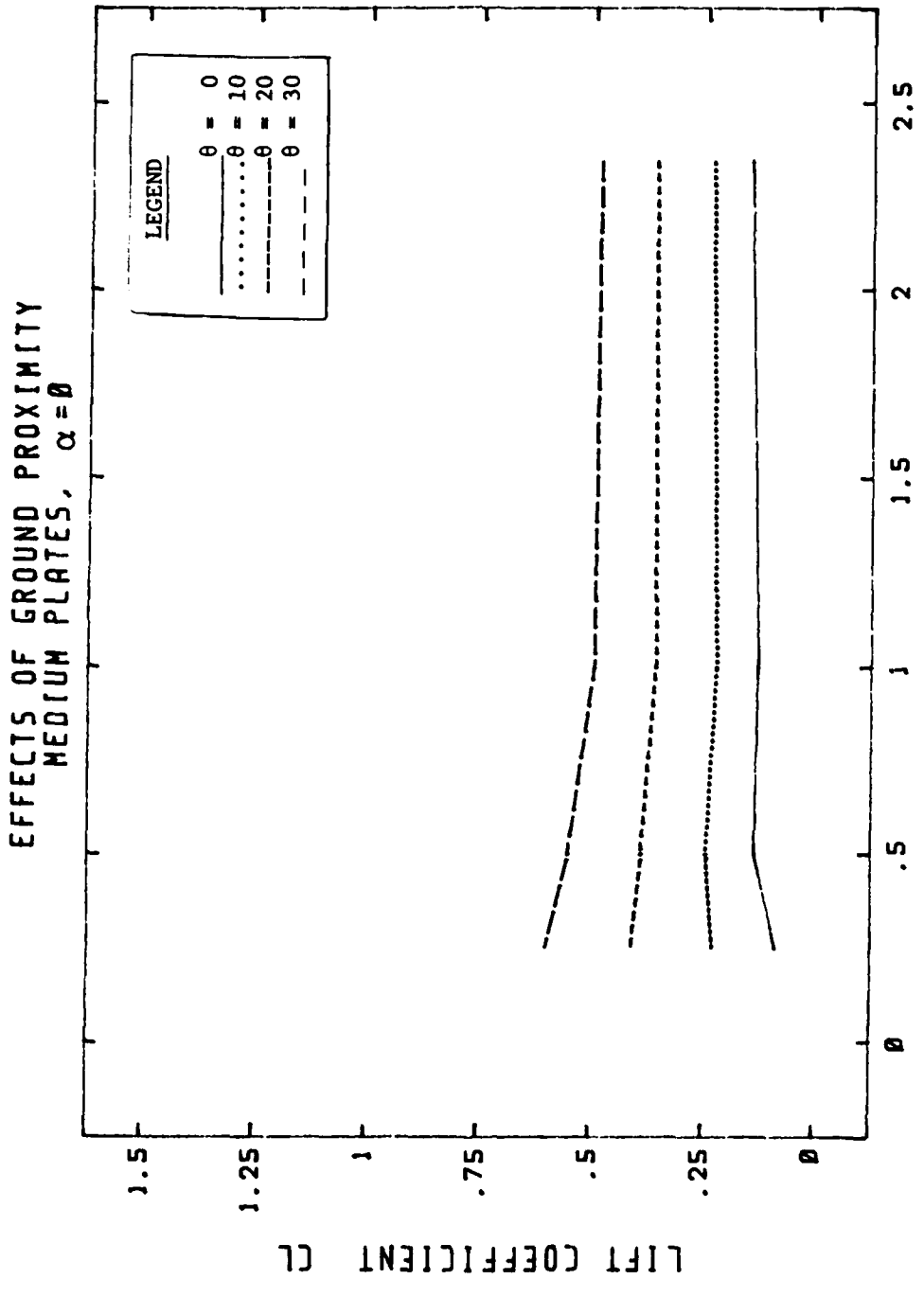

Fig. B-21 Effects of Ground Proximity, CL

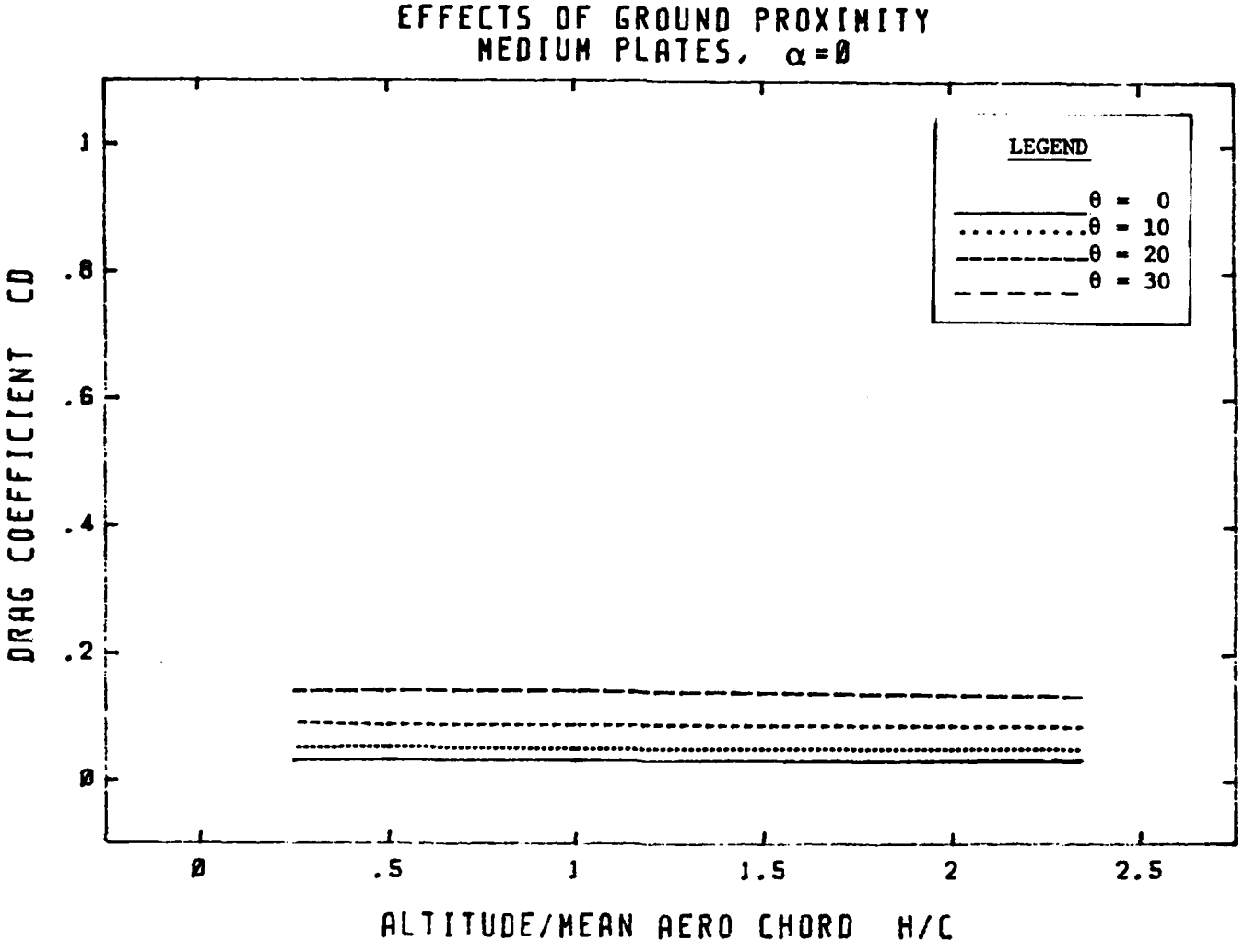

Fig. B-22 Effects of Ground Proximity, CD

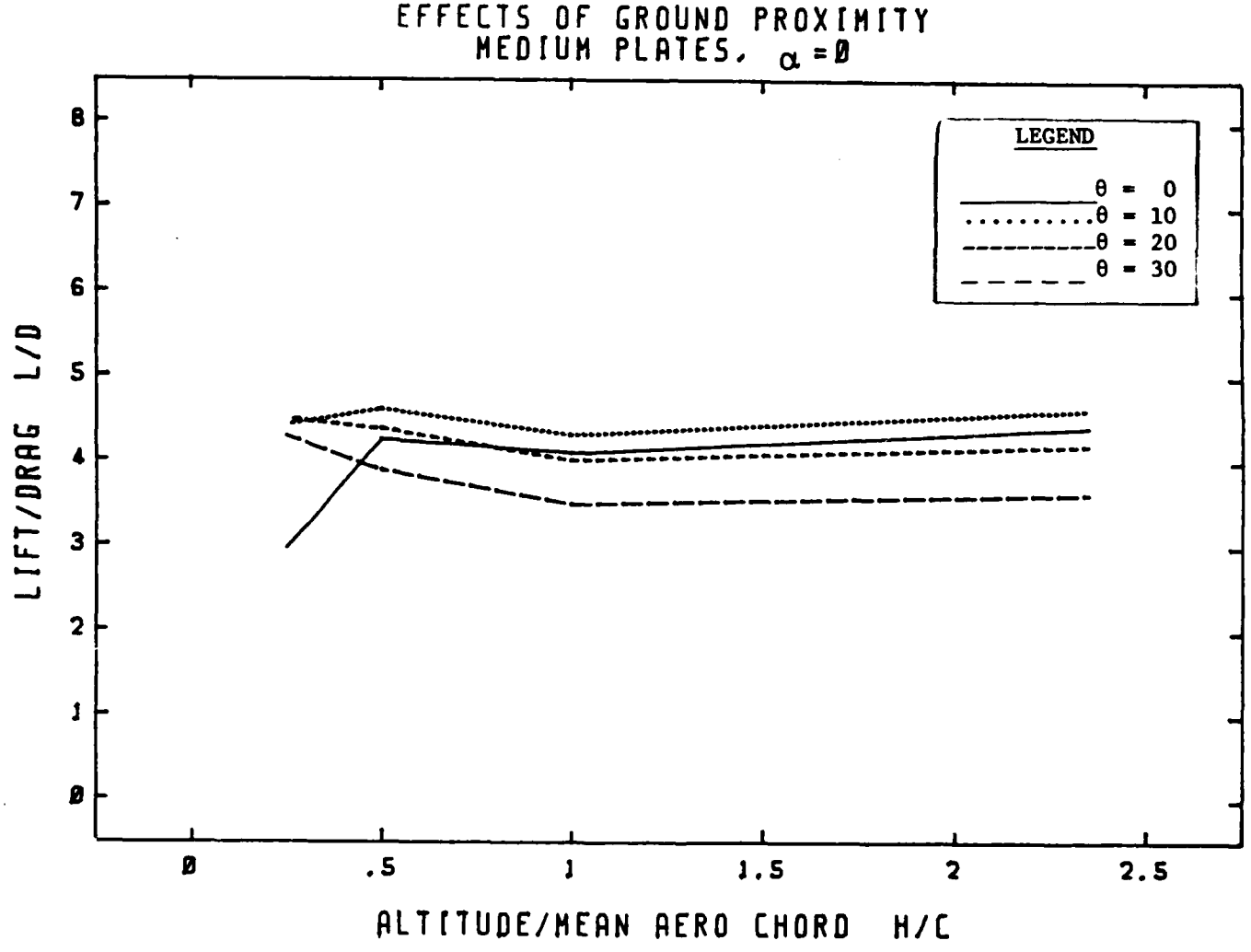

Fig. B-23 Effects of Ground Proximity, L/D

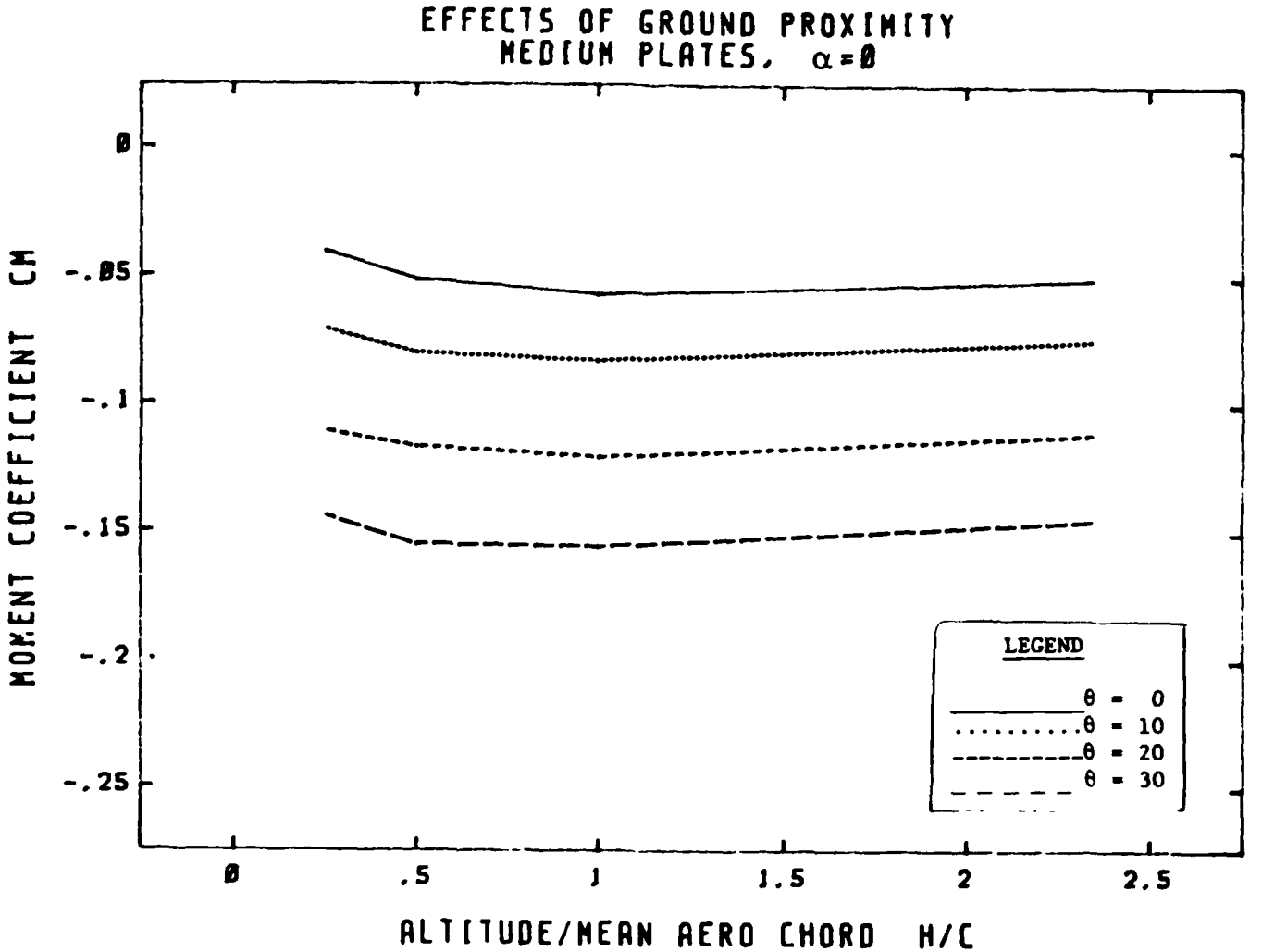

Fig. B-24 Effects of Ground Proximity, CM

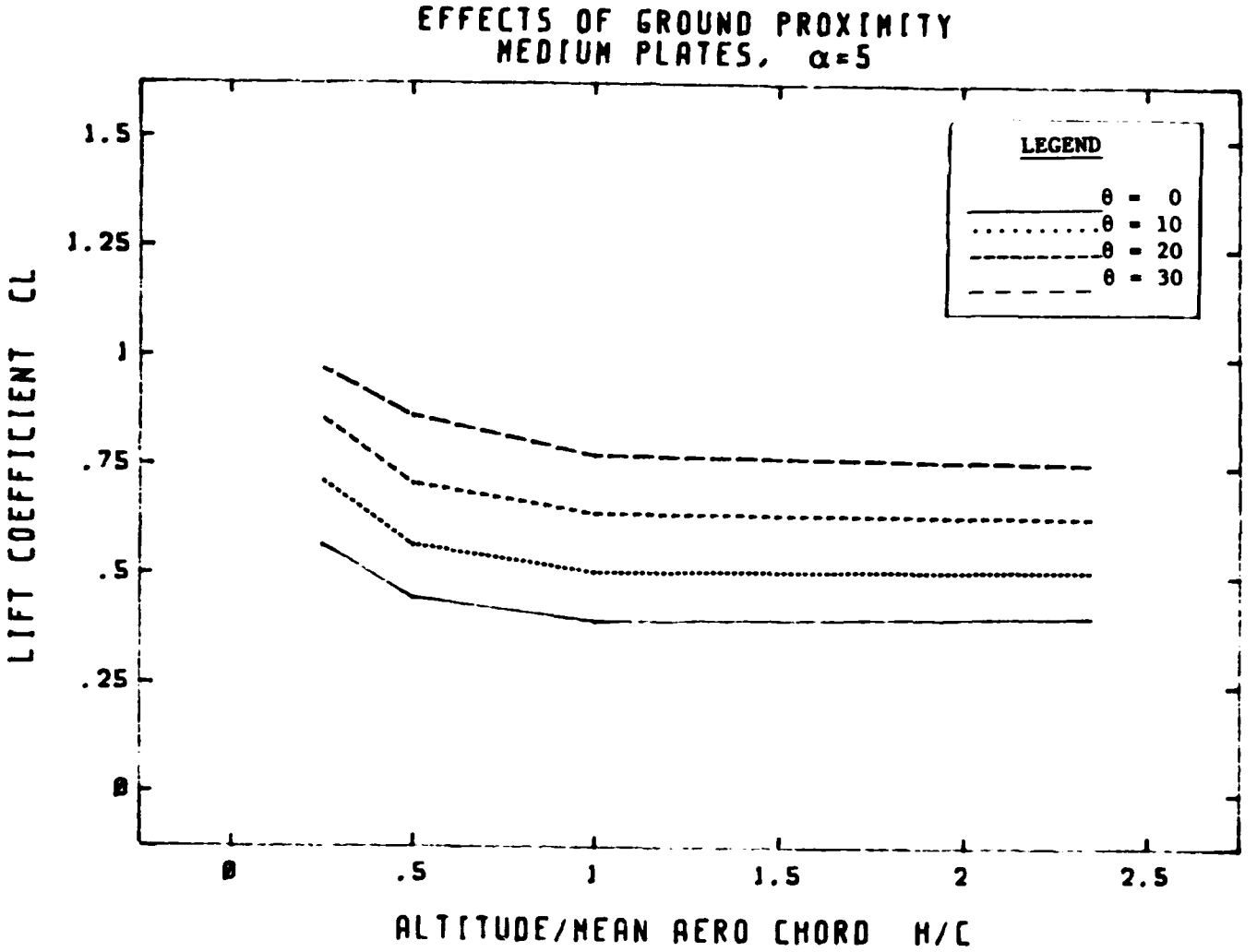

Fig. B-25 Effects of Ground Proximity, CL

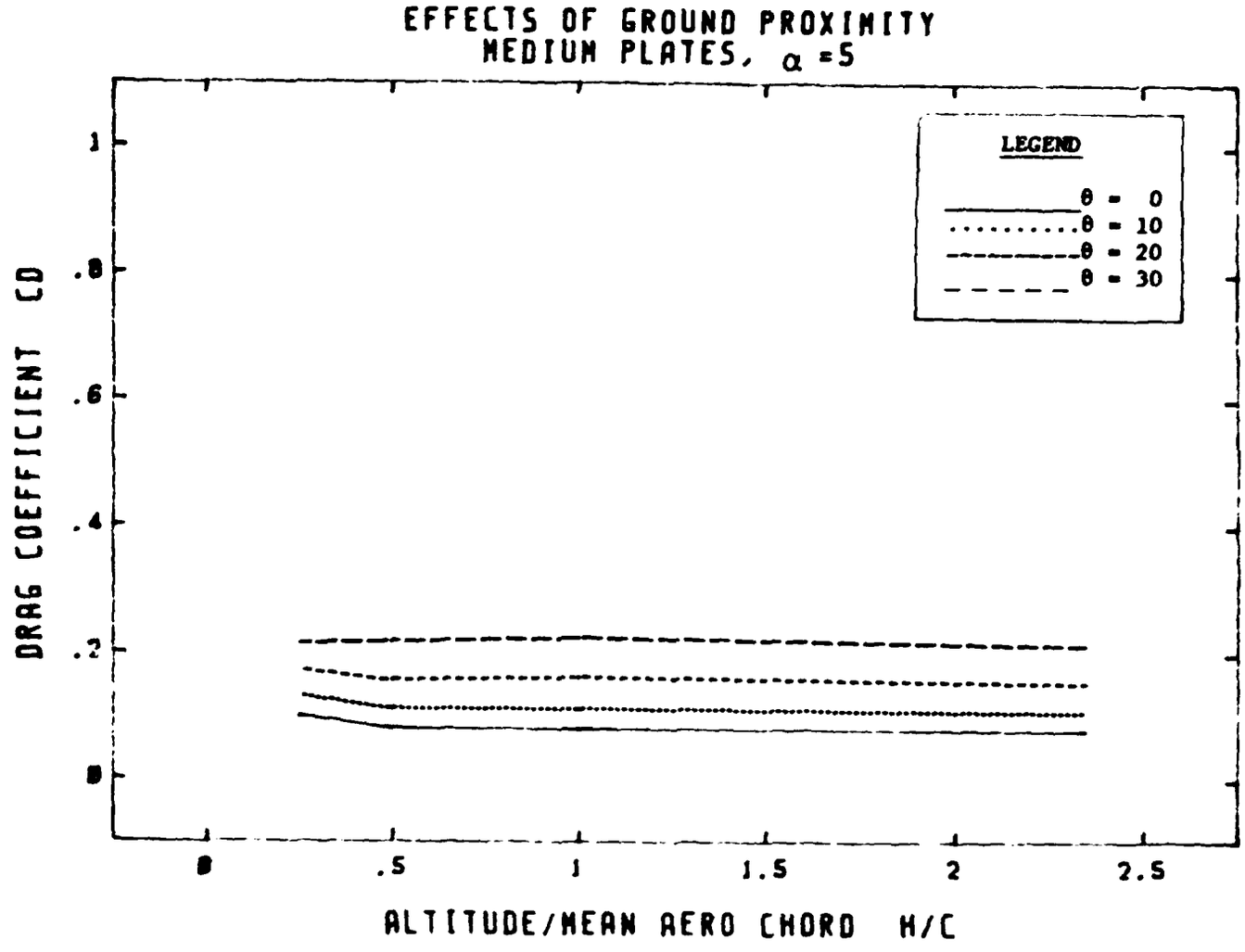

Fig. B-26 Effects of Ground Proximity, CD

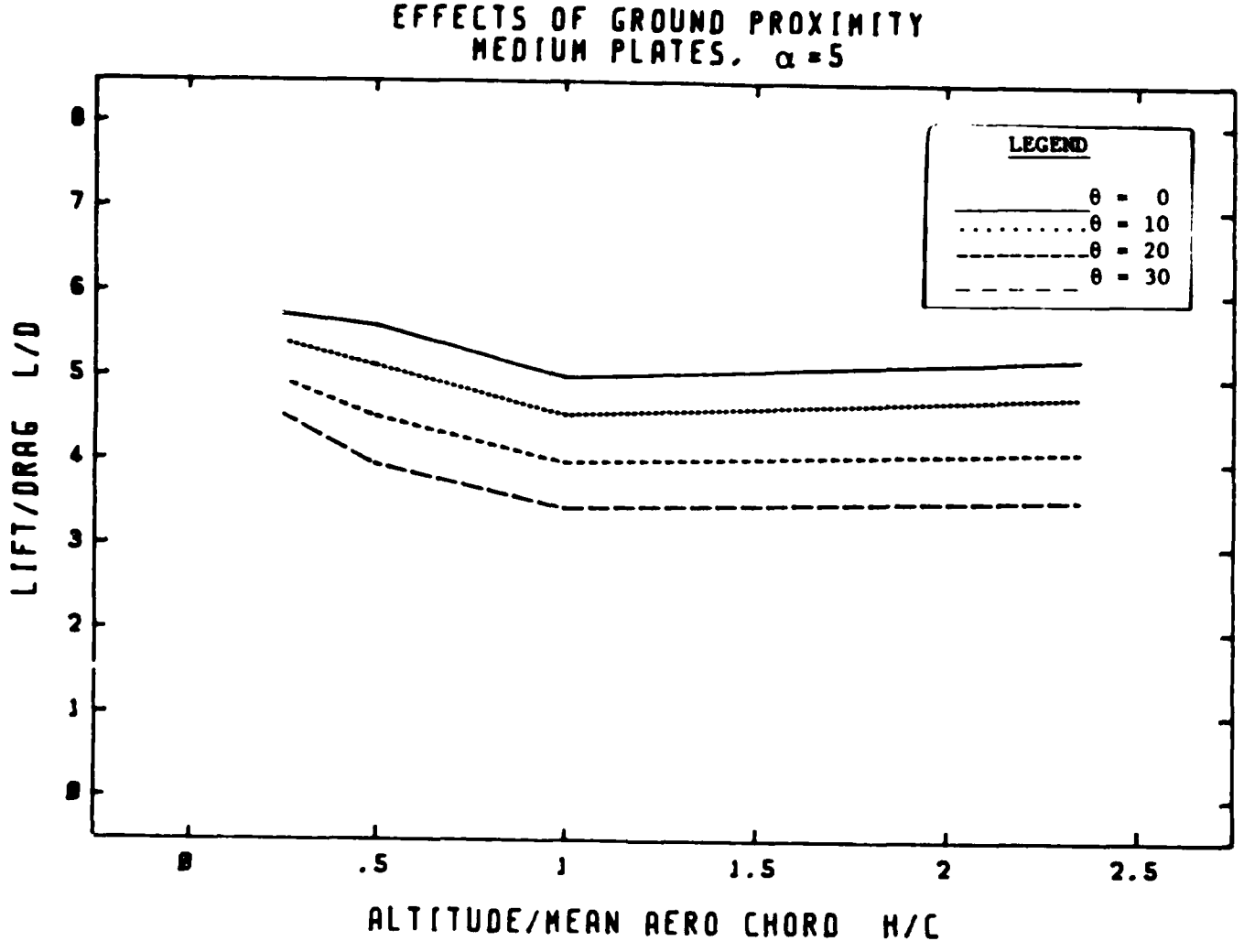

Fig. B-27 Effects of Ground Proximity, L/D

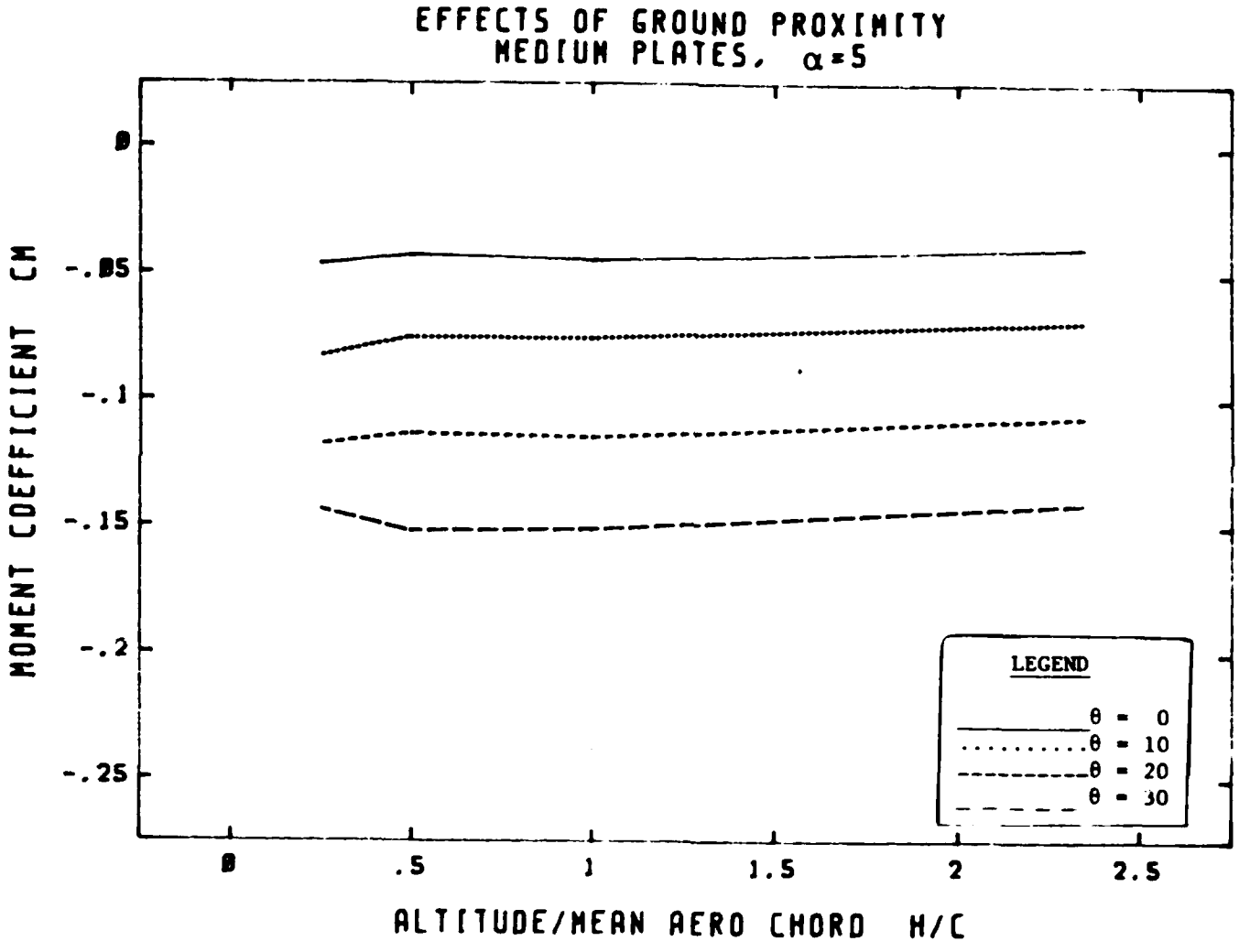

Fig. B-28 Effects of Ground Proximity, CM

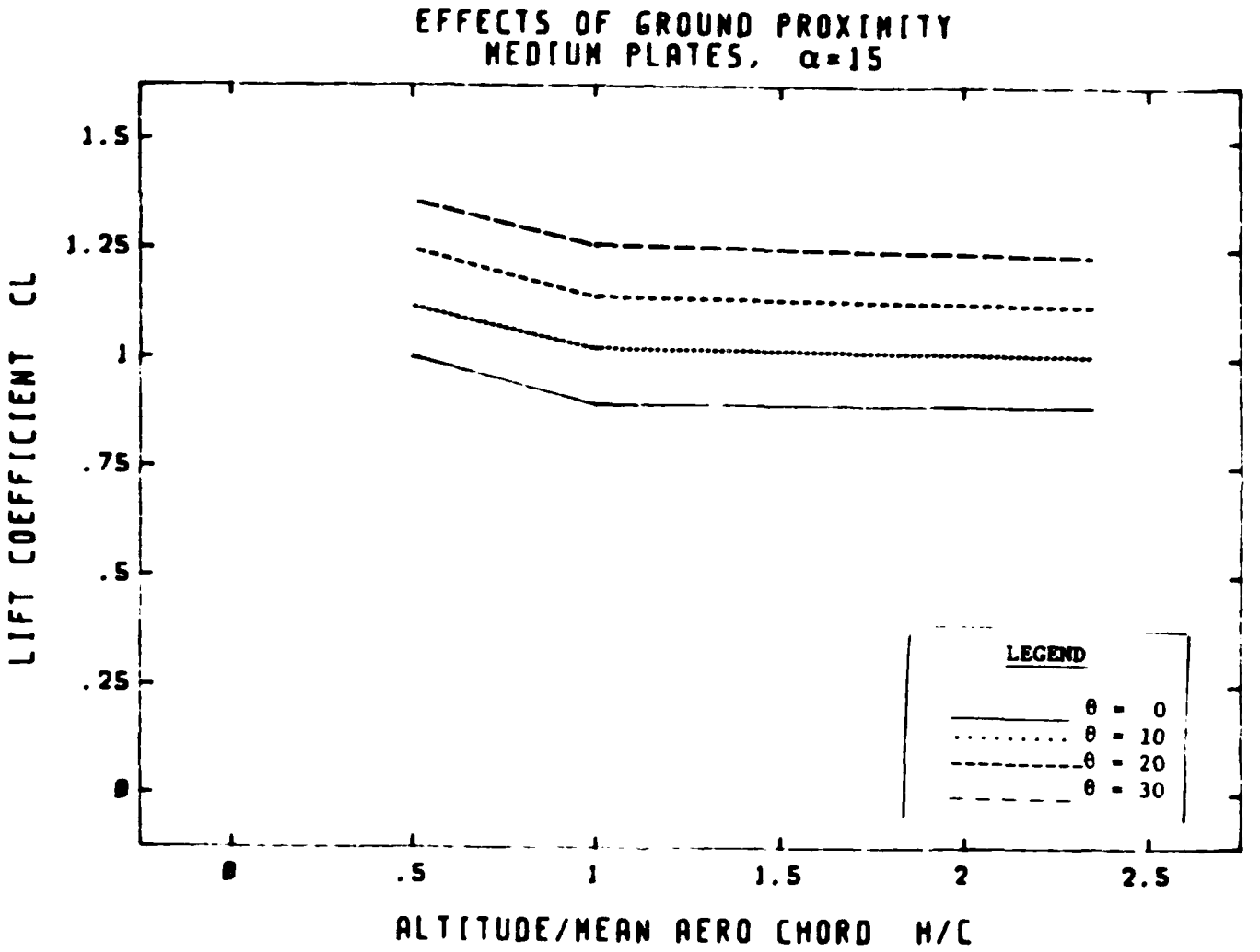

Fig. B-29 Effects of Ground Proximity, CL

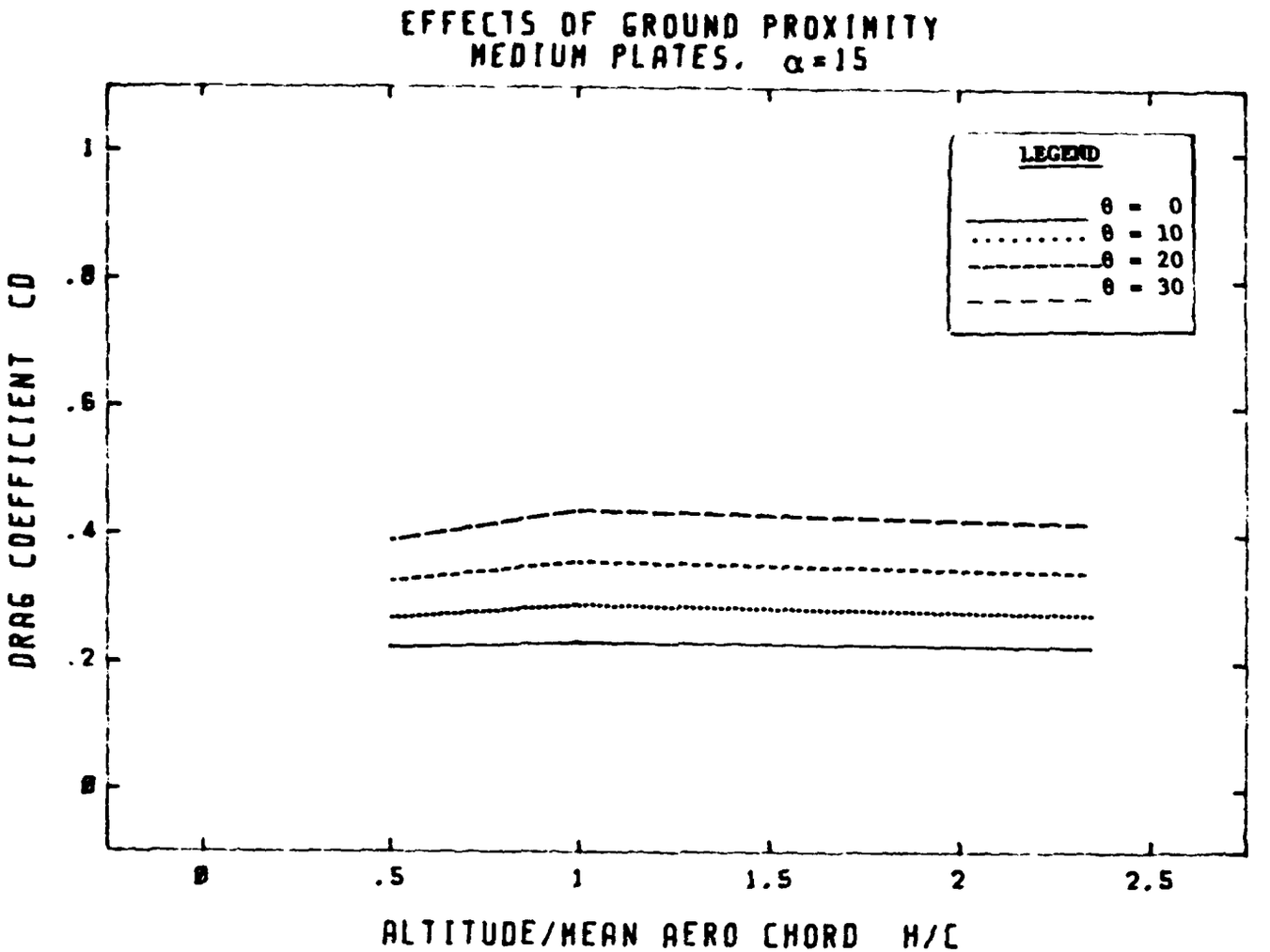

Fig. B-30 Effects of Ground Proximity, CD

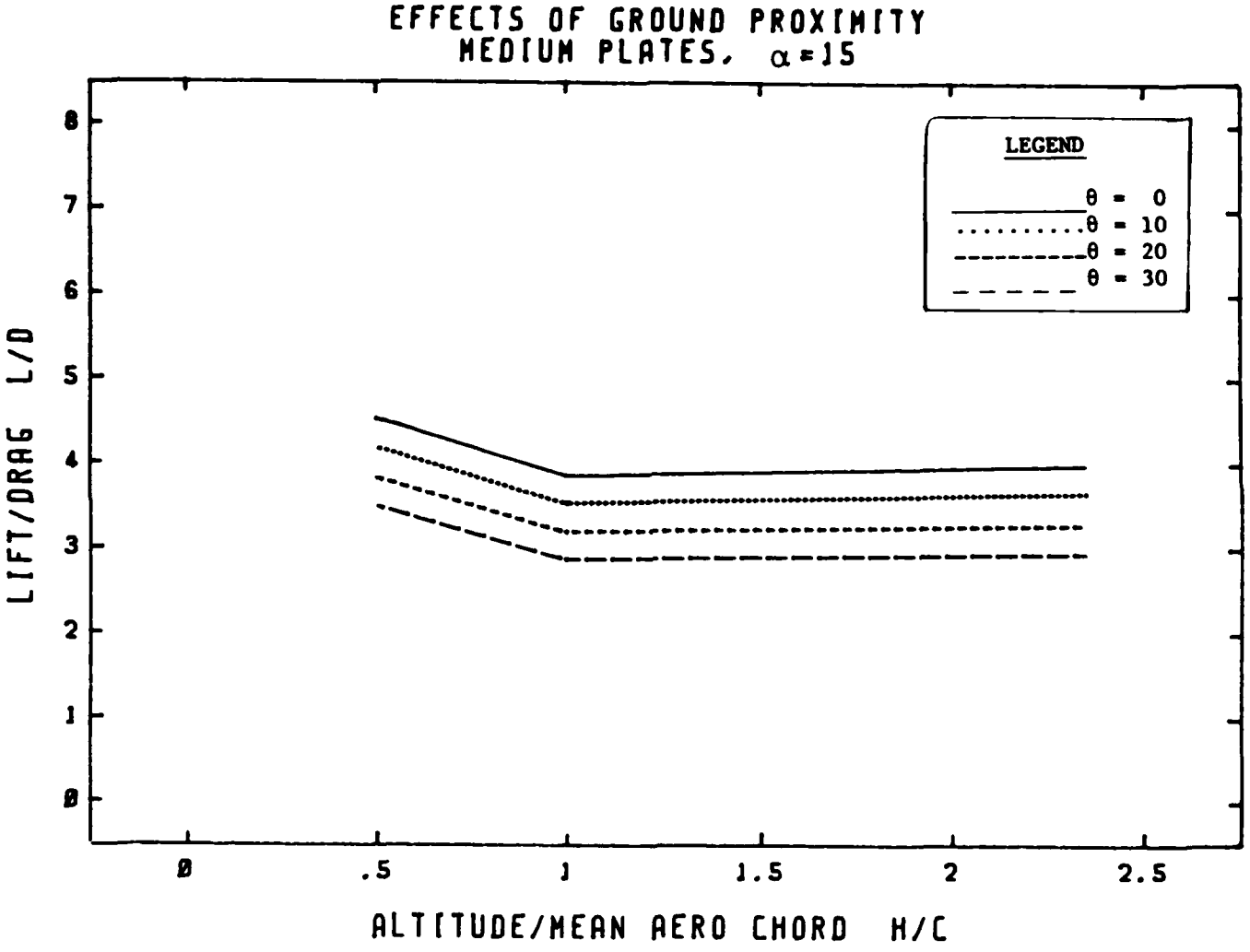

Fig. B-31 Effects of Ground Proximity, L/D

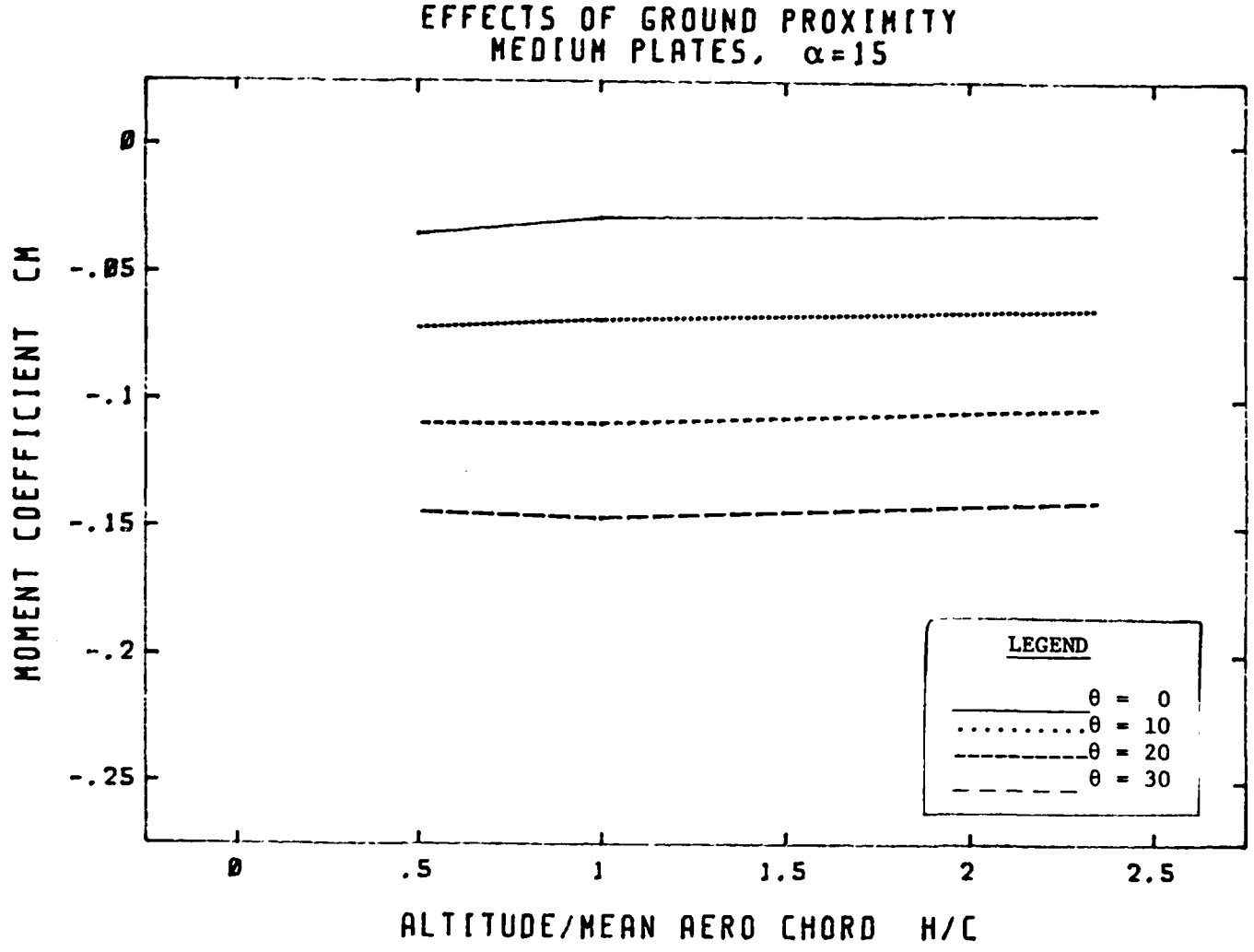

Fig. B-32 Effects of Ground Proximity, CM

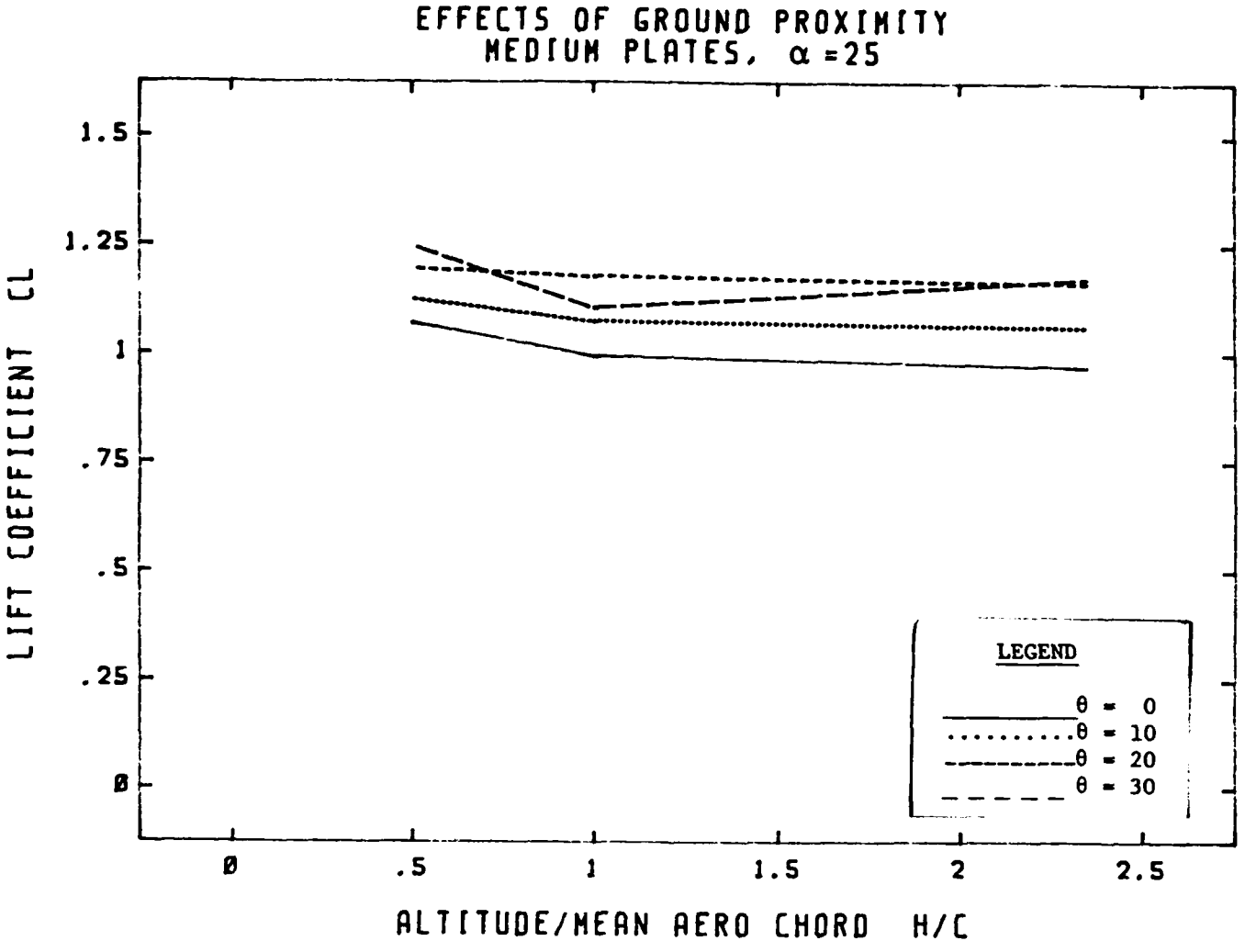

Fig. B-33 Effects of Ground Proximity, CL

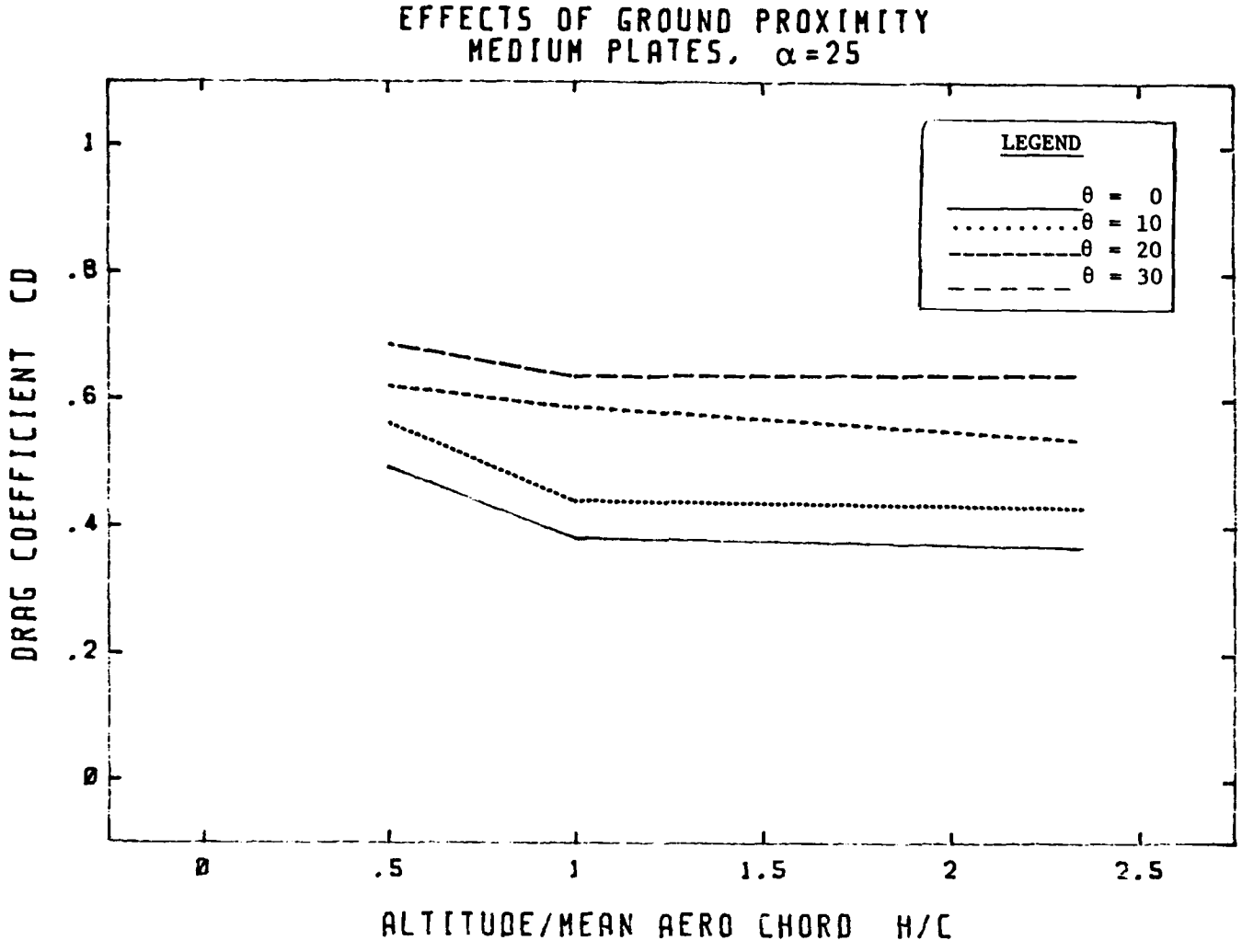

Fig. B-34 Effects of Ground Proximity, CD

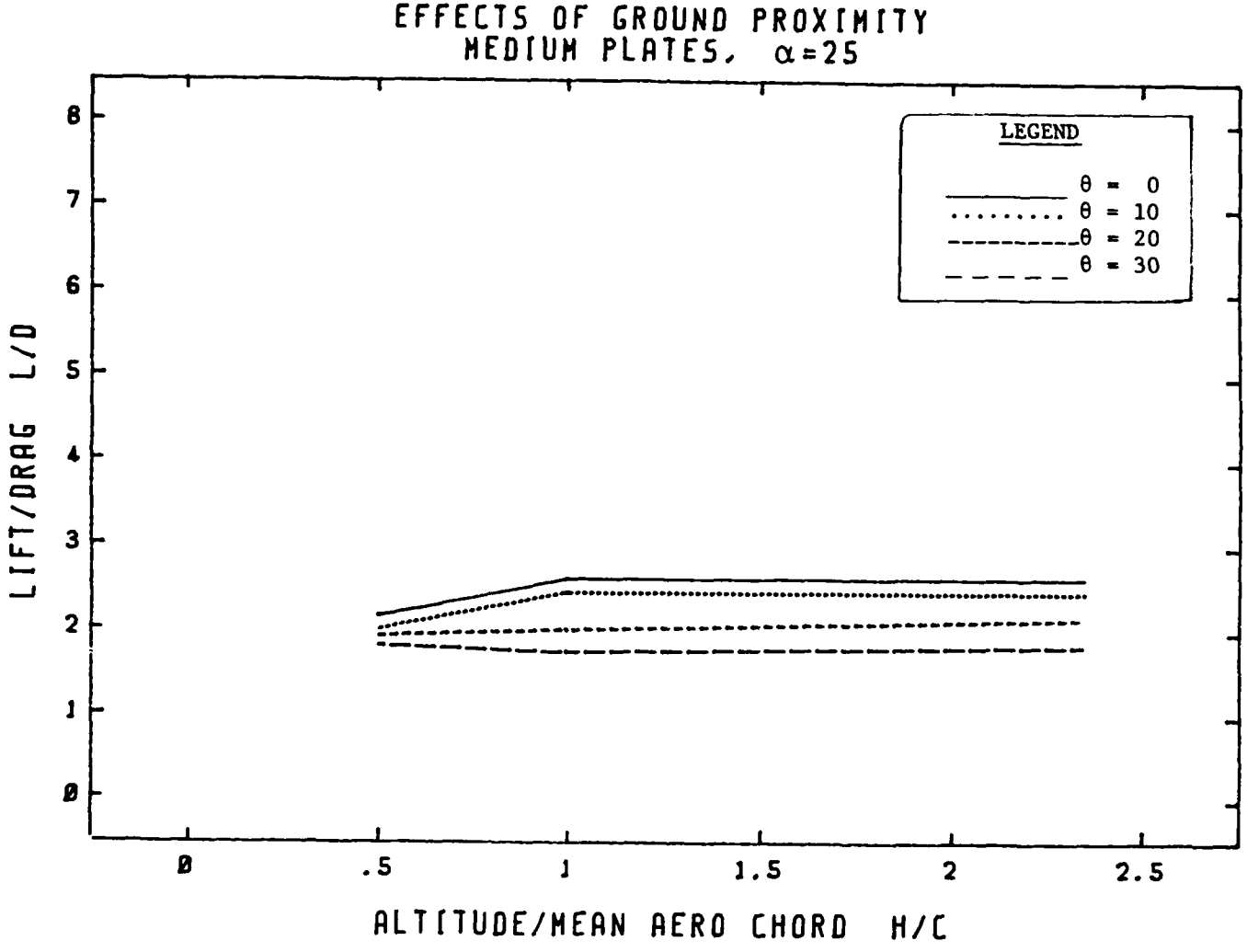

Fig. B-35 Effects of Ground Proximity, L/D

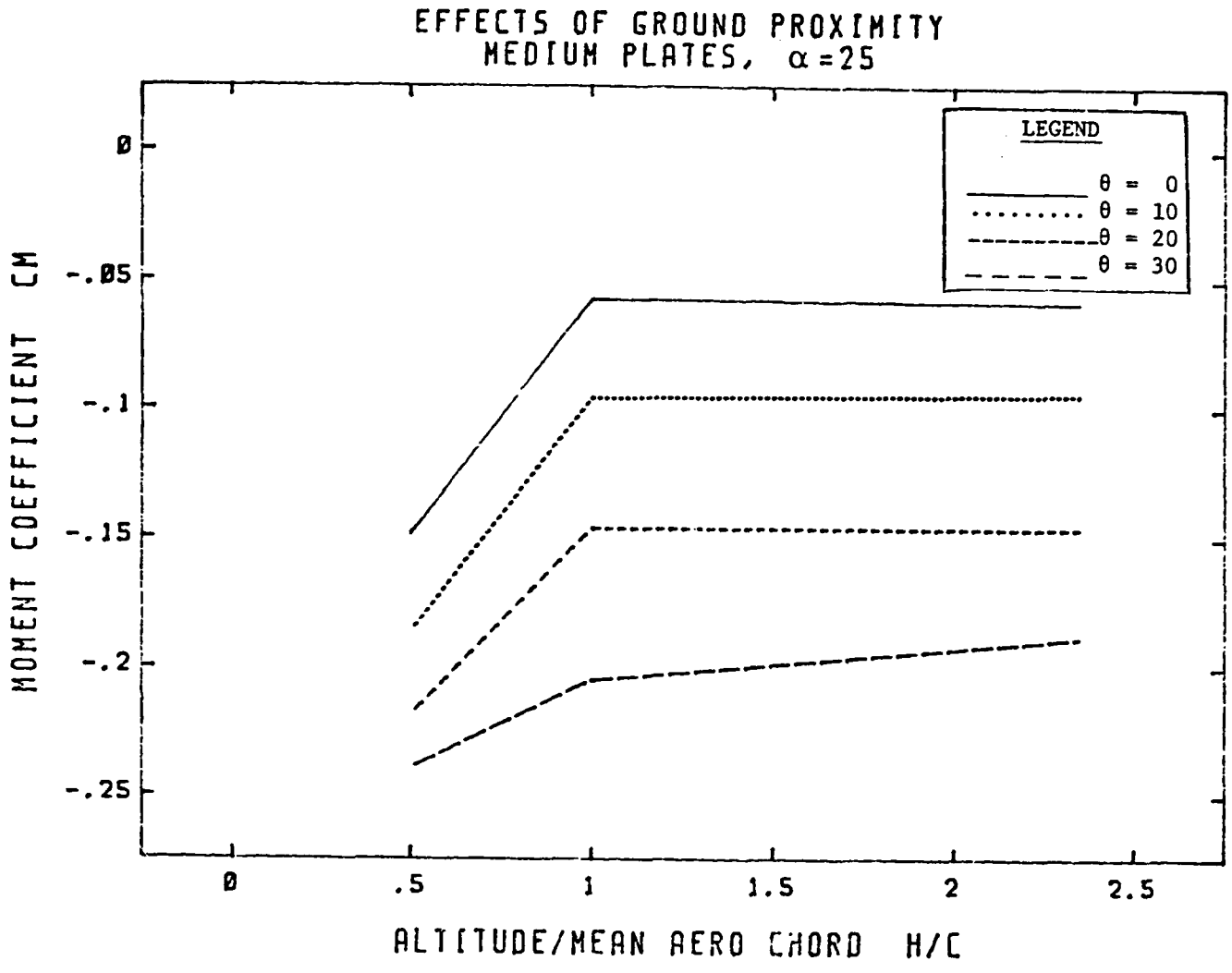

Fig. B-36 Effects of Ground Proximity, CM

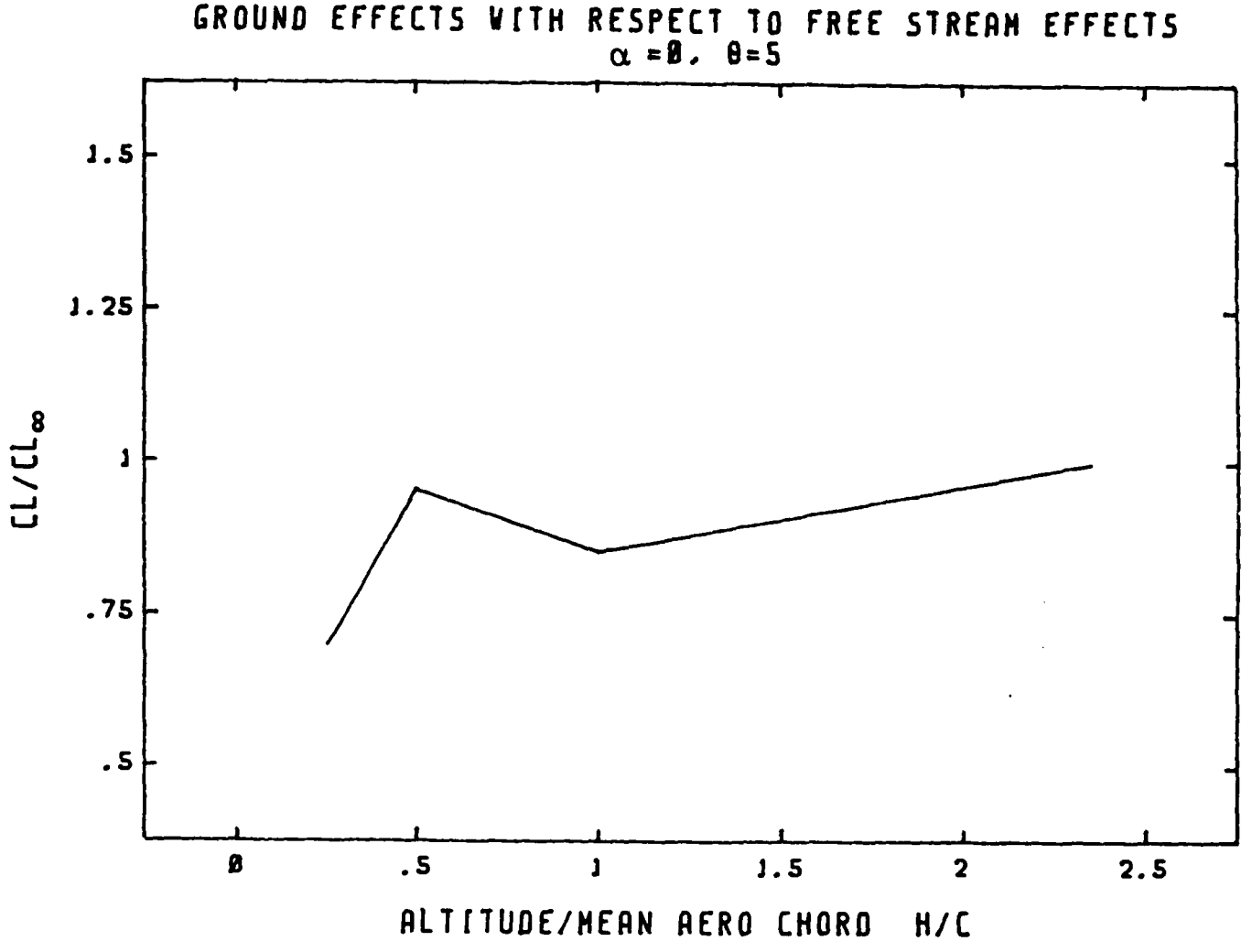

Fig. B-37 Ground Effects With Respect to Freestream Effects, CL

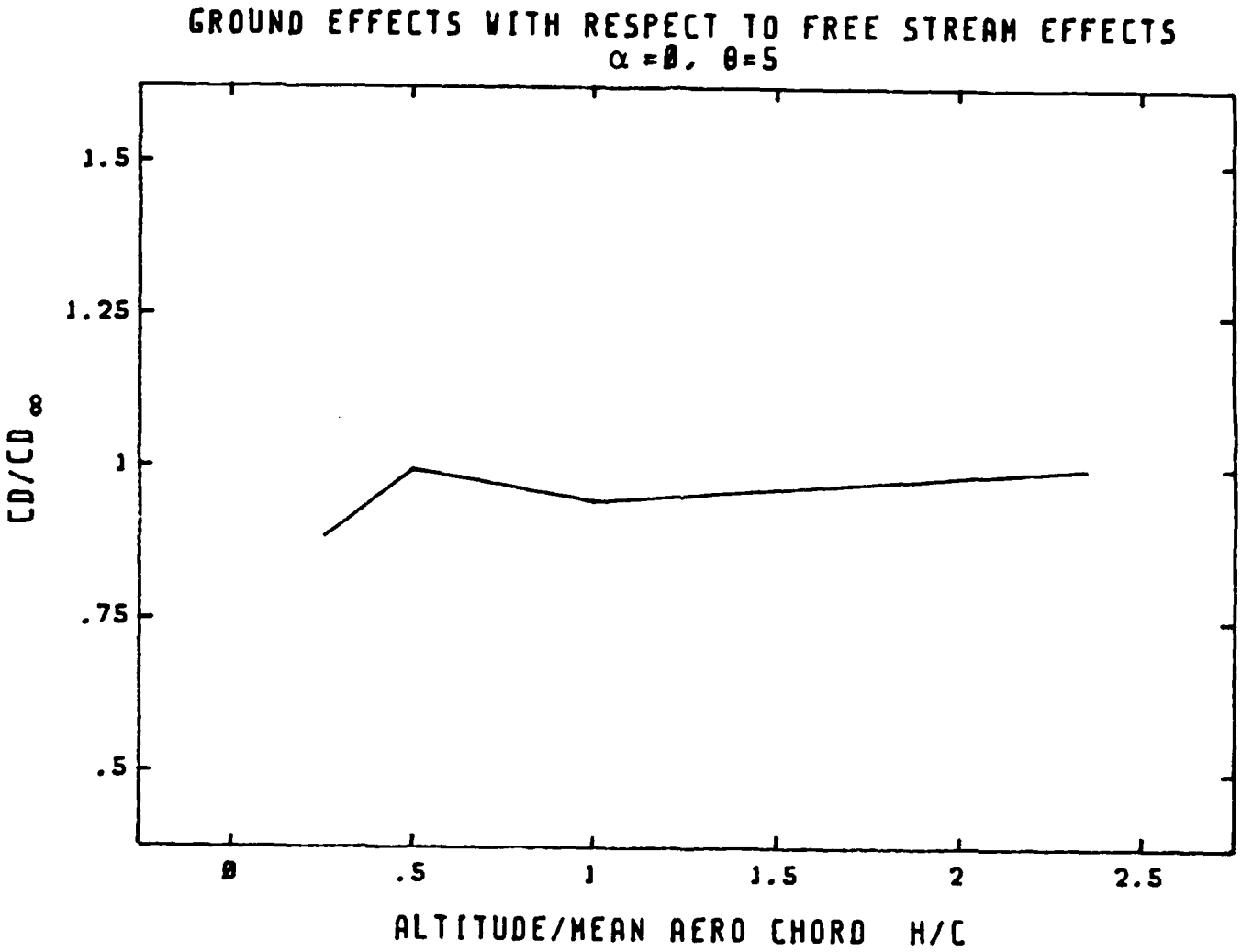

Fig. B-38 Ground Effects With Respect to Freestream Effects, CD

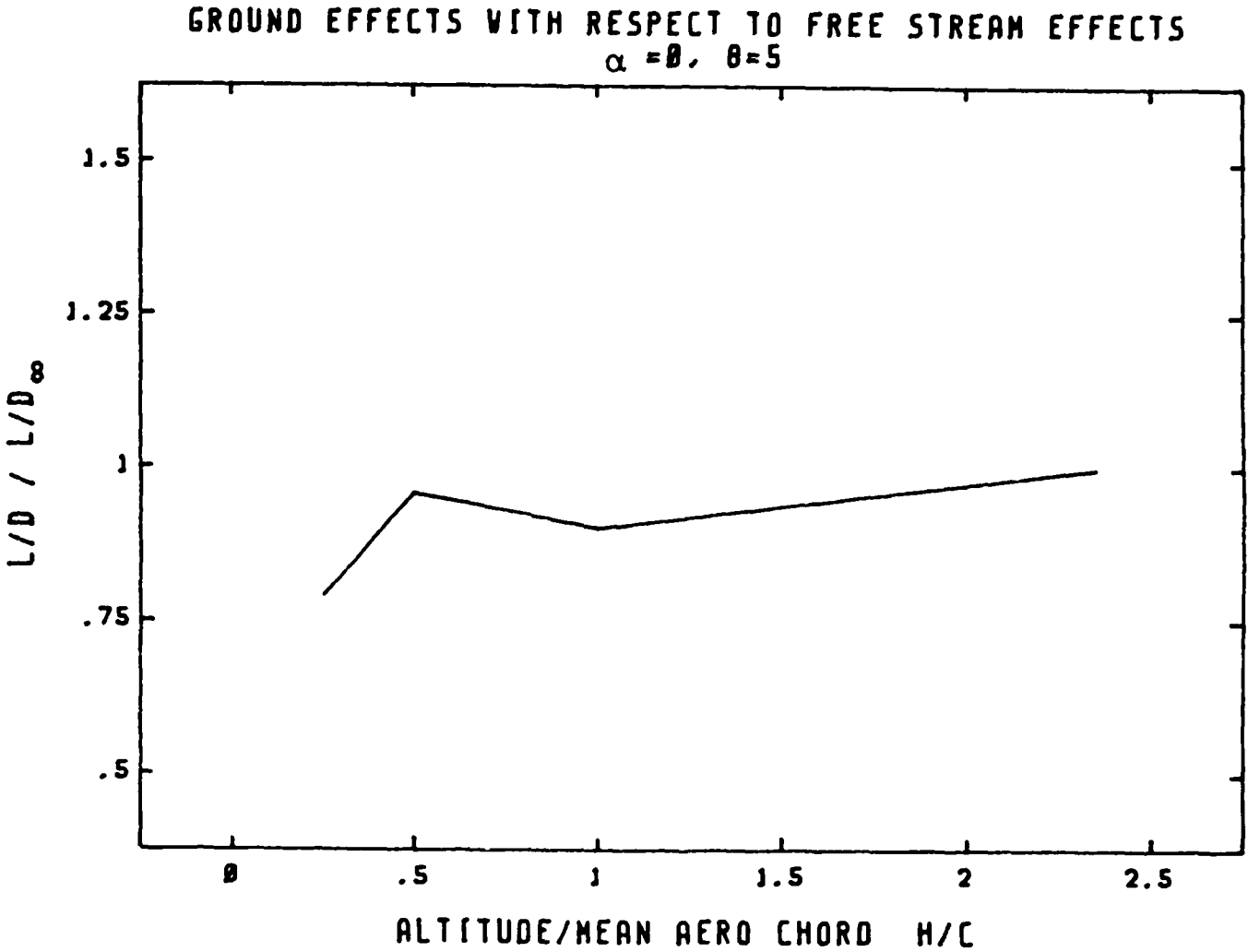

Fig. B-39 Ground Effects With Respect to Freestream Effects, L/D

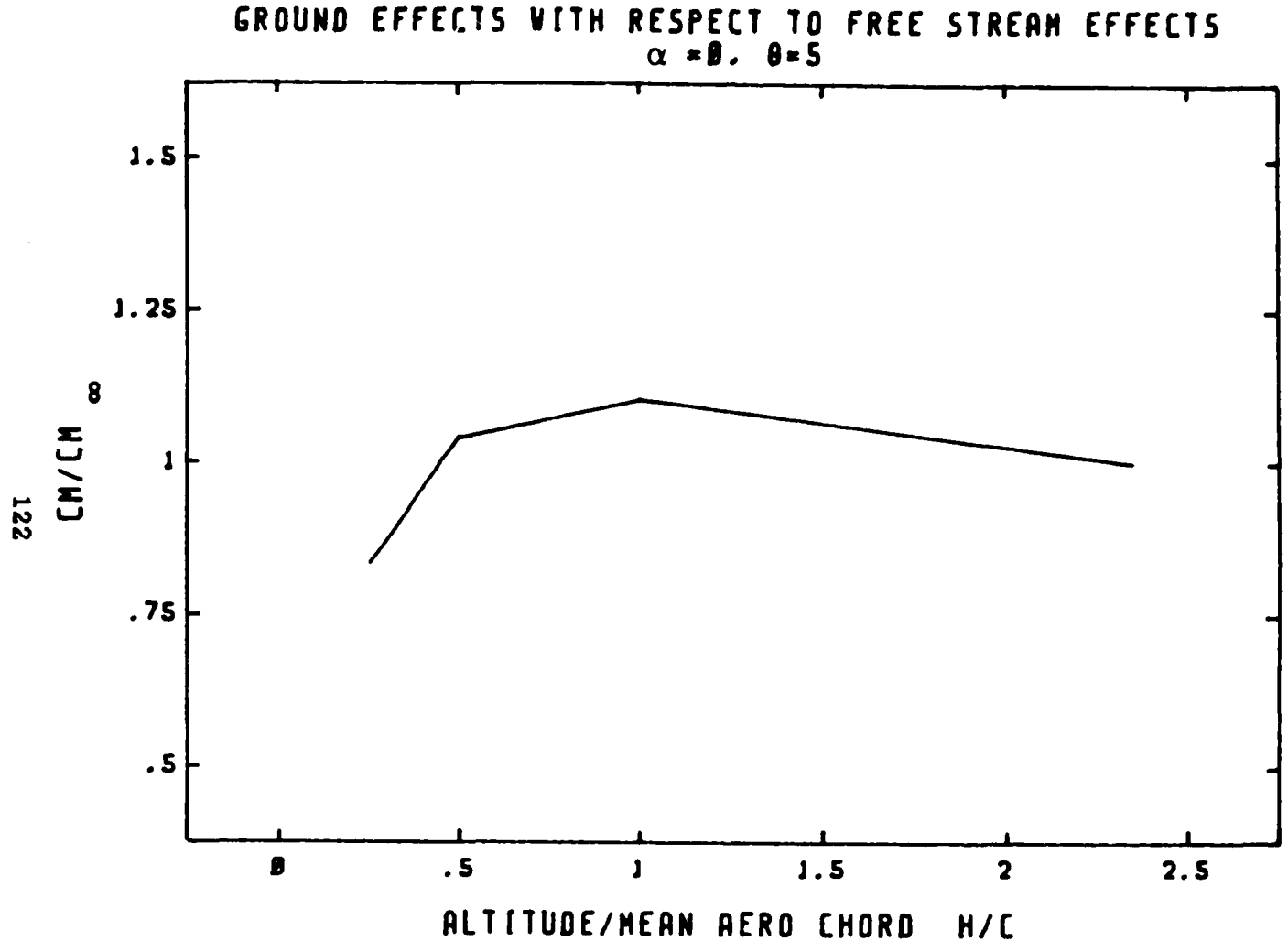

Fig. B-40 Ground Effects With Respect to Freestream Effects, CM

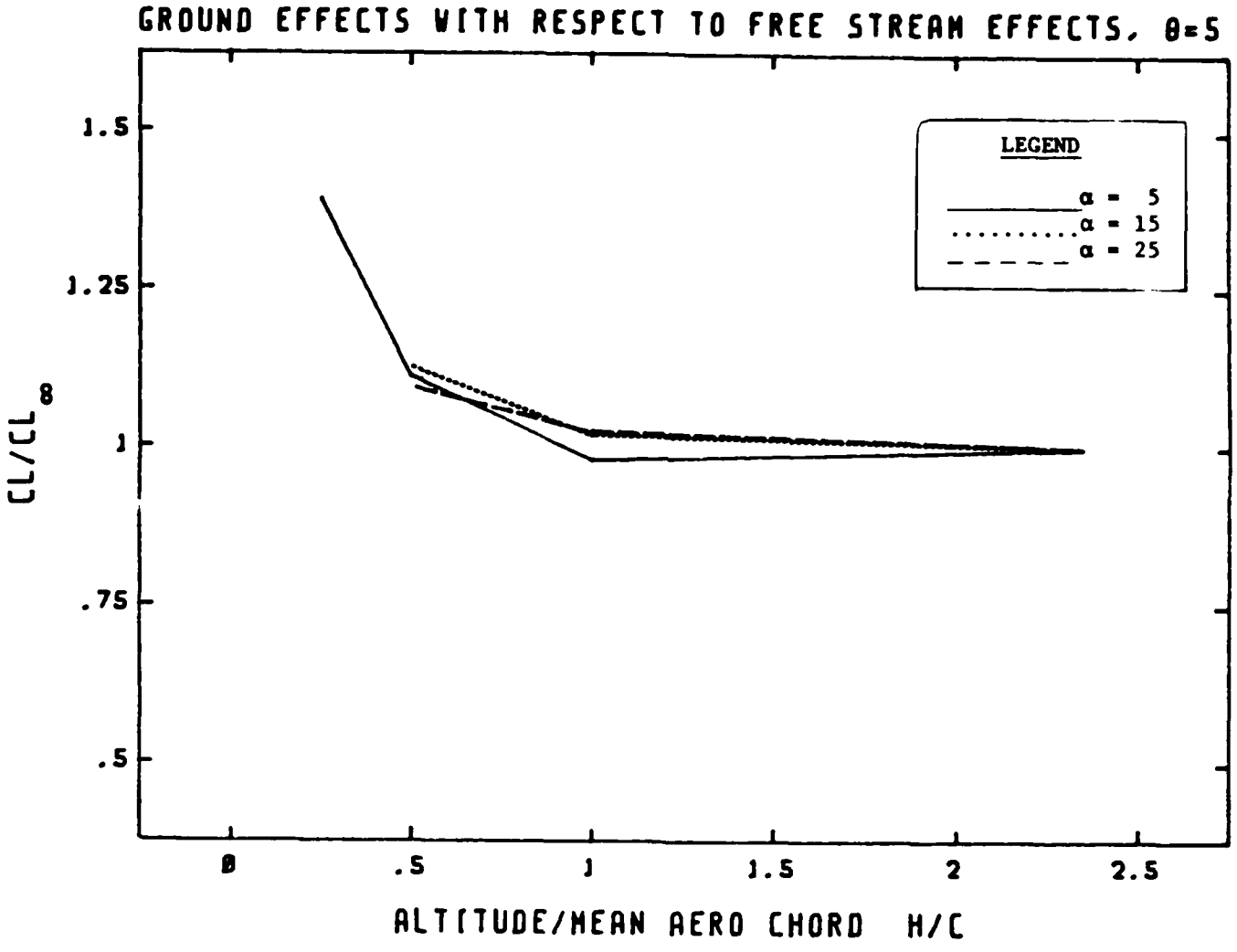

Fig. B-41 Ground Effects With Respect to Freestream Effects, CL

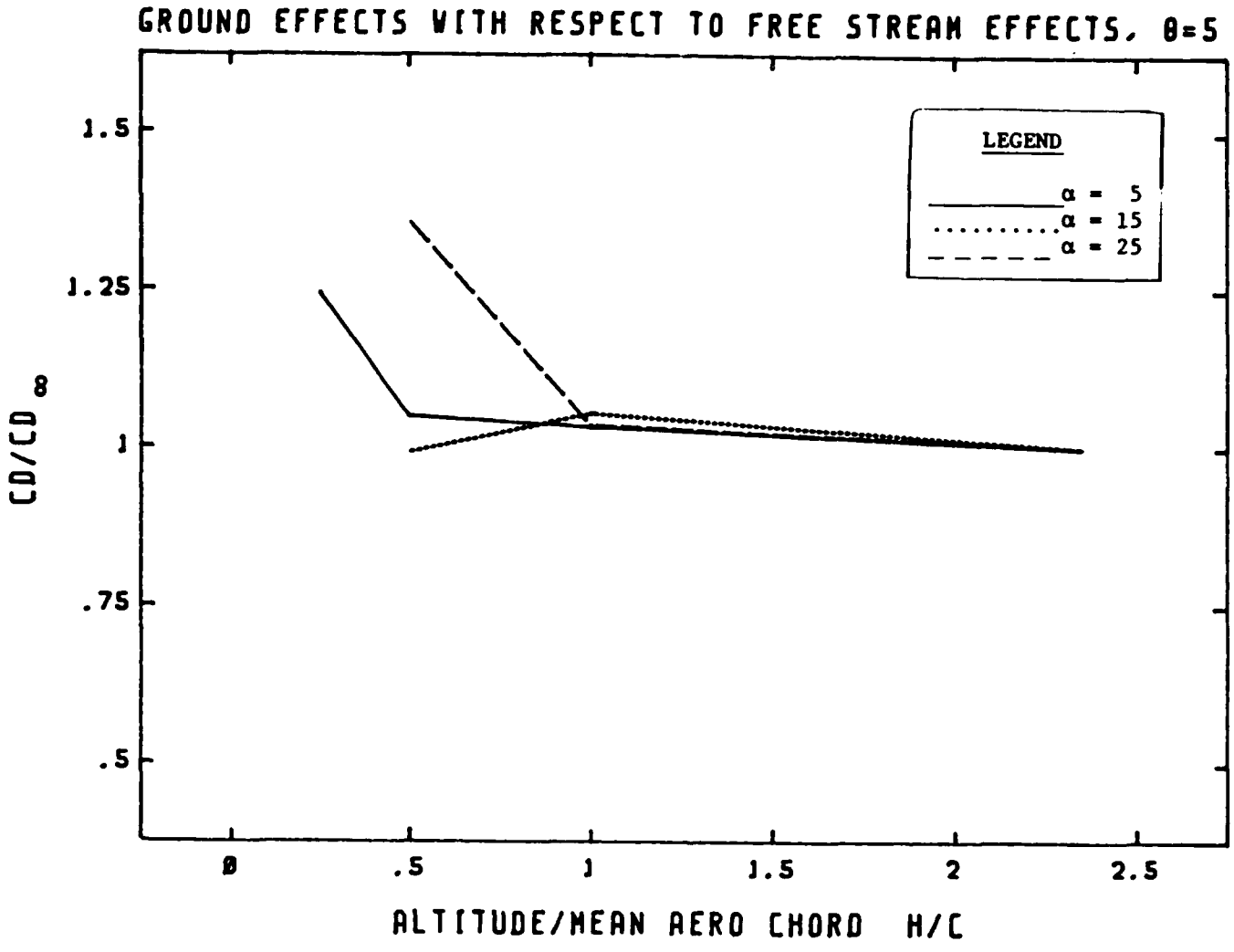

Fig. B-42 Ground Effects With Respect to Freestream Effects, CD

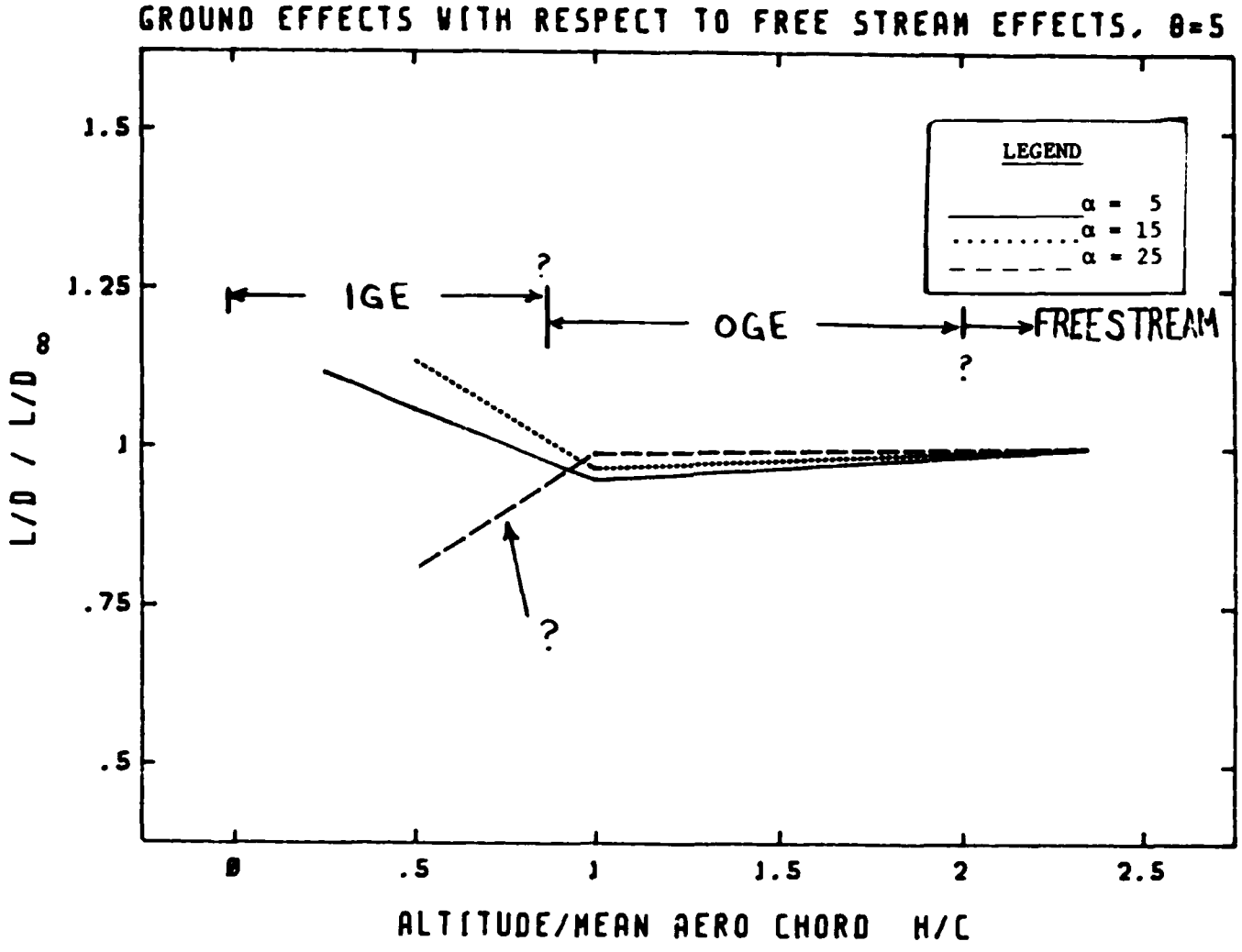

Fig. B-43 Ground Effects With Respect to Freestream Effects, L/D

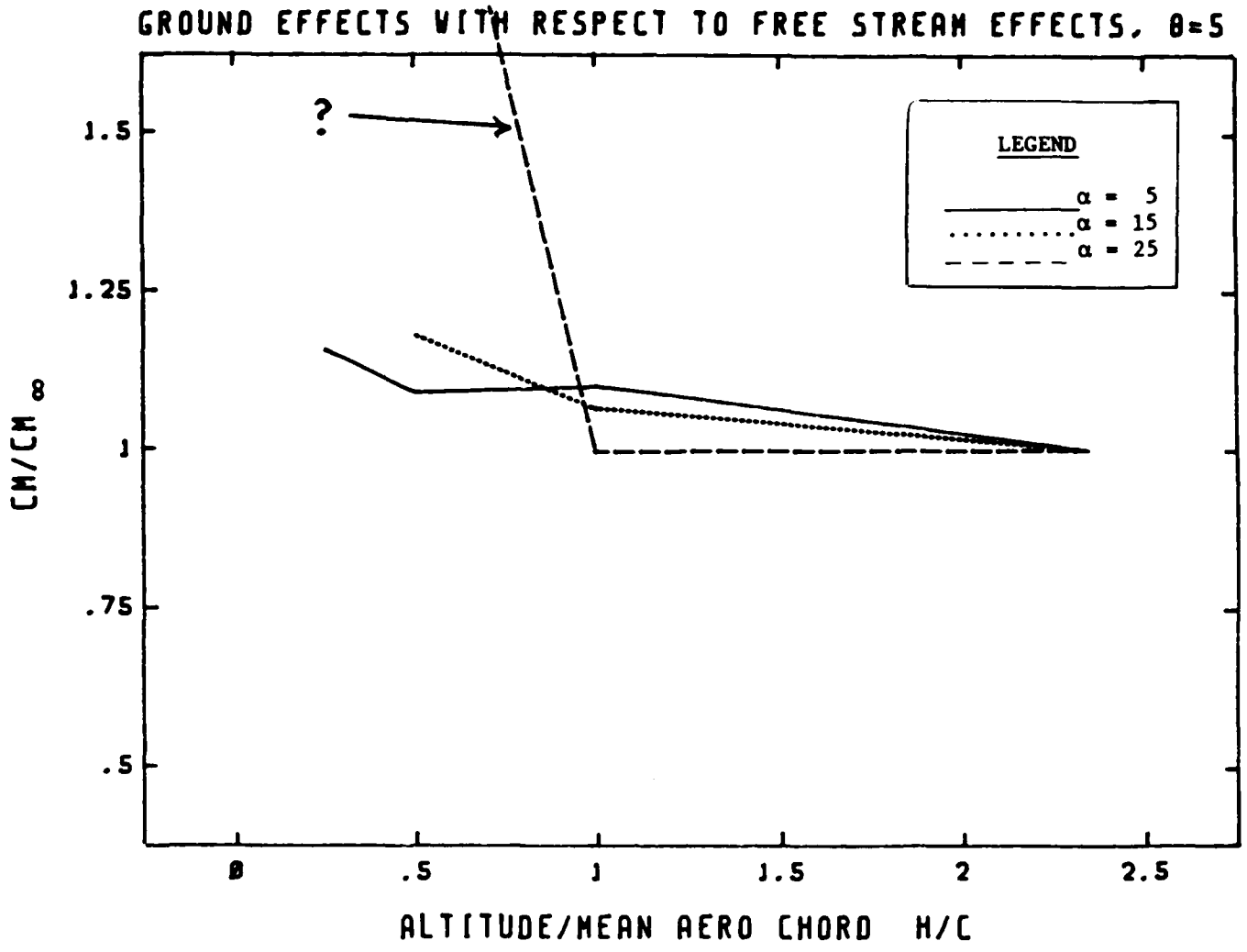

Fig. B-44 Ground Effects With Respect to Freestream Effects, CM

APPENDIX C: GROUND PRESSURE PLOTS

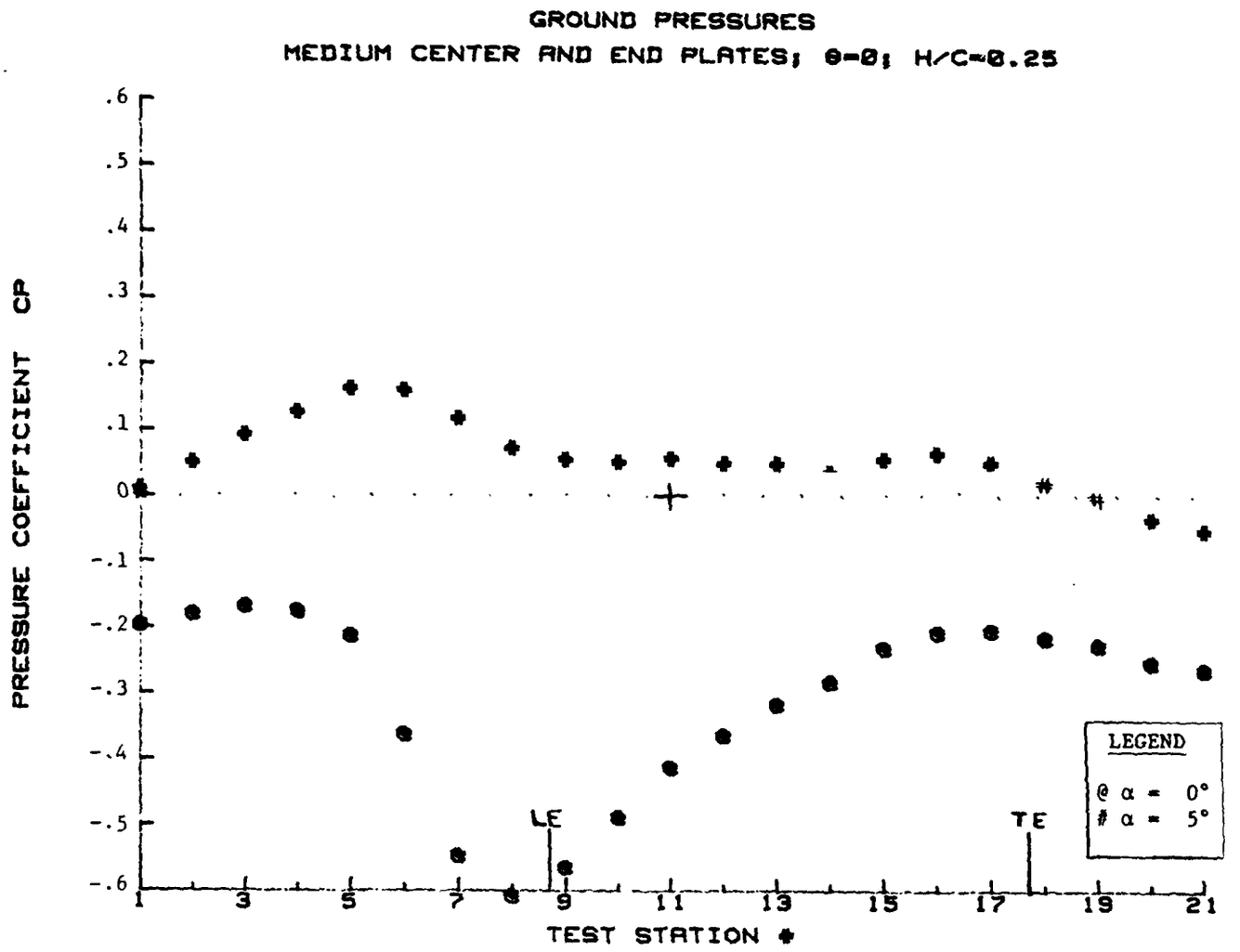

Fig. C-1 Ground Pressures Medium Center and End Plates

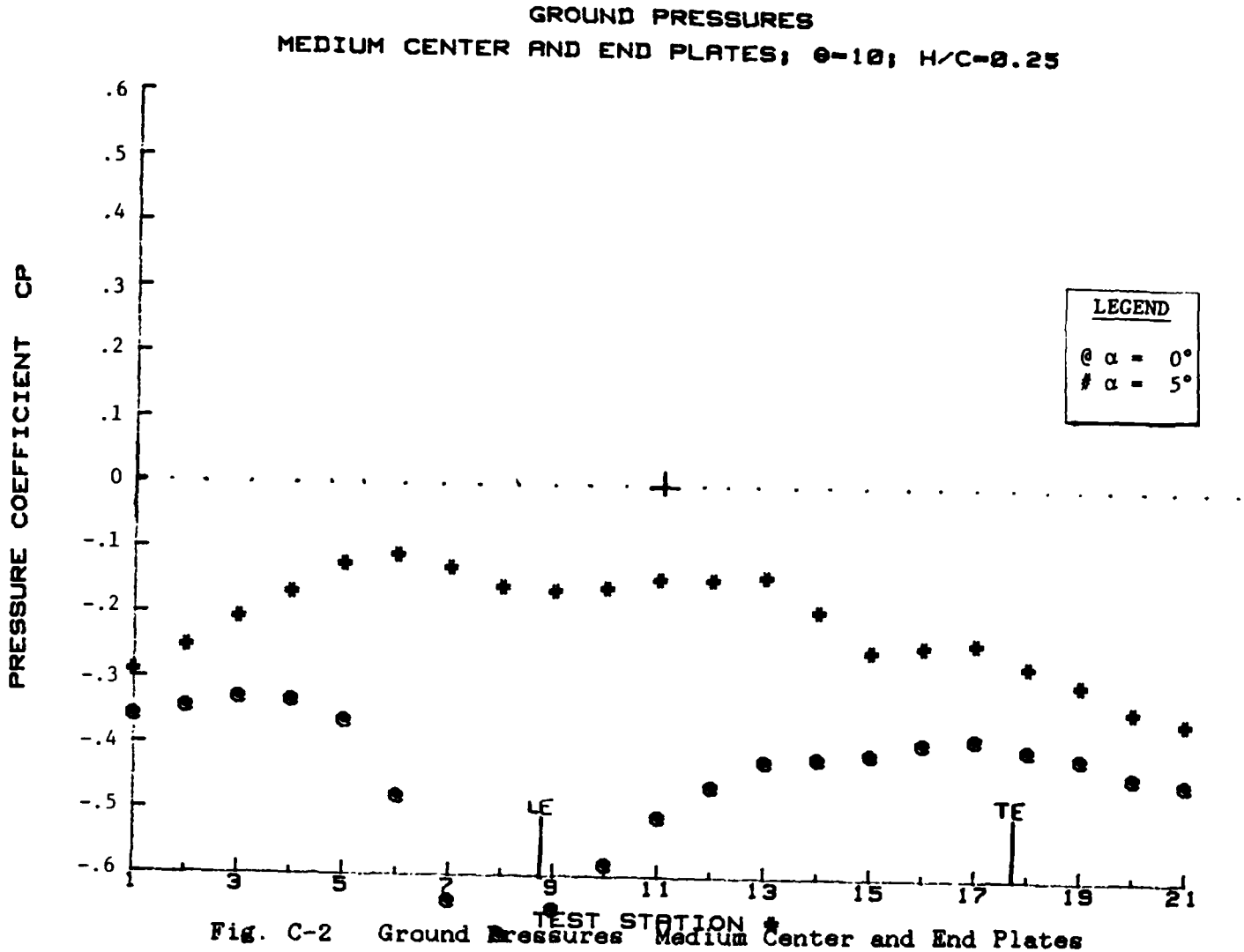

Fig. C-2 Ground Pressures Medium Center and End Plates

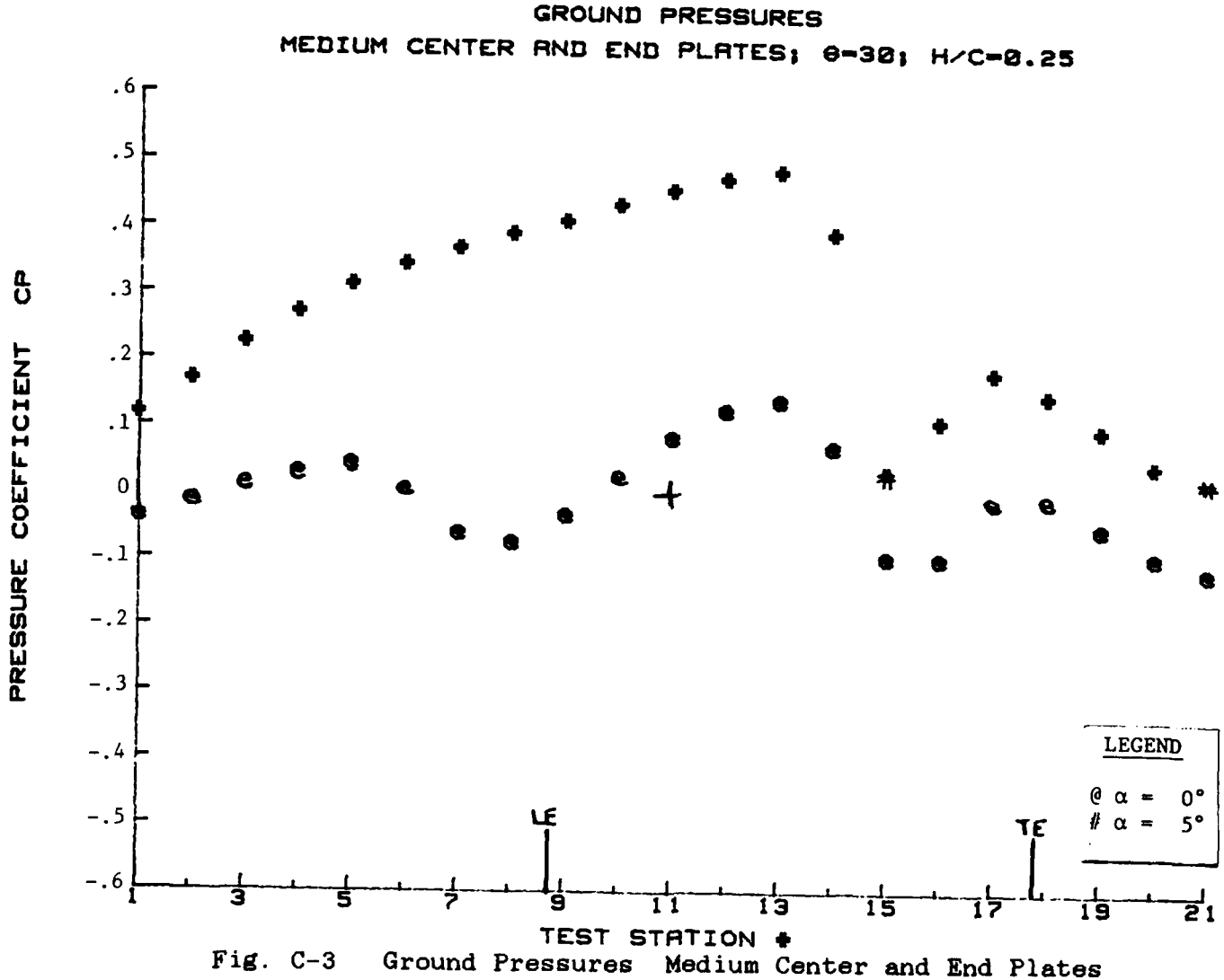

Fig. C-3 Ground Pressures Medium Center and End Plates

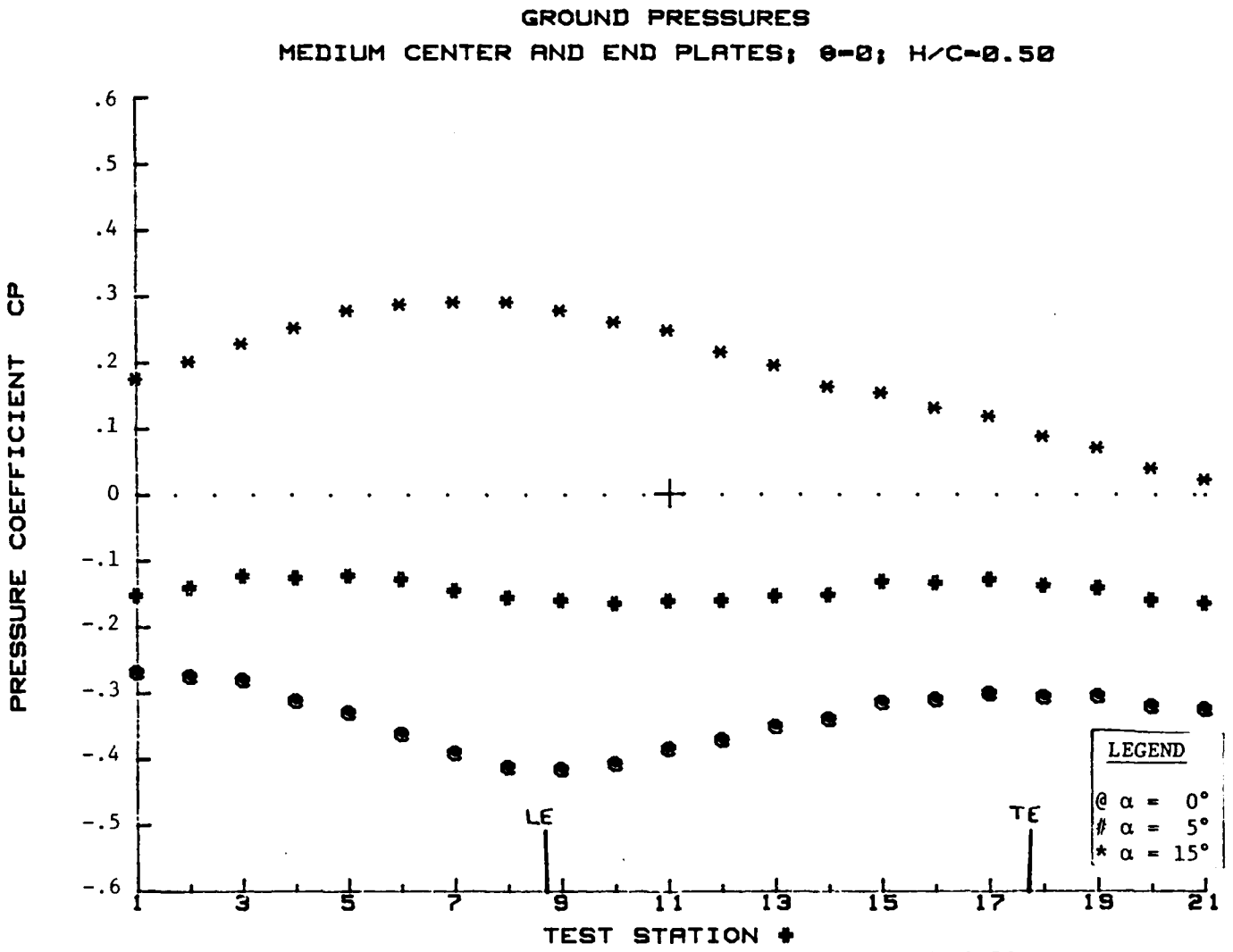

Fig. C-4 Ground Pressures Medium Center and End Plates

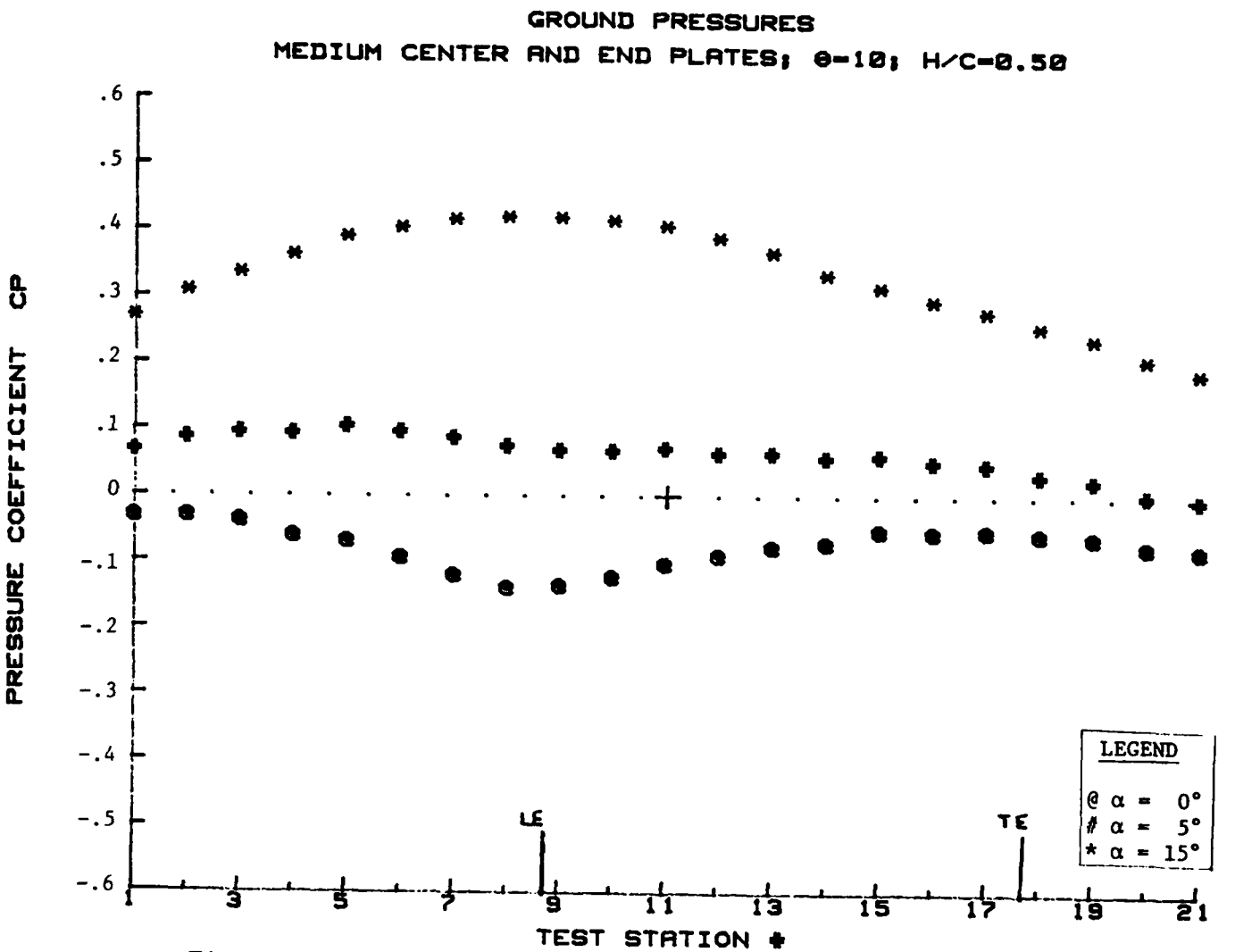

Fig. C-5 Ground Pressures Medium Center and End Plates

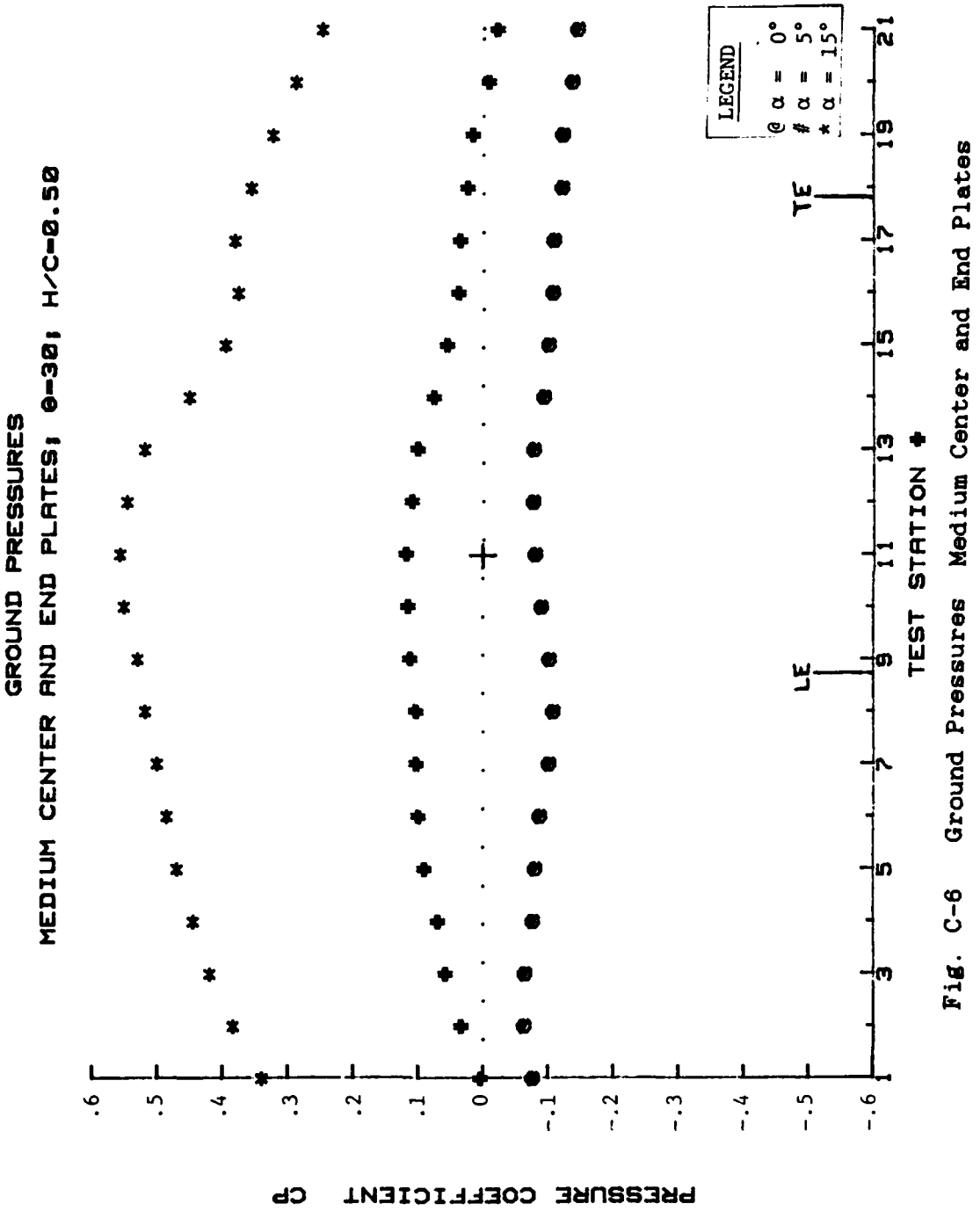

Fig. C-6 Ground Pressures Medium Center and End Plates

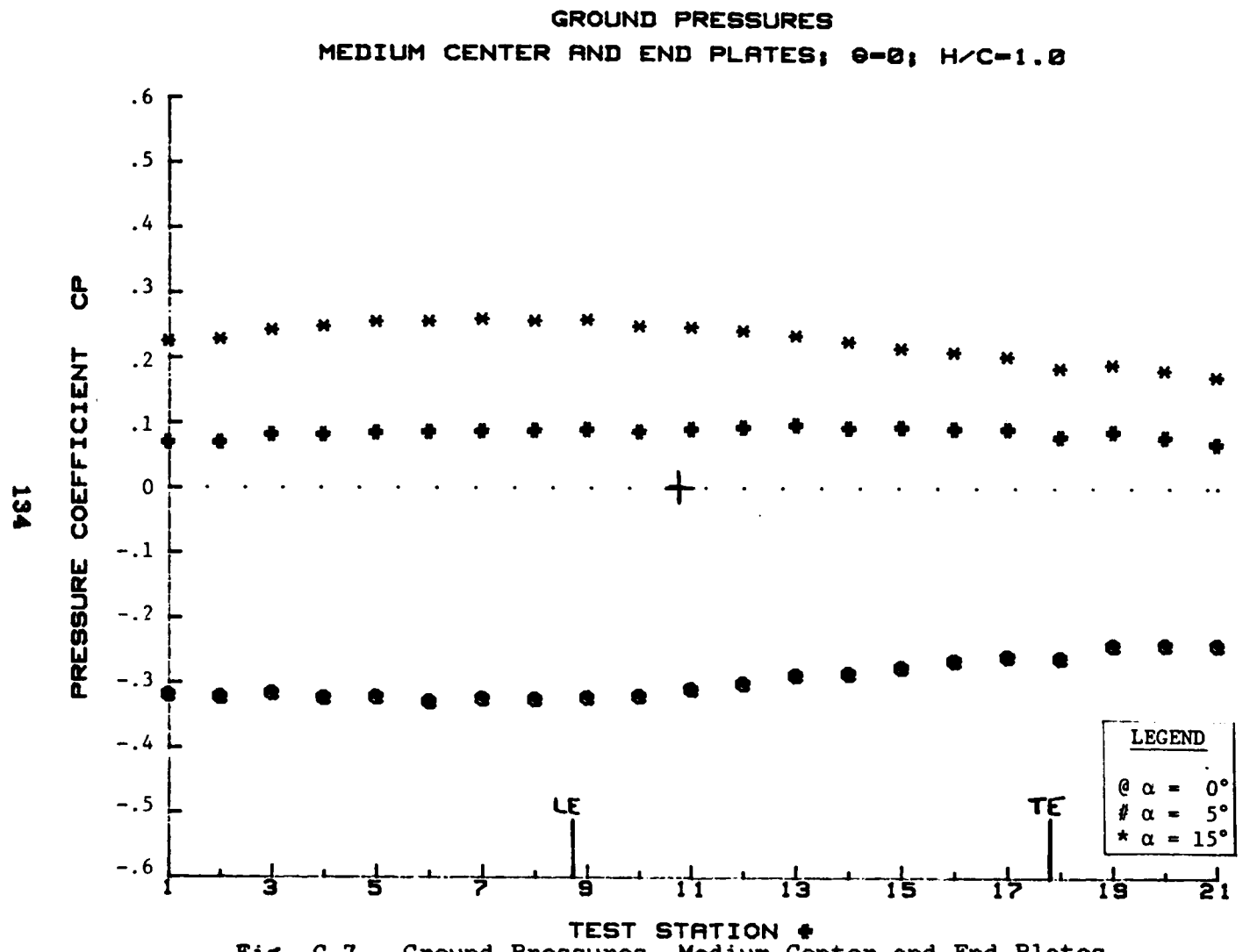

Fig. C-7 Ground Pressures Medium Center and End Plates

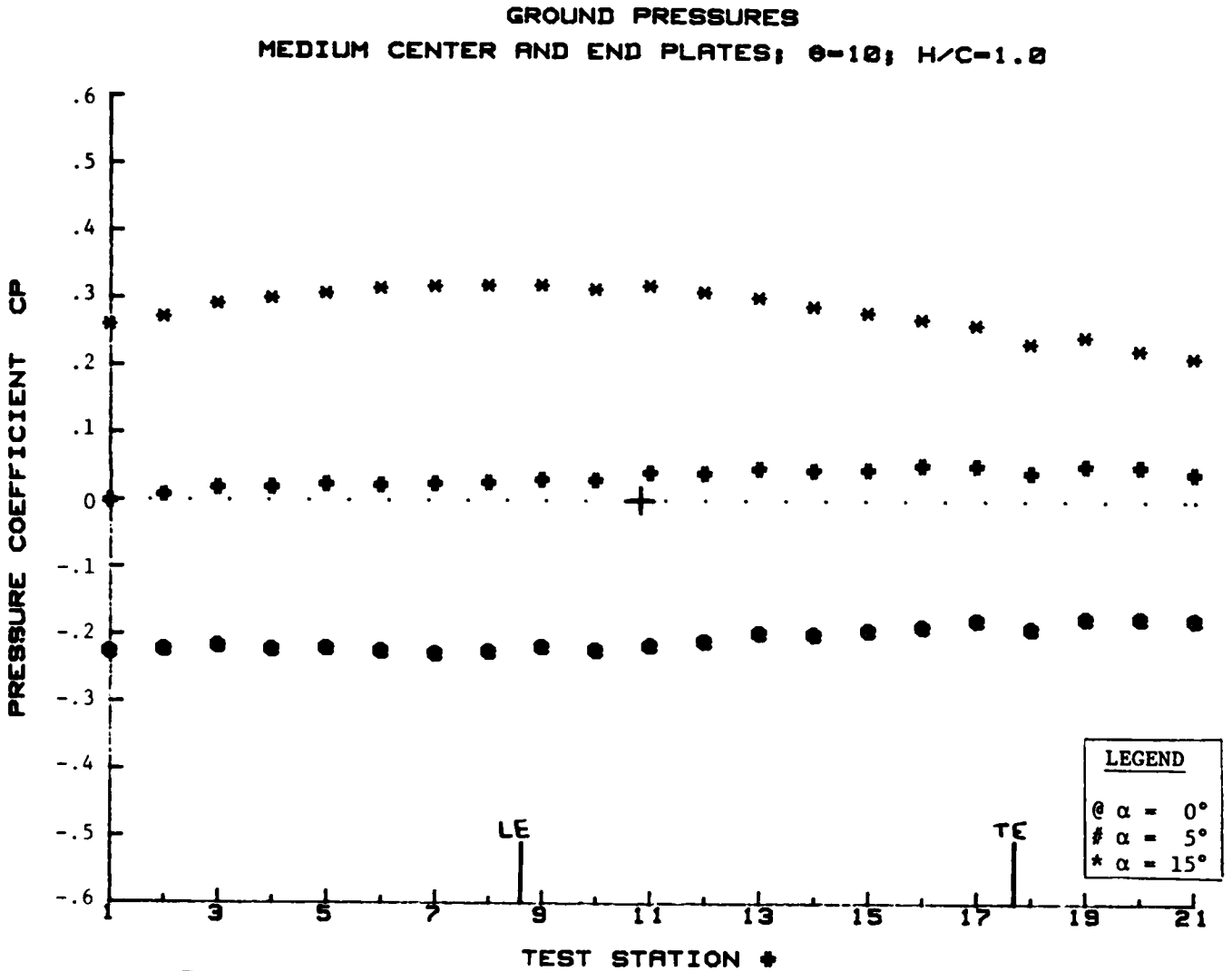

Fig. C-8 Ground Pressures Medium Center and End Plates

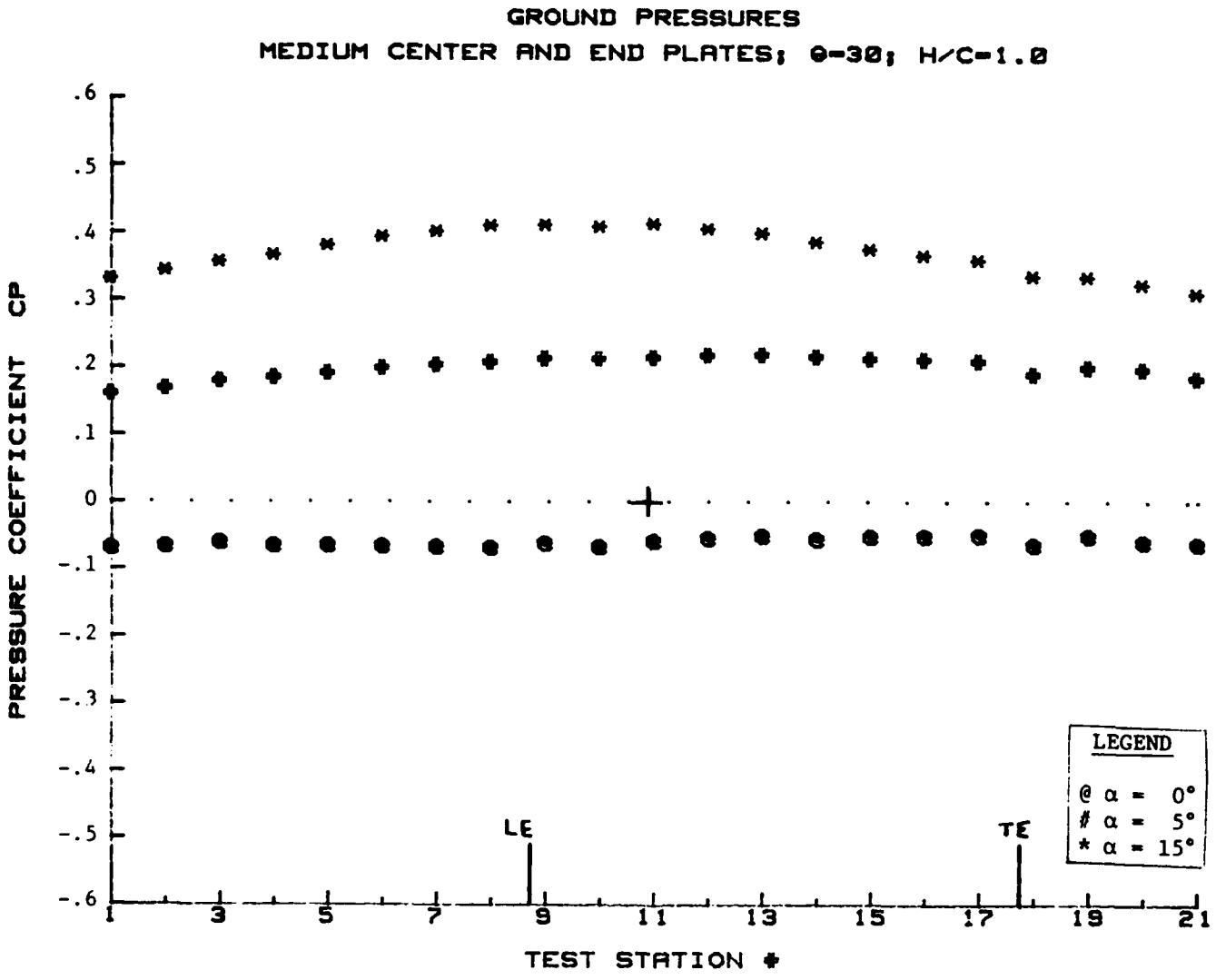

Fig. C-9 Ground Pressures Medium Center and End Plates

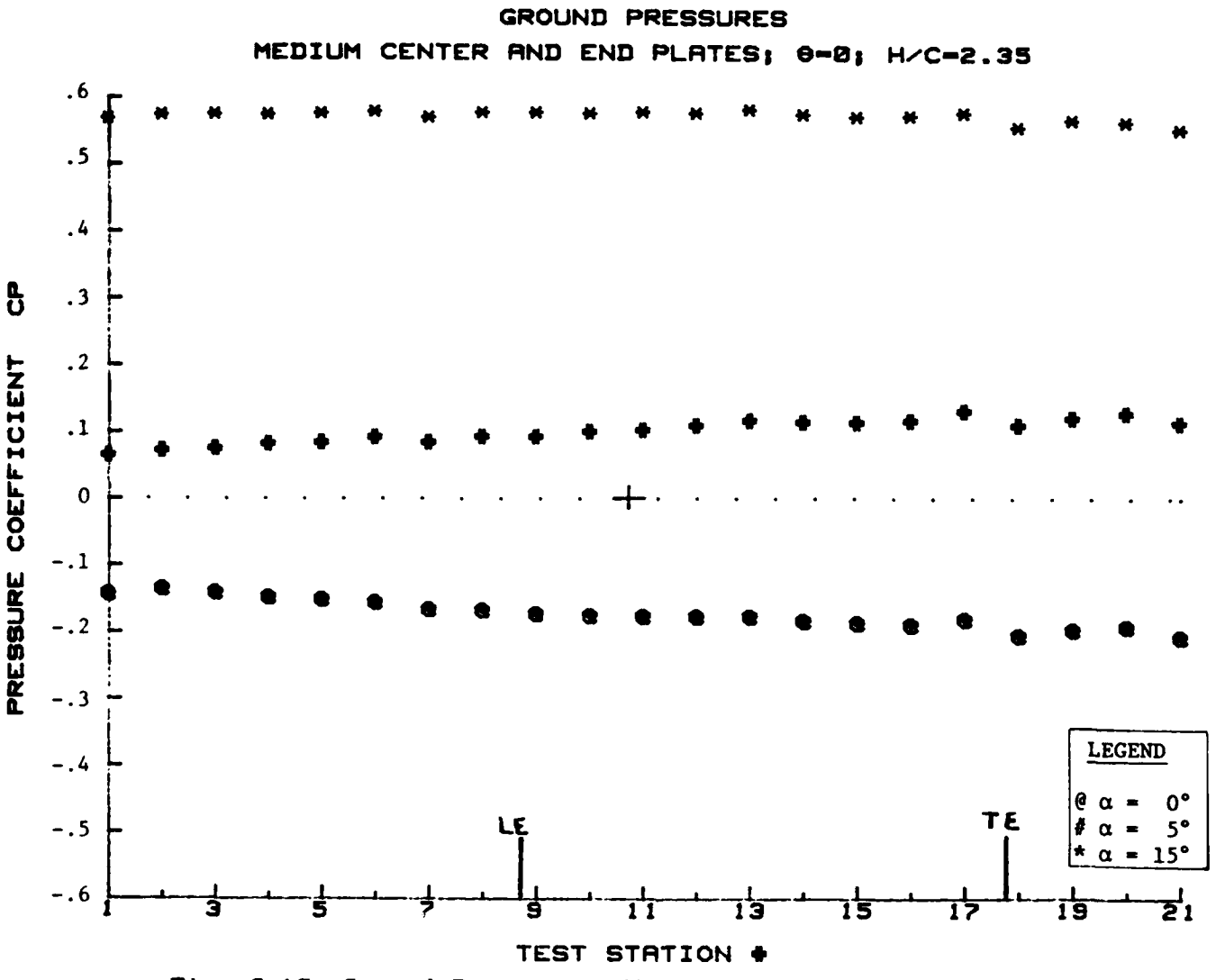

Fig. C-1Ø Ground Pressures Medium Center and End Plates

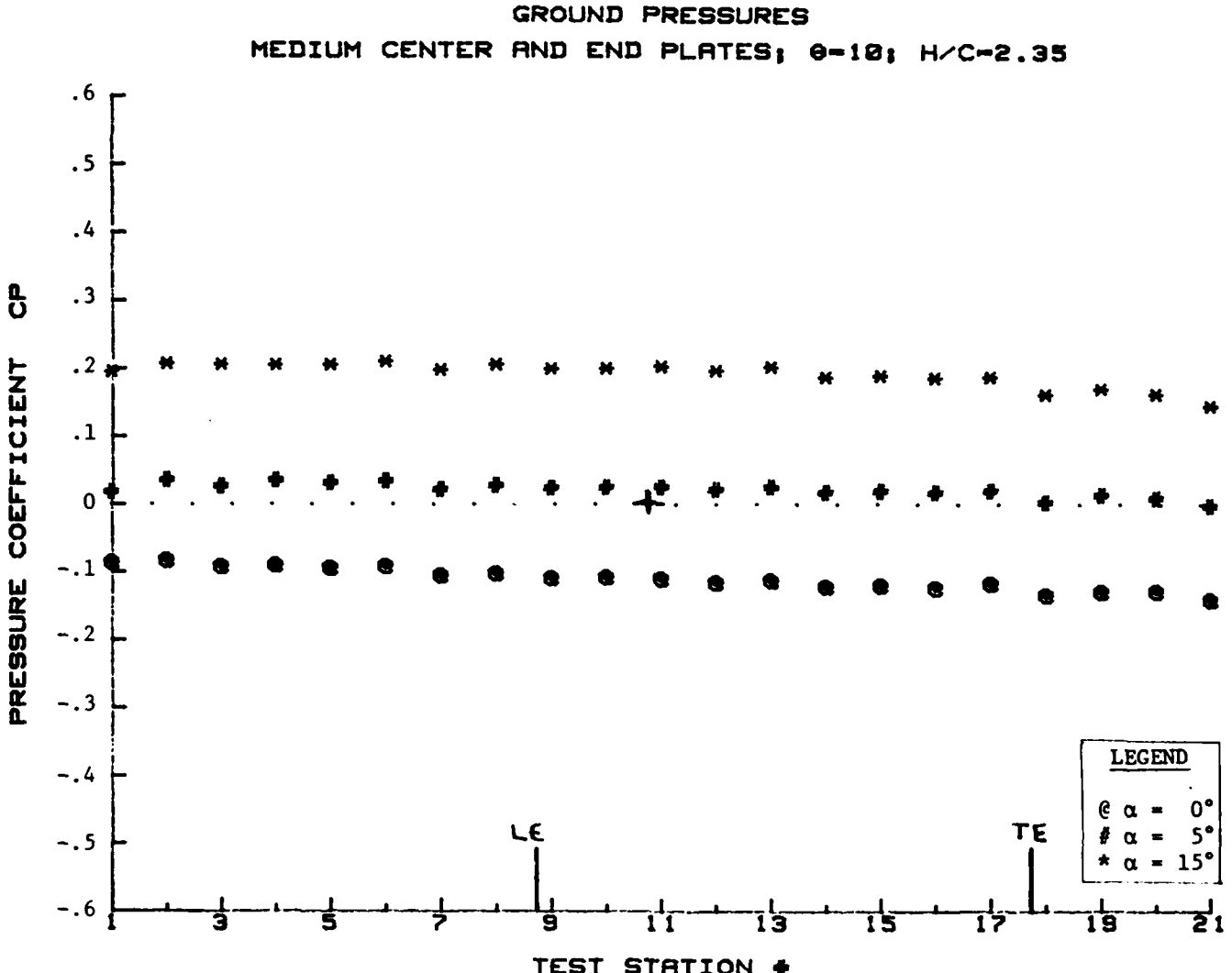

Fig. C-11 Ground Pressures Medium Center and End Plates

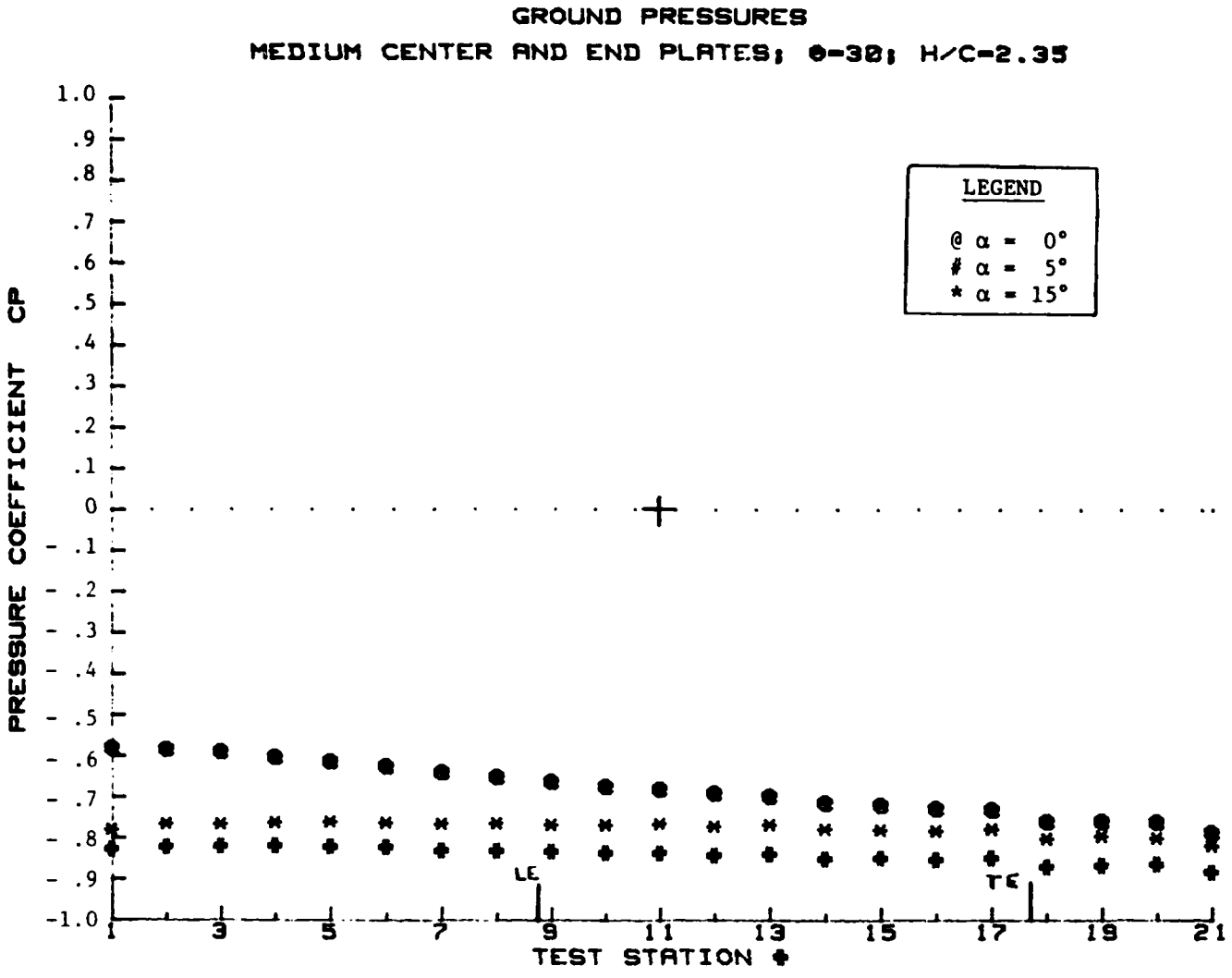

Fig. C-12 Ground Pressures Medium Center and End Plates

APPENDIX D: WING PRESSURE PLOTS

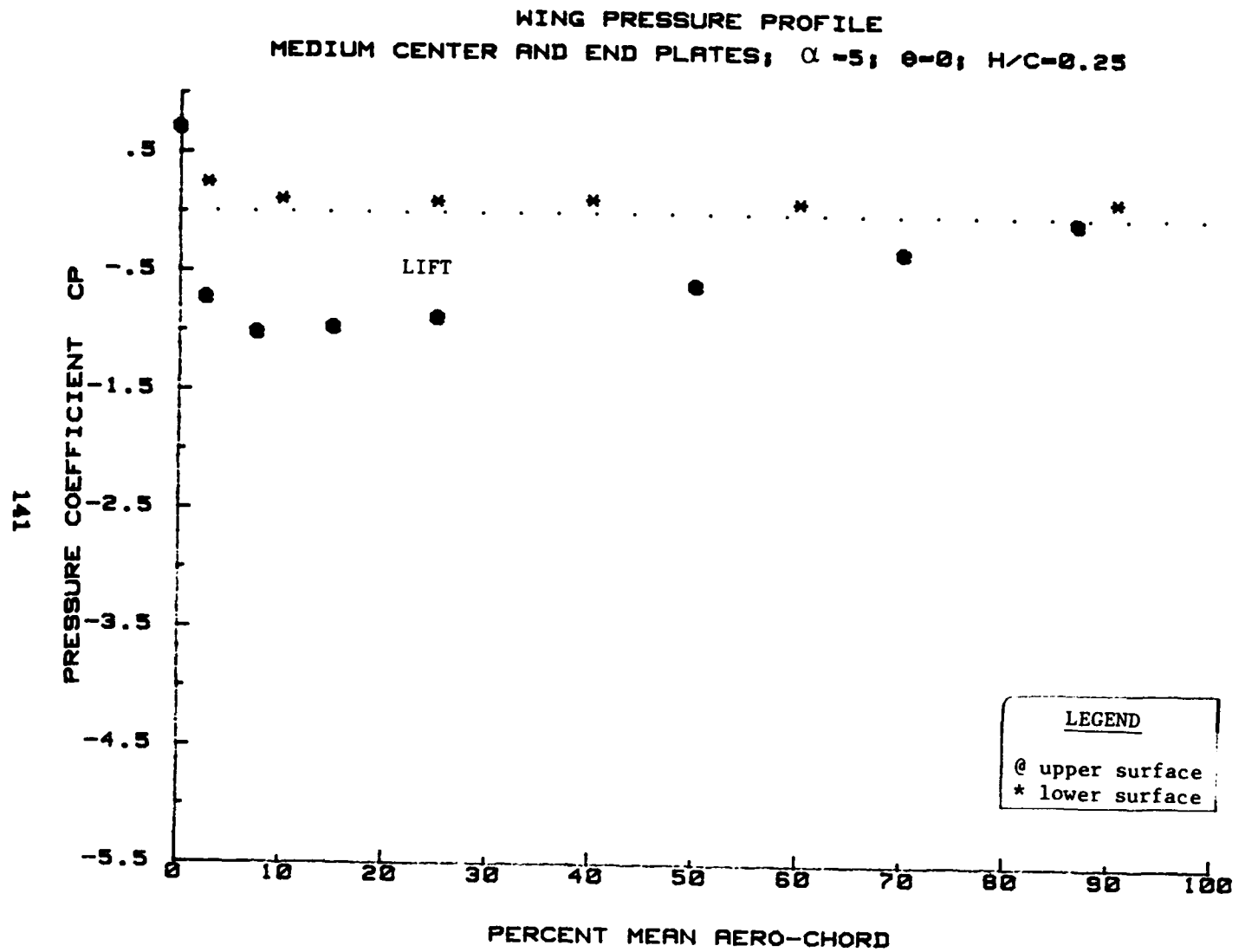

Fig. D-1 Wing Pressure Profile

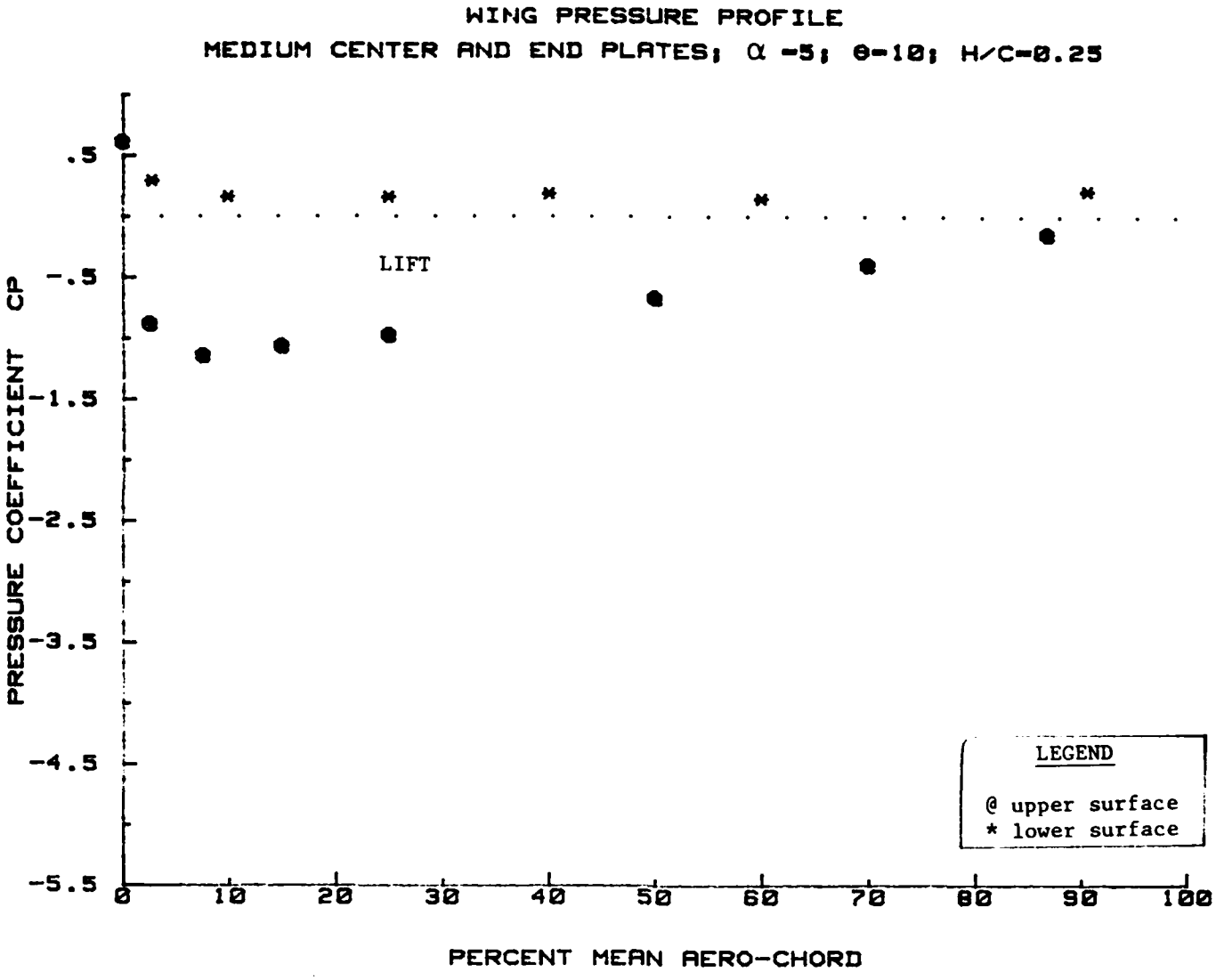

Fig. D-2 Wing Pressure Profile

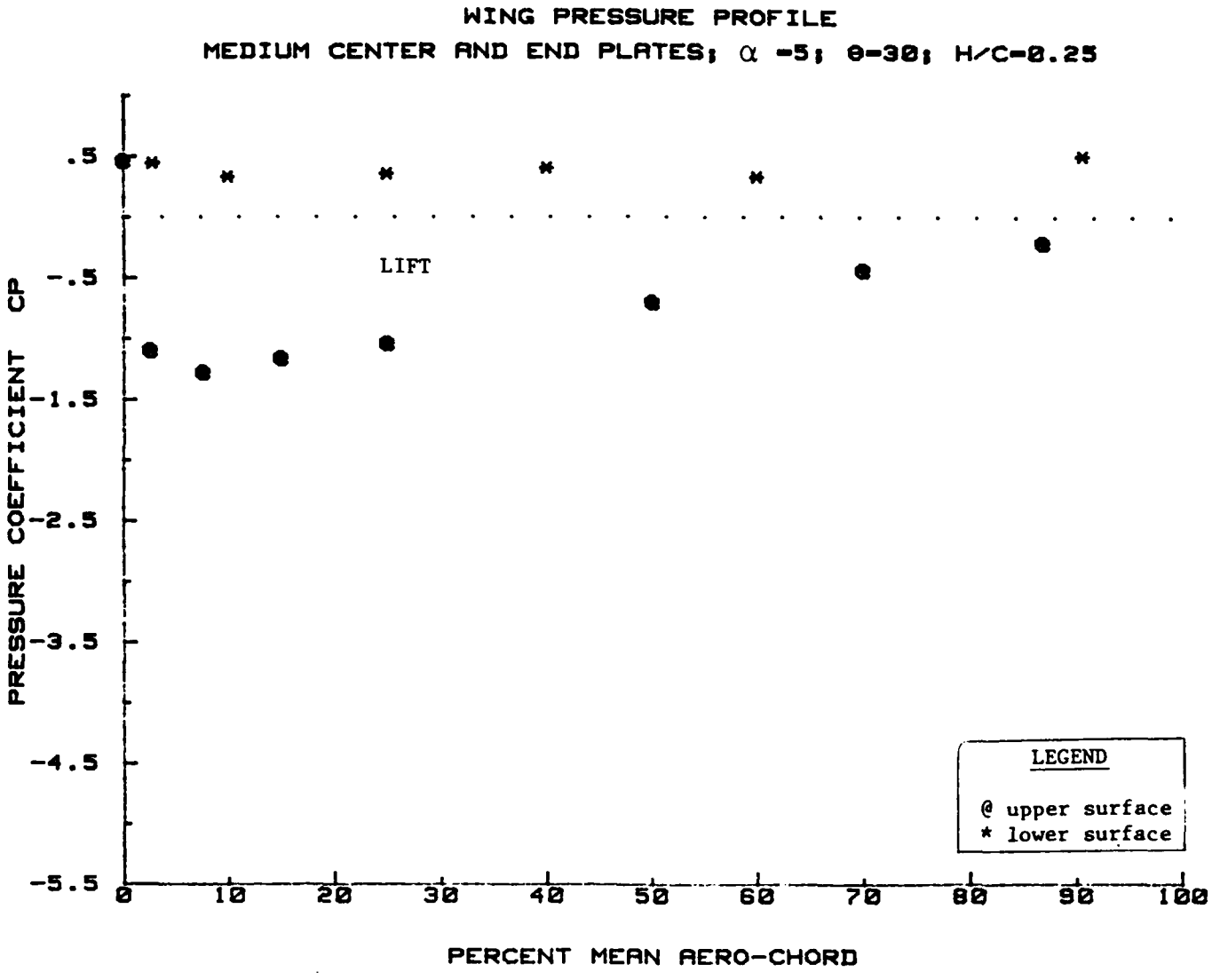

Fig. D-3 Wing Pressure Profile

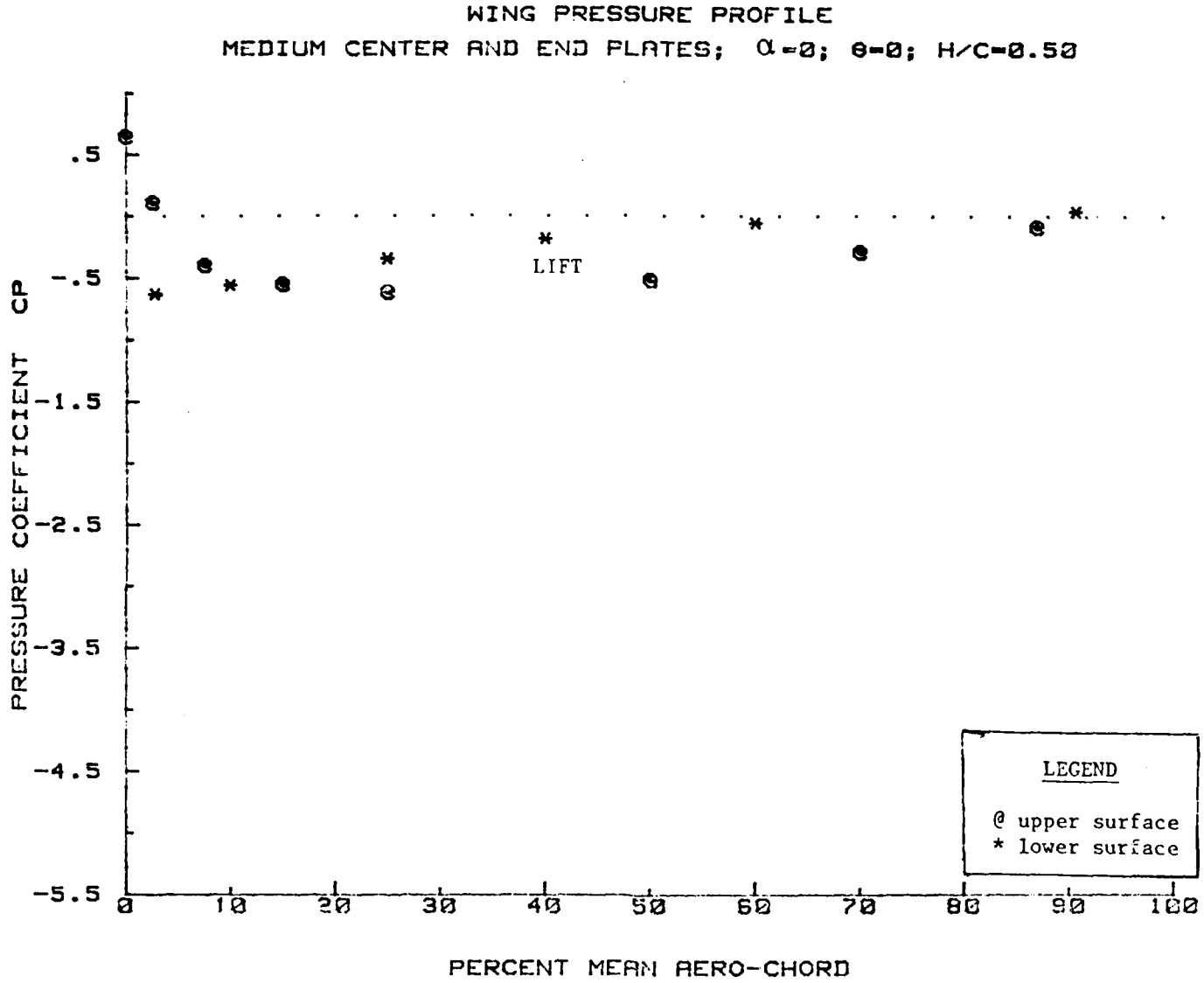

Fig. D-4 Wing Pressure Profile

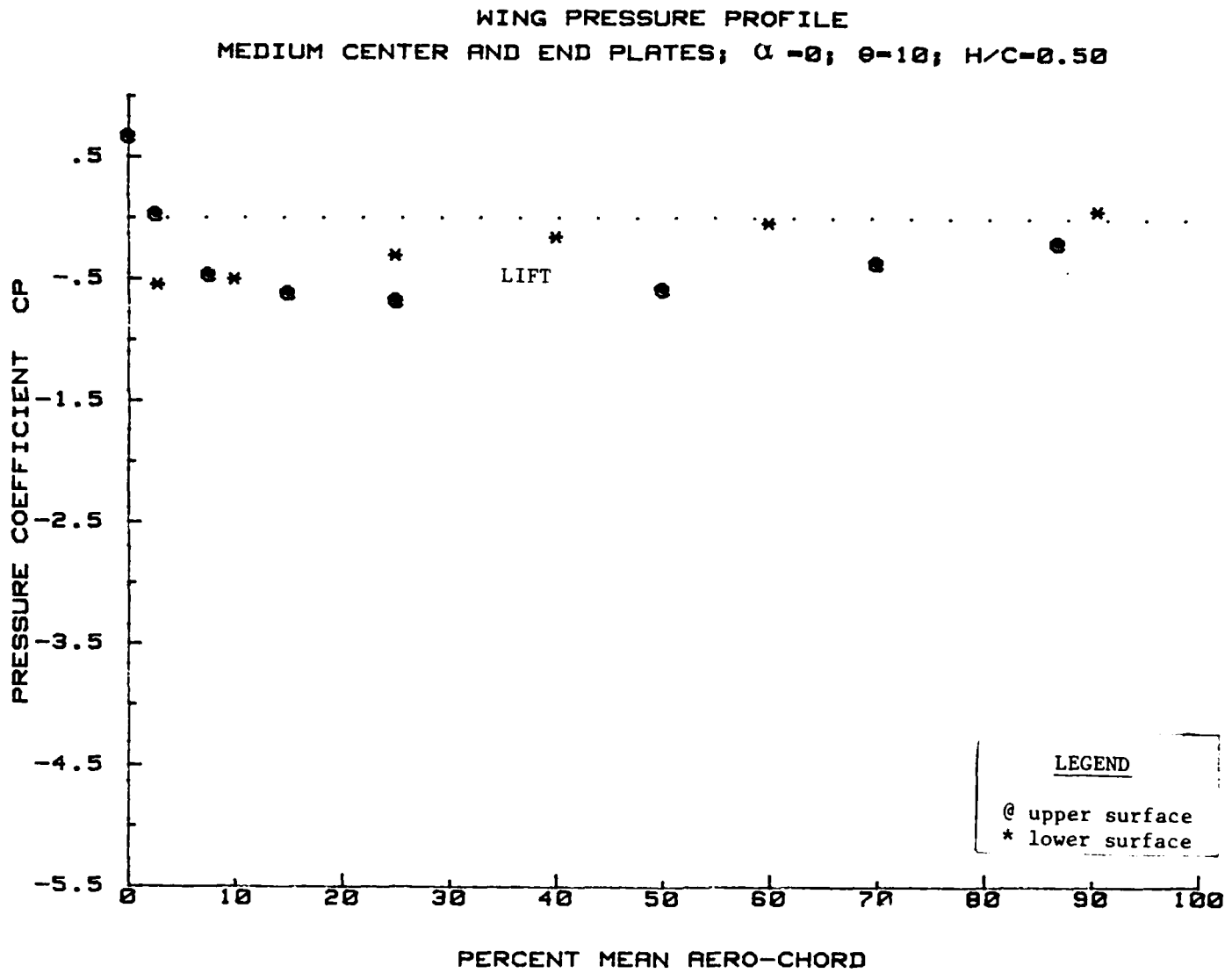

Fig. D-5 Wing Pressure Profile

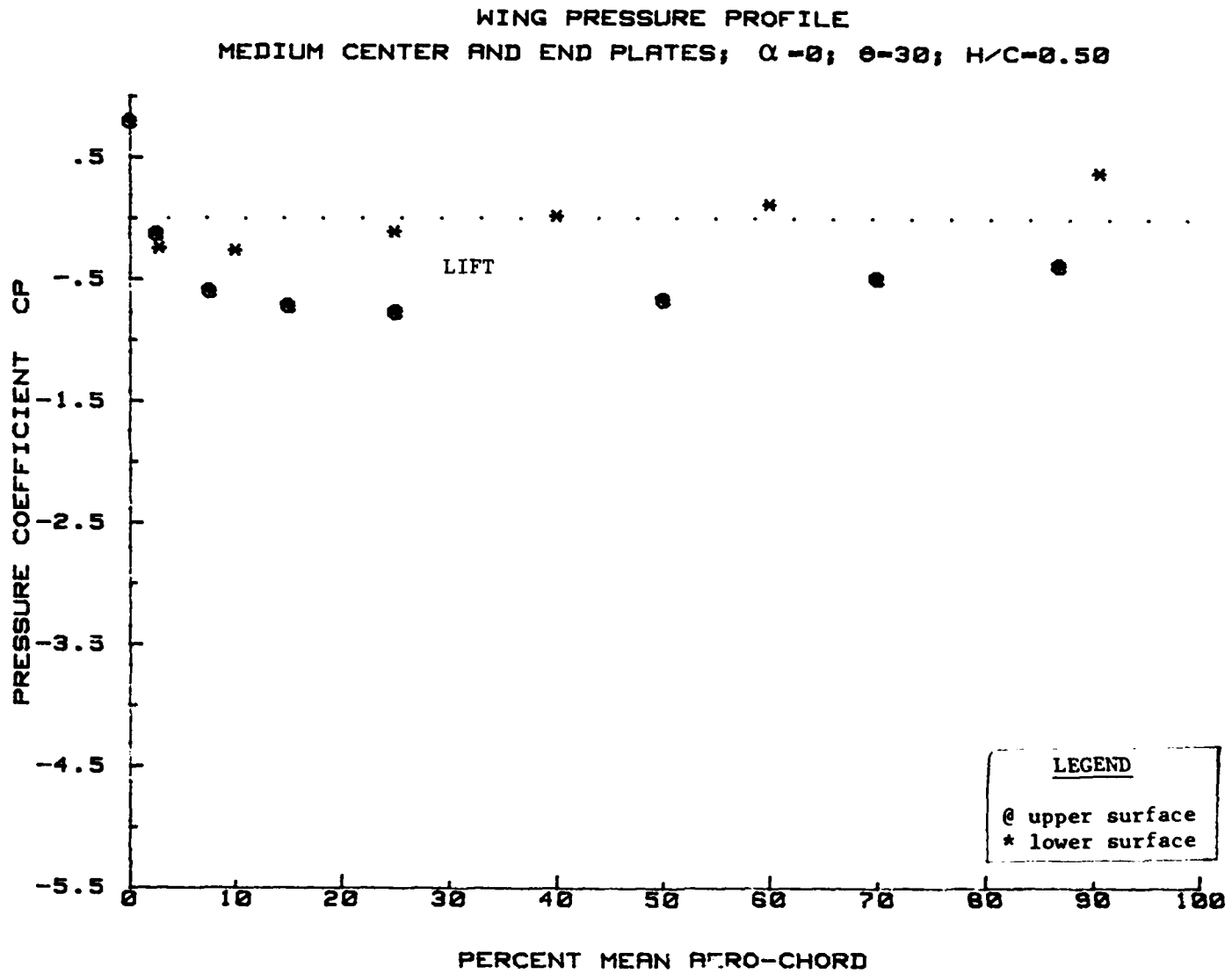

Fig. D-6 Wing Pressure Profile

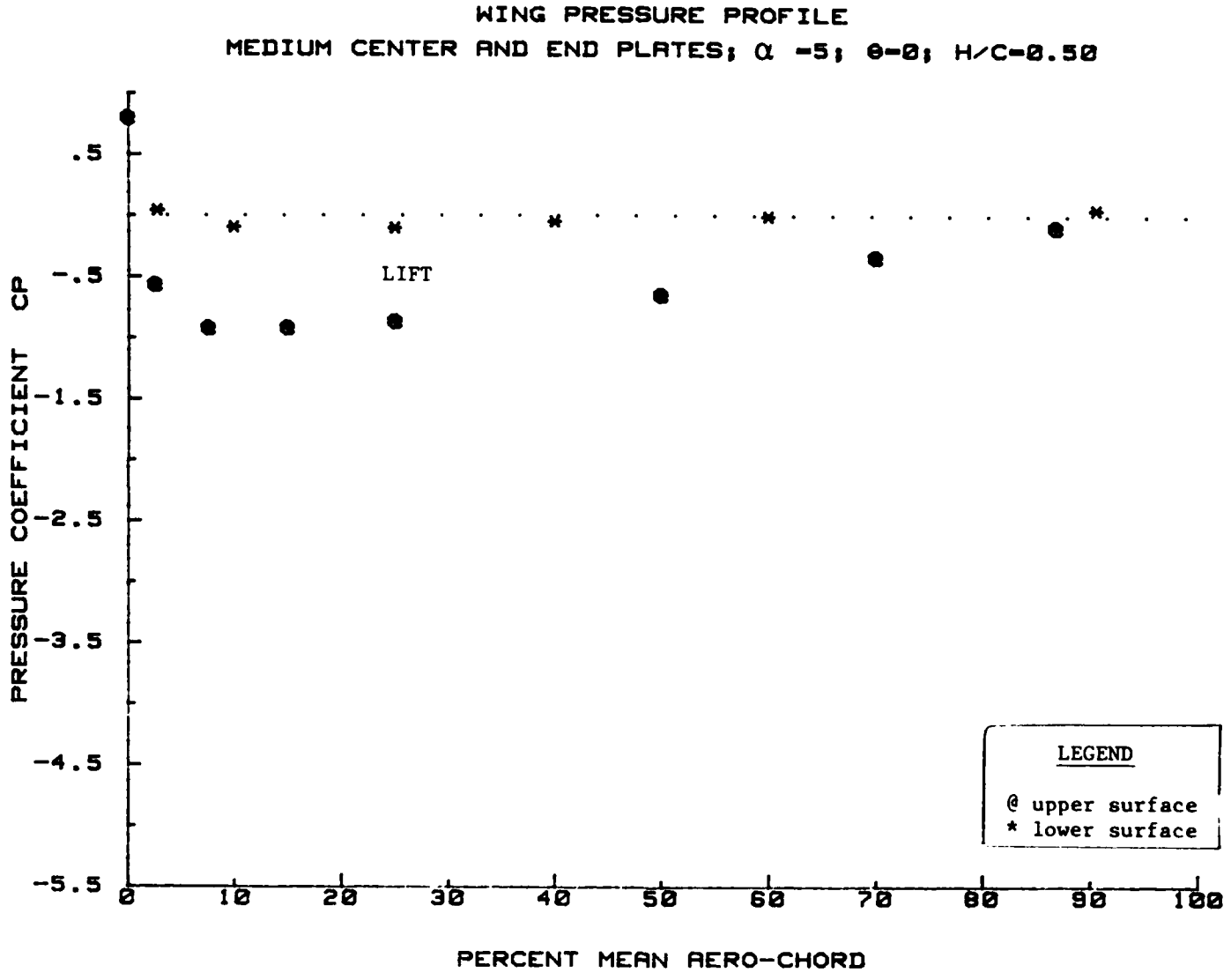

Fig. D-7 Wing Pressure Profile

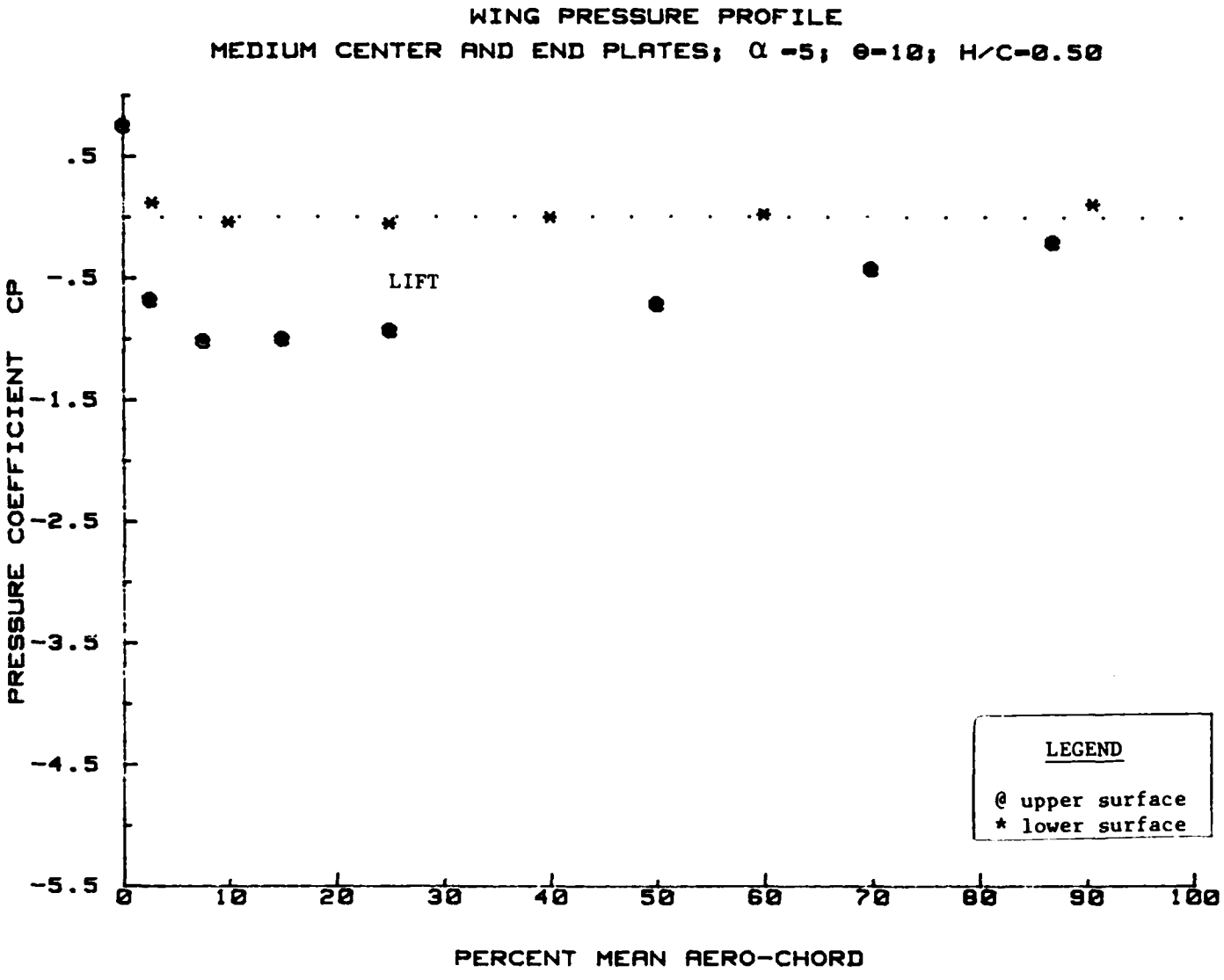

Fig. D-8 Wing Pressure Profile

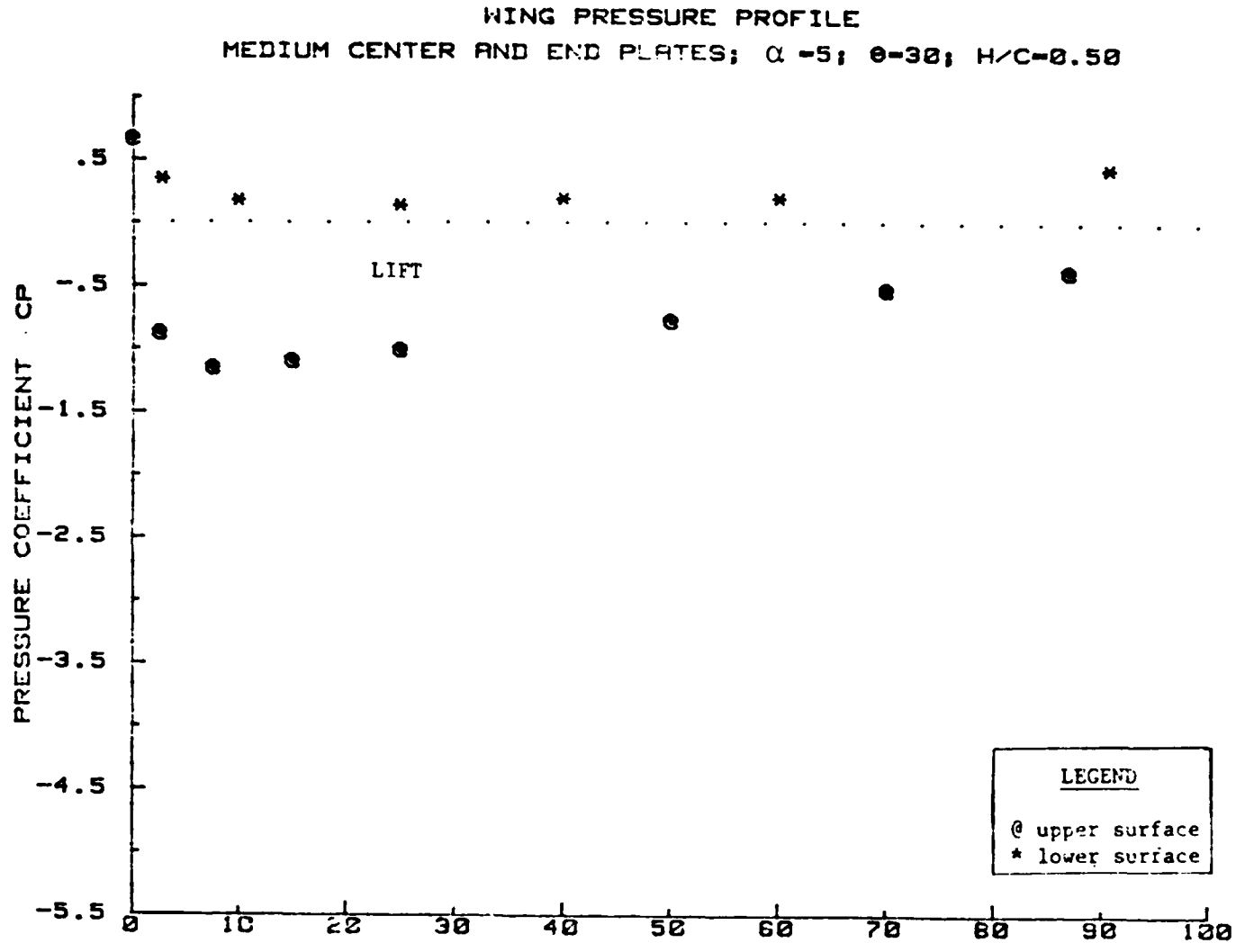

Fig. D-9 Wing Pressure Profile

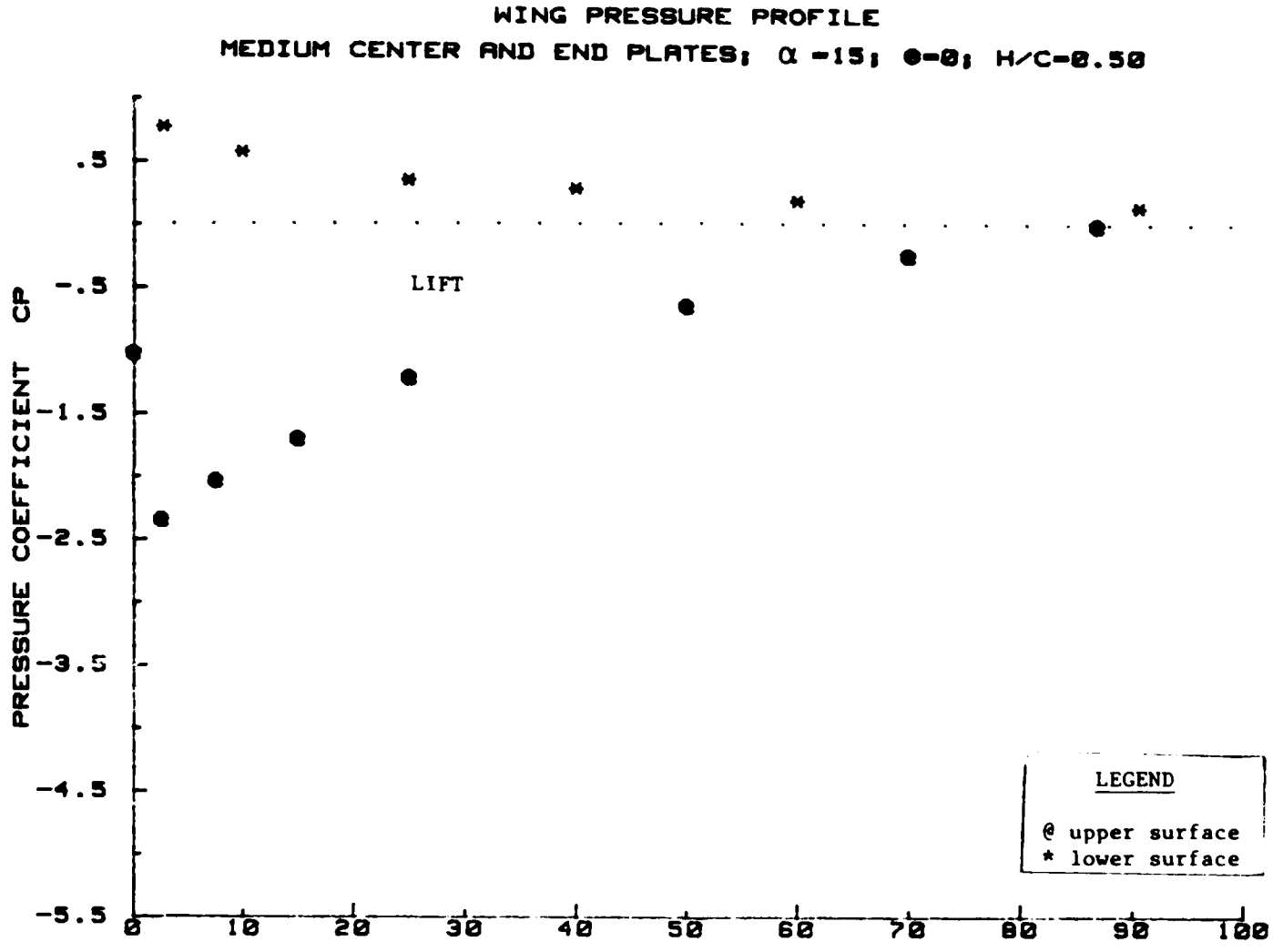

Fig. D-10 Wing Pressure Profile

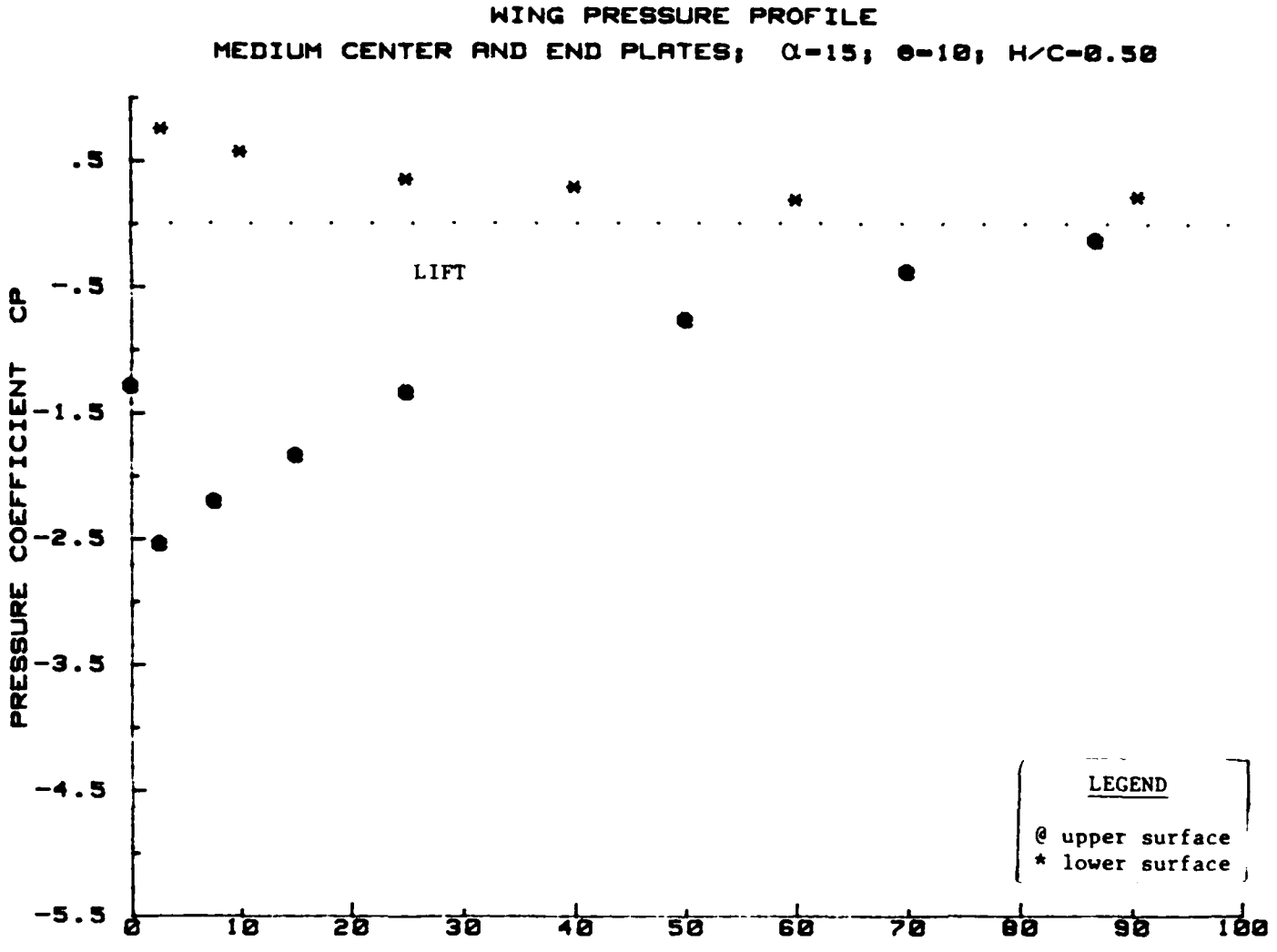

Fig. D-11 Wing Pressure Profile

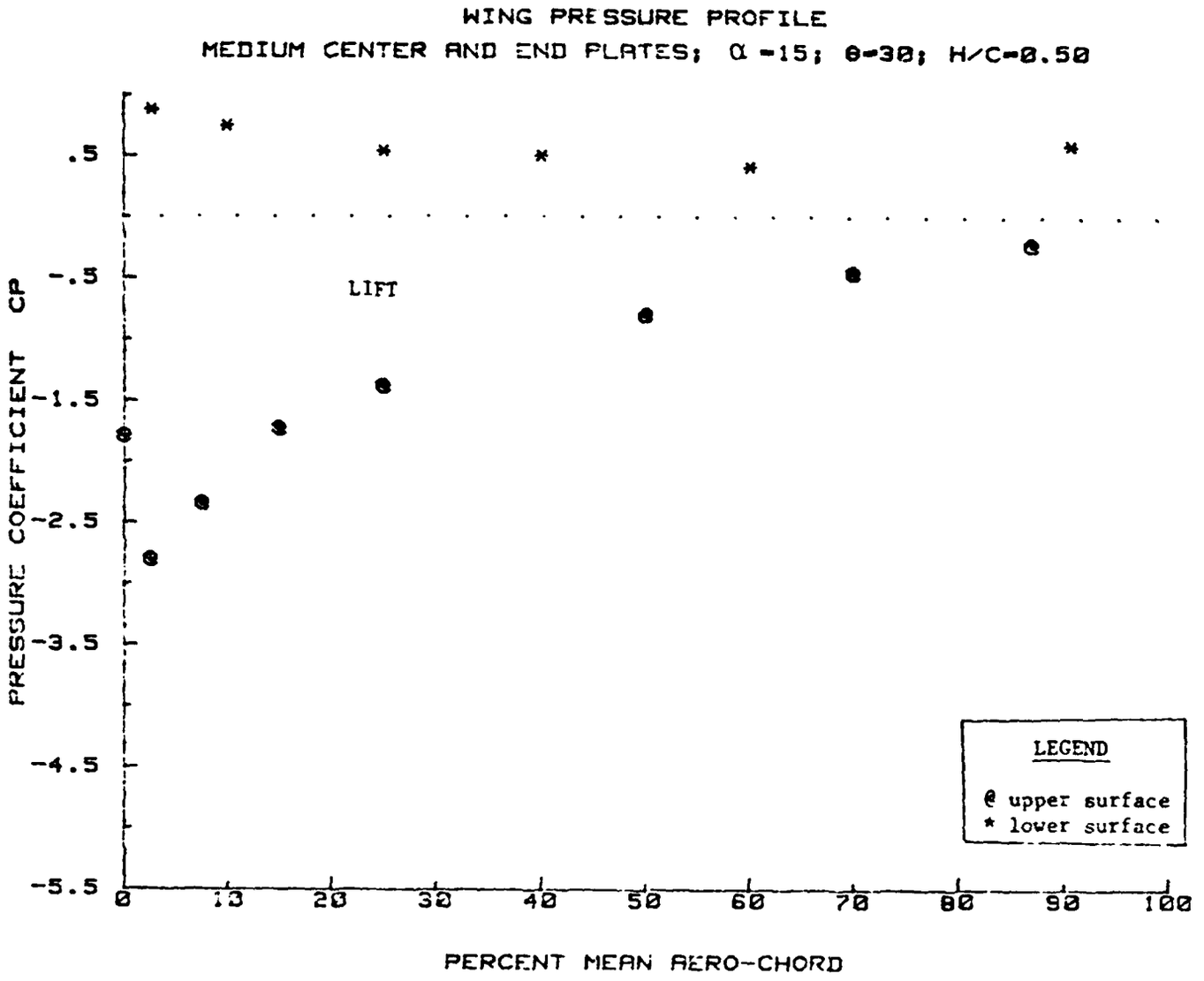

Fig. D-12 Wing Pressure Profile

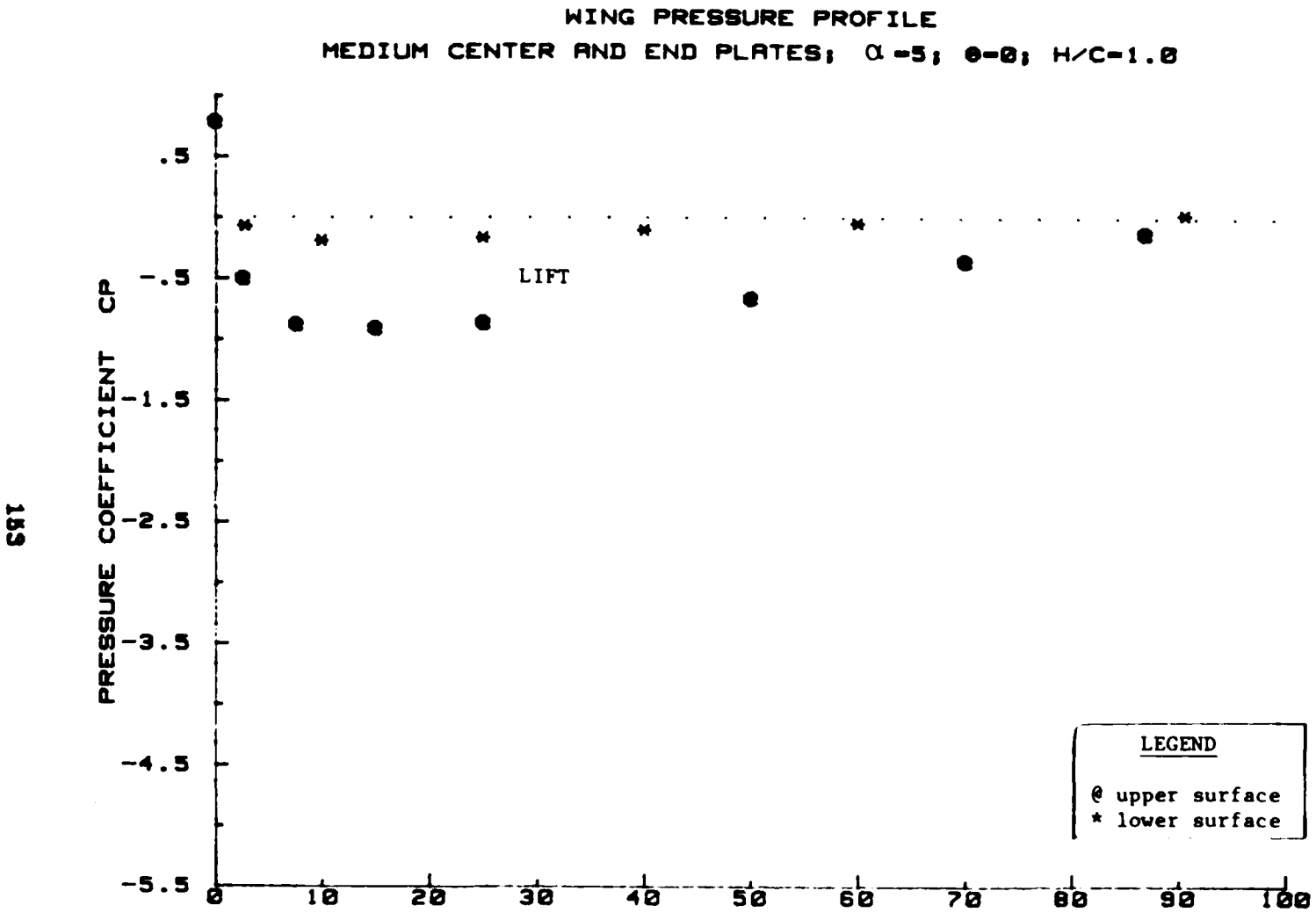

Fig. D-13 Wing Pressure Profile

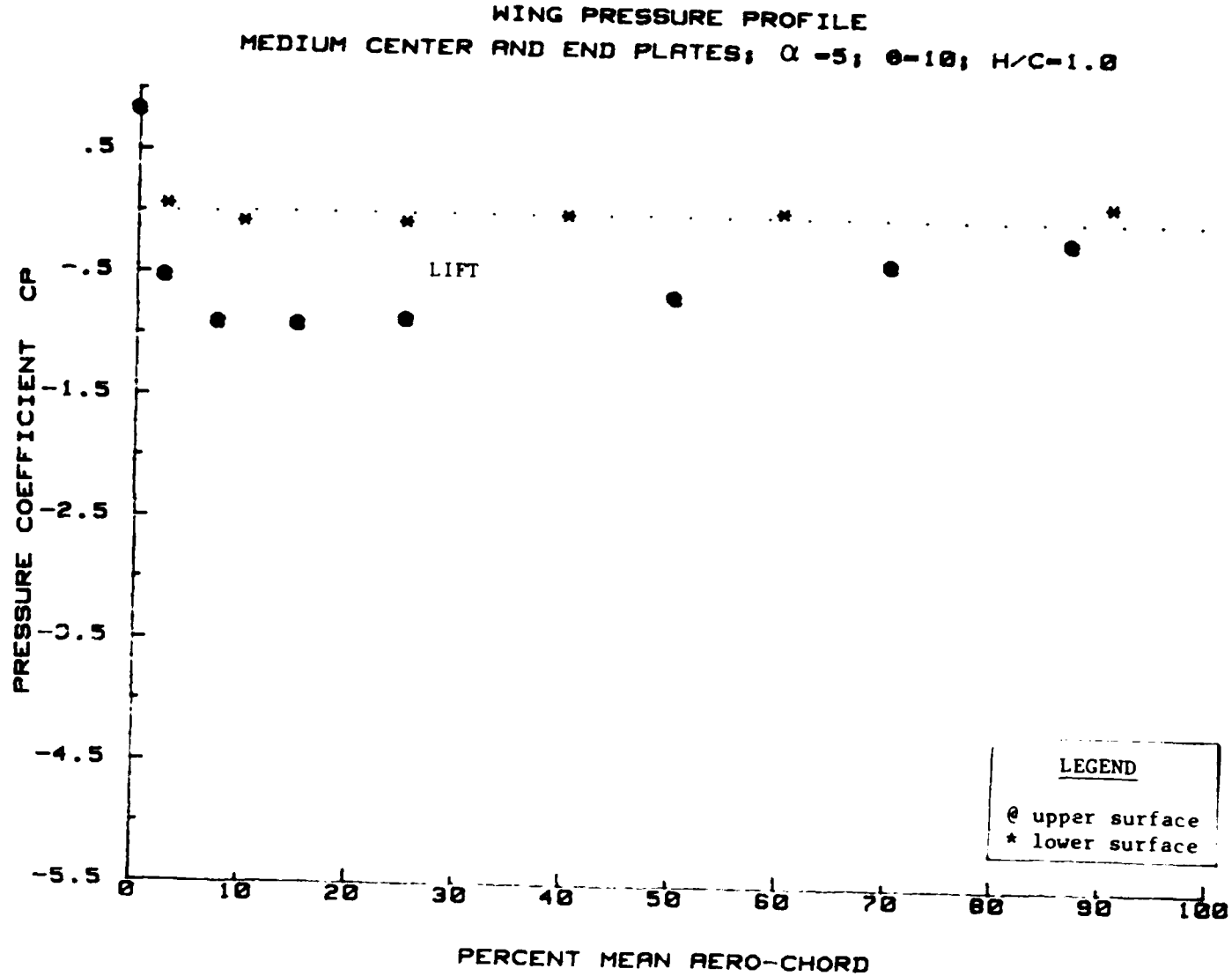

Fig. D-14 Wing Pressure Profile

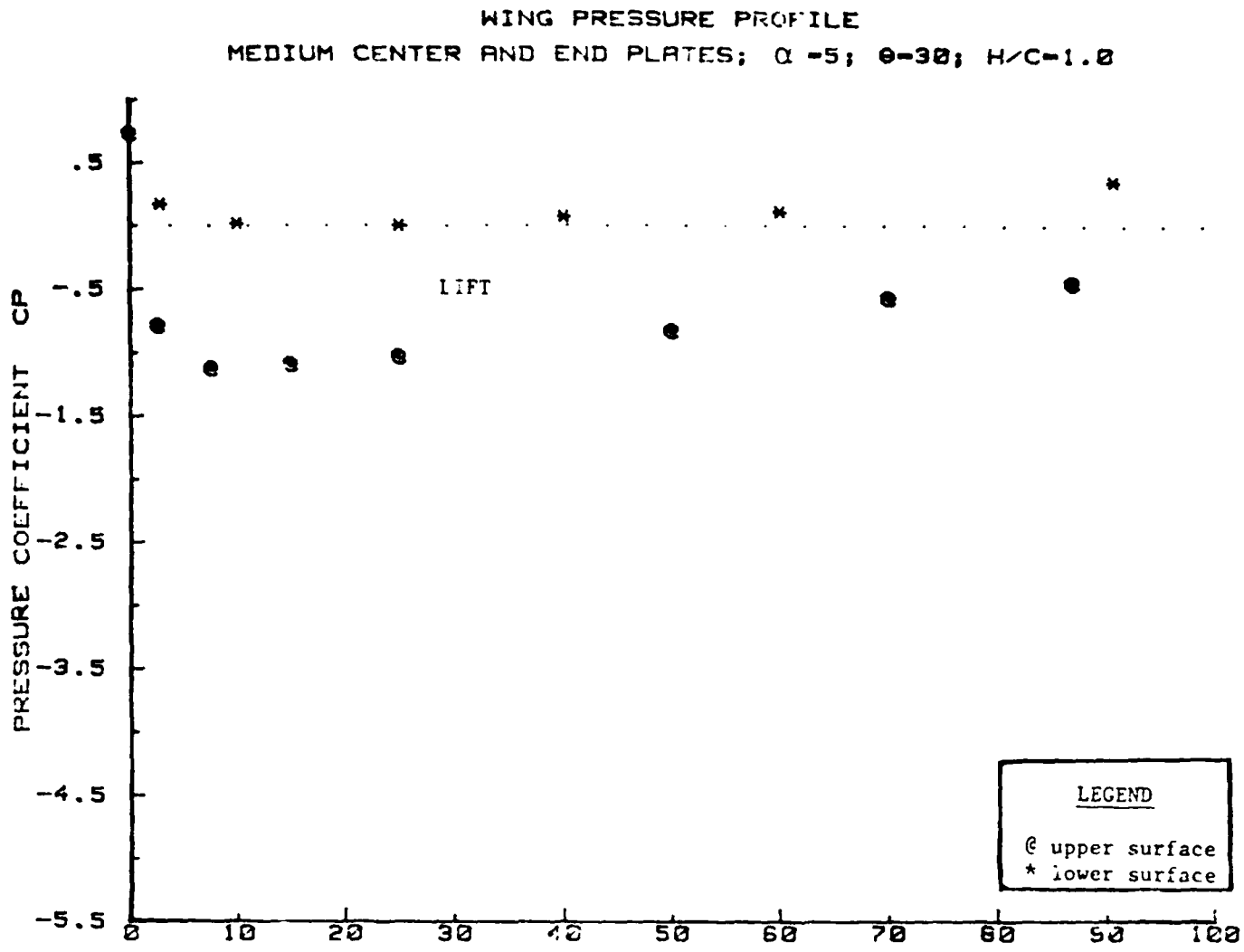

Fig. D-15 Wing Pressure Profile

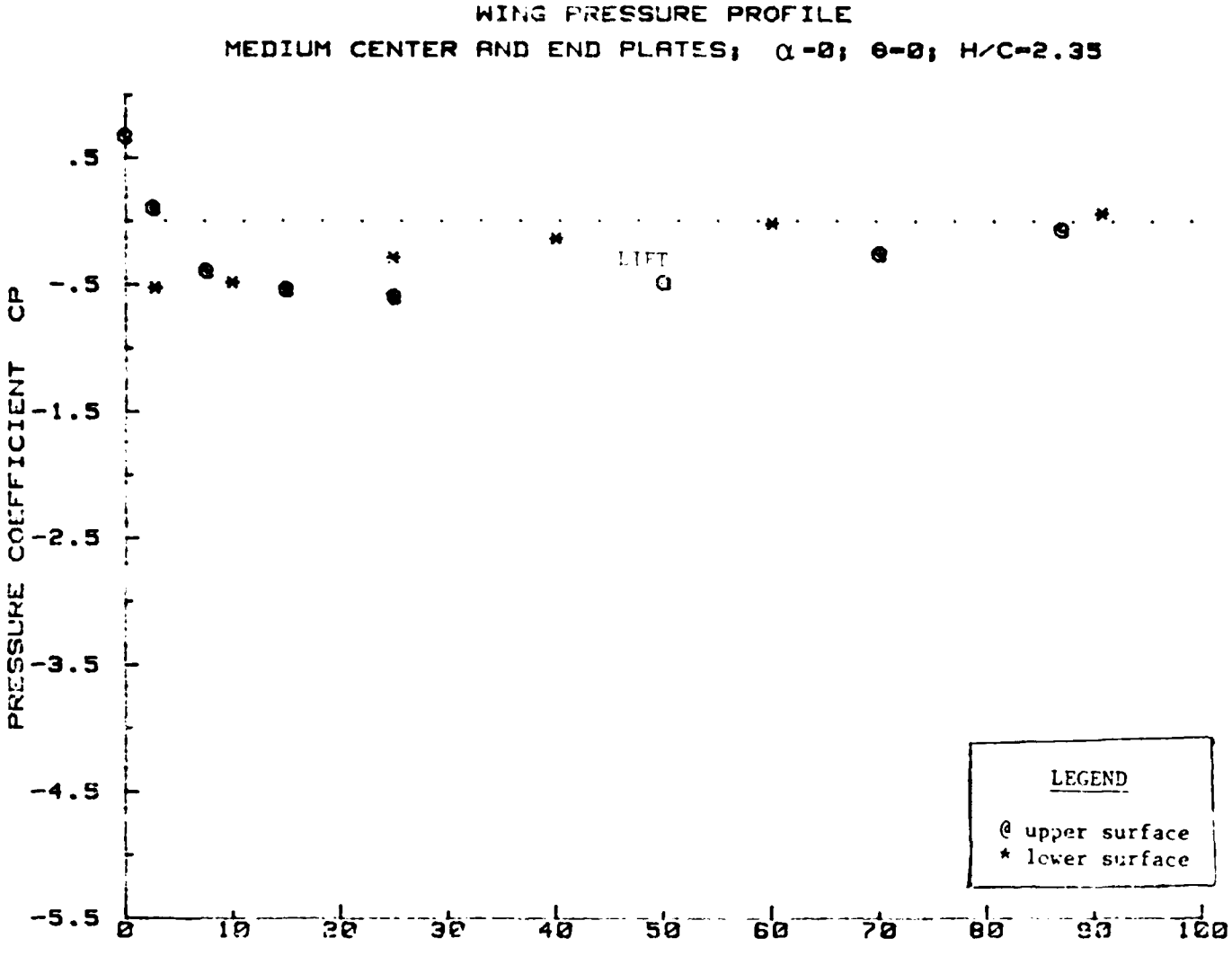

Fig. D-16 Wing Pressure Profile

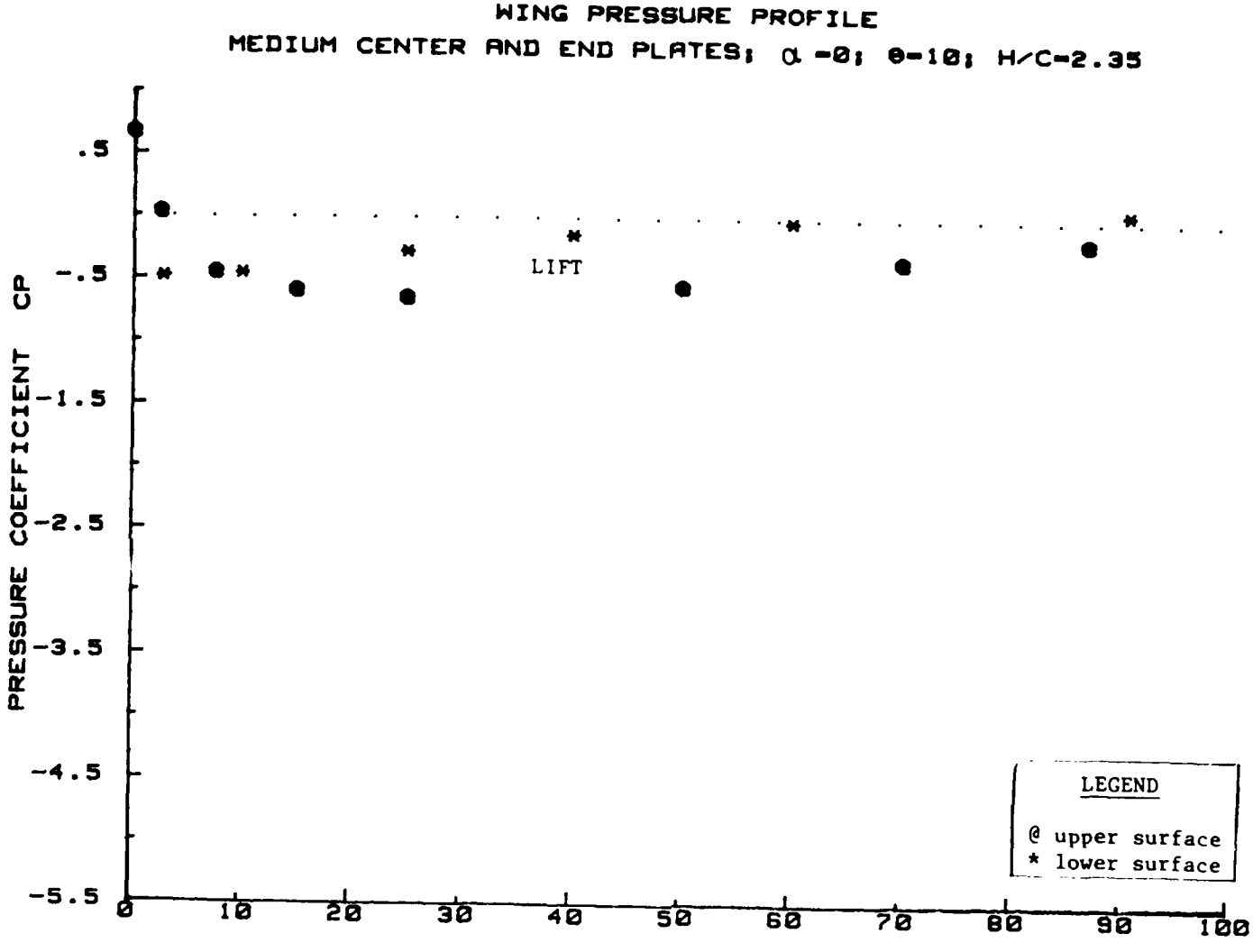

Fig. D-17 Wing Pressure Profile

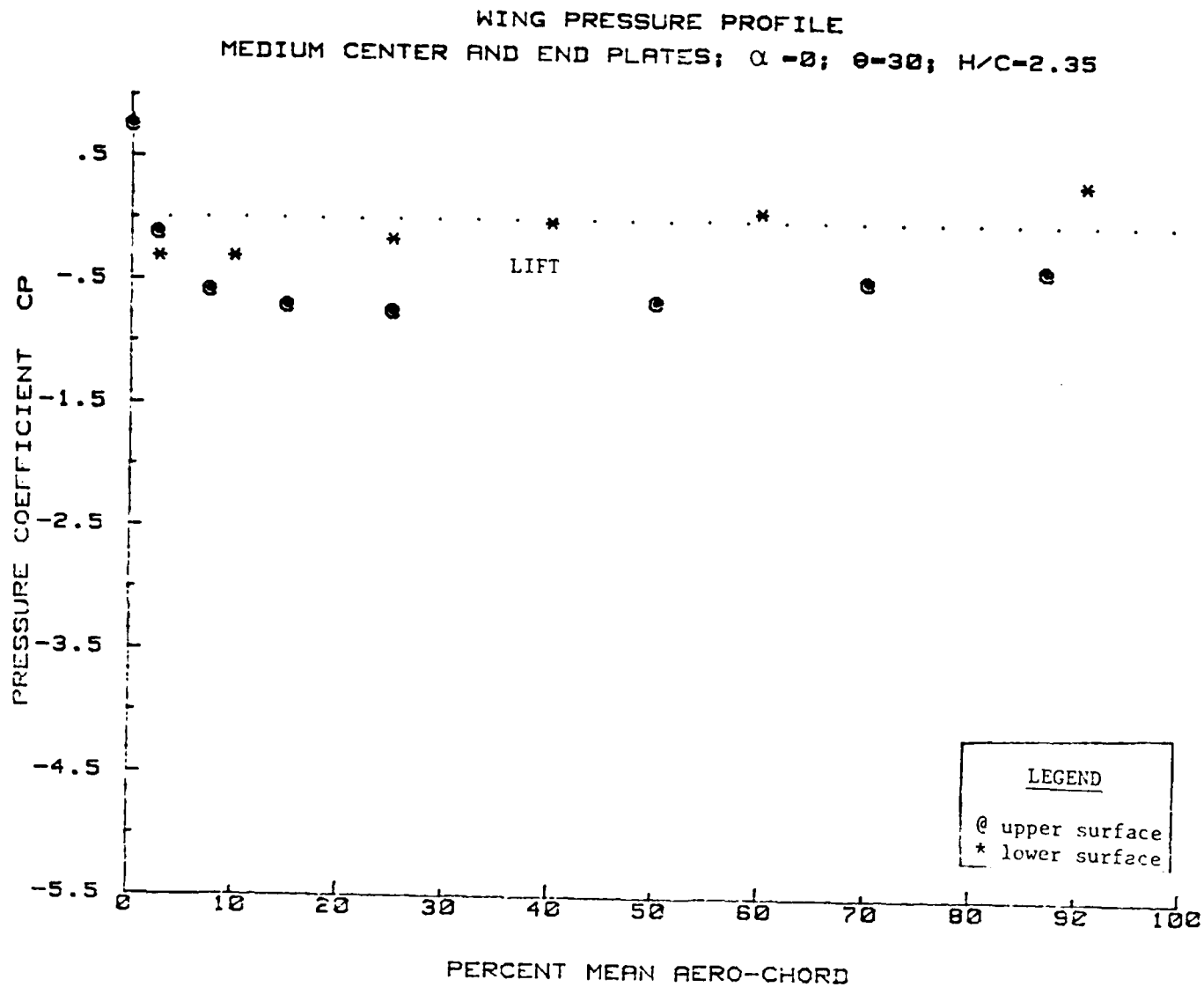

Fig. D-18 Wing Pressure Profile

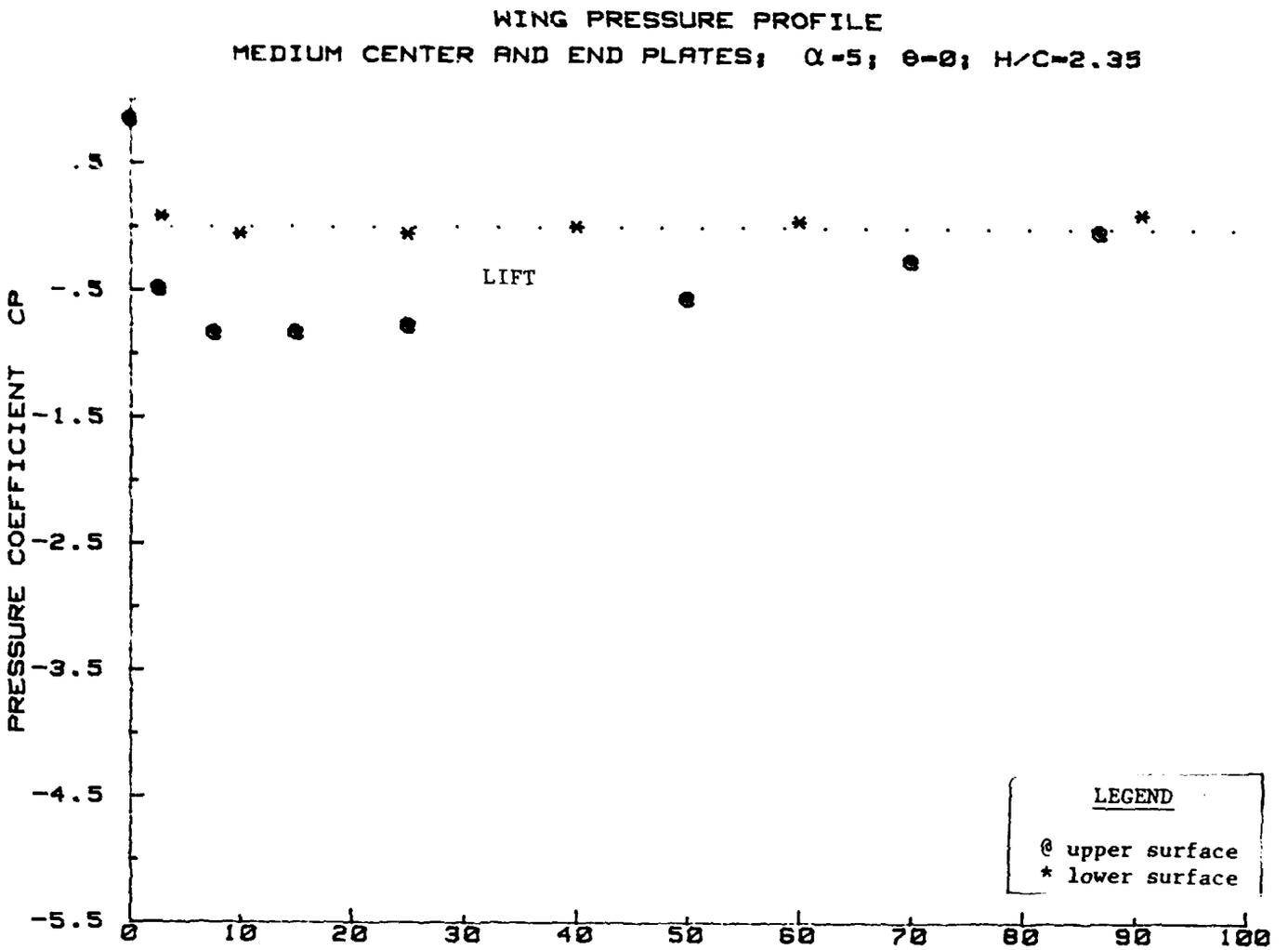

Fig. D-19 Wing Pressure Profile

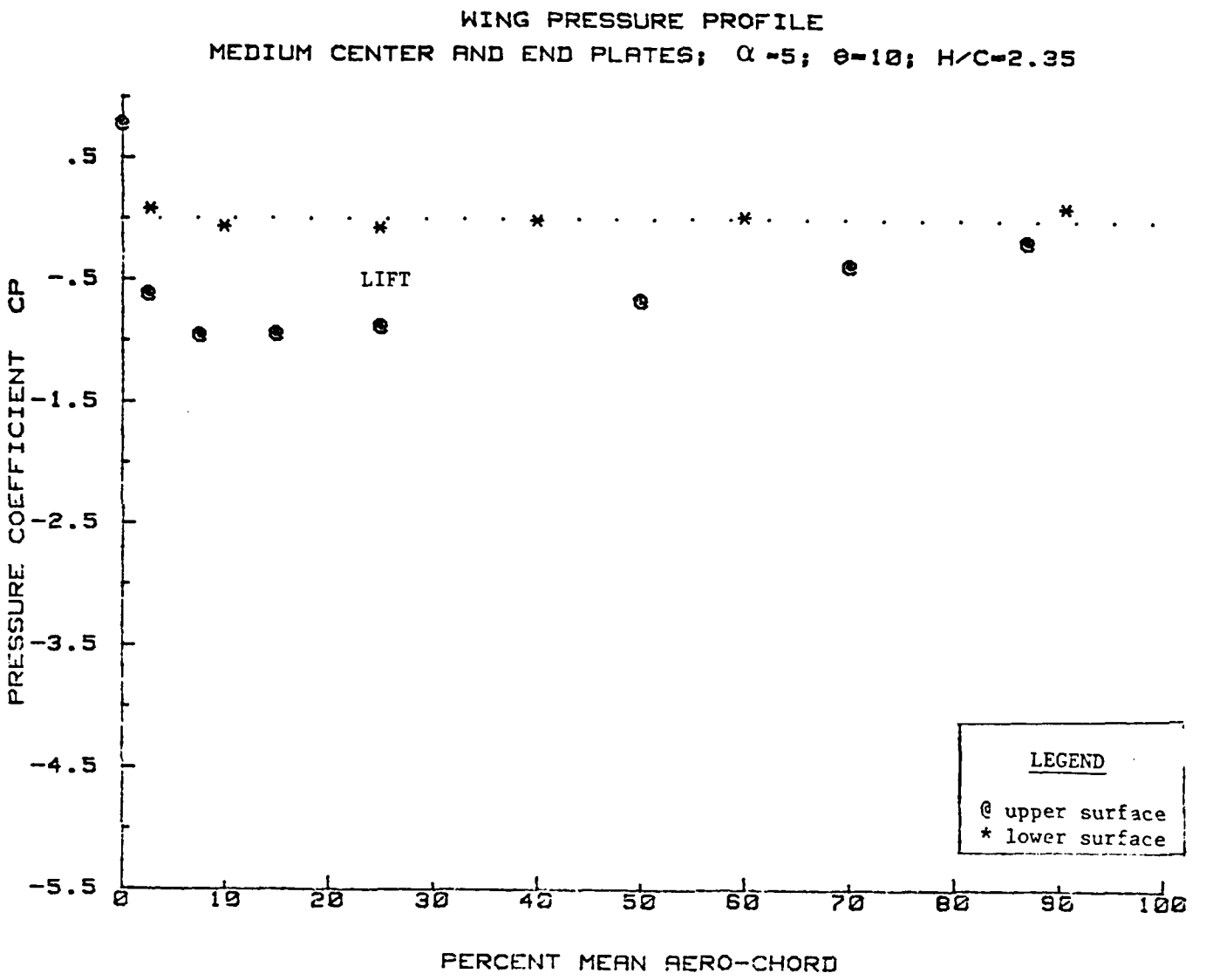

Fig. D-20 Wing Pressure Profile

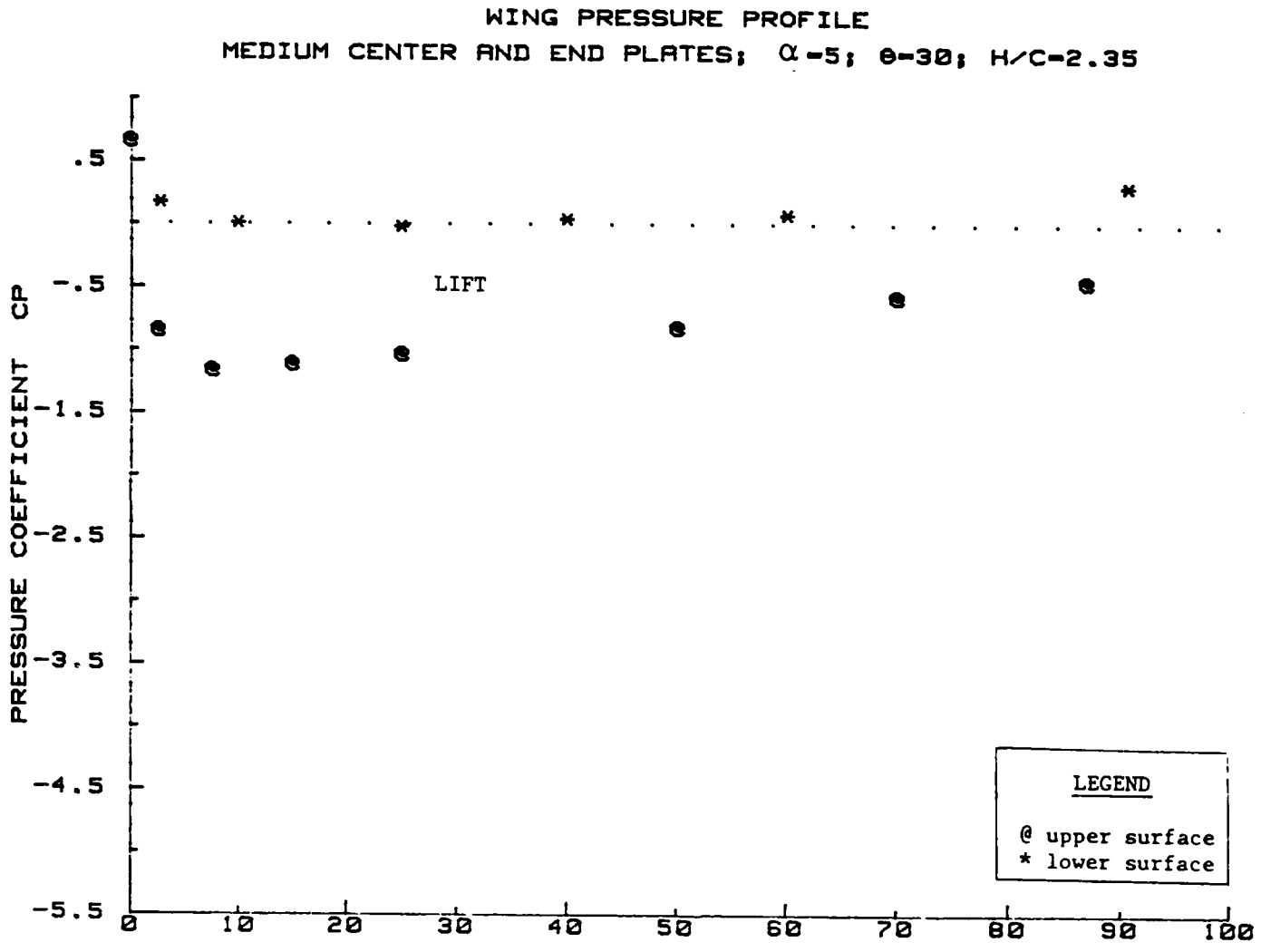

Fig. D-21 Wing Pressure Profile

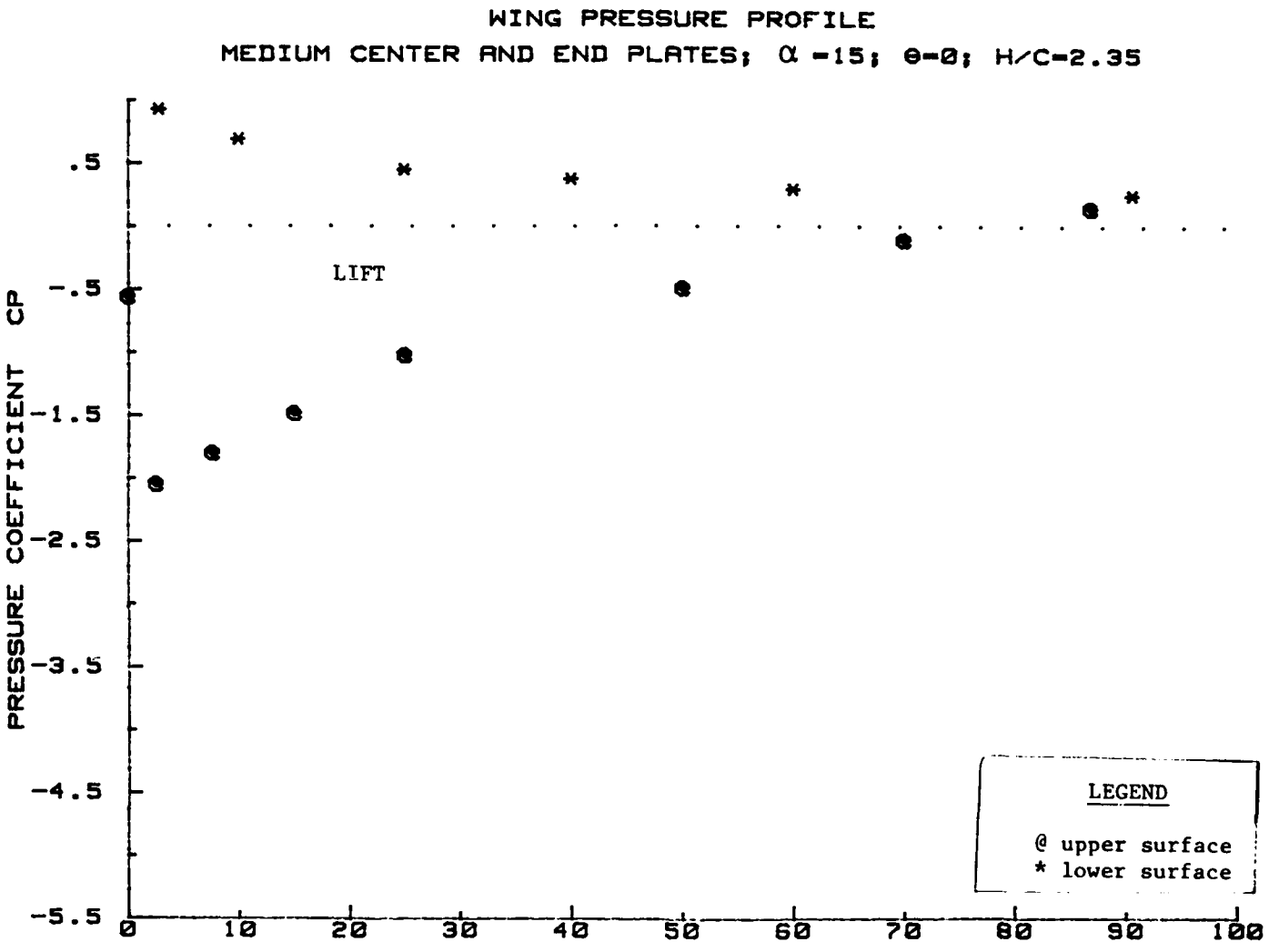

Fig. D-22 Wing Pressure Profile

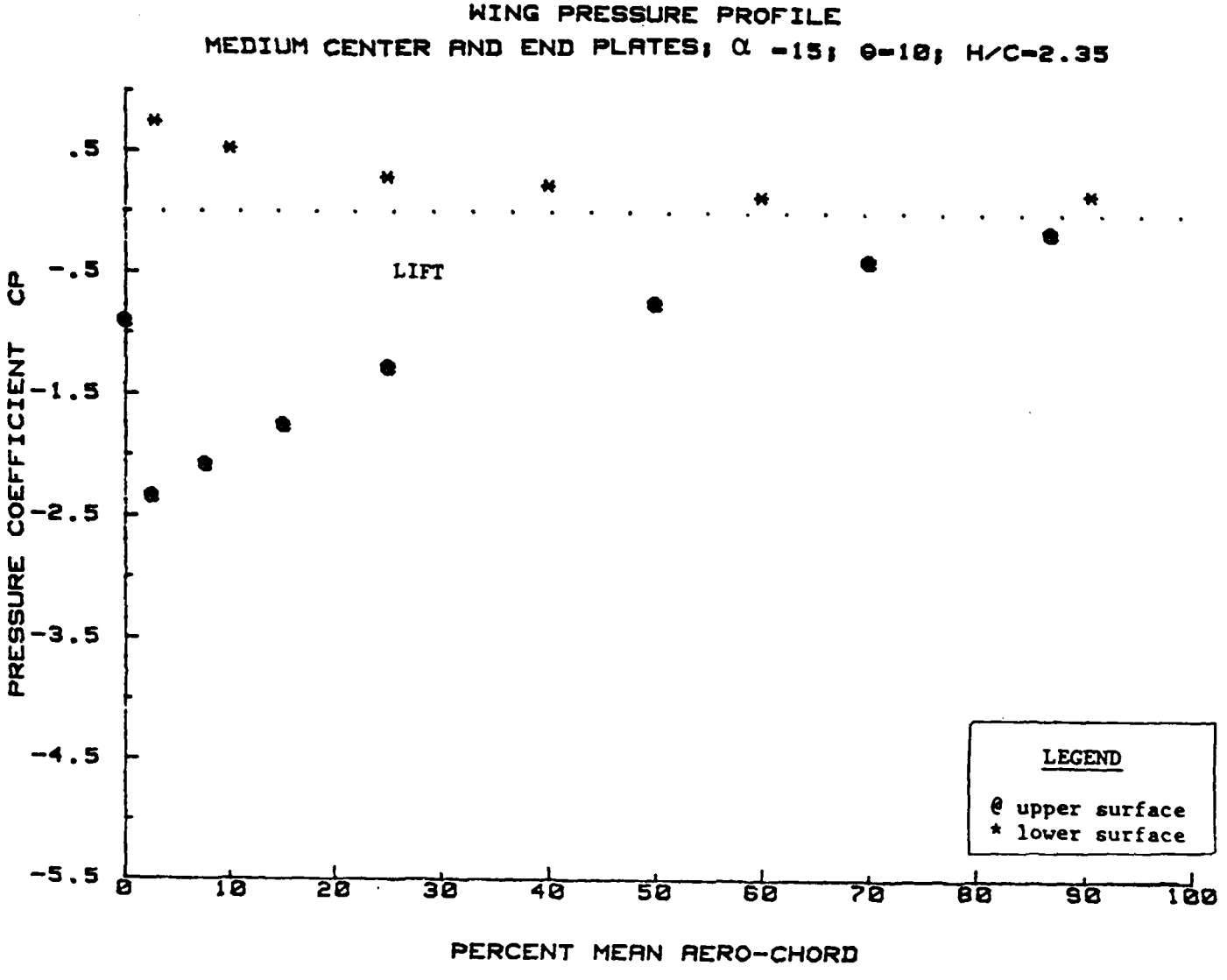

Fig. D-23 Wing Pressure Profile

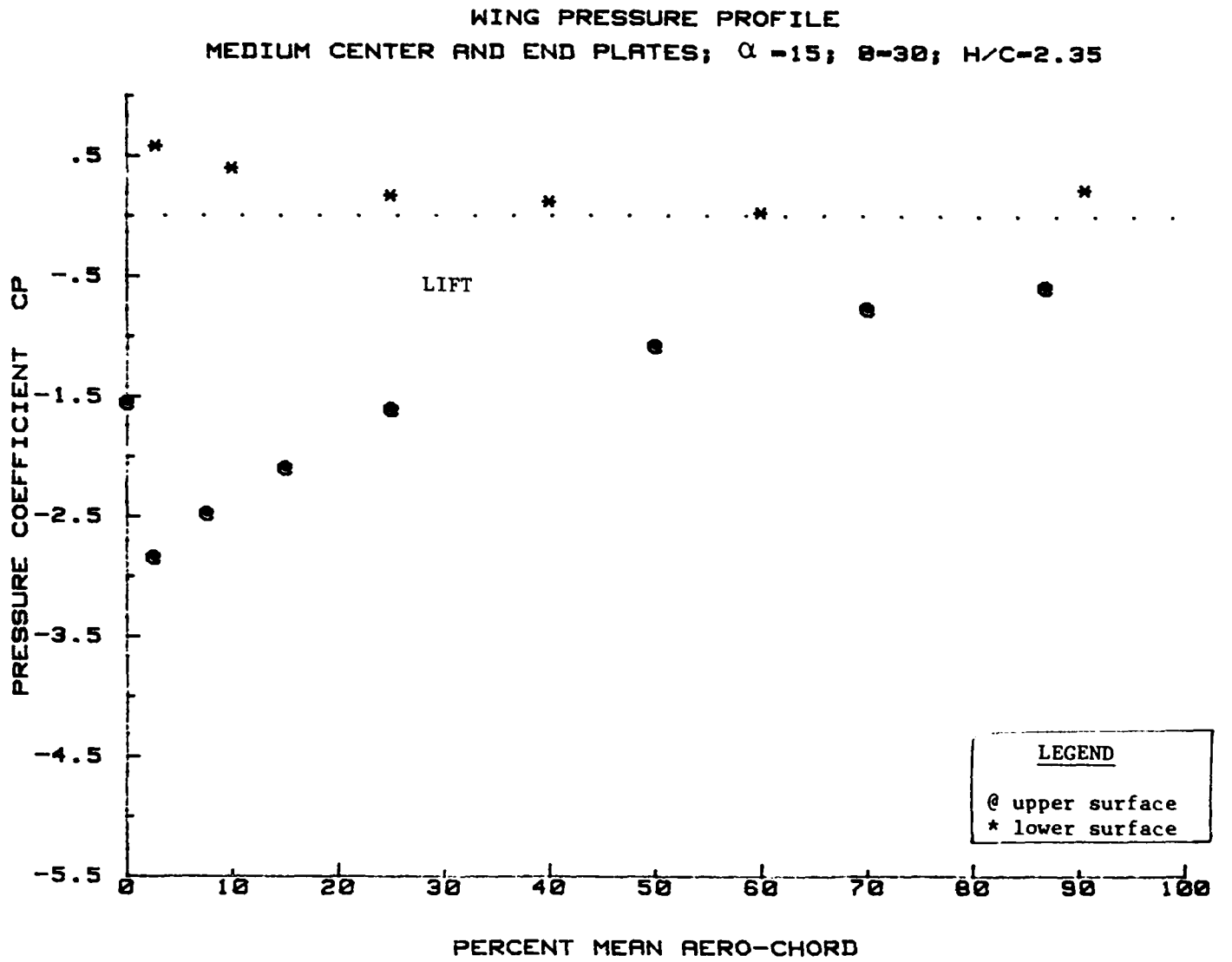

Fig. D-24 Wing Pressure Profile

APPENDIX E: EFFECTS OF α AND θ PLOTS

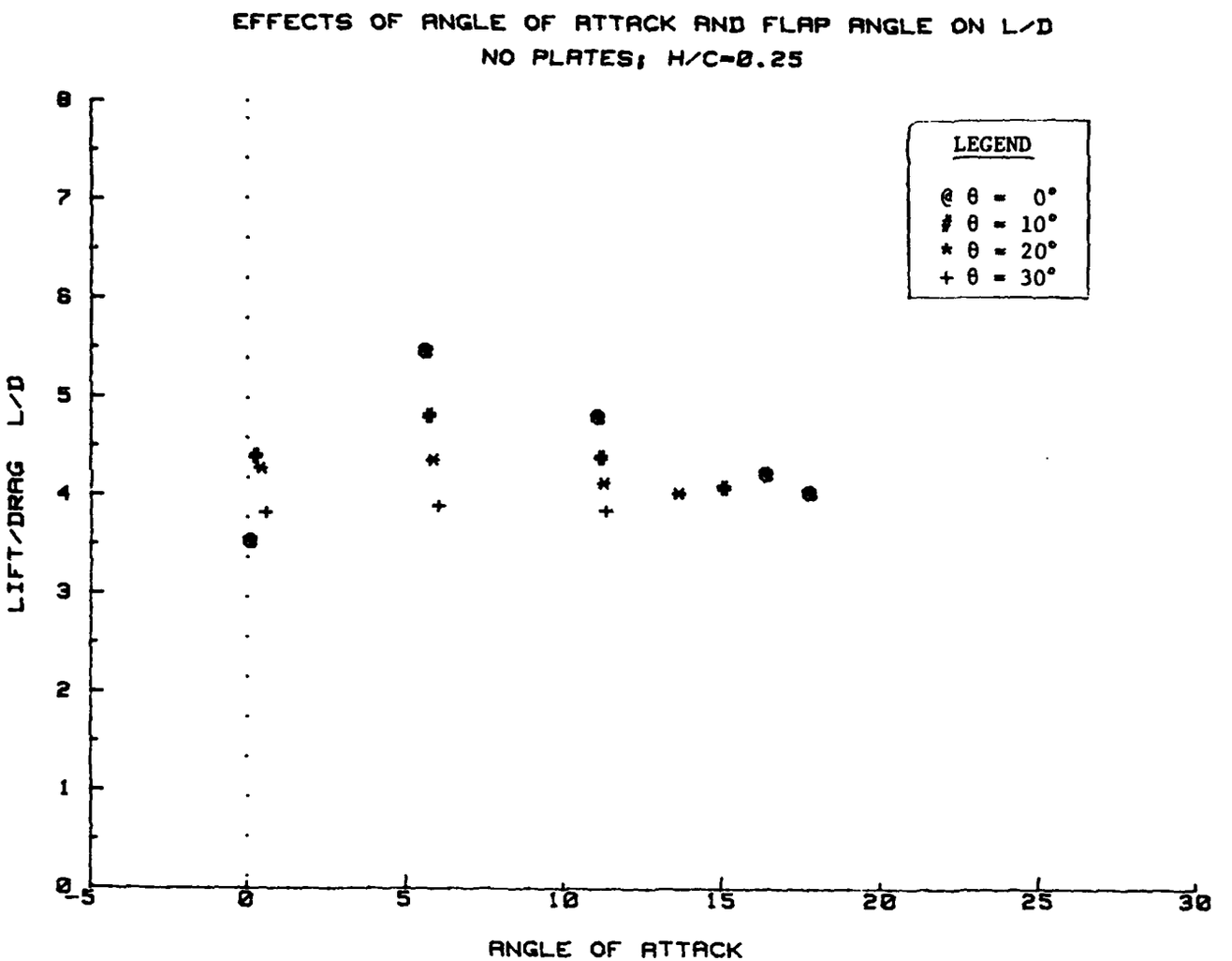

Fig. E-1 Effects of Angle of Attack and Flap Angle on L/D

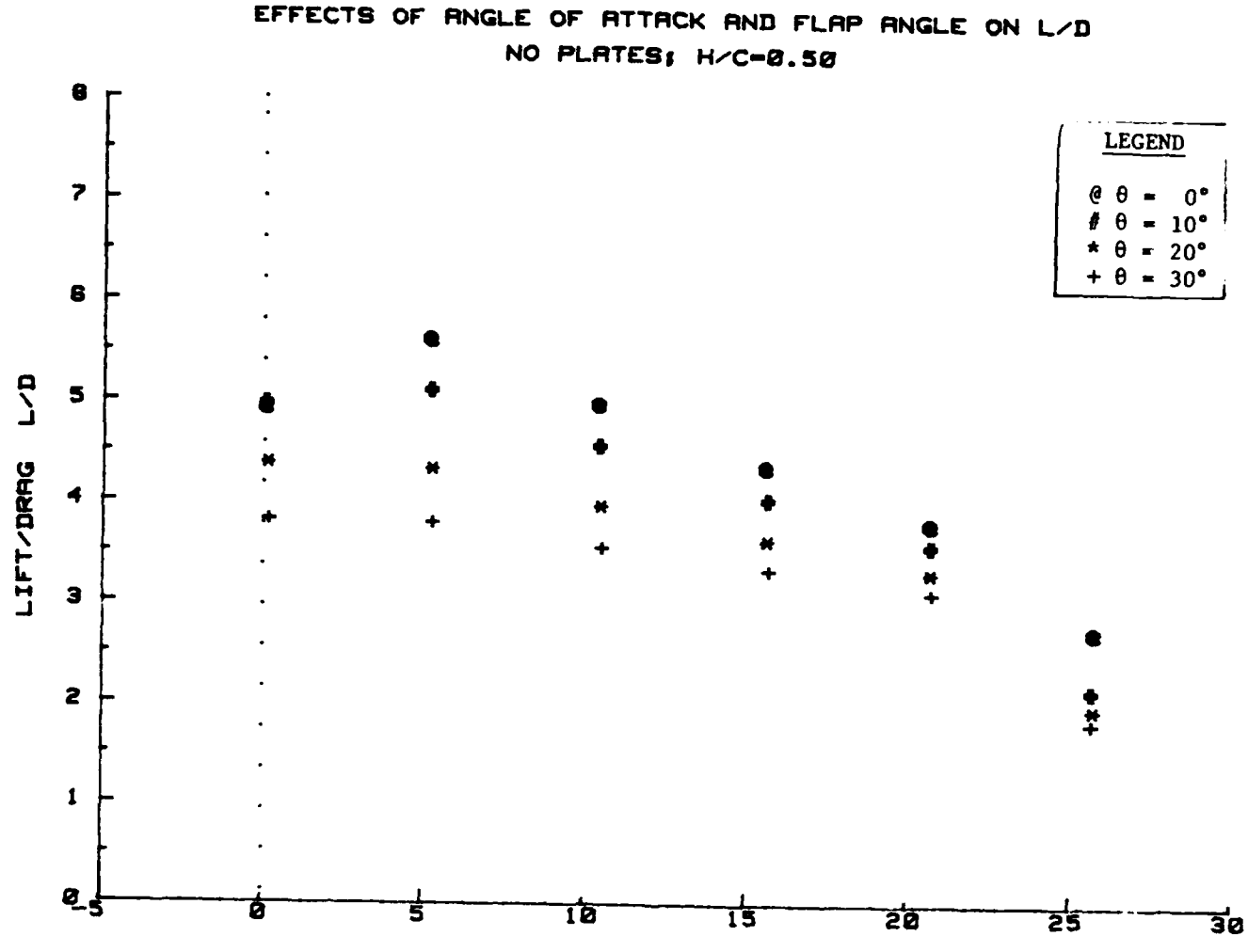

Fig. E-2 Effects of Angle of Attack and Flap Angle on L/D

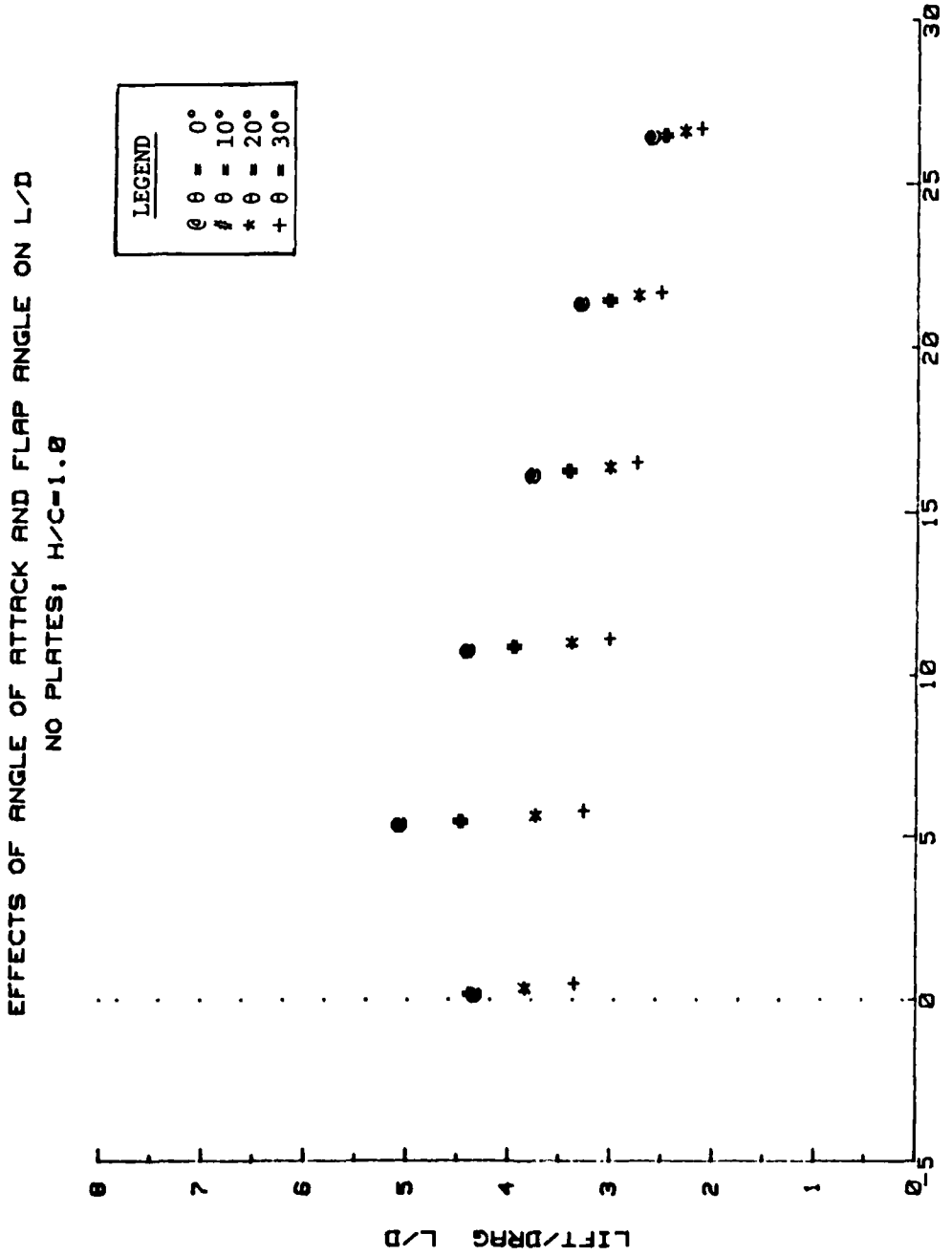

Fig. E-3 Effects of Angle of Attack and Flap Angle on L/D

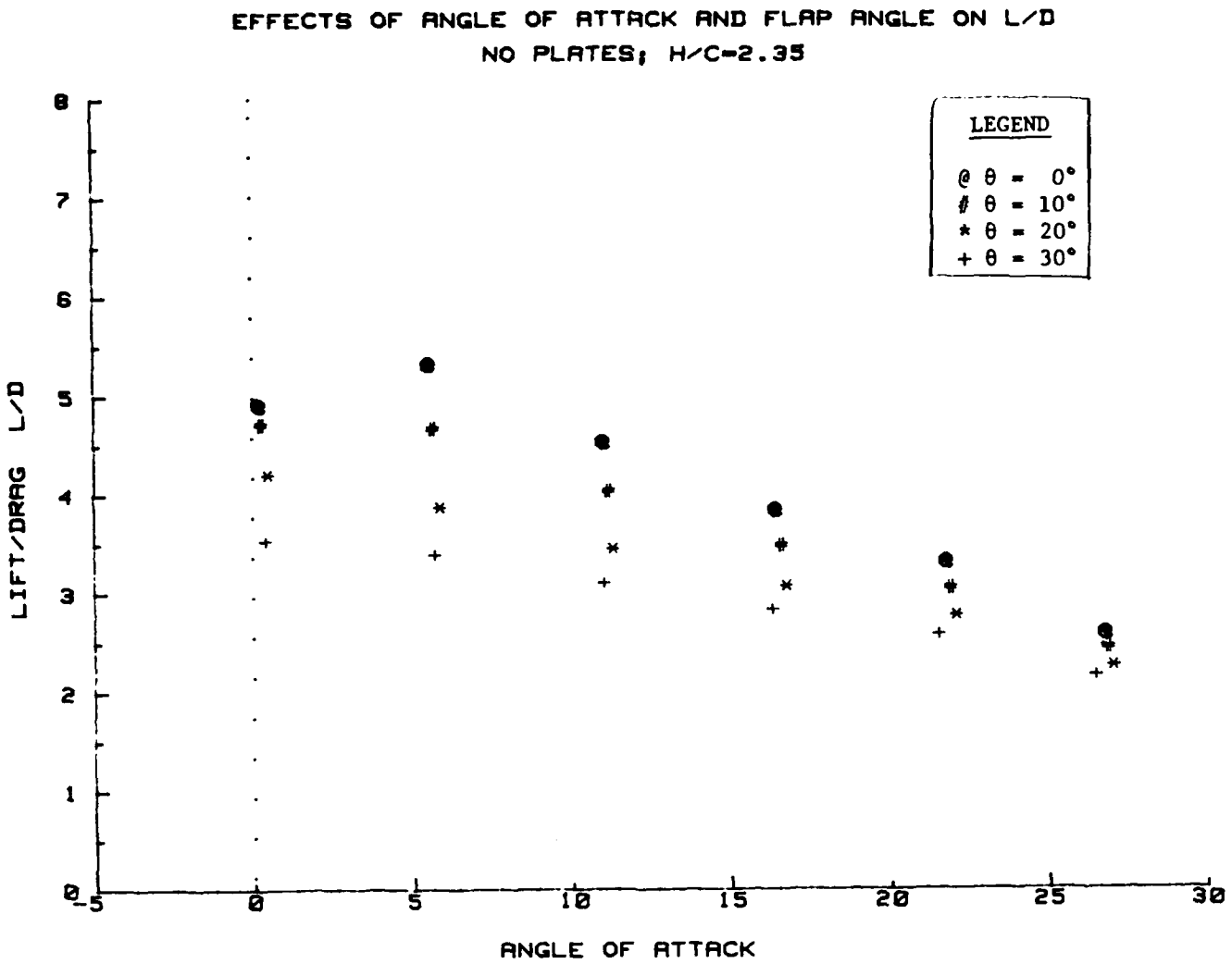

Fig. E-4 Effects of Angle of Attack and Flap Angle on L/D

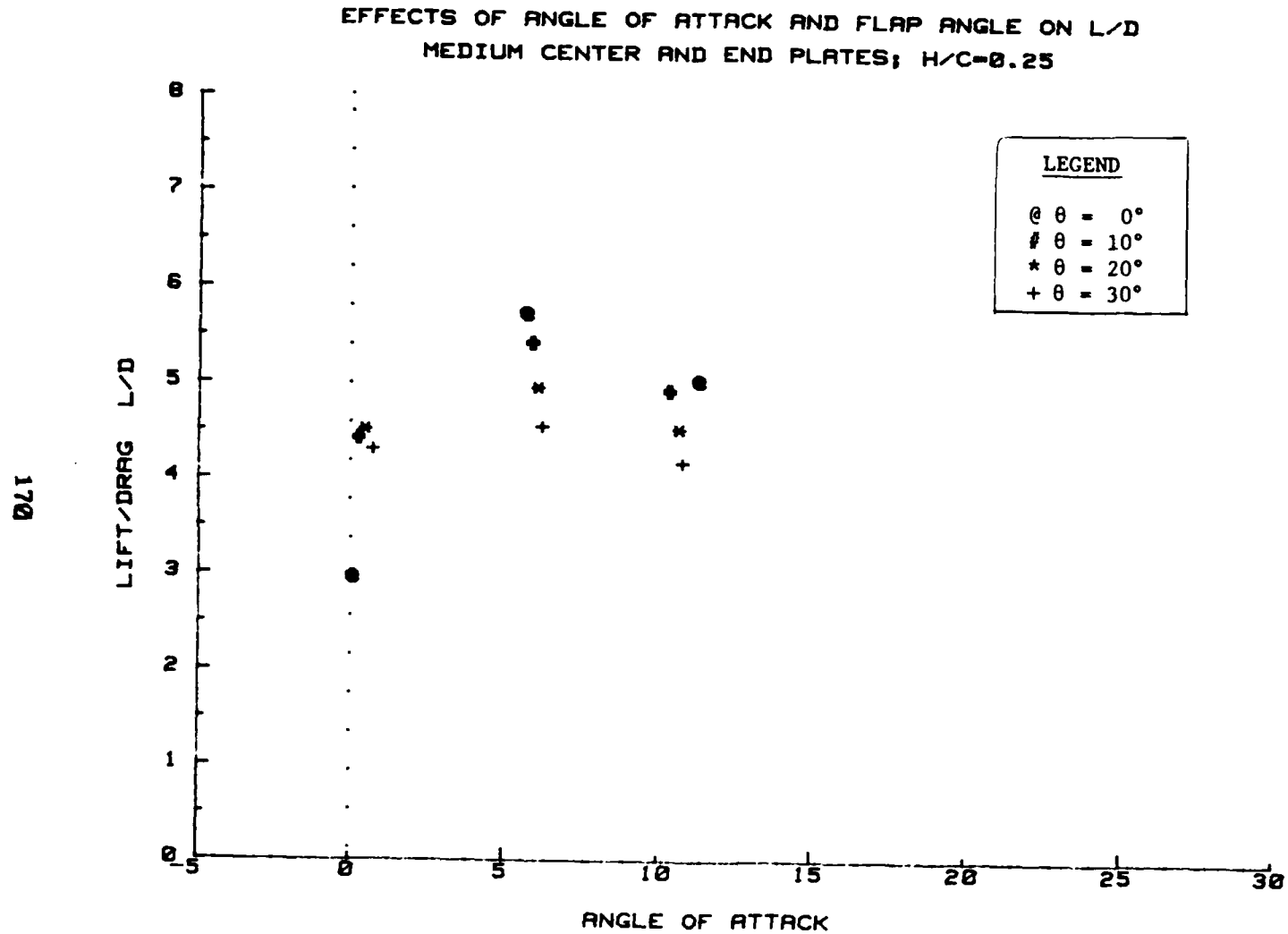

Fig. E-5 Effects of Angle of Attack and Flap Angle on L/D

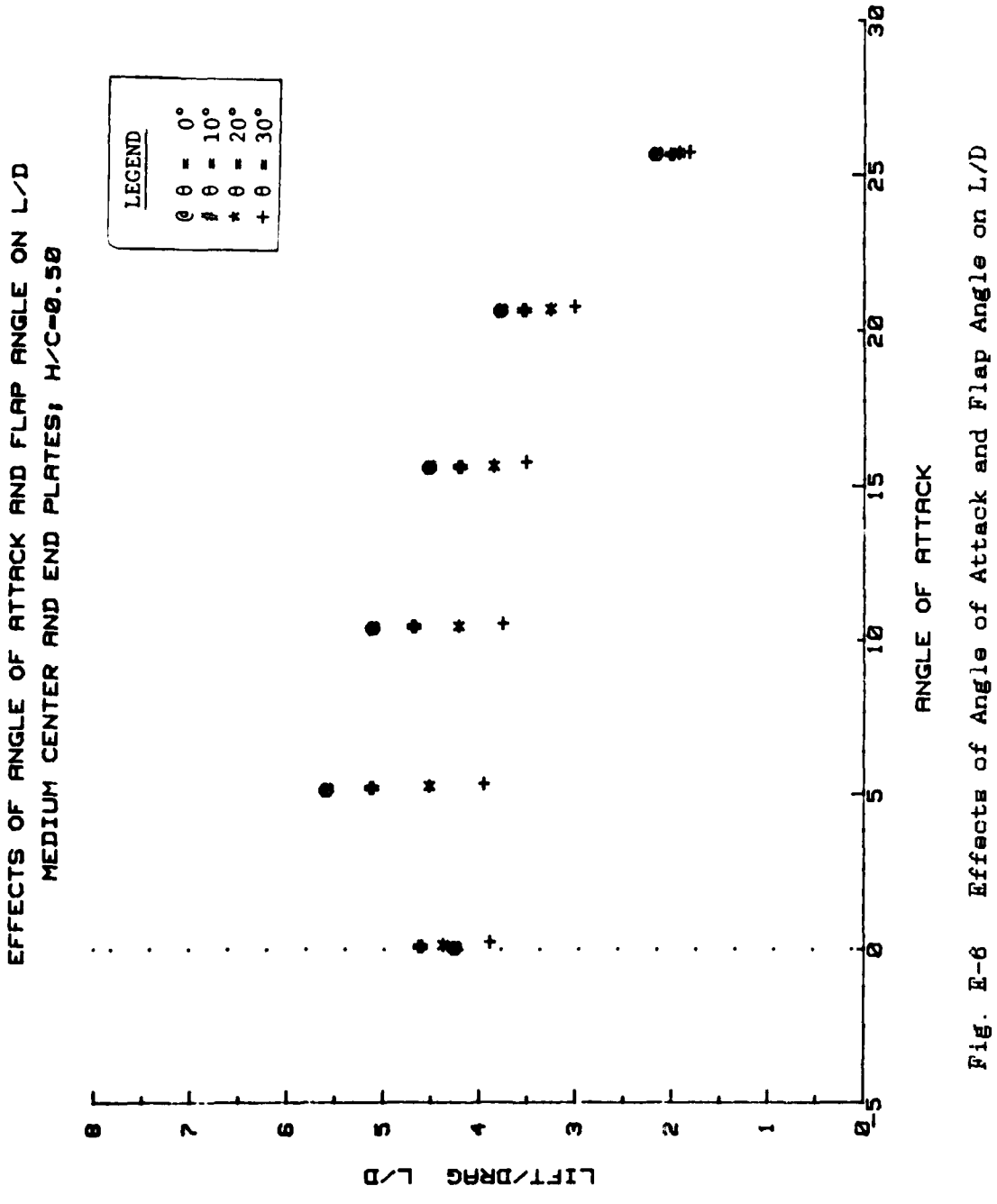

Fig. E-6 Effects of Angle of Attack and Flap Angle on L/D

EFFECTS OF ANGLE OF ATTACK AND FLAP ANGLE ON L/D
MEDIUM CENTER AND END PLATES; H/C=1.0

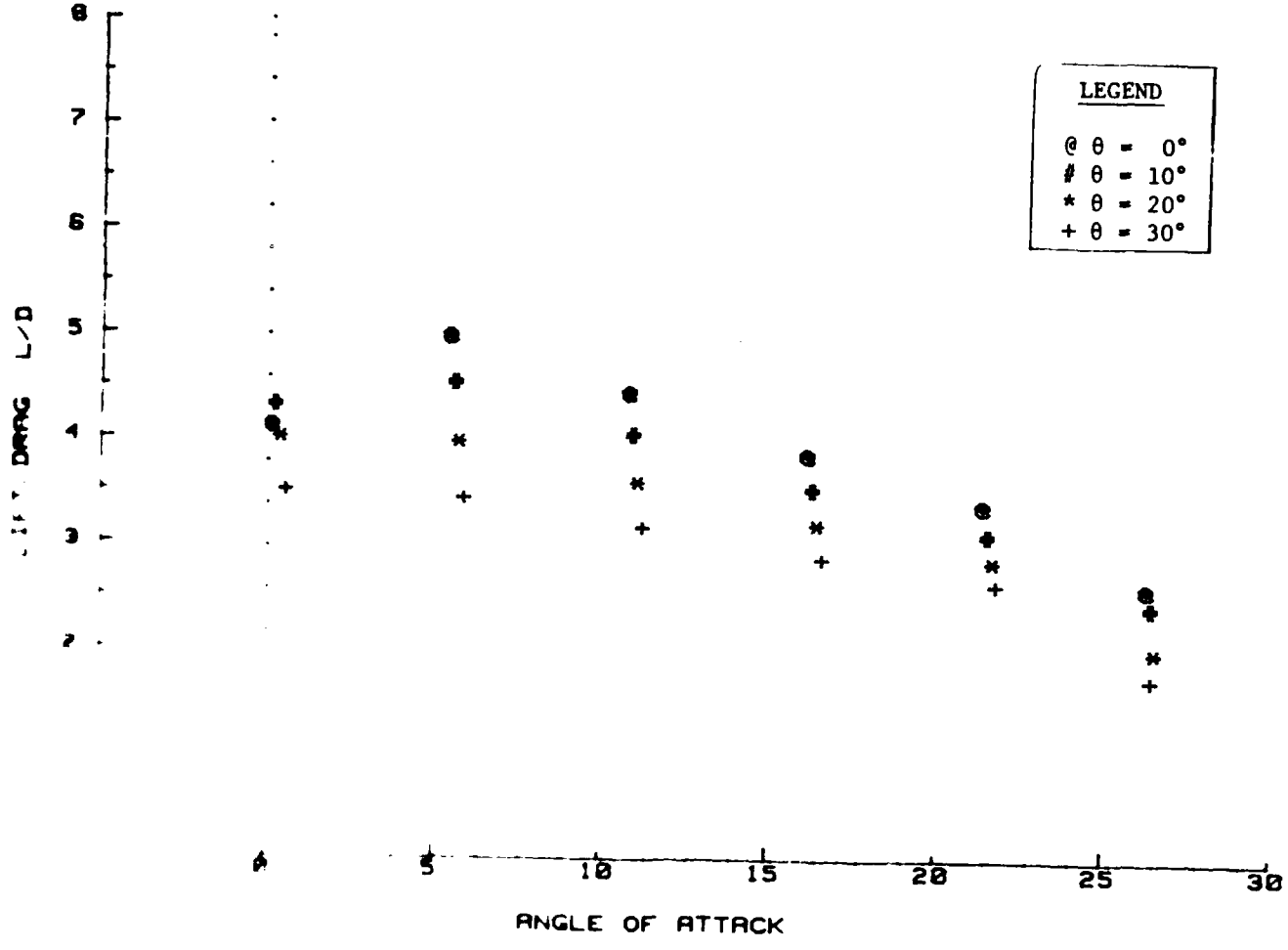

Effects of Angle of Attack and Flap Angle on L/D

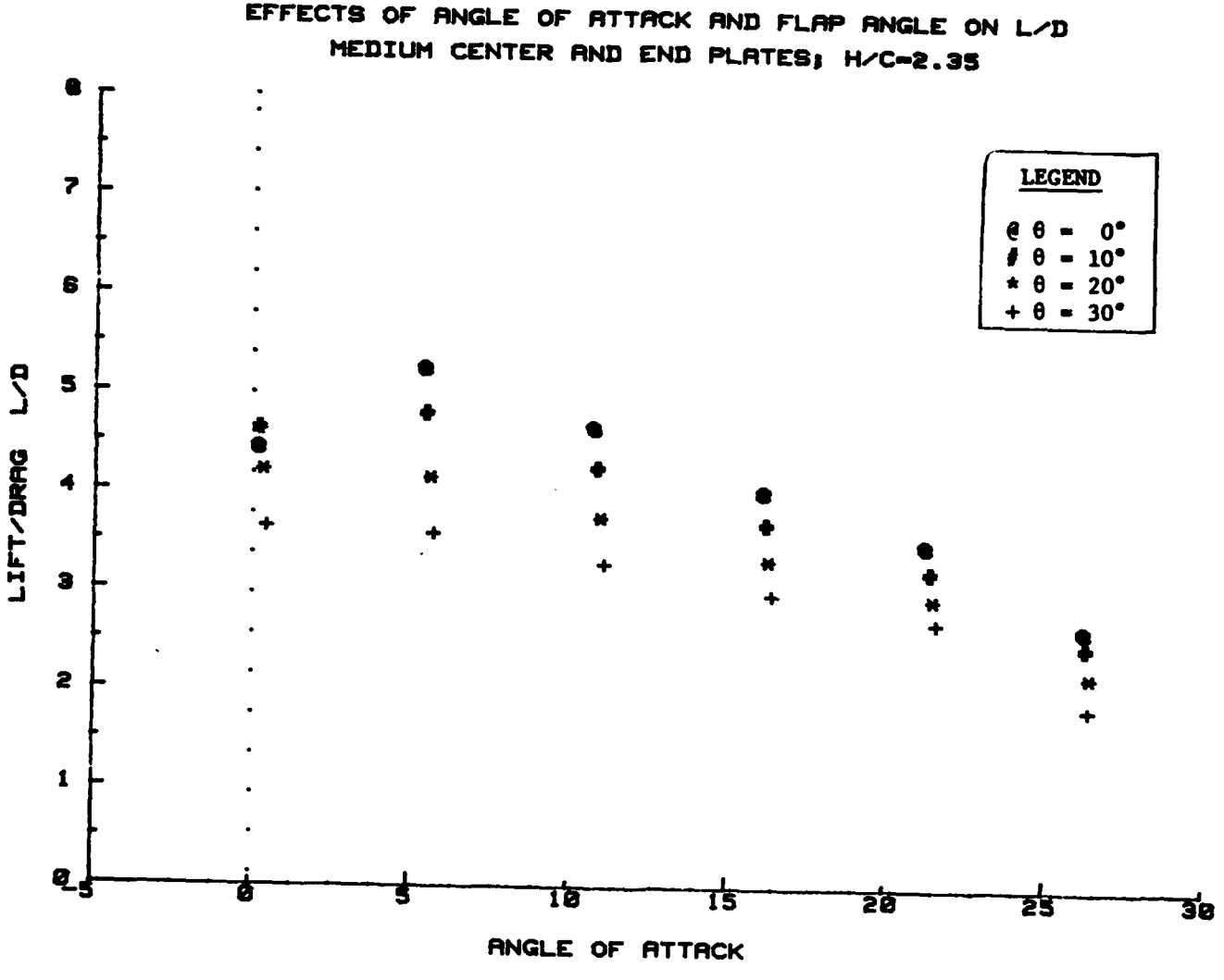

Fig. E-8 Effects of Angle of Attack and Flap Angle on L/D

Bibliography

1. Abbott, Ira H. and Albert E. Von Doenhoff. Theory of Wing Sections. New York: Dover Publications, Inc., 1959.

2. American Power Jet Co. In Ground Effect Cruise Combatant WIG (WIGS) Survivability, Vulnerability and Logistics Considerations. Report No. APJ 815-210. American Power Jet Co., Ridgefield, N.J., September 1977 (AD-B044 500L).

3. Baker, D.C. Ground Effects and Static Stability Characteristics of a Space Transportation Booster Model at Mach Numbers from 0.3 to 0.9. Contract F40600-69-C-0001. Arnold Engineering Development Center, Arnold Air Force Base, TN, February 1970 (AD-869 333).

4. Bagley, J.A. The Pressure Distribution on Two-Dimensional Wings Near the Ground. Report Aero. 2625. Royal Aircraft Establishment, Farnborough, England, February 1960 (AD-238 261).

5. Bagley, J.A. Low-Speed Wind Tunnel Tests on a Two-Dimensional Aerofoil with Split Flap Near the Ground. Tech. Note Aero. 2636. Royal Aircraft Establishment, Farnborough, England, March 1961 (AD-260 653).

6. Belavin, N.I. Wing-In-Ground Effect Craft: The Flying Boats. Paper, Kater i Takhty, No. 15, 1968, U.S.S.R., translated by Naval Intelligenct Support Center, Washington, D.C., October 1976 (AD-A032 507).

7. Belden, T.G. Surface Effects Take-off and Landing Aircraft. Patent APPL-313 860. Department of the Air Force, Washington, D.C., October 1981 (AD-D009 198).

8. Buell, R.L. A Design Study of High Aspect Ratio Wings. Report No. M-5. Bureau of Aeronautics, Navy Department, Washington, D.C., June 1942 (AD-896 716L).

9. Burgan, Elmer T. and Fletcher C. Paddison. Surface Effect Take-off and Landing System (SETOLS). Report No. ARPA/TIO-74-21. Johns Hopkins University, Silver Springs, MD, April 1974 (AD-A000 101).

10. Busch, Steven D. and James R. Martin. The Transatmospheric Vehicle in a Defensive Satellite Role. MS Thesis. School of Engineering, Air Force Institute of Technology (AU), Wright-Patterson Air Force Base, OH, December 1985.

11. Carter, Arthur W. Effect of Ground Proximity on the Aerodynamic Characteristics of Aspect-Ratio-1 Airfoils With and Without End Plates. Tech. Note D-970. NASA, Washington, D.C., October 1961 (AD-265 186).

12. Chawla, Mangal D. "Horizontal Launch System for Transatmospheric Vehicles". Prepared for AIAA 8th Advanced Marine Systems Conference, Air Force Wright Aeronautical Laboratory, Flight Dynamics Modility Branch, September 1986.

13. Engler, P.B.E. and G.F. Moss. Low-Speed Wing-Tunnel Tests on a 1/8 Scale Model of the Handley-Page HP.115. Report No. 3486. Ministry of Technology, London, England, August 1965 (AD-822 748).

14. Fink, Marvin P. and James L. Lastinger. Aerodynamic Characteristics of Low-Aspect-Ratio Wings in Close Proximity to the Ground. Tech. Note D-926. NASA, Washington, D.C., July 1961 (AD-260 640).

15. Foshag, William F. Literature Search and Comprehensive Bibliography of Wings in Ground Effect and Related Phenomena. Report No. 2179. Aerodynamics Laboratory, David Taylor Model Basin, Washington, D.C., March 1966 (AD-633 139).

16. Foster, D.N. and L.F. East. The Theoretical Effect of Ground Proximity on a High-Lift Wing. Report No. 76139. Royal Aircraft Establishment, Farnborough, England, October 1976 (AD-B020 976L).

17. Gallington, Roger W. and Mark K. Miller. "The Ram-Wing: A Comparison of Simple One-Dimensional Theory with Wind Tunnel and Free Flight Results". AIAA Paper No. 70-971. Proceedings of AIAA Guidance, Control and Flight Mechanics Conference, Santa Barbara, CA, August 1970 (AD-715 557).

18. Gallington, Roger W., Mark K. Miller, and Woodrow D. Smith. "The Ram-Wing Surface Effect Vehicle: Comparison of One-Dimensional Theory with Wind Tunnel and Free Flight Results". Project No. 7905, Frank J. Seiler Research Laboratory, U.S. Air Force Academy, Colorado, July 1971. (Update of #17).

19. Gallington, Roger W. Approximate Forces on Hard WIG End Plates Penetrating Waves and Limits on Yaw Angle and Speed. Report No. TM-16-77-107. David Taylor Naval Ship Research and Development Center, Bethesda, MD, January 1977 (AD-B044 480L).

20. Gallington, Roger W. and Michael Sekellick. Assessment of Wing In Ground Effect Vehicle Technology, Vol. I. Contract 12102. David Taylor Naval Ship Research and Development Center, Bethesda, MD, February 1980 (AD-B044 603L).

21. Goddard, V.P. and C.A. Campbell. A Wind Tunnel Free Flight Technique to Determine Lift and Drag of a Wing Configuration. Report No. 1412. Ballistic Research Laboratories, Aberdeen Proving Ground, MD, August 1968 (AD-843 079).

22. Goetz, Alfred R. Aerodynamic Performance of a Wing-In-Ground Effect Using the Panair Program. MS Thesis, AA/84D-7. School of Engineering, Air Force Institute of Technology (AU), Wright-Patterson Air Force Base, OH, December 1984.

23. Hackett, J.E. and E.B. Praytor. Ground Effect for V/STOL Aircraft Configurations and Its Simulation in the Wind Tunnel, Part I, Introduction and Theoretical Studies. Contract NAS 2-66900. Lockheed-Georgia Company, Marietta, GA, December 1972.

24. Harry, Charles W. Wind Tunnel Investigation of Ground Effect on a Rectangular Wing of Several Moderate Aspect Ratios. Report No. 1979. Bureau of Naval Weapons, Washington, D.C., July 1965 (AD-474 257).

25. Harry, Charles W. and Lynn A. Trobaugh. Wind Tunnel Investigation of an Aspect Ratio 10 Tandem Wing Aircraft Configuration in Ground Effect, Part I, Longitudinal Chracteristics. Report No. 2259-1. Bureau of Naval Weapons, Washington, D.C., July 1966 (AD-641 246).

26. Jones, Bradley. Elements of Practial Aerodynamics. New York: John Wiley and Sons, Inc., 1950.

27. Krause, Fred H. and Roger W. Gallington. Static Performance of a Power Augmented Ram Wing. Report No. TM-16-76-76. David Taylor Naval Ship Research and Development Center, Bethesda, MD, May 1976.

28. Kuhn, Richard F. An Engineering Method for Estimating the Induced Life on V/STOL Aircraft Hovering In and Out of Ground Effect. Report No. NADC 80246-60. Naval Air Development Center, Westminster, PA, January 1981 (AD-A098 509).

29. Lockheed-California Company. Wind Tunnel Investigation of Single and Tandem Low-Aspect-Ratio Wings in Ground Effect. TRECOM Technical Report No. 63-63, U.S. Army Transportation Research Command, Ft. Eustis, VA, March 1964 (AD-600 498).

30. McKerhan, Thomas J., Jr. A Wind Tunnel Investigation to Examine Stability and Control Characteristics of the T-46A at High Sideslip Angles. MS Thesis, AA/84D-16. School of Engineering, Air Force Institute of Technology (AU), Wright-Patterson Air Force Base, OH, December 1984.

31. Moore, J.W. and B.T. Farmer, J.F. Honrath, F.E. McBride, R.E. Stephens. Parametric and Conceptual Design Study of Aircraft Wing-In-Ground Effect (WIG) Vehicles. Contract N62269-76-C-0465, Lockheed-Georgia Company, Marietta, GA, May 1977 (AD-B044 634).

32. Nicolai, Leland M. Fundamentals of Aircraft Design. San Jose, CA: METS, Inc., 1984.

33. Pope, Alan and William H. Rae, Jr. Low-Speed Wind Tunnel Testing (Second Edition). New York: John Wiley and Sons. 1984.

34. Rousseau, David G. and Roger W. Gallington. Performance Prediction Method for a Wing-In-Ground Effect Vehicle With Blowing Under the Wing. Report No. 1612-009. David Taylor Naval Ship Research and Development Center, Bethesda, MD, March 1977.

35. Rozhdestvenskiy, K. V. and A.R. Besyadovskiy. Theoretical Evaluation of the Effect of End Plates on Lifting Force of a Low-Ratio Wing in Close Proximity to the Ground. Paper, Trudy Leningradskogo Ordena Lenina Korablestroirlel'nogo Instituta, U.S.S.R., 1977, translated by Naval Intelligence Support Center, Washington, D.C., August 1980 (AD-B050 876L).

36. Schlichting, Hermann. Boundary Layer Theory (Fourth Edition). New York: McGraw-Hill Book Company, Inc., 1960.

37. Spitler, Charles R. A Wind Tunnel Investigation of the Stability and Control Characteristics of the Fairchild T-46 at High Angles of Attack. MS Thesis, AA/84D-27, School of Engineering, Air Force Institute of Technology (AU), Wright-Patterson Air Force Base, OH, December 1984.

38. Strand, T. and J.J. Brainerd. Design of Wing Sections For Use Near the Ground. Report No. 349. Air Vehicle Corporation, San Diego, CA, March 1965 (AD-465 949).

39. Summers, D.R., et al. The General Characteristics of Winged Ground Effect Machines. TRECOM Technical Report No. 63-36. U.S. Army Transportation Research Command, Ft. Eustic, VA, October 1963 (AD-434 300).

40. Trobaugh, Lynn A. and Charles W. Harry. Wind Tunnel Investigation of an Aspect Ratio 10 Tandem Wing Aircraft Configuration in Ground Effect, Part II, - Lateral Characteristics. Report No. 2259-2. Bureau of Naval Weapons, Washington, D.C., January 1967 (AD-650 996).

41. White, Herbert E. Wind-Tunnel Tests of a Low-Aspect-Ratio Wing in Close Proximity to the Ground. Aero. Report No. 1056. David Taylor Model Basin, Washington, D.C., June 1963 (AD-413 890).

42. Widnall, Sheila E. and Timothy M. Barrows. An Analytic Solution for Two- and Three- Dimensional Wings in Ground Effect. Laboratory Report No. 69-1. Massachusetts Institute of Technology, Cambridge, MA, June 1969 (AD-692 562).

43. Wieselberger, Carl. Wing Resistance Near the Ground. Munich, Germany, May 1921, translated by NACA, Tech. Memo No. 77, Washington, D.C., April 1922.

VITA

Major Lawyn C. Edwards was born into the Army family of [redacted] He attended three high schools and graduated from [redacted] in June 1971. He graduated from the United States Military Academy at West Point, New York on 4 Jun 1975 with a Bachelor of Science degree. On the same day, he was commissioned a Second Lieutenant of Armor in the Regular Army. He has been stationed in Armored and Air Cavalry units in Korea, CONUS, and USAREUR over his 11 years of service in combat units. He proudly wears the tabs and badges awarded for Airborne, Ranger, Pathfinder and Senior Army Aviator. He is married to the former [redacted] and has a set of twins, [redacted] as this thesis began.

Permanent Address: [redacted]

UNCLASSIFIED
SECURITY CLASSIFICATION OF THIS PAGE

REPORT DOCUMENTATION PAGE

Form Approved
OMB No. 0704-0188

1a. REPORT SECURITY CLASSIFICATION Unclassified	1b. RESTRICTIVE MARKINGS
2a. SECURITY CLASSIFICATION AUTHORITY	3. DISTRIBUTION/AVAILABILITY OF REPORT Approved for public release; distribution unlimited.
2b. DECLASSIFICATION/DOWNGRADING SCHEDULE	
4. PERFORMING ORGANIZATION REPORT NUMBER(S) AFIT/GAE/AA/87M-1	5. MONITORING ORGANIZATION REPORT NUMBER(S)
6a. NAME OF PERFORMING ORGANIZATION School of Engineering 6b. OFFICE SYMBOL (If applicable) AFIT-ENY	7a. NAME OF MONITORING ORGANIZATION
6c. ADDRESS (City, State, and ZIP Code) Air Force Institute of Technology Wright-Patterson Air Force Base, Ohio 45433	7b. ADDRESS (City, State, and ZIP Code)
8a. NAME OF FUNDING/SPONSORING ORGANIZATION Mobility Development Laboratory Flight Dynamics Laboratories 8b. OFFICE SYMBOL (If applicable) AFWAL/FIEMB	9. PROCUREMENT INSTRUMENT IDENTIFICATION NUMBER
8c. ADDRESS (City, State, and ZIP Code) Air Force Wright Aeronautical Laboratories Wright-Patterson Air Force Base, Ohio 45433	10. SOURCE OF FUNDING NUMBERS PROGRAM ELEMENT NO. / PROJECT NO. / TASK NO / WORK UNIT ACCESSION NO.

11. TITLE (Include Security Classification)
EXPERIMENTAL STUDY OF WING-IN-GROUND EFFECTS IN THE AFIT 5-FOOT WIND TUNNEL

12. PERSONAL AUTHOR(S)
Lawyn C. Edwards, MAJ, USA

13a. TYPE OF REPORT	13b. TIME COVERED	14. DATE OF REPORT (Year, Month, Day)	15. PAGE COUNT
MS Thesis	FROM _____ TO _____	1987 MARCH	

16. SUPPLEMENTARY NOTATION

17. COSATI CODES			18. SUBJECT TERMS (Continue on reverse if necessary and identify by block number)
FIELD	GROUP	SUB-GROUP	In-Ground Effects Out-of-Ground Effects Air Cushion

19. ABSTRACT (Continue on reverse if necessary and identify by block number)

Thesis Advisor: Dr. Milton E. Franke, Professor
Department of Aeronautics and Astronautics

ABSTRACT ON BACK

Approved for public release: IAW AFR 190-1.
LYNN E. WOLAVER 5 May 87
Dean for Research and Professional Development
Air Force Institute of Technology (AFIT)
Wright-Patterson AFB OH 45433

20. DISTRIBUTION/AVAILABILITY OF ABSTRACT	21. ABSTRACT SECURITY CLASSIFICATION
☐ UNCLASSIFIED/UNLIMITED ☒ SAME AS RPT. ☐ DTIC USERS	Unclassified
22a. NAME OF RESPONSIBLE INDIVIDUAL Dr. Milton E. Franke	22b. TELEPHONE (Include Area Code) (513) 255-2362 / 22c. OFFICE SYMBOL AFIT-ENY

DD Form 1473, JUN 86 — Previous editions are obsolete. — SECURITY CLASSIFICATION OF THIS PAGE

UNCLASSIFIED

19. ABSTRACT

The effect of flying close to the earth's surface on the lift to drag ratio (L/D) was investigated. This was accomplished with the model of a NACA 4415 wing in the AFIT 5-foot Wind Tunnel.

The model was equipped with a full-span adjustable flap and three sets of end and center plates. Ground boards were placed in the tunnel to simulate the earth's surface. Five different heights of the model above the ground boards were selected to represent in and out of ground effects regimes.

Data were collected for forces and pressures on the model and on the board. The graphical representation of results displayed the effects of changing model parameters versus force, moment and pressure coefficients.

These conclusions were compared to theory and other literature for correlation. Results were conclusive. The effects of center plates and the variation of plate size were negligible. The presence of the set of end plates was beneficial near the surface but was negligible out of ground effects. The height of the model above the board produced noticeable differences in results. Angle of attack was shown to have a marked influence along with flap angle. Pressure plots also appeared to provide a method of predicting the amount of lift produced.